

Engineering kinetics of immunotherapies & vaccines

by

Sachin Haresh Bhagchandani

B.Tech, M.Tech, Indian Institute of Technology, Roorkee (2017)

Submitted to the Department of Chemical Engineering in partial fulfillment of the requirements for the degree of

Doctor of Philosophy

at the

MASSACHUSETTS INSTITUTE OF TECHNOLOGY

September 2023

© 2023 Sachin H. Bhagchandani. All rights reserved.

The author hereby grants to MIT a nonexclusive, worldwide, irrevocable, royalty-free license to exercise any and all rights under copyright, including to reproduce, preserve, distribute and publicly display copies of the thesis, or release the thesis under an open-access license.

Author
Department of Chemical Engineering
July 21st, 2023

Certified by.....
Jeremiah A. Johnson
Professor of Chemistry, MIT
Thesis Supervisor

Certified by.....
Darrell J. Irvine
Professor of Biological Engineering, MIT
Thesis Supervisor

Certified by.....
Robert S. Langer
Professor of Chemical Engineering, MIT
Thesis Supervisor

Accepted by
Hadley D. Sikes
Professor of Chemical Engineering
Graduate Officer

Engineering kinetics of immunotherapies & vaccines

by

Sachin Haresh Bhagchandani

Submitted to the Department of Chemical Engineering on
July 24, 2023, in partial fulfillment of the
requirements for the degree of
Doctor of Philosophy

Abstract

The dynamic progression of immune responses to infections & tumors points to the possibility of an optimal temporal window for immune modulation as a key parameter that could influence protective outcomes. Altering kinetics in an attempt to orchestrate an immune response in resonance with the biological rhythm of innate and adaptive immunity could have significant returns with respect to improved efficacy and decreased toxicity; all without necessitating the approval of new agents. In this thesis, we explored two distinct strategies to engineer immunotherapy and vaccine kinetics. We show how these kinetics can significantly impact cellular and humoral immune responses, and carried out detailed investigations into the underlying mechanisms that govern these temporal effects.

Firstly, imidazoquinolines (IMDs), small molecule agonists of Toll like receptor (TLR)-7 and/or TLR-8, are of great interest as potential anti-cancer therapeutics due to their ability to activate innate immune cells. Nevertheless, safe and effective systemic administration of these compounds in the clinic is an unsolved challenge due to dose-limiting toxicities, poor bioavailability, and severe immune-related adverse events upon intravenous administration. While attempts to deliver them via nanoparticle technologies have improved the potency of IMDs, achieving these outcomes while minimizing acute systemic inflammation has proven difficult.

Here, we developed a bottlebrush prodrug (BPD) IMD library as a tool to provide a detailed understanding of how the kinetics of drug release impacts safety and tumor immune stimulation. Cylindrical BPDs featuring antibody-like dimensions (~10 nm), coaxial PEG chains, and TLR-7/8 agonists linked through cleavable linkers along their backbone were synthesized using ring-opening metathesis polymerization (ROMP). By tuning the cleavable linker molecular structure,

IMD-BPD constructs were identified that allowed for potent stimulation of innate immune cells in tumors while avoiding systemic increases in inflammatory cytokines, reductions in white blood cell counts, or liver toxicity. These BPDs enabled significant reductions in tumor growth in syngeneic tumor models and improved responses to anti-PD-1 checkpoint blockade. Single-cell RNA-sequencing revealed that IMD-BPDs promote dendritic cell activation and reduce immunosuppressive macrophages in the tumor microenvironment, changes that free TLR7/8 agonists were unable to achieve.

Secondly, “extended dosing” of vaccines – immunization regimens that prolong exposure to antigen/adjuvant– has shown promise as a strategy to significantly augment humoral immune responses to HIV vaccines. Studies in mice and non-human primates have shown that extended dosing of immunogens can trigger long-lived germinal center responses, promote somatic hypermutation, and increase neutralizing antibody breadth. As one form of extended dosing, escalating-dosing (ED) immunization, where a given dose of antigen/adjuvant is administered as 7 injections of increasing dose over 2 weeks (7-ED), has been found to be one of the most effective ways to achieve these effects. This approach provides multifaceted benefits, such as allowing for improved antigen capture on follicular dendritic cells (FDCs) and augmenting follicular helper T cell priming. Furthermore, it results in the generation of long-lived germinal centers (GCs) with a more diverse repertoire of B cell clones that enter these GCs. However, such a multi-dose regimen presents significant feasibility challenges in terms of clinical translation.

Here we explored the parameter space of “reduced ED” immunizations employing fewer injections, aiming to increase clinical feasibility while retaining much of the immunological benefits of ED dosing compared to traditional bolus immunization. We carried out systematic studies varying number of doses, dose ratio, and dose intervals, immunizing mice and analyzing the subsequent immune responses looking for patterns maximizing the size of the antigen-specific GC response. A two shot reduced ED regimen (2-ED) consisting of dose 1 (20% of vaccine dose) on day 0 and a second shot (80% of vaccine dose) with a 7-day interval elicited prolonged optimal responses that were an order of magnitude improved over bolus immunization and enabled antigen capture of the second shot on FDCs, though not reaching the immune response levels elicited by the 7-ED regimen. Computational modeling of the germinal center response indicated that the 7-ED regimen is able to maximize capture of native antigen as a consequence of high antibody titers prior to the final shot. These results suggested that sustained antigen availability at the time of the

second immunization in our 2-ED regimen would boost innate inflammation in lymph nodes & improve antigen capture in follicles. Consistent with these predictions, we found that sustained second prime dosing by anchoring the antigen onto alum via a phosphoserine linker significantly improved the magnitude of the antigen-specific GC responses.

These results pave the way to safer and more potent cancer immunotherapies and vaccines via engineered kinetic approaches to administering these compounds.

Thesis Committee:

Jeremiah A. Johnson (Thesis Advisor), Ph.D.
Professor of Chemistry, **MIT**

Darrell J. Irvine (Thesis Advisor), Ph.D.
Professor of Biological Engineering, **MIT**

Robert S. Langer (Thesis Advisor), Ph.D.
Professor of Chemical Engineering, **MIT**

Stefani T. Spranger, Ph.D.
Professor of Biology, **MIT**

K Dane Wittrup, Ph.D.
Professor of Chemical Engineering, **MIT**

Acknowledgements

I want to express my sincere gratitude to Jeremiah Johnson for his invaluable mentorship during my PhD. Your insightful perspectives, detailed feedback, and expertise in polymer science greatly influenced the direction and quality of my research. Your approachable and down-to-earth demeanor made our interactions incredibly enjoyable and instilled in me a deep passion for polymer science. I am truly thankful for the opportunity to grow under your mentorship, which played a pivotal role in shaping my research journey.

I am deeply grateful to acknowledge Darrell Irvine for his exceptional guidance and mentorship throughout the journey of my PhD. Your profound insights, unwavering support, and dedication to pushing the boundaries of engineering the immune system have been invaluable. Your expertise in immunology has not only shaped the direction of my research but has also inspired me to strive for excellence in this field. Your commitment to fostering a dynamic learning environment has been crucial in my growth as a researcher. I am truly honored to have had the opportunity to work with you as my PhD mentor, and your influence will continue to resonate in my academic and professional pursuits.

I extend my gratitude to Robert Langer, who mentored me throughout this journey. Your influential work has significantly shaped the course of my research, and your guidance has been invaluable in enhancing the quality of my work. Furthermore, I wish to express my sincere appreciation to Stefani Spranger for her expertise and guidance in cancer immunology during my PhD thesis. My time in her lab was invaluable in shaping the focus and insights of my research. Finally, I would like to extend my gratitude to Karl Dane Wittrup for serving as the chair of my thesis committee. Your expertise and insightful feedback have been invaluable assets in shaping the direction and rigor of my research.

I am indebted to Evelyn Yuzhou Tong, Michelle Ramseier, and Alex Shalek for our collaboration involving single-cell RNA sequencing analysis, which greatly enriched the findings presented in my PhD thesis. I am grateful to Leerang Yang and Arup Chakraborty for mentoring and collaborating with me, providing crucial insights using their computational models that allowed me to improve our vaccine formulations. Finally, I extend my sincere appreciation to Shane Crotty, William Schief, and Boris Juelg for their timely feedback and support in my vaccine projects, which significantly contributed to the multifaceted research presented in my PhD thesis.

I would like to thank members of the Johnson Group for the collective support as I navigated my way through learning synthetic chemistry. Specifically, Farrukh Vohidov, Matthew Pearson, Christopher Brown, Bin Liu, Gavin Kiel, Hung V-T Nguyen, Lori Won, Nate Oldenhuis, Wencong Wang, Peter Qin, Peyton Sheih, Keith Husted, David Lundberg, Valerie Lensch, Hadiqa Zafar, Yasmeen Alfaraj, Michael Stolberg, Deborah Ehrlich, Jessica Lamb, Aiden Wang, Shannon Wagner, Lexy Wayne, and Prossy Najjuma. In particular, I am incredibly grateful to Farrukh for mentoring me during my initial years.

I want to acknowledge members of the Irvine lab for their valuable inputs and contributions that enhanced the research presented in this thesis. Specifically, Lauren Milling, Laura Maiorino, Anika Wadhera, Yash Agarwal, Parisa Yousefpour, Anna Romanov, Mariane Melo, Na Li, Jason Chang, Aereas Aung, Asheley Chapman, Shengwei Wu, B.J. Kim, Sasan Jalili, Ivan Susan Pires, Brittany Hartwell, Angela Zhang, Alex Hostetler, Jason Zhang, Leyuan Ma, Kaiyuan Ni, Coralie Backlund, Eric Dane, Kasia Kaczmarek Michaels, Valerie Corapi, Mark Miller, Mariann Murray, Tianyang Mao, Namit Chaudhary, Kristen Rodrigues, Heikyung Suh, Luciano Santollini, Bingxu Liu, Jonathan Dye, Kashif Qureshi, Justin Gregory, Elana Ben-Akiva, Bill Pinney, Maureen Buckley, and Aggi Walsh. In particular, I remain eternally grateful to Lauren for mentoring me during my initial years, and to Laura for her constant support and mentorship throughout the later years, up to this point.

I would like to acknowledge the members of the Spranger lab for their collaborative efforts. Specifically, Timothy Fessenden, Brendan Horton, Maria Zagorulya, Kim Bich Nguyen, and Ellen Duong. Finally, I want to express my gratitude to the members of the Langer lab at MIT for their mentorship and support. Specifically, Padmini Pillai, Malvika Verma Miller, Jamie Webster, Kaitlyn Sadtler, Xueguang Lu, Arnab Rudra, Junwei Li, Rameen Shakur, Lisa Volpatti, and Allen Jiang.

I am deeply grateful for the mentorship I've received from exceptional mentors prior to starting my doctoral journey. Jeffrey Karp's guidance while at Harvard Medical School has profoundly shaped my approach to research. Nitin Joshi's valuable mentorship played a pivotal role in my growth during my time in the Karp lab. Giovanni Traverso's feedback during my time in the Langer lab was instrumental in helping me grow as a scientist. Deepa Khushalani's mentorship during my internship at the Tata Institute of Fundamental Research kindled my passion for scientific exploration, and Gaurav Manik's support during my undergraduate education at the Indian Institute of Technology Roorkee contributed significantly to both my academic and personal development.

I extend my gratitude to Caitlin Stier from the MIT Communication lab for her invaluable mentorship. Being a Communication Lab fellow allowed me the privilege to mentor colleagues in fulfilling their communication needs.

I am thankful for the unwavering support and camaraderie of my friends and colleagues at MIT and Harvard, whose encouragement has been an invaluable part of this journey. In particular, I would like to acknowledge Thomas Kunczewicz, Aaron Mendonca, Prathima Muniyappa, Natalie Landon-Brace, Keir Martyn, Alisa Ugodnikov, Natalie Landon-Brace, Soumya Pasumarthy, Dustin Ammendolia, Sammy Zheng, Cody Cleveland, Vance Soares, Netra Unni, Grace Zhong, and Kelvin Songyu Ng from my time at Harvard.

Furthermore, I'm deeply appreciative of my friends in the Department of Chemical Engineering at MIT, in particular, Lagnajit Pattanaik, Kevin Tenny, Andrew Biedermann, Srinu Pujari, Kara Rody, Patrick Asinger, Anirudh Nambiar, Krishna Srinivas, Supratim Das, Natalie Eyke, Thejas Weasley, Tam Nguyen, Maddie Dery, Sarah Cowles, Arie Havasov, Jennifer Kaczmarek, Brandon Johnson, Arjav Shah, and Simar Kaur. I want to express my heartfelt gratitude to my friends in the 'chai' group, namely, Nidhi Juthani, Rohit Supekar, Shraddha Rana, Prashanth Prakash, Ben Leaker, Chinmay Kulkarni, and Sam Raymond.

I am profoundly thankful to my roommates and closest friends for their unwavering support throughout my PhD thesis journey. Your presence has made this challenging process more rewarding and meaningful than I could have ever imagined. Thank you Elad Deiss-Yehiely, Eesha Khare, Victor Champagne, Johanna Champagne, Pierre Colombe, Safia Dziri, Max L'Etoile, and Katherine Mizrahi. In addition, I want to acknowledge all my friends from other Departments, namely, Jake Song, Jackie Lunger, Kate Reidy, Philip Simons, George Varnavides, Evi Postelnicu, Luke Leissring, Ty Christoff, Parker Buntin, Geoff Vaartstra, Caroline McCue, Vishnu Jayaprakash, Carolyn Sheline, Yohan John, and Katie Hahm.

Finally, I must extend my heartfelt gratitude to my dearest friends from back home in India. Your unwavering support throughout my PhD journey has meant the world to me. Thank you, Jonathan Mendonca, Aditi Talwar, Abhinav Sah, Aman Modi, Niyati Shah, Vaishali Singh, Abhimanyu Lamba, Piyush Subramanian, Bhavesh Vaswani, Kumar Chitresh Sinha, Saurabh Chauhan, Sharukh Moin Khan, Chinmay Saraf, Abhishek Shanbhag, Snehil Shrivastava, Kajal Bhatia, Niharika Anand, Winston Travasso, Aakanksha Singh, Chinmay Vaidya, Anjana Dattani, Darshak Bhagat, Suvir Sharma, Rahul Kapoor and a special shout-out to Krish Mendonsa for his help with my thesis.

I am deeply thankful to my extended family for their unending support during my PhD thesis journey; their belief in me has been a driving force in achieving this milestone. Thank you to the Bahirwani family, Nana, Nani, Didi masi, the Harjani family, Aru didi, Naresh uncle, Shivani, Anika, Megha, the Aswani family, Geetu didi, Kamal uncle, Karan, Bashine, Dimple, Manij, the Jagwani family, Vanisha masi, Jagdish uncle, Tarun, Ntasha, Gaurav, Bhawna, the Manghnani family, Lalitha masi, Kamlesh uncle, Darshan, Vicky, and Erica, the Harjani family, Saroj masi, Moose uncle, Kiran masi, Ashok uncle, Neha (& Jaya), Sanya, Priti, Chinky, the Lalmalani family, Neetu masi, Gopal uncle, Puja, Sapna, Andrew and many others for their support and blessings.

I extend my heartfelt appreciation to my in-laws for their unwavering support throughout my PhD thesis journey; their encouragement and blessings have been invaluable pillars of strength. Thank you, Pa, Ma, Sham uncle, Anita masi, Roshan, Gehna, and family.

I want to take a moment and acknowledge my grandparents, Lakshman and Meena Bhagchandani. Your blessings keep me going and I cherish the time we had together.

Above all, I want to express my deepest gratitude to my dad, my mom, my sister, and my wife for their eternal love and support.

Dad – your constant encouragement and sacrifices have been my source of strength. I deeply respect your guidance throughout my life and truly admire your support along every path that I have taken. I am so so lucky to have you as my role model and my mentor.

Mom – your unwavering faith in my abilities has been my guiding light. Your love, kindness, and generosity has profoundly shaped my moral principles and every good quality I possess is because of you. I aspire to uphold your values, and the thought of having your unwavering love and wisdom as a constant presence in my journey fills me with an immeasurable sense of peace and warmth.

Sonali – your uplifting words have kept me going in the darkest of times. You have always been there for me when I needed you and have deeply influenced who I am as a person. I consider myself incredibly fortunate to have the best sister in the world.

Kiran – your enduring support and boundless love has been my anchor. Every day I wake up endlessly thankful to have my best friend by my side. Your constant encouragement during tough moments, your incredible knack for bringing laughter to my sad days, and your steady support keeps me going. I'm filled with excitement for our future and the adventures that await us.

This thesis is dedicated to my family.

Table of Contents

1 Introduction

1.1	Immune responses in space & time	19
1.2	Spatio-temporal dynamics of cancer-immune system interactions	23
1.2.1	The cancer-immunity cycle	23
1.2.2	Tumor-immune microenvironments	24
1.2.3	Effective local (intra-tumoral) cancer immunotherapies	25
1.2.4	Effective systemic cancer immunotherapies	27
1.2.5	Potential kinetic modulations	29
1.3	Germinal Center dynamics and the evolution of the humoral immune response	31
1.3.1	Anatomy of the Germinal Center (GC)	31
1.3.2	GC Selection	33
1.3.3	Clonal dynamics and evolution over the course of the GC	34
1.3.4	GC duration	35
1.3.5	Potential kinetic modulations	37

2 Evolution of Toll-like receptor 7/8 agonist therapeutics and their delivery approaches

2.1	Introduction	39
2.2	TLR7/8 biology and cellular implications of downstream effects	41
2.2.1	TLR7/8 signaling pathways & downstream effects	41
2.2.2	Cell types responding to TLR7/8 ligands	43
2.2.3	Structure-activity relationships of IMD TLR7/8 agonists	46
2.3	Preclinical and Clinical Development of TLR7/8 agonists	48
2.3.1	Topical therapies for skin conditions	49
2.3.2	IMDs as immunomodulators for Advanced Cancers	50
2.3.3	Systemic delivery of IMDs as Antivirals for Infectious Diseases	56
2.3.4	Anti-inflammatories and bronchodilators for Respiratory Ailments	59
2.4	Bioconjugation and other delivery strategies	60
2.4.1	TLR7/8a conjugates to enhance vaccine efficacy	60
2.4.1.1	Antigen-TLR7/8 conjugates	60
2.4.1.2	Polymer and particulate formulations of TLR7/8 agonists	60
2.4.2	Toward safe, systemic delivery via drug carrier approaches	68
2.4.3	Localized (in situ) delivery approaches to improve intratumoral efficacy	73

2.4.4 In search of synergy: combination delivery approaches.....	76
2.5 Conclusion and Future Outlook	79

3 Engineering kinetics of TLR7/8 agonist release from bottlebrush prodrugs enables tumor-focused immune stimulation

3.1 Introduction	80
3.2 Results	83
3.2.1 Synthesis and characterization of a library of R848-BPDs with varying linkers.....	83
3.2.2 R848-BPDs display tunable release characteristics ranging from a few days to several weeks ...	83
3.2.3 R848-BPDs with optimal linkers have greater maximum tolerated doses (MTDs) and broad therapeutic windows compared to free R848	87
3.2.4 R848-BPDs display tumor accumulation and uptake by innate immune cells in the tumor and tumor-draining lymph nodes compared to R848	89
3.2.5 Systemically administered R848-BPDs elicit therapeutic responses both as monotherapies and in combination with checkpoint blockade therapy in mouse models of colon carcinoma	91
3.2.6 R848-BPDs exert anti-tumor effects via sustained activation of innate immune cell subsets	91
3.3 Discussion	96
3.4 Methods	99

4 Escalating dose immunization of vaccines

4.1 Introduction	109
4.2 Results	110
4.2.1 Escalating dose immunization improves antigen capture on follicles and enhances humoral immune responses to HIV Env trimers	110
4.2.2 Escalating dose immunization improves germinal center and serum antibody responses for the polysaccharide-based typhoid vaccine.....	111
4.3 Discussion	112
4.4 Materials and Methods	113

5 Two-dose “extended priming” immunization amplifies humoral immune responses by synchronizing vaccine delivery with the germinal center response

5.1 Introduction	115
5.2 Results	117
5.2.1 A two-escalating-dose priming regimen greatly augments responses to HIV Env trimer protein immunization over traditional bolus immunization	117
5.2.2 Optimized 2-dose ED priming amplifies both the magnitude and duration of GC responses compared to bolus immunization.....	120
5.2.3 Extended and reduced dosing regimens boost innate inflammation in lymph nodes and allow	

for improved T cell responses.....	121
5.2.4 Computational modeling of the GC response predicts improved native antigen capture following extended-prime immunizations.....	125
5.2.5 A two-dose escalating prime increases antigen capture in follicles compared to bolus immunization	127
5.2.6 Extending antigen availability on the second immunization further boosts humoral responses as a consequence of innate immune activation and Tfh help	129
5.3 Discussion	131
5.4 Materials and Methods	135
6 Concluding thoughts and future directions	
6.1 Modulating kinetics of cancer-immune interactions	141
6.2 The next frontier for tuning kinetics of humoral responses	142
7 References.....	141

List of Figures

Fig. 1A-B: Primary and secondary lymphoid organs (*Adapted from* ¹). (A) Anatomical distribution of lymphoid organs (Primary: Thymus and Bone Marrow, Secondary: Nasal-associated lymphoid tissue [NALT], Spleen, Lymph Nodes, and Gut-associated lymphoid tissue. (B) Generalized structure of a lymph node highlighting activation of adaptive immunity.

Fig. 2: General principles of immune responses: Innate immunity and Adaptive immunity.

Fig. 3: Type I vs Type II immunity in the context of protection against severe disease (*Adapted from* ²).

Fig. 4: Cancer immunity cycle. This is divided into seven major steps, starting with the release of antigens from tumors and ending with the killing of tumor cells.

Fig. 5: Tumor-immune microenvironment schematic highlighting key classes of immune cells and signaling molecules.

Fig. 6: Different types/classes of tumor microenvironments. Representative images of tumor CD8 immunohistochemistry showing patterns of T cells associating with tumor cells (*Adapted from* ³).

Fig. 7: Intra-tumoral immunotherapies. Graphical depiction of biodistribution of intravenously administered systemic, tumor tissue-targeted immunotherapies, and intra-tumorally administered immunotherapies (*Adapted from* ⁴).

Fig. 8: Remodeled systemic immune landscapes in tumors. (A) Bone marrow hematopoiesis skews towards the production of neutrophils and monocytes through increased frequency of hematopoietic stem cells (HSCs) and granulocyte monocyte progenitors (GMPs). (B) Suppressive immature monocytes and neutrophils are mobilized into circulation in the blood along with increased frequencies of suppressive lymphocyte populations, CD4⁺ regulatory T (Treg) cells and regulatory B cells are also observed. Dendritic cell as well as CD8⁺ and CD4⁺ T cell frequencies are decreased in many tumor contexts. Several alterations observed in the blood have been mirrored in the (C) spleen and the (D) tumor draining lymph node (dLN) in mouse models (*Adapted from* ⁵).

Fig. 9: Schematic overview of the germinal center (GC) reaction indicating the key participating cell types (Follicular dendritic cells [FDCs], germinal center [GC] B cells, and T follicular helper [Tfh] cells) and output (Plasma cells and memory B cells).

Fig. 10: Role of antigen affinity in clonal selection.

Fig. 11: Prolonged antigen delivery increases antibody and memory B cell diversity through extended GC duration (Adapted from ⁶).

Fig. 12: Representative structures of widely used synthetic TLR7/8 agonists.

Fig. 13: TLR7/8 signaling pathways and downstream immune-effector modules. (A) Representative structure of TLR7/8 receptor. (B) Schematic of TLR7/8 receptor in the resting and activated states. (C) TLR7/8 signaling pathways from dimerization of the receptors to activation of the 3 transcriptional factors i.e. AP-1, NF- κ B and IRF7.

Fig. 14: SAR studies on synthetic TLR7/8 agonists. (A) Structure of IMDs indicating the sites at which substitutions were studied for improving potency. (B) Crystal structure of TLR7 bound to synthetic TLR7/8 agonist R848 highlighting the important interactions between the receptor and synthetic ligand.

Fig. 15: Bioconjugation approaches to enhance vaccine potency. (A) Dependence of R848-influenza conjugate particles on choice of linker strategy. (B) Charge-modified peptide strategy that results in particulate bioconjugates for personalized cancer vaccines. (C) Self-immolative linker approach for enhancing potency of malaria antigen-TLR7 conjugate.

Fig. 16: Polymer and particulate approaches to improve adjuvant potency. (A) Effect of varying TLR7 agonist density on lymph node residence time of the particle and varying size and architecture of the polymer on antigen-specific T cell response. (B) polymeric nanogel approach toward enhanced lymph node delivery and retention. (C) Adsorption to alum resulting in ‘depot’ effect which minimizes conc of TNF- α in the blood upon administration.

Fig. 17: Toward systemic delivery of synthetic TLR7/8 agonists. (A) TLR7/8 conjugation onto a carrier protein (mouse serum albumin) significantly improves survival in a pulmonary model of *B anthracis* (B) Cyclodextrin nanoparticle (CDNP) formulation of R848 significantly improves survival in the MC38 colon cancer mouse model. (C) β -galactosidase enzyme-mediated tuned release of imiquimod (R837). (D) PD-1 targeting approach localizes effect of R848 NPs upon i.v. administration and significantly improves survival in mice bearing MC38 tumors.

Fig. 18: Localized approaches to maximize intra-tumoral efficacy. (A) C-18 lipid moiety of 3M-052 improves retention at injection site for up to 28 days. (B) HA-R848 scaffold, administered immediately post tumor resection, significantly improves survival in 4T1 mouse model of metastatic breast cancer.

Fig. 19: Combination delivery approaches resulting in synergic efficacy. (A) Combination of TLR7 agonist (R837) and TLR4 agonist (MPLA) encapsulated in PLGA

particles synergistically improves antibody responses against H5N1-influenza-derived HA. (B) A single molecule containing TLR7 agonist (loxoribine), TLR4 agonist (pyrimido-indole) and TLR9 agonist (CpG ODN) improves antibody responses compared to the admixed formulation of the three agonists. (C) Combination of TLR7/8 agonist (R848) and anti-OX40 antibody demonstrates synergistic anti-tumor effects in A20 B cell lymphoma mouse model.

Fig. 20: Development and characterization of the R848-BPD library. (A) Schematic and chemical structure of the R848-BPD library composed of “fast,” “medium,” and “slow” prodrug activation kinetics. (B) Size exclusion chromatography traces of R848-MMs and R848-BPDs show that all of the R848-BPDs have consistent sizes independent of their linker composition. (C) Example cryo-TEM image of slow dMPE R848-BPD. Scale bar, 50 nm. (D) Hydrodynamic diameter of medium MPE R848-BPD as measured by DLS.

Fig. 21: In vitro release studies and immune activation analysis. (A) Release of free R848 from R848-MMs of varied linker structure in neutral PBS buffer. (B) R848 activity in R848-BPDs measuring fold change (relative to saline) in TLR7 reporter activation in HEK-human-TLR7 reporter cells 48 hours after incubation, (C) NF- κ B reporter activation (relative to saline) in mouse NF- κ B reporter cells 48 hours after activation, and (D) representative histograms and (E) quantification of % CD86 expression in mouse bone marrow-derived DCs (BMDCs) upon treatment with saline, a PEG bottlebrush lacking R848, free R848, or R848-BPDs for 48 hours. Data are presented as mean values \pm SEM with $n = 3$ independent samples for each group tested. Statistical comparisons in (E) were tested using one-way analysis of variance (ANOVA) followed by Dunnett’s multiple-comparisons test. * $P < 0.05$, *** $P < 0.001$, and **** $P < 0.0001$.

Fig. 22: MTD and toxicity assessments of free R848 and R848-BPDs. (A) Weight loss measurements for C57BL/6 mice ($n = 3$ per group) following intravenous administration of increasing concentrations of free R848 to define the MTD as 7.5 mg/kg. (B) Weight loss measurements for C57BL/6 mice following intravenous administration of free R848 (7.5 and 15 mg/kg) and R848-BPDs (7.5 mg/kg). (C to F) Serum cytokine measurements taken at 4 and 24 hours postinjection of free R848 (7.5 and 15 mg/kg) and R848-BPDs (7.5 mg/kg). (G) WBC count taken at 24 and 48 hours postinjection of free R848 (7.5 and 15 mg/kg) and R848-BPDs (7.5 mg/kg). (H) Pharmacokinetic (PK) analysis of plasma R848 at 1, 3, 6, and 24 hours postinjection of free R848 (7.5 mg/kg) and medium and slow R848-BPDs (7.5 mg/kg) in C57BL/6 mice ($n = 5$ per group). Data are presented as mean values \pm SEM with $n = 3$ or 5 independent samples for each group tested. Statistical comparisons in (C) to (F) and (G) were tested using two-way ANOVA followed by Dunnett’s multiple-comparisons test. * $P < 0.05$, ** $P < 0.01$, *** $P < 0.001$, and **** $P < 0.0001$.

Fig. 23: Organ and cellular biodistribution and pharmacodynamics of R848-BPDs. (A) Organ biodistribution in digested tissues (means \pm SEM) of Cy5.5 fluorescently labeled medium R848-BPDs (7.5 mg/kg) injected in C57BL/6 mice ($n = 5$ per group) bearing syngeneic MC38 colon carcinoma tumors (~ 25 mm²). (B) Representative flow cytometry histograms and (C to E) cellular biodistribution data of Cy5.5-labeled medium R848-BPDs taken 24 hours postinjection in C57BL/6 mice ($n = 5$ per group) bearing syngeneic MC38 colon carcinoma tumors (~ 25 mm²), indicating uptake by myeloid cells (DC1s, monocytes, and macrophages) in the tumor, tumor-draining lymph node, and spleen. (F and G) Tumor cytokine measurements taken at 4 hours postinjection of free R848, medium, and slow R848-BPDs (7.5 mg/kg) in C57BL/6 mice ($n = 3$ per group) bearing syngeneic MC38 colon carcinoma tumors (~ 25 mm²). (H) Image from intravital imaging showing R848-BPD (in cyan) colocalized with CD11c⁺ DCs (yellow) and other broader myeloid populations (magenta). Scale bar, 50 μ m. Insets highlighting colocalization of R848-BPD (cyan) on CD11c⁺ DCs (yellow) in separate channels. Scale bar, 10 μ m. Statistical comparisons in (F) and (G) were tested using an ANOVA followed by Dunnett's multiple-comparisons test. **** $P < 0.0001$. AU, arbitrary units.

Fig. 24: In vivo efficacy studies with medium and slow R848-BPDs in MC38 and CT26 colon carcinoma models demonstrated lower tumor burden and improved survival rates compared to control groups. (A) Tumor size (means \pm SEM) and (B) Kaplan-Meier survival curves for C57BL/6 mice ($n = 5$ per group) bearing syngeneic MC38 colon carcinoma tumors injected retro-orbitally with R848-BPDs (medium and slow) along with controls. (C) Tumor size (means \pm SEM) and (D) Kaplan-Meier survival curves for C57BL/6 mice ($n = 5$ per group) bearing syngeneic MC38 colon carcinoma tumors injected retro-orbitally with R848-BPDs (medium and slow) in combination with anti-PD-1 checkpoint blockade along with controls. (E) Tumor size (means \pm SEM) and (F) Kaplan-Meier survival curves for BALB/c mice ($n = 10$ per group) bearing syngeneic CT26 colon carcinoma tumors injected retro-orbitally with R848-BPDs (medium and slow) along with controls. (G) Tumor size (means \pm SEM) and (H) Kaplan-Meier survival curves for BALB/c mice ($n = 10$ per group) bearing syngeneic CT26 colon carcinoma tumors injected retro-orbitally with R848-BPDs (medium and slow) in combination with anti-PD-1 checkpoint blockade along with controls.

Fig. 25: Single-cell RNA sequencing (scRNA-seq) of MC38 tumors 24 hours posttreatment with saline, free R848, and medium R848-BPD. (A) Uniform manifold approximation and projection (UMAP) visualization of nonmalignant cells colored by eight broad cell types (left) and by 16 fine cell subsets separated by experimental conditions (right). NK, natural killer. (B) Difference in nonmalignant cell proportional composition across the three experimental conditions. Adjusted P values are only shown for cell subset comparisons (medium BPD versus free R848) that are significant by at least one statistical test: Fisher exact test (shown in #) or Dirichlet regression analysis (shown in *). (C) Enricher (top) and GSEA (bottom) pathway enrichments for the differentially expressed genes in *Cd38*⁺*Saa3*⁺ macrophages compared to the rest of the

macrophage subtypes, showing up-regulations of inflammatory response, IFN, and reactive oxygen species pathways (in boldface). (D) DoRothEA transcription factor (TF) inference for *Spp1*⁺ macrophages versus *Cd38*⁺*Saa3*⁺ macrophages and for DCs versus activated DCs, suggesting inflammation-related TF activities (colored in red) in *Cd38*⁺*Saa3*⁺ macrophages and activated DCs. Only TF-target interactions with a high confidence level were selected for this analysis. ns, not significant. **P* < 0.05, ****P* < 0.001, ##*P* < 0.01, and ###*P* < 0.001.

Fig. 26: Myeloid cell activation is a key requirement for T cell priming and antitumor efficacy of R848-BPDs. (A to C) Immunophenotyping of tumor-draining lymph nodes 24, 48, and 72 hours after R848-BPD dosing of C57BL/6 mice (*n* = 4 per group) bearing syngeneic MC38 tumors (~30 mm²). (D) Mice (*n* = 5 per group) bearing MC38 tumors (~25 mm²) were treated with medium BPD (7.5 mg/kg on days 8, 11, and 14), and tumor growth was followed longitudinally. Treatment experiments in wild-type mice treated with depleting antibodies against F4/80, BATF3 knockout mice, and TLR7^{-/-} mice are shown. (E) C57BL/6 mice bearing MC38 tumors (*n* = 6 per group) were injected with R848-BPDs along with controls, and T cells were isolated on day 7 posttreatment and cocultured with irradiated MC38 cells for IFN- γ enzyme-linked immunosorbent spot (ELISpot) analysis.

Fig. 27: Escalating-dose immunization with HIV Env trimer vaccines in mice. C57BL/6 mice (*n* = 5 animals/group) were immunized with 10 μ g of N332-GT2 trimer & 5 μ g of SMNP adjuvant as bolus or 2-week escalating-dose regimens. GC responses and serum antibody titers were evaluated on day 14 and day 28 respectively. Shown are clarified LNs stained with anti-CD35 to label FDC networks (A), enumeration of GC B cells (B), Tfh cells (C), trimer-binding GC B cells (D) and serum IgG responses (E).

Fig. 28: Escalating-dose immunization with the Typhoid vaccine in mice. Balb/c mice (*n* = 5 animals/group) were immunized with 5 μ g Thyphim Vi vaccine as bolus or escalating-dose regimens. GC responses and serum antibody titers were evaluated on day 21. Shown are raw flow cytometry data of GC B cell staining (A), enumeration of GC B cells (B), and serum anti-Typhim IgG responses (C).

Fig. 29: Going from 7-ED prime immunization comprised of 7 doses to an optimized 2-shot prime immunization. (A) Schematic of different dosing schemes with varying dose number. Representative histograms and total count for (B) GC, (C) Tfh, and (D) trimer-specific GC B cell responses at day 14 for different dosing regimens tested. (E) trimer-specific IgG titer at day 28 for the above groups. (F) Schematic of optimizing ratio for 2-shot immunization. Representative histograms and total count for (G) GC, (H) Tfh, and (I) trimer-specific GC B cell responses at day 14 for different ratios tested. (J) Schematic of optimizing interval for 2-shot immunization. Representative histograms and total count for (K) GC, (L) Tfh, and (M) trimer-specific GC B cell responses at day 14 for different intervals tested.

Fig. 30: Optimized 2-shot prime immunization amplifies & prolongs GC responses & enhances trimer-specific serum antibody titers over time. (A) Schematic of dosing schemes. (B) trimer-specific B cell count, (C) GC B cell count, (D) Tfh cell count, (E) trimer-specific GC B cell count, (F) Plasmablast count plotted, (G) trimer-specific IgM, and (H) trimer-specific IgG titers plotted over time for bolus and 2-ED regimens.

Fig. 31: In Silico modeling & experimental validation of dosing scheme on DC and T cell responses. (A) Schematics of the kinetic model of innate immune response and T cell priming. Prediction of the number of (B) DCs, (C) Ag⁺Adj⁺ DCs, (D) Ag-specific T cells, and (E) Tfh cells for different immunization regimens. (F) Comparing Tfh cell count predicted by the model with the experimental data at day 14. (G) Schematic of dosing schemes and time points for experimental DC measurements. (H) Number of DCs and (I) Representative histograms and (J) Number of trimer⁺ CD86⁺ DC counts over time for bolus, 2-ED, and 7-ED immunization regimens.

Fig. 32: Analysis of 7-ED (adjuvant bolus) regimen. (A) Tfh responses predicted by the model for 7-ED (adjuvant bolus) immunization. (B) Dosing schemes for 7-ED and 7-ED (adjuvant bolus) immunization regimens. (C) GC B cells and (D) Tfh cell responses to the regimens.

Fig. 33: In Silico modeling of antigen capture differences between dosing regimens. (A) Schematics of modeling antigen degradation. (B) Antibody titer from the in silico model for Bolus, 2-ED, and 7-ED immunization regimens. (C) In silico prediction of the amount of native and non-native antigen captured onto FDC over time. (D) Comparison of antigen amounts after the final shot from each dosing scheme. (E) Model prediction for the number of GC B cells. (F) Model prediction for the number of native antigen-binding (i.e. trimer⁺) GC B cells. (G) In silico predictions of trimer-specific GC B cell fraction from bolus, 2-ED, and 7-ED immunization schemes. The results reported are mean values from 10 independent stochastic simulations of the lymph node.

Fig. 34: 2-ED immunization enables antigen capture of the second shot on FDCs. (A) Groups of C57BL/6 mice (n = 3 per group) were by bolus, 2-ED, or 7-ED regimens followed by collection of lymph nodes for imaging at 48 h after bolus or after last injection of 2-ED and 7-ED regimens. FDC networks were labeled in situ by i.p. injection of anti-CD35 antibody 16 h before tissue collection. Collected tissues were clarified and imaged intact by confocal microscopy; shown are maximum intensity projections from z-stacks through FDC clusters (Scale bar, 150 μm). (B) Groups of C57BL/6 mice (n = 3 per group) were by bolus, 2-ED, or 7-ED regimens followed by collection of lymph nodes for imaging at 48 h after bolus or after last injection of 2-ED and 7-ED regimens. Lymph node sections were stained for FDCs (CD35; blue) and N332-GT2 (pink) and analyzed by confocal microscopy (Scale bar, 300 μm). (C-E) Flow cytometry analysis of LN cells (n = 3 pools/group, with each pool containing six LNs from 3 mice) isolated after

immunization with fluorescently labeled trimer using either bolus, 2-ED, or 7-ED dosing regimens. Shown are representative histograms of antigen intensities among LN cells (C), % trimer⁺ FDC population (D), and the mean fluorescence intensity among all trimer⁺ FDCs (E) for the indicated immunization conditions.

Fig. 35: Extended 2nd shot improves native antigen capture & enhances trimer⁺ GC responses. (A) Schematic depicting extended antigen availability on 2nd shot. (B) In-silico prediction of antibody titer upon extended 2 dose immunization (Note: Antigen was assumed to be released at a constant rate over 10 days). (C-D) In-silico prediction of native antigen-binding GC B cells and total GC B cells. (E) Comparison of in-silico prediction for the fraction of GC B cells that are native antigen-binding upon bolus, 2-ED, and 2-ED (Extended) immunization. (F) In-silico prediction of the amount of native and non-native antigen captured on FDC as a function of the duration of antigen release. (G) In-silico prediction of the fraction of GC B cells that are native antigen-binding as a function of the duration of antigen release. (H) Schematic demonstrating anchoring trimer immunogen onto Alum via phosphoserine linker (Alum-pSer). (I) GC and (J) Tfh responses for different groups tested. (K-M) Representative histograms, %, and number of trimer-specific GC B cells for the different dosing regimens.

List of Tables

Table 1: TLR7/8 expression levels and downstream effects.

Table 2: List of synthetic TLR7/8 agonists in different stages of clinical development.

Table 3: List of synthetic TLR7/8 agonists at the pre-clinical stage.

Table 4: One phase decay curve fitting of plasma concentrations for Free R848, Medium BPDs, & Slow BPDs in non-tumor bearing C57BL/6 mice.

Chapter 1

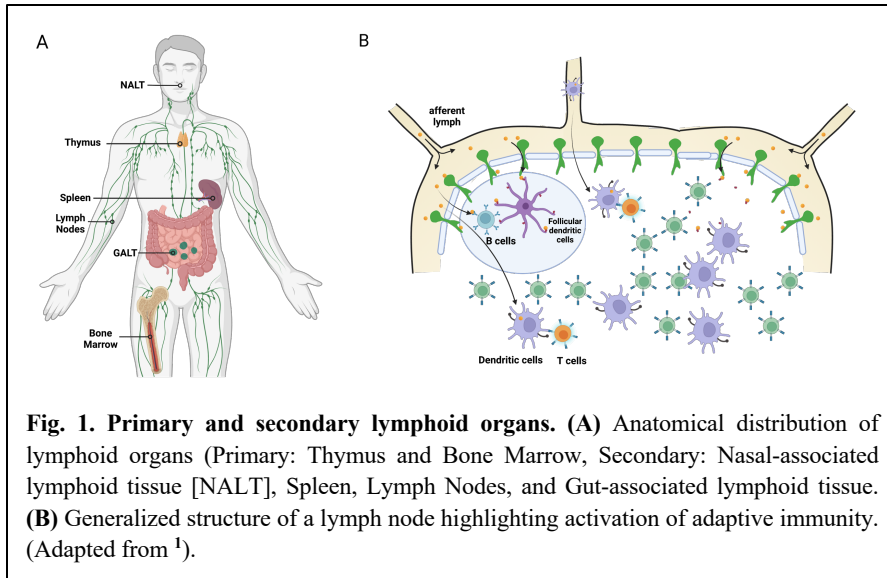
Introduction

1.1 Immune responses in space & time

Host defense mechanisms rely on the appropriate integration and coordination of immune responses in space and time. This coordination ensures that pathogens are effectively recognized and eliminated, and that excessive and damaging inflammation is avoided. Both adaptive and innate immune responses are generated by the coordinated actions of numerous cell types and tissues that promote pathogen recognition and clearance⁷. The fixed spatial arrangement of these organs is also critical for the effective coordination of these responses, as this ensures that immune cells are positioned to interact appropriately with one another as well as with invading pathogens. The availability, distribution, and positioning of immune cells within specific tissues and the distribution of immune-cell enriched tissues (e.g., lymphoid organs) throughout the body can have a substantial impact on the initiation, progression, and resolution of immune responses¹.

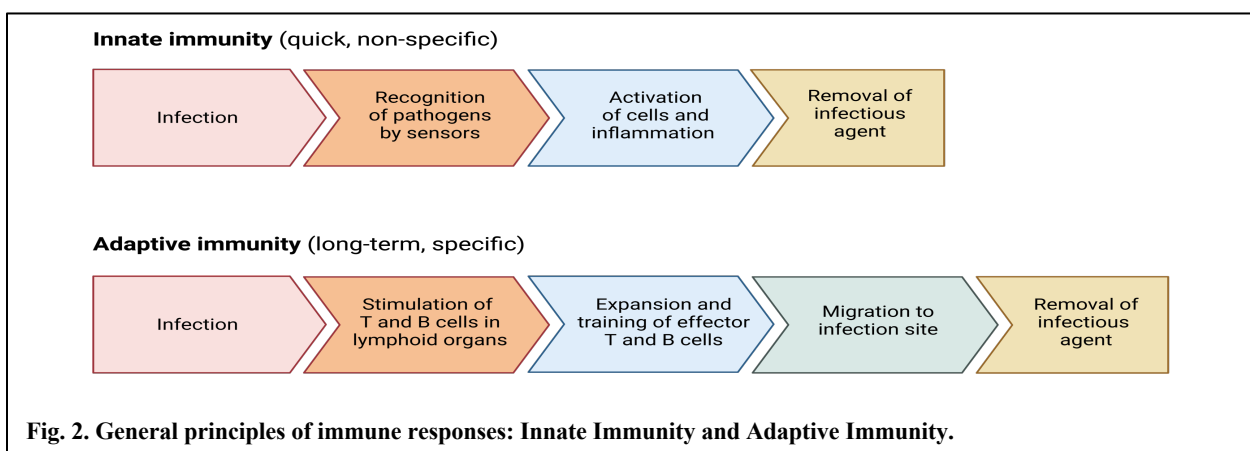
The lymphoid organs coordinate the maturation and migration of immune cells and serve to organize and regulate adaptive immune responses (**Fig. 1A**). In adult mammals, the bone marrow and thymus are primary lymphoid organs that provide niches for lymphocyte development. Secondary lymphoid organs, including the spleen, mucosa-associated lymphoid tissue, and between 600 to 800 lymph nodes distributed throughout the body, are responsible for maintaining and organizing T lymphocytes (T cells), B lymphocytes (B cells), and antigen-presenting cells (APCs)¹. These organs facilitate the activation of naïve B and T lymphocytes and promote the development of an adaptive immune response (**Fig. 1B**). As a result, these organs are frequently critical targets of vaccines and immunotherapies.

In addition to the spatial arrangement of immune cells in the body, immune responses need to be temporally coordinated to sustain effective host defense. The coordination of immune responses in time is influenced by the interplay between innate and adaptive elements (**Fig. 2**). Innate immunity is the first line of defense against invading threats. Innate immune responses are



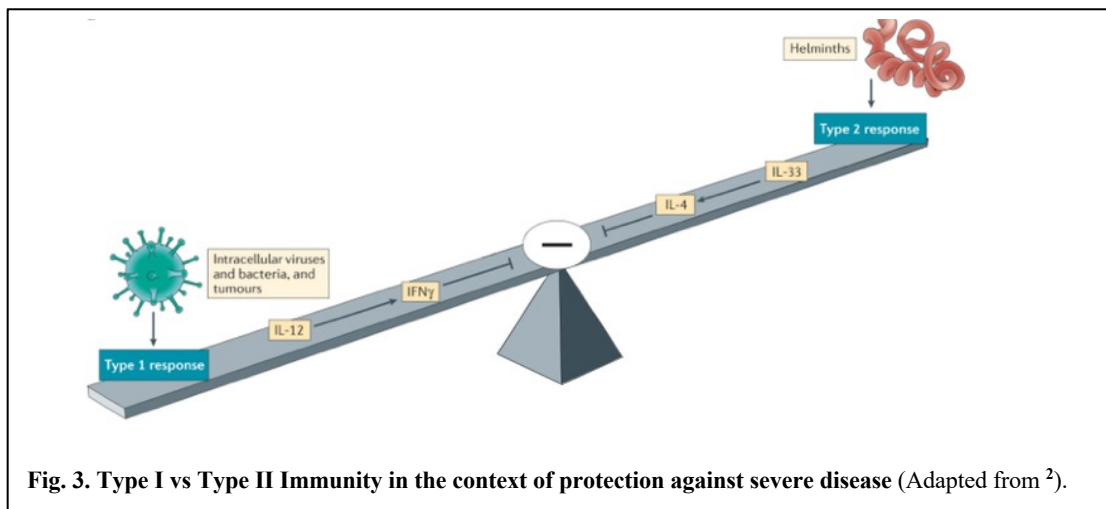
activated rapidly and are generally nonspecific⁸. In addition to its role in promoting immediate pathogen clearance, innate immune responses also activate and modulate the adaptive immune response, which is typically pathogen-specific and characterized

by a slower but longer-lasting response⁹. The consolidation of these two responses is a critical feature of host defense, as it ensures that the response is both balanced and effective. The kinetic progression of the immune response to foreign pathogens or other threats can be divided into three main phases: recognition, activation, and effector responses¹⁰. During the recognition phase, pattern recognition receptors (PRRs) on innate immune cells recognize pathogen-associated molecular patterns and/or damage-associated molecular patterns on invading pathogens or endogenous threats, respectively¹¹. These innate immune cells become activated (i.e., the activation phase) and respond by migrating to draining lymph nodes to initiate an adaptive immune response. This phase includes the activation and differentiation of T and B lymphocytes into effector cells¹². During the final effector phase, pathogens or other threats are eliminated by the immune system. This phase involves the effector functions of both innate and adaptive immune cells, including phagocytosis, cytotoxicity, and cytokine production¹³.



As discussed above, these responses are coordinated and influenced by numerous factors, including the spatial arrangement of immune cells and tissues, the interplay between innate and adaptive immune responses, and their regulation by intracellular signaling pathways¹⁴. A better understanding of the mechanisms underlying the coordination of immune responses will thus be essential for efforts toward developing more effective immunotherapies. For example, additional insight into these mechanisms can be used to inform the development of immunotherapies that target specific immune cells and/or pathways, including both cytokine- and cell-based immunotherapies. Agents that target signaling pathways that regulate immune cell activation and differentiation may be used to modulate the intensity and duration of immune responses with improvements in efficacy and reductions in the number and severity of adverse effects¹⁵.

This approach might also be used to guide the development of immunotherapies that target particular stages of the immune response, including initiation, progression, or resolution. For example, agents that target dendritic cells (DCs) and/or specific cytokines involved in the initiation of an immune response may serve to enhance the host response to pathogens and improve the efficacy of immunotherapies¹⁶. Likewise, agents that alter the duration of an activating signal might change the ultimate outcome of a given interaction. For example, CD4⁺ T cell responses differ based on how long DCs were exposed to lipopolysaccharide (LPS); an eight-hour exposure will result in the production of interferon-gamma (IFN γ) while a 48-hour exposure will lead to the production of interleukin (IL)-4¹⁷. These cytokines trigger distinct effector responses and mediate drastically different physiological outcomes as shown in **Fig. 3**. Similar to responses to LPS, the kinetics of IFN signaling can elicit opposing immune activation



responses. On the one hand, acute IFN-mediated signaling can generate an anti-viral state due to the induction of IFN-stimulated genes that protect against the sequelae of viral infection¹⁸. By contrast, persistent IFN-mediated signaling can be harmful under these circumstances, as it can induce immunosuppression or trigger inflammation and tissue damage^{19,20}. These are only a few of the many examples in which temporally programmed therapeutic interventions might have a significant impact on the efficacy of various immunotherapies and vaccines.

In the Introduction to this thesis, I will examine the mechanisms and therapeutic approaches that involve the spatial and temporal coordination of immune responses that might be used to treat tumors (**Section 1.2**) and for novel vaccination strategies (**Section 1.3**). In **Chapter 2**, I will introduce a more comprehensive outline of the specific kinetic challenges associated with toll-like receptor (TLR) 7/8 agonists as a critical example of a class of cancer immunotherapies that might benefit from an improved understanding of their pharmacokinetics as a means to unlock their therapeutic potential. In **Chapter 3**, I describe the use of a molecular bottlebrush prodrug (BPD) approach to improve the therapeutic index of the TLR agonists reviewed in Chapter 2 and demonstrate their improved anti-tumor efficacy in the absence of systemic toxicity.

In **Chapter 4**, I explore the kinetics of infections compared to vaccines and demonstrate how modulation of vaccine kinetics via escalating dose regimens may provide a significant boost to humoral immunity induced by both T cell-dependent and T cell-independent vaccines. In **Chapter 5**, I will present a systematic approach to the modulation of vaccine kinetics that may be more clinically feasible. I will also probe more deeply into the mechanisms underlying extended vaccine dosing strategies. Finally, in **Chapter 6**, I will review what we have learned from the aforementioned vignettes and suggest future directions that might be taken in the fields of cancer immunology and vaccines using approaches rooted in the modulation of the kinetics of the relevant immune responses.

1.2 Spatio-temporal dynamics of cancer-immune system interactions

Temporal progression is a critical feature of the immune response to tumors as it has been associated with protection against unfavorable outcomes.

1.2.1 The cancer-immunity cycle

The cancer immunity cycle is a complex process that enables the immune system to recognize and eliminate cancer cells (Fig. 4)²¹. The cycle begins when cancer cells die and release a variety of molecules (i.e., antigens) that are recognized as “foreign” by the host immune system. DCs are specialized immune cells that capture, process, and present these antigens to the T cells²². Once they have captured these antigens, DCs undergo a process of maturation that allows them to migrate to lymph nodes to present the processed antigens to T cells as peptide:MHC complexes. This interaction primes and activates the T cells. Once activated, T cells proliferate and are converted into effectors that recognize cancer cells that display the same antigens that were presented to them by the aforementioned DCs. Activated T cells migrate to the site of the tumor, where they must infiltrate into the tumor tissue. Once this has been accomplished, primed and activated T cells can target and kill cancer cells that display the target antigens²³.

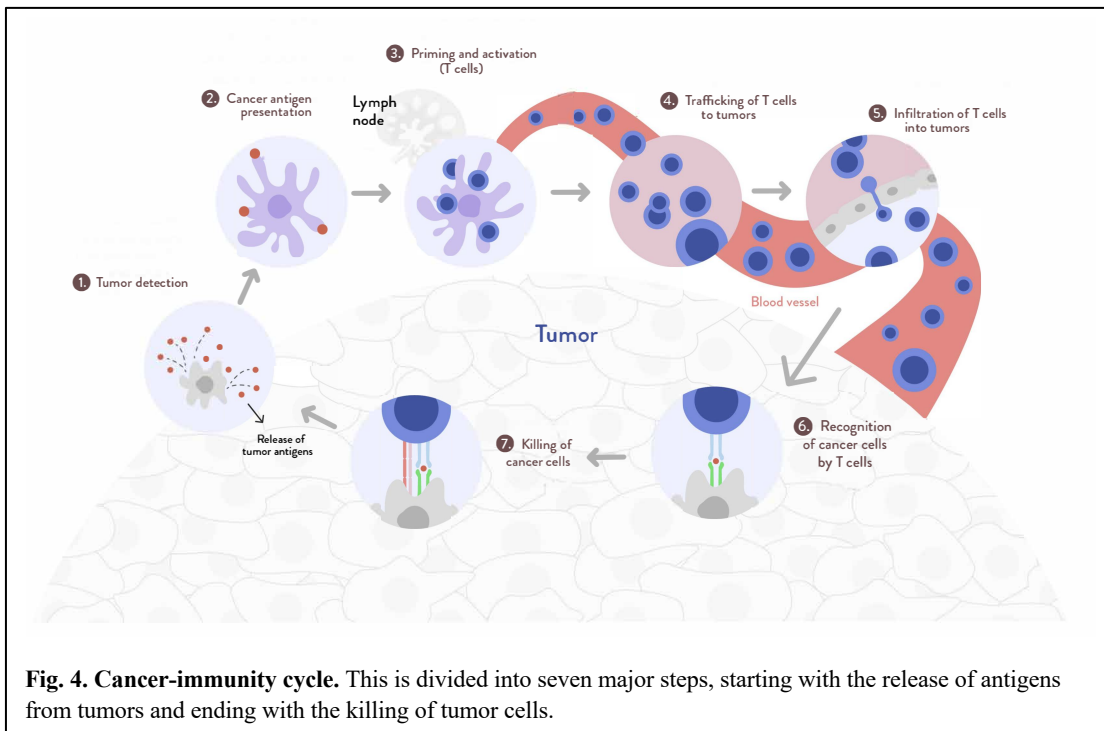
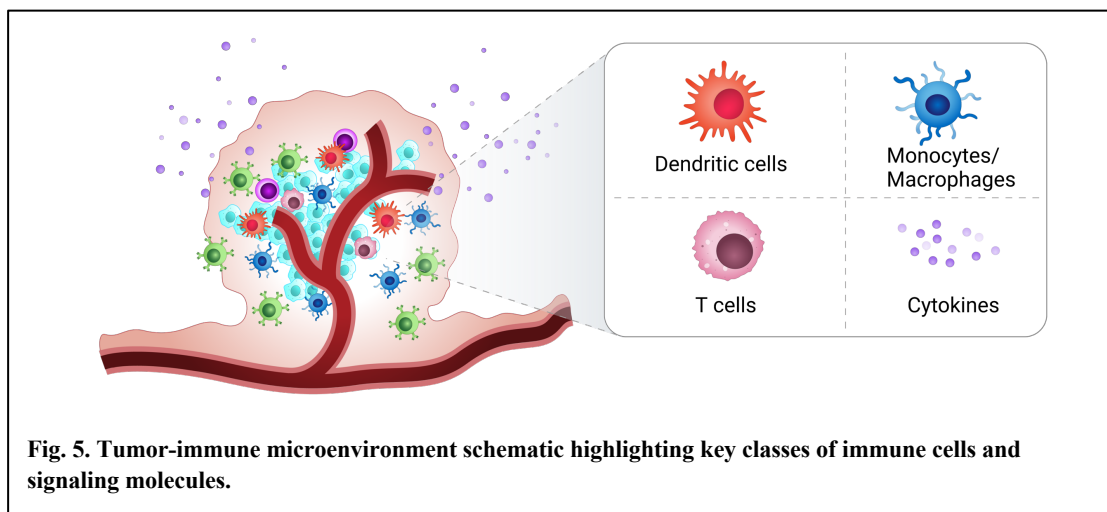


Fig. 4. Cancer-immunity cycle. This is divided into seven major steps, starting with the release of antigens from tumors and ending with the killing of tumor cells.

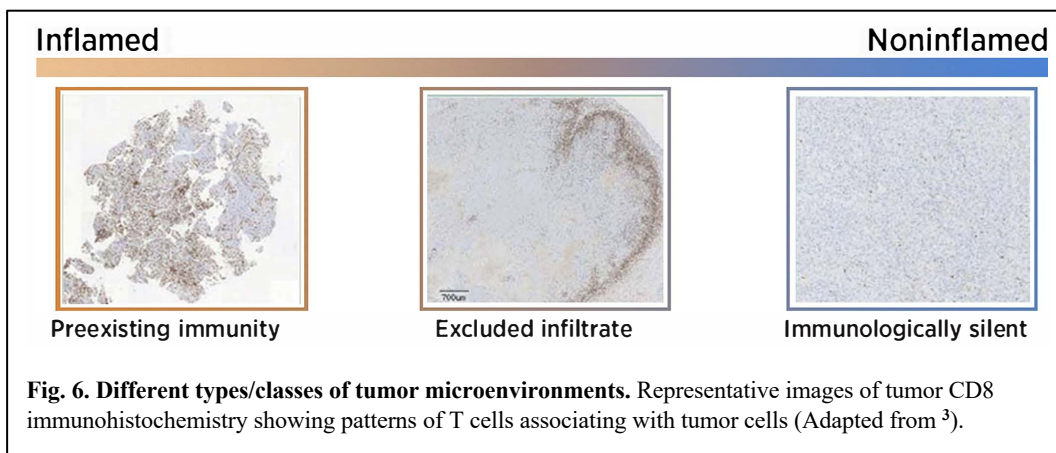
Timing is crucial in each step of this cycle, as the overall success of the immune response depends on the coordination of multiple immune cell types and their activation at the appropriate times. For example, if DCs present antigens too early or too late, the T cell response may be ineffective²⁴. Similarly, if T cells do not infiltrate the tumor site in a timely manner, cancer cells may continue to grow and spread before they can be eliminated by the immune system²⁵. The duration and intensity of the immune response may also have a critical impact on the efficacy of the cancer-immunity cycle. For example, prolonged exposure to a given antigen may lead to T cell exhaustion, which can render the immune system incapable of eliminating the target cancer cells²⁶. Thus, a better understanding of the temporal dynamics of the cancer-immunity cycle may provide us with insight into the development of new and effective immunotherapies.

1.2.2 Tumor-immune microenvironments

The tumor immune microenvironment is a complex network of molecules and cells found within and around a tumor (**Fig. 5**)²⁷, including tumor, stromal, immune, and endothelial cells. The immune cells in the tumor microenvironment (TME) include T, B, natural killer (NK), and myeloid cells (e.g., macrophages and DCs) along with molecules such as cytokines, chemokines, and growth factors. TMEs can be classified into three broad categories: (1) immunologically active or “inflamed”, (2) immune-infiltrated, and (3) immunologically silent (**Fig. 6**)²⁸. Immunologically active microenvironments typically include proinflammatory cytokines and chemokines as well as T lymphocytes and other immune cells. By contrast, the immunologically-silent microenvironment is characterized by an overall lack of inflammation.



Effective cancer therapy requires an in-depth understanding of these microenvironments. In some cases, the microenvironment can be a barrier to effective therapy, as tumors can use them to evade the immune system. For example, tumor cells can downregulate the expression of specific antigens and thus limit the extent to which they can be detected by the immune system. Tumors can also produce immunosuppressive factors, such as transforming growth factor (TGF)- β and IL-10, which inhibit immune cell function²⁹. Tumors can also recruit immunosuppressive cells, including myeloid-derived suppressor cells (MDSCs) and regulatory T cells (Tregs), which will further inhibit the function of tumor-suppressive immune cells^{30,31}.

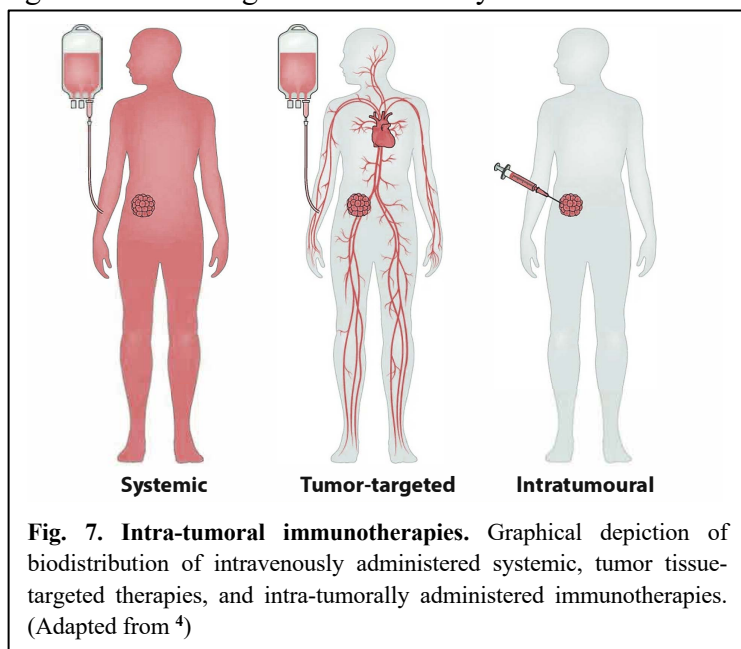


The timing of therapy is also important for the development of effective TME-focused approaches³². Tumor cells found in immunologically-active microenvironments typically respond better to immunotherapy than those found in regions that are immunologically silent. Of note, immunologically-active microenvironments are not fixed and can vary over time³³. Therefore, therapeutic approaches need to be tailored to take advantage of the specific characteristics of the TME that are present at a given time. For example, therapies that activate the immune system (e.g., immune checkpoint inhibitors) may be more effective at combatting tumors within an environment that is rich in CD8⁺ T cells³⁴. By contrast, therapies that target the stroma (e.g., anti-angiogenic agents) may be more effective against tumors in an immunologically-silent environment³⁵.

1.2.3 Effective local (intra-tumoral) cancer immunotherapies

Intratumoral immunotherapies are immune-modulating agents or cells delivered directly into the tumor that aim to prime or enhance a pre-existing anti-tumor immune response (**Fig. 7**)⁴.

One common example of this approach is the use of oncolytic viruses, which are viruses that have been modified so that they can selectively infect and replicate within cancer cells³⁶. Oncolytic viruses can induce tumor cell death and release tumor-specific antigens that can trigger an immune response against the cancer cells. These viruses can also be engineered to express immunostimulatory molecules that will further enhance the anti-tumor immune response within a given microenvironment³⁷. Another strategy involves the direct intra-tumoral injection of immune checkpoint inhibitors (e.g., anti-PD-1 or anti-CTLA-4 antibodies). These antibodies block the inhibitory signals generated by cancer cells to evade immune detection and thus permit the immune system to mount a stronger anti-tumor response. Intratumoral delivery leads to higher drug concentrations within the tumor with enhanced therapeutic efficacy and fewer adverse systemic effects³⁸. Thus, intra-tumoral immunotherapies offer targeted and localized approaches to maximize the therapeutic index of several immunomodulatory therapies³⁹. This approach can have a significant impact on the outcomes of combination therapies. For example, systemic chemotherapy can disrupt peripheral immune integrity and thus impede the therapeutic benefit of PD-1 blockade; the net result will be systemic lymphodepletion and loss of long-term immune memory⁴⁰. By contrast, local chemotherapy avoids this shortcoming and may synergize with PD-1 blockade to induce DC infiltration into the tumor and clonal expansion of antigen-specific effector T cells⁴⁰. Similarly, intratumoral injection of proinflammatory agents can provide local adjuvant activity to turn lesions into “*in situ*” cancer vaccines with the capacity to induce immunity against tumor antigens also shared by metastatic and micrometastatic foci⁴¹.



Advances in interventional radiology and associated imaging modalities have facilitated access to most if not all lesions, thus paving the way for their clinical application of this approach⁴². Similarly, novel strategies used to enhance the residence time of intra-tumoral therapeutics have been developed and are the subject of ongoing research and clinical trials focused on their optimization and

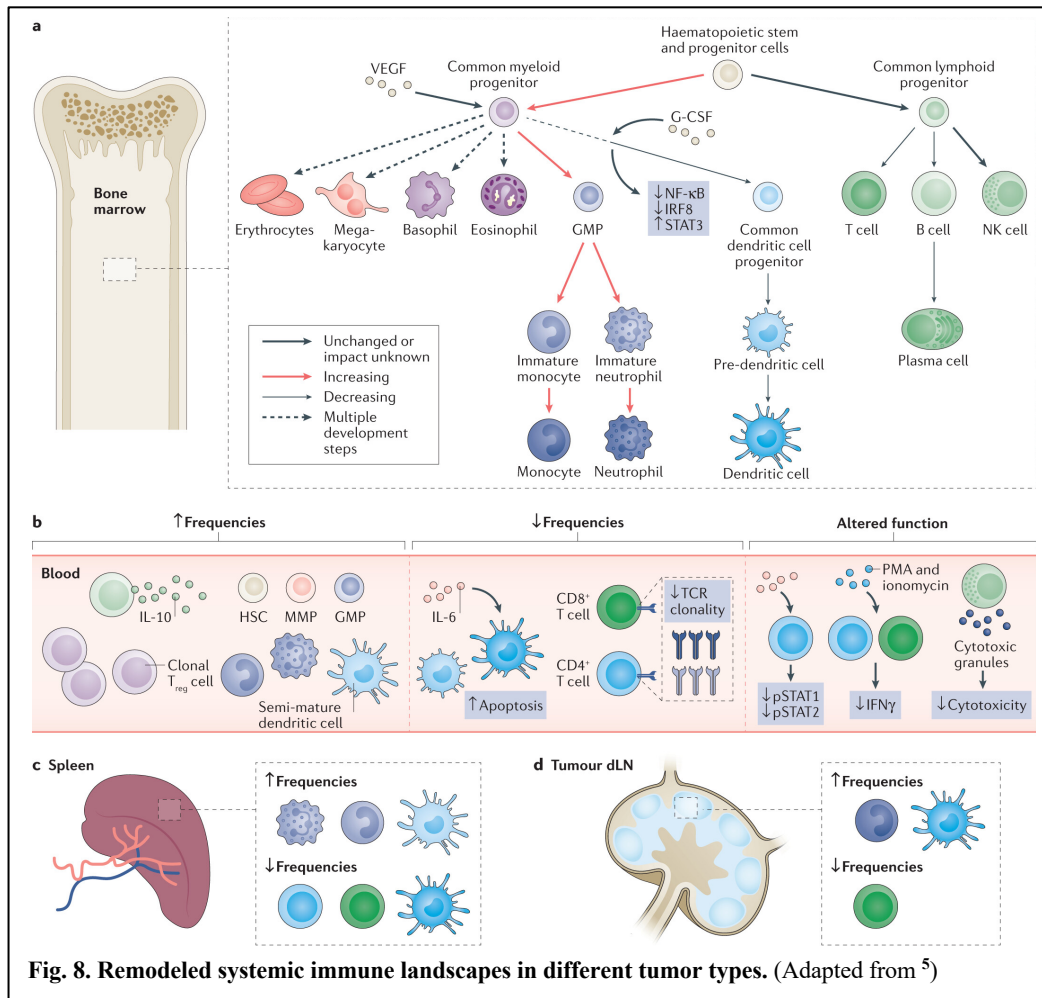
expanded use to target various types of cancer⁴³. Kinetic strategies designed to prolong local bioavailability will need to be developed so that intratumoral therapies will be able to achieve their full clinical potential.

Several preclinical examples highlight the use of focused kinetic strategies as a means to support intratumoral therapy. In one approach, retention of collagen-anchored cytokines was substantially prolonged following intratumoral injection⁴⁴. This strategy, which was introduced in several different mouse models, revealed synergistic anti-tumor activity from combinations of IL-2 and IL-12 while limiting systemic exposure. Results from another mouse model study initially revealed that the simultaneous introduction of anti-PD-1 and anti-OX40 immunotherapy had less of an impact on tumor growth than anti-PD-1 alone⁴⁵. However, the researchers found that if one staggered the administration times, the combination of two agents (anti-PD-1 followed by anti-OX40) substantially reduced the rate of tumor growth and resulted in extended survival time. Interestingly, the anti-tumor effect was not observed when the therapies were administered in reverse order. Thus, it is clear that practical considerations, including appropriate timing and optimal local delivery of immune stimulatory agents both play an important role in the safety and efficacy of this approach.

1.2.4 Effective systemic cancer immunotherapies

While the prevailing view of cancer immunotherapy focuses on strategies that might be used to reinvigorate cytotoxic effectors within the TME, there is a growing appreciation for the systemic aspects of effective anti-tumor immunity. Beyond the TME, strategies designed to assess the systemic immune landscape will be essential to unlocking the full therapeutic potential of cancer immunotherapies, particularly those intended to target metastatic disease. For example, results from a recent study that examined multiple models of breast cancer in a variety of mouse strains revealed extensive remodeling of splenic immune cells that included phenotypic shifts, increased frequencies of neutrophils, eosinophils, and monocytes, and reductions in the DC, T cell, and B cell populations⁴⁶. Strikingly, either surgical resection of the tumor or cytokine blockade treatment reversed many of these changes, suggesting that peripheral reorganization of the immune microenvironment was subject to substantial plasticity. Collectively, these data demonstrate that tumor development dramatically restructures the global immune landscape across multiple lineages (**Fig. 8**). These findings also support the notion that systemic corruption of immune

organization occurs in response to a variety of diverse tumor types.



Conventional therapeutic strategies in cancer, including chemotherapy, radiation, and surgery all perturb the global immune landscape. A better understanding of these systemic immune responses will be important in the effort to design strategies that augment rather than impede critical anti-tumor immune responses, including strategies such as optimal timing, dosing, and combination therapy. For example, in non-small cell lung cancer, standard prolonged radiotherapy, but not chemotherapy, led to myeloid cell expansion, reduced APC function, and impaired T cell responses⁴⁷. The results of several published studies have highlighted the role of myeloid immune cell remodeling induced by systemic wound healing programs with elevated levels of circulating IL-6, granulocyte colony-stimulating factor (G-CSF), and CC chemokine ligand (CCL)2 as ultimately driving myeloid subsets toward immunosuppressive states⁴⁸. Immunosuppressive mechanisms associated with wound healing may provide an opportunity for the growth of disseminated cancer cells⁴⁹. However, reduced primary tumor burden can ultimately restore the

capacity for strong systemic adaptive immune responses. Modulation of myeloid subsets in an adjuvanted setting can prevent the development of post-surgical metastasis. Efforts in this direction include the use of gemcitabine to deplete MDSCs or gefitinib to alter the inflammatory macrophage state⁵⁰. The appropriate pairing of conventional therapies with immune modulation can be a powerful tool to combat cancer; consideration of the systemic immune context may also lead to improved outcomes⁵¹. It is also important to consider the immunologically vulnerable period following surgery and to investigate the mechanisms driving these states as well as the therapeutic interventions with the potential to restore immune function and prevent tumor recurrence and metastasis. Although many patients diagnosed with tumors exhibit altered systemic immunity, the mechanisms underlying many of these responses remain unknown. Future studies focused on mechanistic insights into the dynamics of systemic immune reorganization may lead to the development of therapeutics that will restore a healthy homeostatic set point.

1.2.5 Potential kinetic modulations

In Section 1.2, I reviewed several different features of cancer-immune system interactions based on our current understanding of the cancer-immunity cycle, tumor-immune microenvironments, intratumoral treatments, and the generation of effective systemic immune responses against cancer. In each of the subsections, I highlighted the pivotal role of spatiotemporal dynamics and highlighted how simple but carefully planned temporal modulations might lead to a successful anti-tumor immune response that eradicates tumors and promotes immune memory. In the paragraphs to follow, I will provide a few examples of how kinetic modulations may be used to reveal a successful anti-tumor immune response.

As discussed previously, intratumoral injection of proinflammatory agents such as TLR agonists is currently one of the most promising approaches used to potentiate responses to immune checkpoint blockade therapy. These agonists can provide effective local adjuvant activity and will turn lesions into “*in situ*” cancer vaccines⁵². However, these agents typically reside only briefly at the site of injection. They can disperse into the circulation and elicit immune-related adverse events, for example, systemic pro-inflammatory cytokine production⁵³. One way to address this problem would be to alter the local pharmacokinetics after intratumoral administration of these agents using biomaterial-based depots. This approach has shown promise toward boosting anti-tumor efficacy while minimizing systemic toxicities. For example, intratumoral injection of TLR

agonist-releasing hydrogels resulted in improved anti-tumor efficacy in combination with chemotherapy in a mouse model of colon cancer⁵⁴. Interestingly, while the use of this approach also limited the recurrence of breast or lung cancer tumors that were implanted at surgical resection sites in mouse models, it was ineffective when the TLR agonist was administered in the absence of hydrogel⁵⁵.

In a similar vein, the addition of a phosphoserine peptide tag to IL-12 facilitated its stable and high-avidity binding to aluminum hydroxide, which is a commonly-used clinical vaccine adjuvant⁵⁶. Intratumoral injection of IL-12-loaded alum particles allowed the drug to be retained in the tumors for more than two weeks and resulted in pronounced regression and complete responses in several mouse tumor models. Similar results were obtained in studies involving intratumoral injection of spherical nucleic acids and liposomal nanoparticles with surface-conjugated oligonucleotides as ligands for TLR9. These approaches led to strong immunomodulatory activity and led to a current Phase II clinical trial⁵⁷. Another promising approach featured “*in situ*” vaccination using nanoparticles that contained elements of virus cowpea mosaic virus. Using this method, the immune composition of the TME shifted toward a pro-inflammatory profile⁵⁸. Biomaterials are also under consideration as depots for the local release of immunotherapy payloads within the TME. For example, chitosan microparticles that release IL-12 over 1–2 weeks following intratumoral injection have been developed. The use of this agent elicited complete tumor regression in 80–100% of the animals featured in murine cancer models⁵⁹.

In addition to modulating local and/or intratumoral kinetics, we also need to focus on developing systemic immunotherapies with narrow therapeutic indices. As discussed above, TLR agonists failed to provide clinical benefit when administered systemically because of their dose-limiting toxicities⁶⁰. In Chapters 2 and 3, I provide an in-depth evaluation of TLR7/8 agonists as a model to explore the potential benefit of modulating immunotherapy kinetics for improved anti-tumor immune responses overall.

1.3 Germinal Center dynamics and the evolution of the humoral immune response

The rate at which an immune response to infections and/or synthetic immunizations (vaccines) progresses can be a critical factor when determining the degree of protection against unfavorable outcomes. In this section, I will discuss several features of the humoral immune response and its evolution over time.

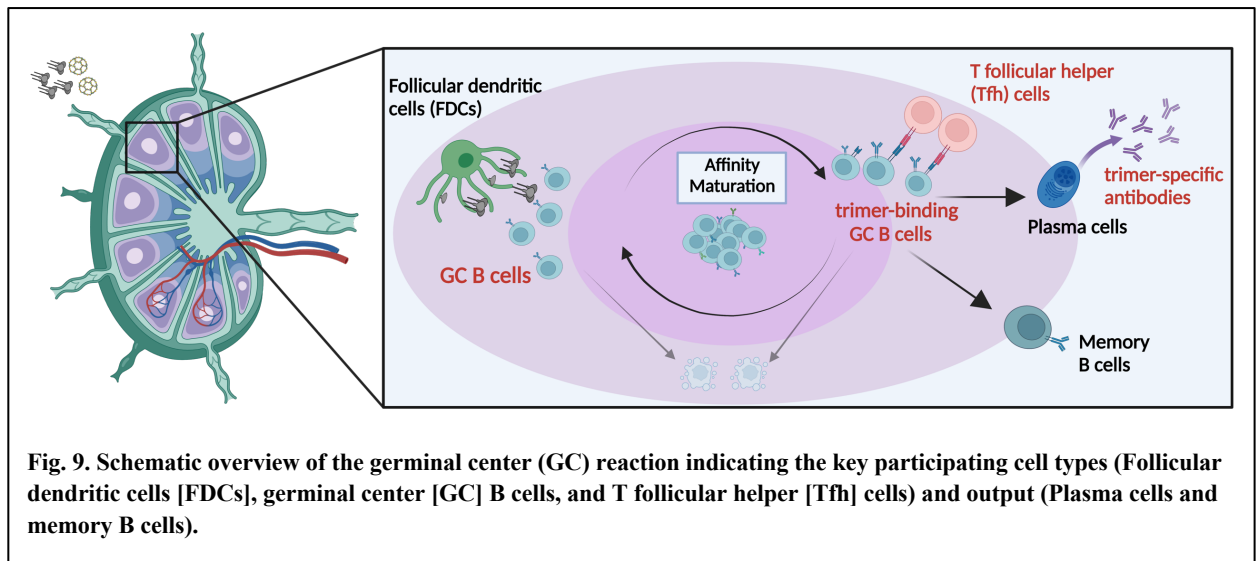
1.3.1 Anatomy of the Germinal Center (GC)

One well-characterized hallmark of the humoral immune response is antibody affinity is progressively enhanced over time⁶¹. This process is the direct result of somatic hypermutation (SHM) occurring within the antigen-binding variable regions of immunoglobulin (Ig) genes⁶². This generates a diverse repertoire of B cells that is ultimately subjected to purifying selection. Selected B cells then proliferate and differentiate into antibody-secreting plasma cells (PCs) and memory B cells (MBCs)⁶³. This selection process takes place within specialized microanatomical structures known as germinal centers (GCs).

GCs are established at the core of B cell follicles in the secondary lymphoid organs. GCs are surrounded by a network of stromal cells known as follicular dendritic cells (FDCs)⁶⁴. FDCs provide a critical long-term reservoir for intact antigens within complement-coated immune complexes, thereby facilitating the affinity-driven assessment of B cell receptors (BCRs) that have undergone SHM⁶⁴. FDCs also support and maintain GC B cells and contribute to the overall robustness of the GC reaction. Notably, findings from several studies revealed that inhibition of FDC activation results in diminished GC size and reduced antibody titers in response to immunization^{65,66}.

GC formation commences with antigen capture by quiescent B cells. These B cells then migrate toward the border between the B cell follicle and the T cell zone, a region known as the T:B border⁶⁷. At this location, B cells receive co-stimulatory signals from CD4⁺ helper T cells and initiate a phase of vigorous proliferation (**Fig. 9**)⁶⁸. A fraction of these cells assemble into compact clusters at the center of the follicle, thereby giving rise to early GCs. Mature GCs are partitioned into two distinct compartments, known as zones. The dark zone (DZ) is proximal to the T cell zone in lymph nodes and the spleen and has few to no FDCs. Conversely, the light zone (LZ) is distal

to the T cell zone and close to the capsule or marginal zone in the spleen. The LZ includes a rich abundance of FDCs.



The DZ contains densely packed and highly proliferative B cells referred to as centroblasts. These cells are notable for their robust expression of the chemokine receptor, CXCR4^{69,70}. The stromal component of the DZ is comprised of an intricate network of reticular cells that express CXCL12, which is a chemokine involved in maintaining the spatial separation between DZ B cells and FDCs. Notably, DZ B cells express high levels of activation-induced cytidine deaminase (AID). DZ B cells also express the error-prone DNA polymerase *eta*, which introduces point mutations into DNA while repairing AID-induced lesions^{70,71}. This expression profile strongly implicates the DZ as the primary site at which Ig genes undergo SHM to generate clonal variants with varying affinities for a specific target antigen.

The LZ exhibits greater diversity than the DZ. In addition to GC B cells and FDCs, the LZ includes a substantial proportion of infiltrating naïve B cells and a somewhat smaller population of Tfh cells⁷². The convergence of antigen, Tfh cell-mediated activity, and the activated phenotype of resident B cells strongly implicate the LZ as the site in which SHM B cell variants with high affinity are selected. It is important to note that this separation (i.e., segregation of proliferation and SHM processes in the DZ from antigen-driven selection in the LZ) indicates that cells must be able to migrate between these two zones to facilitate their affinity maturation, as described below.

B cells within the GC engage in a cyclic process known as affinity maturation. To begin, B cells in the DZ undergo proliferation while mutations are introduced into their antigen receptors.

These cells then migrate to the LZ, where they have the opportunity to acquire antigens from FDCs. The acquired antigen is then processed, complexed with class II MHC molecules, and presented to Tfh cells. The B cells that interact with Tfh cells can continue in this cyclical process. B cells can also exit the GCs at this point and serve as either short-lived antibody-producing cells termed plasmablasts (PBs), long-lived antibody-producing PCs, or memory cells (MBCs)⁷³. The kinetics of antigen availability on FDCs will have an impact on these fate choices⁷⁴.

1.3.2 GC Selection

The process of affinity maturation is based on the selection of B cells in the GCs based on the affinity of their BCRs for the target antigen (**Fig. 10**). B cells have access to two potential antigen-based signals while within the LZ⁷⁵. They first encounter the antigen, which is securely tethered to FDCs in a conformation that allows it to bind and activate the BCR. The second antigen-dependent signal arises from a cognate interaction between GC B cells and Tfh cells⁷⁶. GC selection is driven by the competition between GC B cells displaying varying amounts of peptide-MHC II complexes for a limited number of Tfh cells. The interactions between GC B cells and Tfh cells often involve feed-forward loops. For example, the presence of the ICOS ligand (ICOSL)

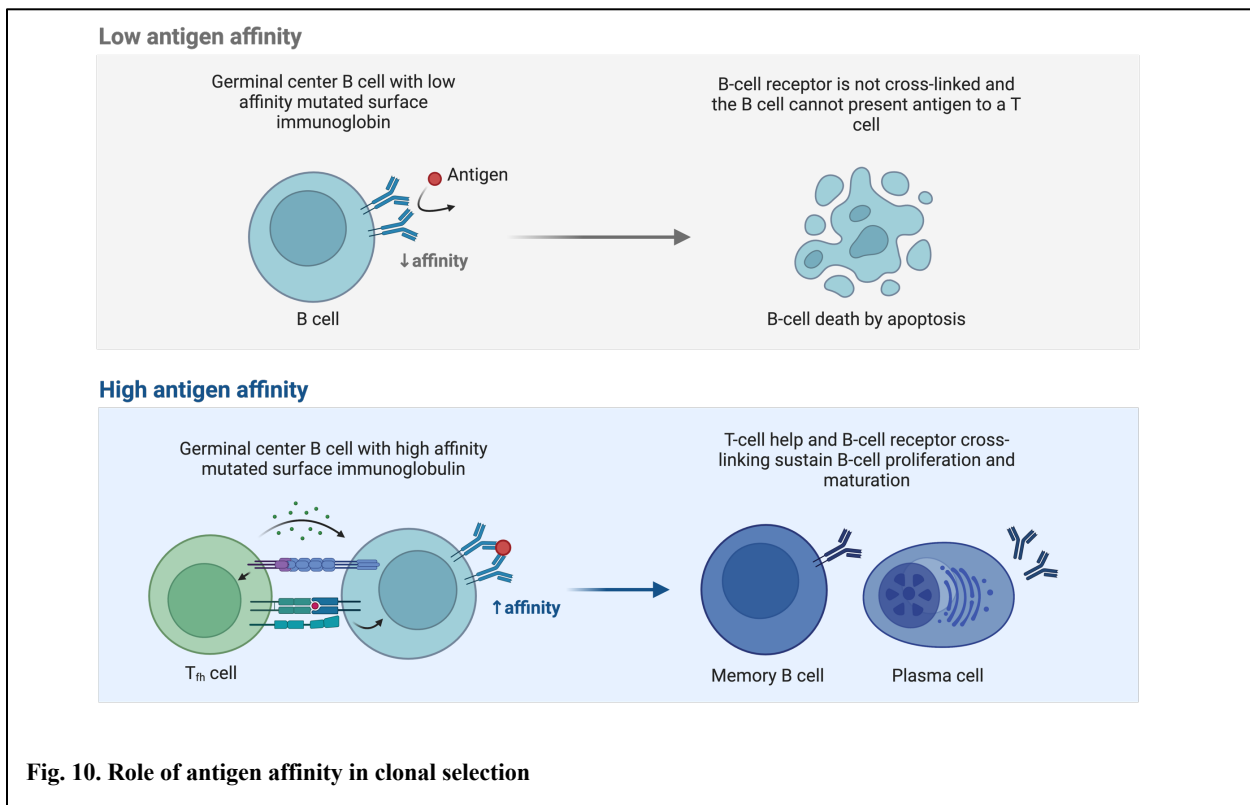


Fig. 10. Role of antigen affinity in clonal selection

in B cells promotes the upregulation of CD40L in T cells. This results in additional increases in the expression of ICOSL on B cells⁷⁷. These interactions also lead to the production of B cell helper cytokines IL-4 and IL-21 by Tfh cells⁷⁸. Tfh cells also serve as the primary source of the prosurvival cytokine, B-cell activating factor (BAFF), within the GC. BAFF produced by Tfh cells supports the survival of B cells that carry high-affinity mutations⁷⁹. Consequently, the kinetics of antigen availability play a critical role in the selection processes taking place in the GC. Improved antigen availability facilitates stronger BCR-mediated signaling and enhances the retrieval of antigens for presentation to T cells.

1.3.3 Clonal dynamics and evolution over the course of the GC

The results of seminal studies performed by Victora and colleagues^{69,80} provided valuable insights into clonal diversity within GCs. Among their findings, they demonstrated that individual GCs can exhibit considerable clonal diversity. For example, more than 100 different clones were identified in a single GCs following immunization with chicken gamma globulin (CGG) in alum. The level of clonal diversity can vary significantly depending on the antigen employed. The extent of early GC clonal diversity appears to be influenced by antigen-specific factors, for example, the frequency of specific naïve precursor cells and/or the immunodominance hierarchy among the antigenic epitopes. These antigen-related properties can be modulated by the kinetics of antigen presentation, a finding that highlights the impact of timing on the generation of clonal diversity within GCs.

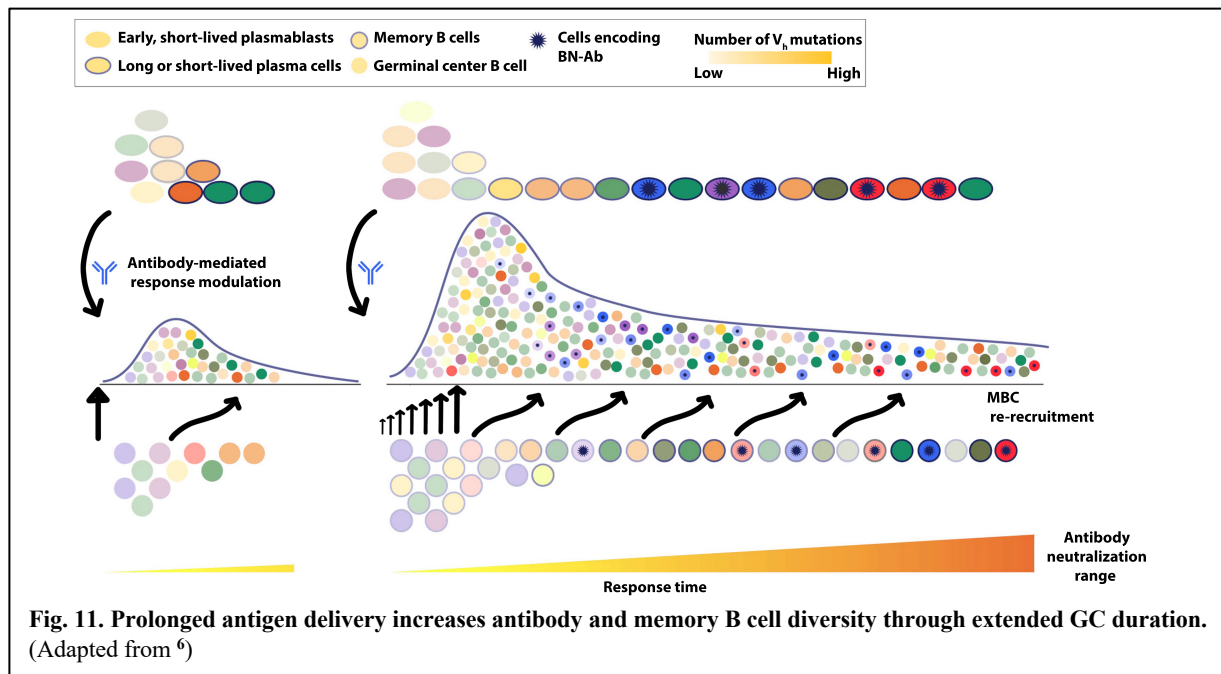
Once the GC structure has been established, a dynamic competition process unfolds. This process involves both interclonal competition between clones with different V(D)J rearrangements and intraclonal competition among variants generated by SHM⁸¹. Notably, Tas and colleagues⁸⁰ revealed that while many GCs maintain considerable clonal diversity throughout the three-week lifespan of the response, a subset undergoes rapid and extensive expansion of higher-affinity SHM variants and thus a notable reduction in diversity. This phenomenon, referred to as a "clonal burst", highlights the fact that B cells with a wide range of affinities can coexist within the same GC. These findings challenge the notion of stringent GC selection and suggest that the process might also be influenced by the kinetics of vaccination which may permit fine-tuning of the GC response.

To fulfill their effector and memory functions, B cells must first differentiate into either PCs or MBCs, respectively. This fate decision can take place at two distinct stages⁸². First, upon

reaching the T:B border, recently activated B cells can either enter the GC or differentiate directly into PCs or MBCs. Alternatively, B cells that have entered the GC that have undergone positive selection can interrupt the re-entry cycle between the LZ and the DZ; the B cells will then exit the GC and undergo differentiation into PCs or MBCs⁸³. The precise mechanism via which affinity influences B cell differentiation into PCs or MBCs is not fully understood, but it likely involves signals from both the B cell receptor (BCR) as well as T cell help. In addition to affinity, the propensity of B cells to differentiate into MBCs or PCs changes throughout the course of an antibody response. MBCs are generated predominantly during the pre-GC and early GC phases; by contrast, differentiation into long-lived PCs becomes more prominent as the response progresses⁸². These dynamic shifts in differentiation patterns highlight the temporal aspects of B cell fate determination during the antibody response.

1.3.4 GC duration

The lifespan of a GC can vary significantly based on the nature of the immune stimulus. For instance, protein antigens adsorbed in alum typically generate short-lived GCs that collapse within one month following immunization⁸⁴. By contrast, certain viral infections and immunization approaches can generate GCs that remain active for much longer duration; in some cases, these GCs can persist indefinitely (**Fig. 11**)^{85,86}. This discrepancy is particularly notable considering that infections typically generate more GCs in mice, particularly in the secondary



lymphoid organs associated with the affected tissues^{87,88}. GCs with prolonged lifespans may exhibit higher levels of SHM compared to younger GCs and generate MBCs on a continuous basis. These findings underscore the significance of GC persistence and its role in promoting subsequent antibody responses with increased affinity^{85,87}. Prolonged GC lifespans enable B cells to achieve a higher degree of affinity maturation and help with responses to antigenic drift frequently observed in viral infections⁸⁹. However, it is also critical to recognize that prolonged periods of SHM within chronic GCs may lead to the emergence of self-reactive variants. These variants may evade negative selection and ultimately contribute to autoimmune responses⁹⁰.

Despite the critical contributions of persistent GCs, the specific factors needed to maintain GCs over the long term as well as those governing the dynamics of B cell selection under these conditions remain poorly understood. Antigen persistence on FDCs may be a specific prerequisite for sustained GC selection. FDCs are uniquely capable of recycling and retaining immune complexes that are free of degradation for extended periods. Thus, FDCs serve as a continuous source of intact antigens needed to fuel ongoing selection within the GC^{91,92}. In addition to antigens, innate immune signaling contributes to GC maintenance. Thus, efforts to modulate the formulation and kinetics of vaccines so that they will be more effective at stimulating innate immune PRRs may lead to prolonged GC responses. For example, immunization of mice and non-human primates (NHPs) with influenza hemagglutinin (HA) nanoparticles combined with TLR4 and TLR7 agonists generate GCs that persist for several months⁹³. The innate immune signals provided by these agonists contribute to the priming of T cells that play crucial roles in determining GC persistence. Of note, GC stimulation by T cell-independent antigens is not sustained as long as conventional T cell-dependent GC responses⁹⁴. Increased help from Tfh cells serves to "refuel" GC B cells by promoting their survival and proliferation within the DZ and ultimately facilitating the selection and polyclonal responses⁹⁵. In the absence of Tfh cell help, B cells are unable to receive the growth and proliferation signals that are vital for the establishment of long-lived GCs⁹⁶.

Cells that have left the GC differentiate into long-lived bone marrow PCs and circulating MBCs. These effector B cells are critical mediators of long-term protection against a pathogen and their formation is thus a major goal of vaccine development. Specific modulation of vaccine exposure kinetics may serve to improve the magnitude and duration of the GC response. Of note, GC-dependent MBCs are poised to undergo rapid differentiation into short-lived extrafollicular PBs in the event of pathogen re-exposure. This will result in the production of high-affinity

antibodies that can work together with mature PC antibodies to promote rapid clearance of cells expressing the target antigen^{97,98}. MBCs can also re-enter the GC and undergo additional rounds of SHM and affinity maturation, thereby enhancing subsequent antibody responses⁷¹. Thus, efforts to enhance GC responses by altering vaccine formulations and kinetics may contribute to the overall response by influencing GC duration. This will be discussed further in the section to follow.

1.3.5 Potential kinetic modulations

Numerous kinetic disparities between antigen and innate immune signals are observed in live infections compared to synthetic immunizations. These discrepancies highlight a potential critical mismatch that may be addressed via the manipulation of vaccine kinetics. Using this strategy, significant improvements in the humoral immune response can be achieved without the need to alter the antigen. In the paragraphs to follow, I will outline several approaches that can be used to modulate vaccine kinetics. Each of these approaches will have an impact on different aspects of the humoral response.

While somewhat impractical for large-scale vaccinations, the vaccine formulation might be divided into multiple doses. The vaccine can then be administered in a progressive, regressive, or constant manner while maintaining a consistent total dose of antigen and adjuvant⁹⁹. Notably, the results of investigations conducted in both murine and NHP experimental models demonstrated that dosing at exponential increments over a two-week period, a strategy referred to as “escalating dose immunization”, enhances both GC and antibody responses^{99,100}. Further studies that feature this approach are detailed in Chapters 4 and 5.

Several alternative strategies employ synthetic chemistry and materials engineering to extend the duration of antigen and/or adjuvant exposure. This is a general approach that can be used to enhance humoral responses to a wide variety of vaccine formulations¹⁰¹. Seminal investigations conducted by Hem and colleagues^{102,103} revealed a robust binding affinity between phosphorylated proteins and alum that was achieved via ligand exchange reactions with surface hydroxyl groups found on aluminum hydroxide particles. Building on this knowledge, Moyer and colleagues¹⁰⁴ introduced phosphoserine (pSer) tags to human immunodeficiency virus (HIV) Env protein immunogens. This led to a substantial increase in the time required for alum-conjugated antigen clearance from a few days to several weeks. This controlled release profile also significantly augmented antigen-specific GC B cell responses, elicited long-lived PCs, and

markedly improved the induction of neutralizing antibody responses. Similarly, ligand exchange reactions have been used in the design of molecular adjuvants that exhibit a high affinity for alum. To overcome pharmacokinetic and pharmacodynamic limitations of imidazoquinolines (IMDs), synthetic TLR7/8 agonists, Wu and colleagues¹⁰⁵ synthesized derivatives featuring a phosphate moiety that facilitated ligand exchange with hydroxyl groups on the aluminum surface. By exploiting this engineered alum-binding capability, systemic exposure to the TLR7/8 agonist was reduced and enhanced humoral responses to anthrax protein vaccination were observed. Chapter 2 of this thesis provides a comprehensive insight into several additional synthetic approaches that have been used to modulate adjuvant kinetics, particularly those focused on manipulating imidazoquinolines. Finally, biomaterials-based strategies, for example, the use of solid polymer matrices as vaccine carriers, including microparticles or nanoparticles that facilitate sustained release, have emerged as a common means of fine-tuning vaccine kinetics. Notably, the clinical track record of poly(lactic-co-glycolic acid) (PLGA)-based polymers has already been established. These compounds exhibit both biocompatibility and the capacity for controlled release when used in vaccine formulations¹⁰⁶. As but one example, Jaklenec and colleagues¹⁰⁷ demonstrated that a single injection of an inactivated polio vaccine formulated with PLGA microparticles resulted in superior neutralizing antibody responses when compared to multiple doses of the liquid form of the vaccine.

In summary, the studies presented here highlight the promise of modulating vaccine kinetics as a means to enhance humoral immune responses. The results presented also emphasize the need for further exploration of GC biology and to elucidate the molecular mechanisms that are contributing to these effective immunization strategies. In Chapters 4 and 5, I will discuss the impact of escalating dose immunization. I will also consider several engineering approaches that might be used to reduce the number of doses needed so that these kinetic modulations can be more clinically feasible.

Chapter 2

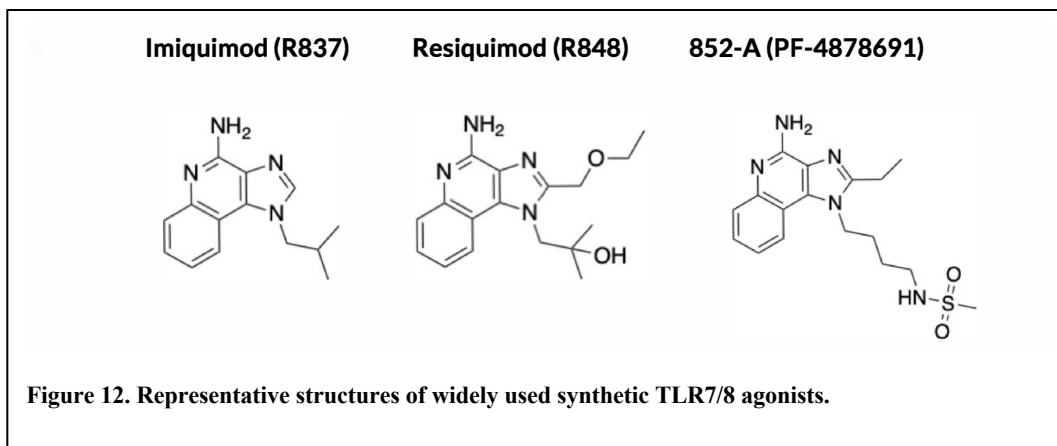
Evolution of Toll-like receptor 7/8 agonist therapeutics and their delivery approaches

This chapter is adapted in part from Bhagchandani et al Adv Drug Deliver Rev (2021) doi:10.1016/j.addr.2021.05.013.

2.1 Introduction

In the mid-1980s, 3M Pharmaceuticals discovered that imidazoquinoline derivatives (IMDs) could possess antiviral properties¹⁰⁸. At that time, the functions of Toll-like receptors (TLRs) were not defined and the antiviral feature of IMDs was not known to be related to TLR7/8 activation¹⁰⁹. The first patent filing on this class of compounds focused on topical administration and detailed their efficacy in a guinea pig model of herpes simplex virus¹¹⁰. One of the first IMDs reported, imiquimod (also known as R837; **Fig. 12**), progressed through clinical trials and was approved by the United States Food and Drug Administration (FDA) in 1997 for the topical treatment of genital and perianal warts and actinic keratosis (Aldara, 5%). It has since been approved for topical treatment of basal cell carcinoma¹¹¹. Following the success of R837, a library of more potent and selective IMDs was developed and tested in preclinical studies and clinical trials^{112,113}. A prominent compound in this class is resiquimod (R848; **Fig. 12**), which was shown to be 100 times more potent than R837 in stimulating TLR7¹¹⁴. Nevertheless, R848 has followed a more difficult path to the clinic, with multiple human trials in genital herpes and hepatitis C yielding no positive outcomes¹¹⁵. These disappointing results led 3M to discontinue development of R848 and license it to Spirig Pharma, which conducted clinical trials testing R848 on basal cell carcinoma and actinic

keratosis without success¹¹⁶. Spirig Pharma was acquired by Galderma, and R848 has since received orphan status from the European Medicines Agency and is in continued clinical development for the treatment of cutaneous T cell lymphoma¹¹⁷.



The transition from treating viral infections to malignant tumors using IMDs was bolstered by several mechanistic insights into the biology of these molecules as activators of TLR7/8¹¹⁸. In addition to inducing an antiviral state through secretion of type I interferons (IFNs), synthetic TLR7/8 agonists trigger acute inflammation and stimulate adaptive immunity by activating the nuclear factor kappa-light-chain enhancer of activated B cells (NF- κ B) pathway¹¹⁹. This mechanistic rationale led compounds such as 852-A (**Fig. 12**) to be tested for treatment of hematological malignancies (e.g., chronic lymphocytic leukemia) and solid tumors (e.g., ovarian, cervical, and breast cancers)¹²⁰. In fact, 852-A and R848 generated sufficient excitement that, in 2008, they were both featured on the National Cancer Institute's list of 20 agents with the highest potential for treating cancer¹²¹. Nevertheless, while potent immune activation was a consistent feature of the 852-A and R848 trials, severe adverse events associated with on-target, off-tumor activity hindered attempts to take these compounds from bench to bedside¹²². In parallel, mechanistic insights into the impact of TLR signaling on T cell immunity prompted studies focused on the use of IMDs as allergy and asthma treatments with the goal of skewing pathological Th2 immune responses toward a non-pathologic Th1 functional profile¹²³. Promising results were obtained in large animal models and preliminary clinical work, but the toxicity of IMDs once again dampened success and forced the field to address systemic side effects using approaches rooted in medicinal chemistry,

formulation, prodrug design, and drug delivery¹²⁴.

Despite the challenges described above, there is maintained clinical interest in the development of IMDs and related synthetic immune agonists, which is driven by significant progress in understanding innate immune sensors and their link to the adaptive immune system⁸. Crystal structures of TLR8 and TLR7 both with and without ligands have recently been elucidated, enabling structure-based compound development aimed toward enhanced receptor specificity¹²⁵. These advances are especially important because R837 has been shown to have immune effects independent of TLR7/8, which could hamper attempts to reduce its off-target toxicity¹²⁶. Today, in response to the multitude of toxicity-induced failures, research focus is moving toward localized delivery approaches, especially in the context of cancer, and prodrug or delivery formulations aiming to target IMDs to desired tissues and/or cells¹²⁷. Here, we review preclinical and clinical studies of IMDs and related compounds, highlighting new strategies to overcome the safety challenges and address early clinical failures.

2.2 TLR7/8 biology and cellular implications of downstream effects

Pioneering work by Akira and others laid the foundation of TLR7/8 biology, and demonstrated the structural basis for recognition of guanosine- and uridine-rich viral single-stranded RNA (the likely natural ligands for these TLRs)^{128–130}. We provide here a brief overview of the currently known signaling pathways and immune effector modules downstream of TLR7/8 agonists that will allow for an appreciation of the complexities involved and highlight the important players—the cells and proteins in the immune cascade—that will be discussed in later sections focused on preclinical and clinical studies.

2.2.1 TLR7/8 signaling pathways & downstream effects

The TLRs are a family of 13 type 1 transmembrane proteins expressed both by tissue cells and immune cells that function as pattern recognition receptors (PRRs); that is, they identify conserved molecular structures on microbes or molecules released by

dying cells and thereby comprise a major form of innate immune sensing¹³¹. TLRs share a common general structure: The N-terminal ectodomain consists of leucine-rich repeats (LRRs), formed in a horseshoe shape, followed by a single transmembrane domain and a cytosolic Toll-interleukin-1 receptor (TIR) domain¹³² (**Fig. 13A**). TLRs dimerize upon binding their cognate ligand (**Fig. 13B**), leading to conformational changes that allow for the recruitment of adapter molecules and initiating signaling cascades that ultimately induce transcription of inflammatory mediators¹³³. In the case of TLR7/8, dimerization initiates the TIR signaling cascade, which results in association with the adaptor protein myeloid differentiation primary response 88 (MyD88) at its carboxy terminus¹³⁴. MyD88 also has an N-terminal death domain that recruits and associates with similar death domains present on two serine-threonine protein kinases: IL-1-receptor associated kinase (IRAK4) and IRAK1¹³⁵ (**Fig. 13C**).

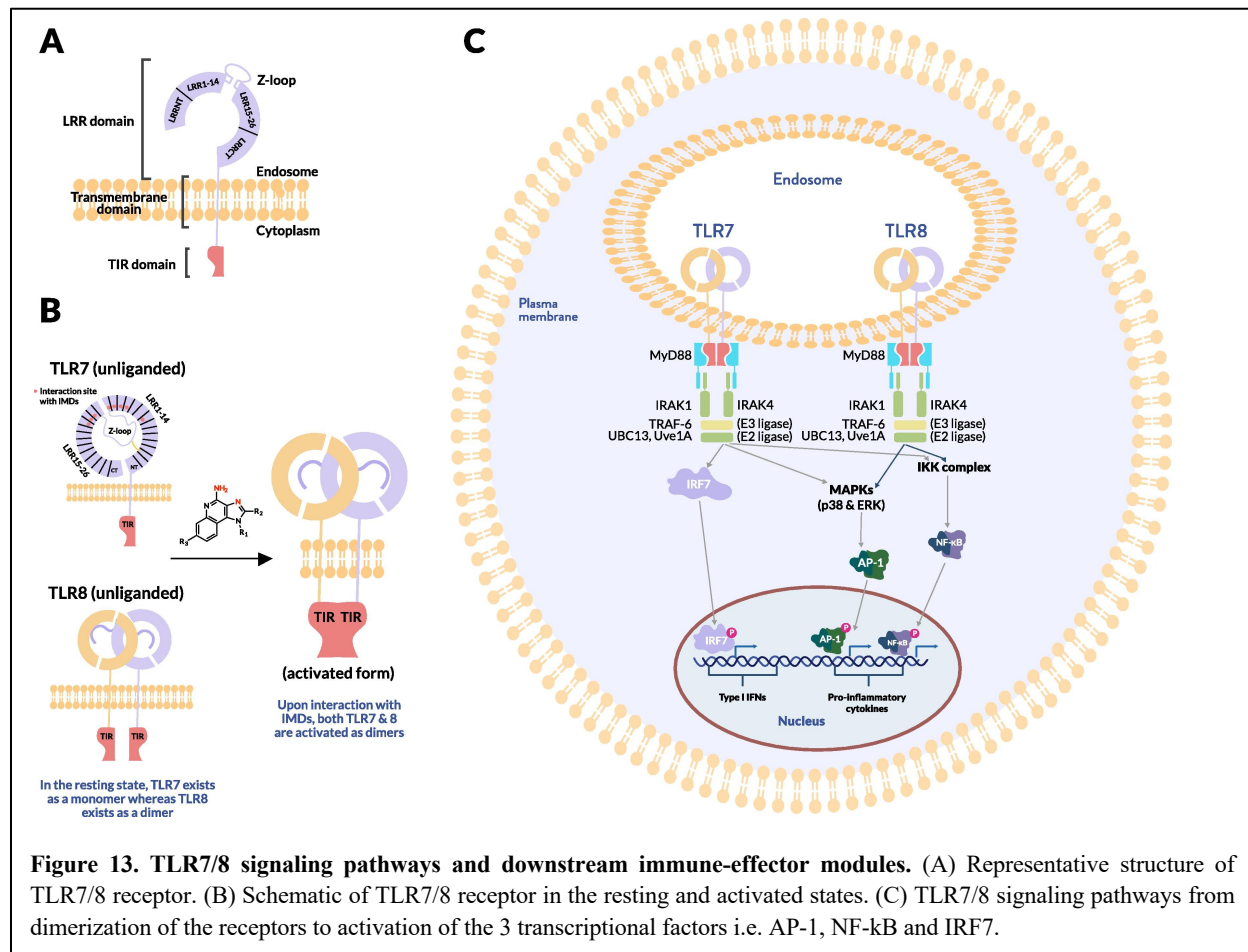


Figure 13. TLR7/8 signaling pathways and downstream immune-effector modules. (A) Representative structure of TLR7/8 receptor. (B) Schematic of TLR7/8 receptor in the resting and activated states. (C) TLR7/8 signaling pathways from dimerization of the receptors to activation of the 3 transcriptional factors i.e. AP-1, NF-κB and IRF7.

The above complex consisting of MyD88, IRAK4, and IRAK1 recruits the enzyme tumor necrosis factor (TNF) receptor-associated factor 6 (TRAF6)¹³⁶. TRAF-6 is an E3

ubiquitin ligase that, in combination with UBC13 (an E2 ubiquitin ligase) and Uve1A (a cofactor), initiates polymerization of ubiquitin via K63 linkages¹³⁷. This polymerized scaffold recruits a signaling complex, resulting in activation of the AP-1 family transcription factors that transcribe cytokine genes such as TNF- α . The same scaffold also leads to the phosphorylation of the inhibitor of κ B (I κ B), the protein responsible for keeping NF- κ B in the cytoplasm. This action results in the degradation of I κ B, which releases NF- κ B into the nucleus where it drives transcription of genes encoding proinflammatory cytokines such as IL-6 and TNF- α , resulting in a state of acute inflammation¹³⁸ (**Fig. 13C**).






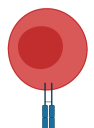

In addition, IRAK1, as part of the IRAK complex, can physically associate with interferon regulatory factor 7 (IRF7), which is highly expressed in specific cell subsets such as plasmacytoid dendritic cells¹³⁹. Phosphorylated IRF7 enters the nucleus to induce expression of type I IFNs, inducing an antiviral state (**Fig. 13C**).

2.2.2 Cell types responding to TLR7/8 ligands

Although the immune-effector modules of TLR7/8 activation can be broadly classified into “acute inflammation” and “antiviral state,” the downstream effects of TLR7/8 activation vary by cell type. **Table 1** summarizes the current understanding of TLR7/8 expression in different cells across species^{140–143}. Defining TLR expression patterns has been confounded by a lack of reliable antibodies for TLRs, conflicting results with different primer sequences used in reverse transcription (RT)-PCR measurements, and species-specific differences in TLR7/8 expression across cell types. Additionally, similar cell types might express different levels of TLR7/8 in different tissues, and this pattern of expression can be further altered by the activation, maturation or differentiation of the cells¹⁴⁴. Under certain circumstances, expression may be induced even in cells with low basal TLR7 levels, in particular immune cells such as macrophages and monocytes¹⁴⁵. Most studies have focused on quantifying TLR7/8 expression in immune cells and less is known about expression levels in other cell subsets, such as epithelial, endothelial or hematopoietic cells.

Dendritic cells (DCs) are broadly classified into conventional/myeloid DCs (cDCs), which express CD11c, or plasmacytoid DCs (pDCs), which do not express

CD11c¹⁴⁶. In humans, cDCs express TLR8 mRNA, but their expression of TLR7 is still under debate¹⁴⁷. In mice, cDCs can be further subdivided into CD4⁺, CD8⁺, or double negative cells, of which only CD8α⁺ DCs lack TLR7 expression and fail to respond to synthetic TLR7 ligands¹⁴⁸. pDCs, unlike cDCs, express high levels of TLR7 mRNA but lack TLR8 expression¹⁴⁹.

	Species	Sub-classification	TLR7/8 expression	Downstream effects (autocrine)	Response	References
 pDC	mouse	CD11c ⁺ Ly6c ⁻	7++ : 8-	type I IFNs	anti-viral state	[60] [38] [45] [33] [35]
	macaque	CD123 ⁺				
	human	CD123 ⁺				
 cDC	mouse	DN	7++ : 8++	pro-inflammatory cytokines and chemokines including TNF-α, IL-6, IL-12 and MCP-1	acute inflammation, maturation of DCs and expression of costimulatory molecules for priming T cells	[32] [33] [35] [39] [40]
		CD4 ⁺	7+/- : 8++			
	human	CD11c ⁺	7+ : 8+			
 Monocyte	mouse	GR1 ⁺ Ly6c ^{high}	7++ : 8++	activation of FcγR, differentiation into Mφ and DCs, secretion of pro-inflammatory cytokines such as IL-12	acute inflammation	[32] [33] [35] [47] [54]
	human	CD14 ⁺	7+/- : 8++			
 Macrophage	mouse	RAW264.7	7++ : 8++	pro-inflammatory cytokines including TNF-α and IL-12	M1 type polarization effects	[33] [35] [x]
		Bone-marrow derived macrophages				
 Neutrophil	mouse	Ly6G ⁺ CD11b ⁺	7+ : 8?	cytokines including IL-8, release of reactive oxygen species	acute inflammation	[x] [x] [49] [50]
	human	CD62L ⁺ CD16 ⁺	7+/- : 8++			
 T cell	mouse	CD4 ⁺	7+ : 8+*	pro-inflammatory cytokine secretion, suppression of T _{reg} activity	Proliferation and IL-2 production, Shift toward Th1 response	[x] [x]
	human					
 B cell	mouse	CD19 ⁺ or CD20 ⁺	7++ : 8-	increased proliferation, antibody secretion, cytokine production such as TNF-α and IL-6	humoral response	[59] [x] [62] [60] [x]
	macaque					
	human					

*a particular subset of CD4 T cells which also express CD25 referred to as regulatory T cells (Tregs) express TLR8

Table 1: TLR7/8 expression levels and downstream effects.

Upon TLR7/8 ligation in the presence of antigens, cDCs undergo multiple functional changes, including maturation and expression of co-stimulatory markers, such

as CD80 and CD86, and secretion of proinflammatory cytokines, including IL-12, TNF- α , and IL-6¹⁵⁰. The migration of DCs to draining lymph nodes (dLNs) to stimulate naïve T cells is triggered by TLR7/8-induced downregulation of inflammatory chemokine receptors such as CCR6 in concert with upregulation of receptors for lymphoid chemokines such as CCR7¹⁵¹. Activation of naïve T cells by DCs is contingent on receiving three signals: the first is provided by binding of the T cell receptor (TCR) to antigenic peptide presented by the major histocompatibility complexes (MHCs) present on DCs; the second signal is provided by co-stimulatory molecules such as CD80, CD86, or CD40, which trigger CD28 expression on naïve T cells; and the third signal is provided by cytokines, especially IL-12, which have further downstream effects on multiple immune subsets¹⁵². For example, increased IL-12 levels lead to IFN- γ secretion by T cells and natural killer (NK) cells, further amplifying the immunological cascade^{153–155}. Thus, T cell activation depends upon the class of MHC that presents the antigenic peptide, the co-stimulatory environment, and the cytokine milieu¹⁵⁶.

Type 1 IFNs are one of the key products of TLR7/8 activation. In both humans and mice, upon TLR7 ligation, pDCs secrete large amounts of type I IFNs (IFN- α and IFN- β)¹⁵⁷. Although ligands for other innate immune receptors such as TLR9 and more recently the Stimulator of Interferon Genes (STING) have been explored for their capacity to induce type I IFNs^{158,159}, targeting TLR7/8 with synthetic agonist drugs may have some advantages over these other innate immune receptors. For example, the substantial difference in cellular distribution of TLR9 between rodents and humans and the rapid degradation of the most common cyclic-dinucleotide STING agonists by circulating and cell-bound enzymes are but a few of the limitations that widen the appeal of TLR7/8 agonists as potent immune modulators. The downstream effects of this type 1 IFN production are discussed in disease-specific contexts in Section 3.

Beyond DCs (arguably the most important cell type for TLR7/8 agonists), other innate immune cells such as monocytes, macrophages, neutrophils, mast cells, and eosinophils also express TLR7/8 and secrete a host of cytokines and chemokines upon ligation by synthetic agonists, as shown in **Table 1**^{160–169}.

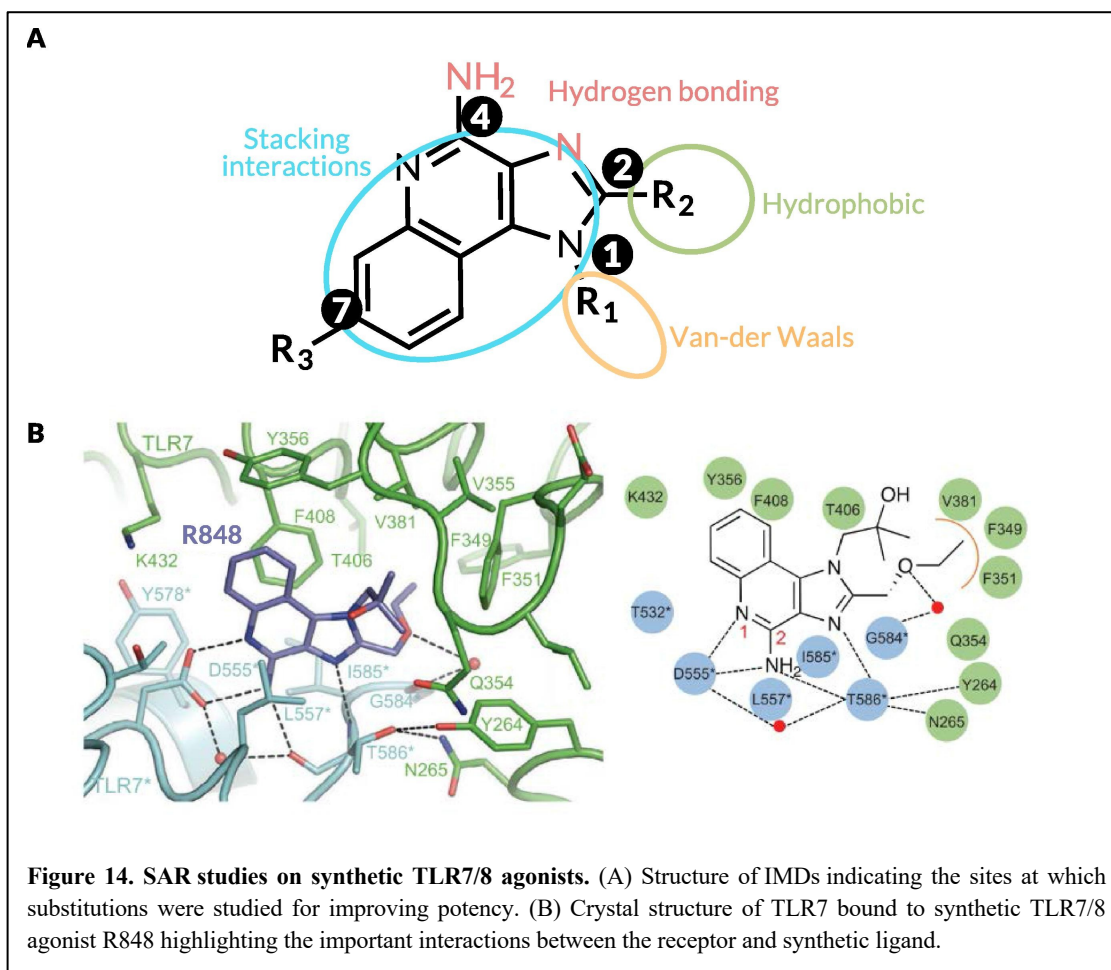
One thought-provoking aspect of the cellular effects of TLR7/8 ligation is the duality of direct and indirect immune processes¹⁷⁰. Jakubzick and coworkers demonstrated that, in the mouse lung microenvironment, CD11b⁺ DCs need to be directly

activated by TLR7 to efficiently cross-present antigens, whereas CD103⁺ (CD8 α ⁺) DCs require TLR3 activation¹⁷¹. This observation further supports theories by Reis e Sousa and colleagues on the requirement for direct DC activation to efficiently prime T cell activity¹⁷². Multiple studies, however, have indicated a role for indirect DC activation in priming the adaptive immune system. For example, type I IFN secreted from pDCs has been shown to activate cross-presenting CD8 α ⁺ DCs^{170,173}. Apart from cellular immunity, B cells also express TLR7; ligation by synthetic TLR7 agonists has been shown to enhance activation of multiple B cell subsets¹⁷⁴⁻¹⁷⁹.

2.2.3 Structure-activity relationships of IMD TLR7/8 agonists

The biological effects of these TLR7/8 agonists are heavily dependent on their chemical structures. Most of the structure–activity relationship (SAR) studies on IMDs were performed before the crystal structures of liganded TLR8 and TLR7 were elucidated in 2013 and 2016, respectively^{180,181}. Moreover, in early SAR studies, Gerster and colleagues measured *in vitro* production of IFN- α in human peripheral blood mononuclear cells (hPBMCs) as a surrogate biomarker for potency (TLR7-specific bioassays were not available at the time)¹⁸². Nevertheless, important insights were gained from these earlier studies. As shown in **Fig. 14A**, the major sites for derivatization of the IMD core have been the N-1, C-2, C-4 amine, and the C-7 position. These studies showed that attachment of long alkyl chains or bulky substituents at N-1 or C-2 reduced IFN production, whereas short-chain alkyl substituents at C-2 and short hydroxyl chains at N-1 enhanced IFN production. Most importantly, the C-4 amine was shown to be a key requirement for activity; all substitutions at this position completely abrogated IFN- α production. Moreover, most substitutions on the aryl ring were not tolerated except at the C-7 position. David and colleagues synthesized a library of more than 50 compounds to further demonstrate the increased potency obtained via substituents at N-1 and C-2 using both IFN- α production from hPBMCs and the current standard HEK-TLR7/8 reporter gene assay¹⁸³. The lead compounds were shown to be exceptionally potent inducers of cytokine production in human newborn and adult leukocytes, and the crystal structures generated for the liganded TLRs validated the positive effects of the N-1 and C-2 substituents¹⁸⁴. Ferguson and colleagues showed improved potency with C-7 methoxy

carbonyl derivatives, hypothesizing that this result could be due to inflammasome activation¹⁸⁵. The same group further studied the effects of C-2 and N-1 substituents on the C-7 substituted scaffold and showed that TLR8 activity correlated with a hydrogen bond donor at the N-1 position, with compounds that contained a terminal amino group showing the highest potency^{186,187}. These studies followed work by David and colleagues that showed quinoline amine-based derivatives lacking the imidazole groups were more potent and selective TLR8 agonists, with the terminal amino substituent extending into a pocket within the TLR8 ectodomain, forming hydrogen bonds with glycine 351¹⁸⁸. The same group explored IMD-based dimers (linked at N-1), trimers, and hexamers with improved potency that were validated *in vivo* in vaccine studies^{189,190}. Extensive SAR studies on imidazopyridines, thiazoquinolines, furopyridines, and furoquinolines have been conducted by the David group in search of potent and specific TLR7 and TLR8 agonists¹⁹¹⁻¹⁹⁴.



The elucidation of the crystal structures of liganded TLR8 and TLR7 by Shimizu and colleagues, and the resulting identification of key interactions between the ligands and the receptors, has paved the way for the more targeted design of potent TLR7/8 agonists (**Fig. 14B**)¹⁹⁵. For TLR7, the effects of N-1 substituents depended on van der Waals contacts with the loop region of LRR11¹⁹⁶. The pocket formed by phenylalanine 349, phenylalanine 351, valine 381, and phenylalanine 408 interacts with C-2 substituents via hydrophobic interactions (**Fig. 14B**). This interaction was particularly essential for TLR7 activity because R837 lacks the C-2 substituent and demonstrates weak TLR7 agonism. Similarly, for TLR8 agonism, stacking interactions or hydrogen bonds with phenylalanine 405 and aspartic acid 543 are critical components that need to be conserved in the ligand structure¹⁹⁷. These insights have led to the development of synthetic ligands with higher potency and represent a key milestone on the path to TLR7/8 agonism for improved therapeutic outcomes^{198,199}.

Although we focus here on SAR studies of IMDs because they are the most studied, other classes of synthetic TLR7/8 agonists that expand upon nucleobase and ribonucleoside analogs include adenine-, guanosine-, and pteridinone-based derivatives in addition to benzazepines, benzonaphthyridines, and pyrrolopyrimidines^{200–204}. Each of these series of agonists, particularly 8-oxo-adenine derivatives, have been expanded significantly via SAR studies to generate lead compounds that are in clinical trials^{205–211}.

2.3 Preclinical and Clinical Development of TLR7/8 agonists

In this section, we review preclinical and clinical studies using synthetic TLR7/8 agonists and focus on the clinical results, exploring in detail some of the unexpected outcomes and the hypotheses underlying these responses. Summaries of all of the compounds discussed, organized in order of progress toward clinical approval, are provided in **Tables 2 and 3**. Additionally, the compounds are classified by application into four areas: (1) skin conditions, the most widespread, with the FDA-approved imiquimod (R837) now having multiple generic formulations²¹²; (2) advanced cancers, wherein these molecules serve as tumor immunomodulators and adjuvants; (3) infectious diseases, as antiviral agents, and vaccine adjuvants; and (4) respiratory ailments, as bronchodilators and anti-inflammatories.

Active	Drug Name	Company Name	Therapy Area	Development Stage	Route of Administration	Target
1	Imiquimod	3M Pharmaceuticals	Skin conditions, Infectious Diseases, Advanced Cancers	Marketed	Topical	TLR7
2	Resiquimod (R-848)	Galderma (Originally 3M Pharmaceuticals)	Skin conditions, Infectious Diseases, Advanced Cancers	Orphan Status from EMA	Topical, Oral, Intra-tumoral	TLR7/8
3	Motolimod (VTX-2337)	Bristol-Myers Squibb Co (previously VentriX Pharmaceuticals)	Advanced Cancers	Phase II	Subcutaneous, Intra-tumoral	TLR7
4	Selgantolimod (GS-9688)	Gilead Sciences Inc	Infectious Diseases	Phase II	Oral	TLR7
5	NKTR-262	Nektar Therapeutics	Advanced Cancers	Phase II	Intra-tumoral	TLR7/8
6	RG-7854 (RO 7020531)	F. Hoffmann-La Roche Ltd	Infectious Diseases	Phase II	Oral	TLR7
7	DSP-0599	Sumitomo Dainippon Pharma Co Ltd	Advanced Cancers	Phase II	Intravenous	TLR7
8	BDB-001	Seven and Eight Biopharmaceuticals Corp	Advanced Cancers	Phase I	Intravenous	TLR7/8
9	BDC-1001	Bolt Biotherapeutics Inc	Advanced Cancers	Phase I	Intravenous	TLR7/8 (HER2+ cells)
10	LHC-165	Novartis AG	Advanced Cancers	Phase I	Intra-tumoral	TLR7
11	SHR-2150	Jiangsu Hengrui Medicine Co Ltd	Advanced Cancers	Phase I	Oral	TLR7
12	JNJ-4964 (TQ-A3334)	Johnson & Johnson, Chia Tai Tianqing Pharmaceutical Group Co Ltd	Infectious Diseases, Advanced Cancers	Phase I	Oral	Not specified
13	Vesatolimod (GS-9620)	Gilead Sciences Inc	Infectious Diseases	Phase I	Oral	TLR7
14	RO-7119929	F. Hoffmann-La Roche Ltd	Advanced Cancers	Phase I	Oral	TLR7
15	DN-1508052	Shanghai De Novo Pharmatech Co Ltd	Advanced Cancers	Phase I	Subcutaneous	TLR8
16	VTX-1463	Bristol Myers Squibb Co (previously VentriX Pharmaceuticals)	Respiratory Ailments	Phase I	Intra nasal	TLR8
17	BNT-411 (SC1)	BioNTech SE	Advanced Cancers	IND/CTA Filed	Intravenous	TLR7
18	APR-003	Apros Therapeutics	Advanced Cancers	IND/CTA Filed	Oral	TLR7
Inactive/Discontinued						
1	Btopiramine	Pfizer Inc	Advanced Cancers	Discontinued/Inactive (Phase III)	Oral	TLR7
2	PF-4876691 (852-A)	Pfizer	Infectious Diseases, Advanced Cancers	Discontinued/Inactive (Phase II)	Intravenous, subcutaneous, Oral	TLR7
3	GSK-2245035	GlaxoSmithKline Plc	Respiratory Ailments	Discontinued/Inactive (Phase II)	Intra-nasal	TLR7
4	RG-7795 (ANA-773, RO-6864018)	F. Hoffmann-La Roche Ltd	Infectious Diseases, Advanced Cancers	Discontinued/Inactive (Phase II)	Oral	TLR7
5	Epirimod (R-851)	Takeda (Originally 3M Pharmaceuticals)	Skin conditions	Discontinued/Inactive (Phase II)	Topical	TLR7
6	DSP-3025 (AZD-8848)	AstraZeneca Plc, Sumitomo Dainippon Pharma Co Ltd	Respiratory Ailments	Discontinued/Inactive (Phase II)	Intra-nasal	TLR7
7	Sotirimod (R-850, S-30594)	Meda AB	Skin conditions	Discontinued/Inactive (Phase II)	Topical	TLR7
8	Tetratolimod (3M-052, MEDI-9197)	MedImmune, AstraZeneca Plc	Advanced Cancers	Discontinued/Inactive (Phase I)	Intra-tumoral	TLR7/8
9	Isatoribine (ANA-245)	F. Hoffmann-La Roche Ltd	Infectious Diseases	Discontinued/Inactive (Phase I)	Intravenous, Oral	TLR7
10	Lxoribine	Johnson & Johnson	Advanced Cancers	Discontinued/Inactive (Phase I)	intramuscular	TLR7
11	ANA-971	F. Hoffmann-La Roche Ltd	Infectious Diseases	Discontinued/Inactive (Phase I)	Oral	TLR7
12	ANA-975	Novartis AG	Infectious Diseases	Discontinued/Inactive (Phase I)	Oral	TLR7
13	RG-7863 (RO6870868)	F. Hoffmann-La Roche Ltd	Infectious Diseases	Discontinued/Inactive (Phase I)	Not specified	TLR7

Table 2: List of synthetic TLR7/8 agonists in different stages of clinical development.

Drug Name	Company Name	Therapy Area	Route of Administration	Target
ALT-702	Altimmune Inc	Advanced Cancers	Intra-tumoral	TLR7/8
GS-986	Gilead Sciences Inc	Infectious Diseases	Oral	TLR7
KUP-101	Kupando GmbH	Advanced Cancers	Intravenous	TLR4/7
PRTX-007	Primmune Therapeutics Inc	Infectious Diseases, Advanced Cancers	Oral	TLR7
PRX-034	Primmune Therapeutics Inc	Advanced Cancers	Oral	TLR7
S-34240	Pfizer Inc (previously 3M Pharmaceuticals)	Skin Conditions	Topical	TLR7
TRANSCON	Ascendis Pharma	Advanced Cancers	Intra-tumoral	TLR7/8
SBT-6050	Silverback Therapeutics Inc	Advanced Cancers	Intravenous	TLR8 (HE
SBT-6290	Silverback Therapeutics Inc	Advanced Cancers	Intravenous	TLR8
ZM-TLR8 agonist	Zheming Biopharma	Infectious Diseases	Not specified	TLR8
VX-001	Vaccex	Advanced Cancers	Intra-tumoral	TLR7/8
MBS-8	MonTa Biosciences ApS	Advanced Cancers	Intravenous	TLR7
APR-002	Apros Therapeutics	Infectious Diseases	Oral	TLR7
SNAP	Avidea Technologies	Advanced Cancers	Intravenous	TLR7/8
R848-HA scaffold	STIMIT Technologies	Advanced Cancers	Intra-tumoral (intra-operative)	TLR7/8

Table 3: List of synthetic TLR7/8 agonists at the pre-clinical stage.

2.3.1 Topical therapies for skin conditions

Topical administration of small molecule TLR7/8 agonists formulated as creams or gels overcomes the issues of poor circulation half-life and systemic toxicity that limit the systemic administration of these compounds²¹³. Upon topical administration, TLR7/8 agonists induce significant accumulation of pDCs at the treatment site²¹⁴. As discussed previously, pDCs secrete large amounts of type I IFNs in response to TLR7 activation, setting in motion a process that creates an antiviral state in the tissue. The levels of type I IFN-inducible products such as 2'-5'-oligoadenylate synthase (2'-5'-AS) and Mx proteins are increased in the affected area²¹⁵. These products play a crucial role in inhibiting viral replication and survival. For example, 2'-5'-AS is an antiviral enzyme that counteracts viral attack by degrading viral RNA²¹⁶. In addition, TLR7/8 activation causes Langerhans cells (LCs), a type of DCs resident in the epidermis, to differentiate into mature APCs, resulting in the generation of antigen-specific T cells²¹⁷. Finally, the release of proinflammatory cytokines, such as IL-6 and TNF- α , upon NF- κ B activation lead to increased NK cell activity and macrophage activation that furthers cytokine release, nitric oxide secretion, and B cell proliferation²¹⁸.

The first clinical application of synthetic TLR7/8 agonists was for the treatment of human papillomavirus (HPV)-associated genital and perianal warts. The standard treatment— injection of IFN- α —was expensive but also short-lived, associated with multiple side effects, and mostly unable to prevent recurrence²¹⁹. These warts result from proliferation of keratinocytes infected with HPV and are difficult to treat because they activate basal keratinocytes without activating LCs, the latter of which are necessary for the generation of virus-specific T cells²²⁰. Topical administration of R837 (imiquimod) was shown to activate LCs, which migrate to the lymph nodes and prime HPV-specific T cells with both cytotoxic and memory phenotypes²²¹. Two pivotal phase III studies showed that patients treated with R837 had over 75% reduction in wart area^{222,223}. Side effects were minimal, with the most common being erythema at the application site, which correlated with mRNA expression of TNF- α , IFN- γ , and MCP-1. Skin biopsies showed decreases in CD1a mRNA in LCs, indicating activation and migration, as well as upregulation of IFN- γ , IL-2, IL-12p40, CD4, and CD8 mRNA in R837-treated patients. Wart regression was correlated with a decrease in viral load, as shown by decreases in HPV DNA and HPV E7 and L1 mRNA. Based on these results, R837 received FDA approval in 1997 for the treatment of genital and perianal

warts.

Another promising, but ultimately unsuccessful, clinical application of R837 and R848 was in the treatment of herpes simplex virus (HSV). There are multiple reports of anecdotal evidence for the successful treatment of both acute and chronic HSV lesions that have resulted in off-label usage of these IMDs^{224,225}; however, clinical trials failed due to insufficient efficacy at safe doses (i.e., narrow therapeutic indexes)²²⁶. Another off-label usage of these synthetic TLR7/8 agonists was for treatment of vaginal or cervical HPV lesions. Multiple clinical trials demonstrated the efficacy of R837 combined with photodynamic therapy or HPV therapeutic vaccines for treatment of vulvar intraepithelial neoplasia (lesions caused by HPV-16)^{227,228}. Side effects were significant, however, with one patient needing hospitalization for severe vulval erythema. Moreover, clinical trials in patients with cervical intraepithelial neoplasia have been unsuccessful due to side effects and insufficient enrollment²²⁹.

Beyond virus-induced topical lesions, R837 and R848 have shown promising results in topical treatment of precancerous and cancerous lesions. R837 is FDA-approved for treatment of actinic keratosis, a precancerous skin condition that can develop into squamous cell carcinoma or basal cell carcinoma²³⁰. In clinical trials, R837 had to compete with photodynamic therapies using 5-aminolevulinic acid as the standard of care²³¹. In two phase III trials, R837 showed disease clearance rates greater than 50% (vs. 3% for the control arm)²³². When the lesions were biopsied, significantly increased levels of CD11c⁺ DCs and CD4⁺ and CD8⁺ T cells were detected. The third and final indication for which R837 received FDA approval, in 2004, was for basal cell carcinoma, with disease clearance rates of 75% in two phase III trials²³³. Skin biopsies revealed Th1 polarization, significantly increased type I IFN signaling, and recruitment of CXCR3⁺ lymphocytes. Mild erythema, edema, erosion, and ulceration were observed in 50% of patients. Recent clinical results using R848 for treatment of cutaneous T cell lymphoma have also been promising^{234,235}. In a phase I trial, 9 of 12 patients showed significant improvement, with 4 experiencing complete clearance of all lesions²³⁶. The patients who responded to treatment showed significantly increased production of IFN- γ and TNF- α by CD4⁺ T cells, granzyme B by CD8⁺ T cells, and IFN- γ , perforin, and granzyme by CD56⁺ NK cells in skin biopsies of lesions. For treatment of melanoma, some anecdotal successes using topical administration of IMDs have

been reported, but no clinical approvals have been achieved²³⁷. R837 was studied in clinical trials as the primary treatment for an early form of melanoma called lentigo maligna, but the pathological complete regression rate did not reach the predefined end points needed to replace surgery as the standard treatment²³⁸. There is anecdotal evidence of topical R837 displaying efficacy in primary and metastatic melanoma with increased levels of CD4⁺ and CD8⁺ T cells in treated skin and sentinel lymph nodes (LNs), as well as regression of skin metastases in breast cancers, but large-scale randomized clinical trials have yet to demonstrate efficacy²³⁹.

Recent clinical studies of IMD topical formulations have been focused on their use as vaccine adjuvants. Over 100 clinical trials using topical imiquimod as a vaccine adjuvant for cancer (mostly DC vaccinations), infectious diseases (hepatitis B vaccination), and respiratory ailments (influenza vaccines) are currently listed on clinicaltrials.gov. These clinical applications are discussed in detail below; it is important to note that despite the success of topical administration of synthetic TLR7/8 agonists, this route of administration has been associated with dose-limiting side effects, such as fever and pemphigus-like lesions, in some cases. These side effects need to be addressed through further molecular design to advance the use of IMDs as vaccine adjuvants^{240–242}.

2.3.2 IMDs as immunomodulators for Advanced Cancers

In the late 1990s, synthetic TLR7/8 agonists were touted as an alternative to FDA-approved high-dose exogenous IFN- α ; widespread use of the latter in treating cancer was limited by significant toxicity and exorbitant cost²⁴³. Type I IFNs suppress tumor cell proliferation, upregulate expression of MHCs, and increase levels of IFN- γ in synergy with IL-12, thus improving cross-priming by DCs²⁴⁴. In certain cancers, synthetic TLR7/8 agonists have been shown to cause apoptosis of tumor cells^{245,246}. Other studies, however, show they can promote tumor growth in the lung; thus, the effects of TLR7/8 ligands on different types of tumor cells are cancer and tissue context-dependent²⁴⁷. By contrast, the direct and indirect effects of TLR7/8 agonism on immune cells are well defined, with increased infiltration of cytotoxic T cells (via DCs) and NK cells, macrophage polarization, and decreased levels of myeloid-derived suppressor cells combining to yield potent antitumor efficacy^{248,249}.

The first attempts to demonstrate antitumor efficacy of IMDs studied parenteral administration of 852-A and progressed to phase II clinical trials before discontinuation due to considerable side effects^{250,251}. Urosevic and colleagues tested intravenous administration of 852-A in patients with metastatic melanoma²⁵². With thrice-weekly dosing, only 4 out of 21 patients showed disease stabilization and 1 patient had a partial response. This lack of efficacy was particularly puzzling given the pharmacologic activity measured; that is, significantly increased levels of type I IFN and activation markers such as CD86 on monocytes in peripheral blood. The authors hypothesized that immune activation might have been decoupled from tumor antigens and that the level of immune activation was insufficient for treating metastatic disease. Other failed attempts at parenteral delivery of TLR agonists for cancer therapy include research on loxoribine, a guanosine analog-based TLR7 agonist. Loxoribine significantly augmented NK cell activity of murine splenocytes, increased cytolytic activity when combined with IL-2 (the synergy was NK cell dependent), and prevented lung metastases in the B16 melanoma mouse model^{253,254}. Nevertheless, when loxoribine was evaluated in a phase I trial in 20 patients with advanced cancers, the disease was stabilized in 6 patients but progressed in 14 patients²⁵⁵. Moreover, one patient experienced a 46% decrease in absolute lymphocyte count on day 2 (which returned to baseline by day 8); the trial was discontinued following numerous other immune-related adverse events (irAEs). Preclinical work by Stratford and colleagues on DSR-6434 (a compound from the 8-oxoadenine library discussed in Section 2.3), showed synergy with ionizing radiation in mice bearing CT-26 tumors, with increased levels of IFN- α , IFN- γ , and TNF- α ²⁵⁶. As a monotherapy, however, DSR-6434 could not elicit effective CD8⁺ T cell responses in animal models. Each of these compounds, although having ultimately failed, provided important insights that have guided current preclinical and clinical developments of synthetic TLR7/8 agonists as antitumor therapies.

Lessons learned from these unsuccessful attempts at parenteral delivery paved the way for next-generation TLR agonists, with a focus on supplementing immune checkpoint inhibitors rather than testing the TLR agonists as monotherapies. Activation of innate immune cells such as DCs by TLR agonists assists in generating potent, tumor-specific immune responses capable of significant tumor regression and long-lasting memory against tumor recurrence^{257,258}. Moreover, TLR agonists can directly influence the immunological status of the tumor microenvironment by generating pro-inflammatory cytokines, thus complementing checkpoint inhibitors in overcoming

immunosuppressive pathways in tumors²⁵⁹. The most clinically advanced TLR agonist in this context is DSP-0509, which is currently in a phase I/II trial in combination with pembrolizumab, the latter of which targets programmed cell death protein 1 (PD-1). Preclinical studies have shown DSP-0509 to have high water solubility, which allows for intravenous administration, resulting in increased serum levels of IFN- α . Antitumor efficacy was demonstrated in CT26 and 4T1 murine tumor models concomitant with upregulation of IFN- γ signature genes, CD8⁺ and effector memory tumor-infiltrating lymphocytes, and MHC class I expression on tumor cells, in addition to decreased levels of myeloid-derived suppressor cells²⁶⁰. Systemically administered liposomal formulations of IMDs have also been used in combination with checkpoint blockade therapy. For example, BDB-001, a TLR7/8 agonist formulated in liposomes, is in phase I clinical trials in combination with pembrolizumab. Antibody conjugation has also been explored to enable tumor-targeted IMD delivery. BDC-1001, a TLR7/8 agonist conjugated to the anti-HER2 IgG₁ monoclonal antibody trastuzumab, is currently in phase I trials in combination with pembrolizumab^{261,262}. In the same vein, SBT-6050 is an antibody conjugated TLR8-specific agonist that is advancing toward the clinic based on strong preclinical results. Potent antitumor activity was observed upon intravenous administration in CT26 Her2⁺ tumors, with minimal production of serum cytokines such as IL-6, IL-10, TNF- α , and MCP-1^{263,264}. Thus, parenteral administration of synthetic TLR7/8 agonists continues to receive significant clinical attention, despite failures, because of the potential to treat metastatic disease.

Oral delivery of synthetic TLR7/8 agonists has also been pursued for cancer treatments with the goal of increasing widespread use due to ease of administration and patient compliance. Initial clinical attempts have failed, however, due to insufficient efficacy and unacceptable toxicity. ANA773 (RG-7795) is an orally available TLR7 agonist that was developed by Anadys Pharmaceuticals. Preclinical studies showed promising NK cell-mediated antitumor activity with increased levels of cytokine secretion, cytolysis of tumor cells via increased levels of IFN- γ , and antibody-dependent tumor cytotoxicity mediated by increased levels of IFN- α ²⁶⁵. Nevertheless, in a phase I clinical trial, only 1 of 20 patients had a partial response and significant irAEs were reported, including grade 3 neutropenia, grade 3 fatigue, nausea, diarrhea, headaches, vomiting, and weight loss²⁶⁶. Another orally administered TLR7 agonist called bropirimine was compared

with bacillus Calmette-Guérin (BCG) intravesical immunotherapy (standard treatment for carcinoma in situ bladder cancer) in a pivotal phase III trial and showed lower levels of toxicity and treatment discontinuation (4% of patients in the bropirimine group withdrew vs. 14% in the BCG group). Unfortunately, antitumor efficacy was not sufficient to merit FDA approval²⁶⁷. Roche is currently developing orally available synthetic TLR7/8 agonists for advanced cancers. For example, the compound RO-7119929 is being tested in a phase I clinical trial in patients with metastatic hepatocellular carcinoma with the IL-6 inhibitor tocilizumab, the latter of which is to be administered in case of severe steroid refractory cytokine release syndrome. Additionally, Primmune Therapeutics is continuing where Anadys left off with two orally available TLR7/8 agonist prodrugs, PRTX-007 and PRX-034. Preclinical data show increased levels of type I IFNs, IL-6, and IL-1Ra upon incubating the prodrugs with human PBMCs, with no increases in IFN- γ , IL-2, or IL-12p70; these results indicate minimal engagement of the NF- κ B proinflammatory pathway, which might minimize systemic toxicities²⁶⁸.

Given the history of failed attempts at systemic delivery of synthetic TLR7/8 agonists, considerable effort has also focused on localized administration of these compounds to circumvent systemic toxicity²⁶⁹. Early work on local delivery evaluated a liquid formulation of R837, based on excipients such as poloxamers and β -cyclodextrin, for the treatment of non-muscle invasive bladder cancer²⁷⁰. A formulation called TMX-101 or Vesimune progressed through phase I and II trials, with promising results in patients with carcinoma *in situ* bladder cancer^{271,272}. Among compounds that are currently in trials, VTX-2337, a benzazepine-based TLR8 agonist, was shown to be well tolerated in phase I and is currently in phase II trials in combination with Doxil (doxorubicin) for ovarian cancer treatment and with cetuximab for squamous cell carcinoma of the head and neck²⁷³⁻²⁷⁵. Intratumoral administration of MEDI-9197 (or 3M-052) was evaluated in a phase I clinical trial in combination with durvalumab, another anti-PD-1 antibody. Although the preclinical data were very promising, further development of this compound has been discontinued by AstraZeneca²⁷⁶. NKTR-262 is another TLR7/8 agonist being evaluated in the context of intratumoral administration in advanced cancers in combination with the CD122 agonist NKTR-214. Similarly, LHC165, a benzonaphthyridine TLR7 agonist adsorbed to aluminum hydroxide, is being tested in a phase I clinical trial with the anti-PD-1 antibody spartalizumab. Preclinical

compounds that have shown promise in mitigating systemic toxicity by localized retention include ALT-702, TransCon-R848, and VX-001; ALT-702 is based on a depot-forming peptide technology and the latter two are described as “sustained-release R848 formulations.” These systems are discussed in greater detail in Section 2.4, where we focus on formulation and carrier-based approaches.

2.3.3 Systemic delivery of IMDs as Antivirals for Infectious Diseases

In addition to treatment of skin conditions as discussed in section 3.1, IMDs are being explored as systemic treatments for chronic infectious diseases such as hepatitis C (HCV), hepatitis B (HBV), and HIV. The development of orally available prodrug forms of TLR7/8 agonists has been extensively evaluated in the treatment of chronic infectious disease, with the goal of improving patient compliance and minimizing side effects²⁷⁷. As in the application to cancer, however, the transition from treating topical infectious conditions to chronic systemic infections has also been limited by narrow therapeutic indexes of systemically/orally administered TLR7/8 agonists. Low doses have insufficient therapeutic effects and higher doses are associated with vomiting, fatigue, lymphopenia, and fever, in addition to hepatic and renal impairment²⁷⁸. Although toxicity remains a concern, the antiviral state generated by type I IFN induction upon TLR7 ligation makes these agonists promising antiviral agents for chronic infectious diseases²⁷⁹. For example, type I interferons elicited by TLR7/8 activation can induce viral RNA transcript degradation and activation of protein kinase R, which blocks translation of viral mRNAs²⁸⁰.

The first clinical attempts at treating chronic infectious diseases with synthetic TLR7/8 agonists focused on chronic HCV. Oral administration of R848 was extensively evaluated but failed in two phase IIa clinical trials because of toxicity at higher doses, similar to issues with PEGylated IFN- α injections, the standard treatment for chronic HCV²⁸¹. Oral administration of PF-4878691 (852-A) was tested in a phase I trial in patients with chronic HCV but showed low bioavailability and highly variable absorption compared with parenteral administration. This drug was therefore discontinued for treatment of HCV but further evaluated in the context of advanced cancers²⁸². ANA975 and ANA971 are oral prodrug formulations that are converted to active compound by first-pass metabolism²⁸³. They were also tested in phase I clinical trials in patients

with chronic HCV but failed due to inadequate therapeutic indexes.

Although synthetic TLR7/8 agonists are no longer, to our knowledge, being tested for chronic HCV, treatments for chronic HBV have shown promising results. HBV infects hepatocytes in the liver without activating hepatic non-parenchymal cells such as Kupffer cells and liver sinusoidal endothelial cells or surrounding immune cells such as myeloid DCs (mDCs), pDCs, and macrophages²⁸⁴. TLR7/8 agonists play a role in preventing viral transmission and replication by mechanisms similar to those discussed earlier, including upregulation of IFN-stimulated genes (ISGs) and the generation of an antiviral state by type I IFN signaling²⁸⁵. One of the many lead compounds in the clinic, RO-7020531, has completed a phase I trial and is currently in phase II trials in combination with direct-acting antivirals^{286–288}. This compound is a double prodrug of a TLR7 agonist that has shown promising preclinical results. In an AAV-HBV mouse model, RO-7020531 induced both innate pharmacodynamic responses and adaptive immune responses²⁸⁹. GS-9620 is another oral TLR7 agonist that was tested clinically for treatment of chronic hepatitis B. This compound exhibited high first-pass hepatic clearance and increased levels of type 1 IFN upon oral administration compared with intravenous administration, with similar systemic exposure in nonhuman primates (NHPs)²⁹⁰. At low doses, GS-9620 was shown to activate ISGs without inducing systemic interferons, which suggested the presence of a therapeutic window for inducing an anti-HBV response²⁹¹. Ferrari and colleagues demonstrated sustained antiviral effects against woodchuck hepatitis virus (WHV) in a woodchuck model of HBV and against HBV in a chimpanzee model, with significantly increased production of IFN from monocytes rather than direct activation of antiviral pathways in hepatocytes. These findings indicated that GS-9620 could be used in concert with other standard antiviral treatments^{292,293}. The same researchers observed significantly increased levels of antigen presentation in hepatocytes, which led to improved HBV-specific immune responses. In a phase 1b trial with 1 or 2 doses of oral GS-9620 administered 7 days apart, no change in serum HbsAg or HBV DNA levels were detected, despite induction of interferon-stimulated genes²⁹¹. Clinical development of GS-9620 for chronic HBV has since been discontinued, but is still being examined for treatment of HIV (*vide infra*). APR002, a liver-targeted TLR7 agonist designed to act locally in the liver and gastrointestinal tract, is being developed by Apros Therapeutics. Preclinical studies in NHPs showed that retention in the liver is partly mediated by organic anion transporting polypeptide transporters²⁹⁴. These studies

demonstrated sustained suppression of serum WHV DNA, lowered levels of serum WHsAg, and durable antibody responses in a woodchuck model of chronic WHV.

Bertoletti and colleagues probed purified hepatic immune cells from healthy and HBV-infected human livers with numerous TLR agonists and demonstrated that only TLR8 agonists were able to selectively activate liver-derived cells, resulting in substantial production of IFN- γ , which has been shown to mediate clearance of HBV in infected chimpanzees^{295,296}. GS-9688, a selective TLR8 agonist currently in phase II clinical trials for treatment of chronic HBV, can activate TLR8-expressing gut and hepatic immune cells, leading to secretion of immune mediators in the portal vein²⁹⁷. An effective dose of 3 mg/kg was defined in WHV-infected woodchucks and 3 mg in virally suppressed and viremic patients with chronic HBV²⁹⁸.

Beyond treatment of HCV and HBV, recent work has shown the potential of TLR7/8 agonists in reversing HIV latency (a state where cells are infected and contain an integrated and functional HIV viral genome, but where active viral transcription is silent). GS-9620, discussed earlier in the treatment of chronic HBV, is currently in a phase I trial for reversing HIV latency. Preclinical data indicated that TLR7/8 agonist-induced increases of IFN- α effectively inhibited HIV-1 replication *in vitro* in activated lymphocytes and macrophages²⁹⁹. Work done by Barouch and colleagues combining Ad26/MVA vaccination with oral TLR7 agonists GS-9620 or GS-986 (a GS-9620 analog) in an NHP model showed significantly reduced viral DNA in lymph nodes and peripheral blood³⁰⁰. They also observed improved virologic control and delayed viral rebound following discontinuation of antiretroviral therapy³⁰¹. Whitney and colleagues demonstrated the ability of these oral TLR7 agonists to induce transient viremia in rhesus macaques (RMs)³⁰². Thus, TLR7/8 agonists may have a role to play in HIV cure strategies.

Although we have focused here on viral infections, it is important to note the role that synthetic TLR7/8 agonists play as adjuvants in vaccines against bacterial infections. The mechanisms underlying TLR7/8 sensing of bacterial RNA are gradually being established³⁰³⁻³⁰⁵. Preclinical studies of these agonists in vaccine formulations against bacterial pathogens demonstrate the ability of these compounds to activate both neonatal and adult DCs alike thus also highlighting their potential in boosting neonatal immunizations³⁰⁶⁻³⁰⁸.

2.3.4 Anti-inflammatories and bronchodilators for Respiratory Ailments

In addition to their utility as potential anti-viral compounds, synthetic TLR7/8 agonists are being explored as agents to shift the polarization of immune response and as bronchodilators for treatment of allergic conditions such as asthma and rhinitis. Allergic reactions are characterized by highly Th2-polarized immune responses and the production of allergen-specific IgE antibodies. One approach to treatment of such disorders has been to therapeutically shift the polarization of the immune response from pathology-causing Th2 to a non-pathologic Th1 response. Preclinical studies using R848 as a model compound have demonstrated its ability to activate DCs, airway epithelial cells, and Th1 cells, leading to Th1 immune polarization³⁰⁹. In animal models of allergy, R848 treatment decreased airway hyperreactivity, airway remodeling, and activation of airway nerves, leading to increased nitric oxide production³¹⁰. R848 was also able to reverse airway reactivity to allergen challenge, thus preventing airway smooth muscle proliferation and goblet cell hyperplasia³¹¹. Initial use of synthetic TLR7/8 agonists in allergic asthma was motivated by work done on administration of CpG oligodeoxynucleotides (CpG ODN; TLR9 agonists) to airways, which were shown to induce a redirection of the immune response polarization from Th2 to Th1. Inappropriate Th2 responses to harmless environmental antigens need to be counterbalanced by a strong Th1 cytokine response to reduce the downstream effects of the allergy³¹². Asthma therapies have focused on addressing airway inflammation and excessive bronchoconstriction³¹³. Preclinical work using murine models of asthma has shown the potential of synthetic TLR7/8 agonists to significantly reduce ovalbumin (OVA)-induced airway hyperreactivity and eosinophilic inflammation³¹⁴. TLR7/8 agonists inhibit IgE synthesis in favor of IgA synthesis in human B lymphocytes and can reverse airway hyperresponsiveness by IFN- γ -mediated effects. Intracellular signaling through NF- κ B and the AP-1 family of transcription factors is implicated as the mediator of this response *in vitro*, whereas acute bronchodilation effects are shown to be mediated via production of nitric oxide upon TLR7 activation.

Synthetic TLR agonists have also been evaluated for the treatment of allergic asthma and rhinitis clinically. GSK-2245035 was investigated in clinical trials for the treatment of allergic asthma and allergic rhinitis³¹⁵. This compound was designed to preferentially upregulate IFN- α secretion without significant changes in TNF- α as a means to alter the immune microenvironment

of the airway and thus to modify the Th2 response to aero-allergens³¹⁶. Preclinical work on the development of the 8-oxo-adenine antedrug series, possessing an ester moiety that cleaves to an inactive acid in the presence of plasma esterases, allowed for lowered systemic toxicities³¹⁷. AZD-8848 was the result of this selective antedrug TLR7 agonist library optimized for airway treatment³¹⁸. However, AstraZeneca has since discontinued development of TLR7 agonists. VTX-1463, a selective TLR8 agonist, is currently undergoing phase I trials for treatment of allergic rhinitis. Preclinical data have shown significant upregulation of Th1 inflammatory mediators, such as IL-12, IFN- γ , and MCP-1, that shift the balance of the Th1:Th2 ratio toward lowering allergic effects³¹⁹. This compound was well tolerated in a phase I clinical trial for grass pollen allergy, with improved levels of total nasal symptom scores, the primary clinical endpoint³²⁰.

2.4 Bioconjugation and other delivery strategies

The discussion above demonstrates the breadth of preclinical and clinical applications of synthetic TLR7/8 agonists, but also highlights the myriad unsuccessful attempts at clinical translation. Overall, two main problems have dominated failures in clinical trials: insufficient therapeutic efficacy and unacceptable toxicity (i.e., narrow therapeutic index). Therefore, significant research has focused on bioconjugation and other delivery strategies to overcome these limitations and realize the full potential of these synthetic small-molecule immunomodulators.

2.4.1 TLR7/8a conjugates to enhance vaccine efficacy

2.4.1.1 Antigen-TLR7/8 conjugates

Some of the early research on improving the potency of vaccine formulations involved conjugating synthetic TLR7/8 agonists to vaccine antigens as a means to prevent the former from entering the bloodstream and to focus their effects precisely on antigen-specific B cells and those DCs that acquire antigen and are most relevant for T cell activation. The hypothesis was that covalent conjugation would allow for colocalization of antigen and adjuvant, thus greatly

increasing the likelihood that the antigen and adjuvant are taken up by the same APC, which in turn could enhance antigen presentation to CD4⁺ and CD8⁺ T cells³²¹.

Work done by Seder and colleagues comparing the efficacy of R848 to that of the TLR9 agonist CpG ODN as vaccine adjuvants showed that R848 induced lower levels of antigen-specific CD4⁺ and CD8⁺ T cells and reduced IgG₁ and IgG_{2a} responses to the HIV-1 Gag protein³²². Using a reactive derivative of R848, the TLR agonist was conjugated to HIV-1 Gag protein, and the IMD-conjugated protein elicited elevated cytokine production by antigen-specific CD4⁺ and CD8⁺ T cells to the antigen. This study indicated that the discrepancy between innate activation of DCs and lack of T cell response from free R848 could be a delivery problem, wherein the timing of antigen presentation was not optimized with the activating effects of R848. Follow-up studies in rhesus macaques (RMs) comparing the TLR7/8 agonist-Gag protein conjugate with the Gag protein itself or with CpG ODN showed increased Th1 responses and Gag-specific CD8⁺ T cell responses for the conjugate³²³. The mechanism of action of the TLR7/8 bioconjugate was hypothesized to be due to enhanced migration of 6 distinct DC populations to dLNs, thus significantly increasing the total number of specific DC subsets in the dLNs. Increased uptake of OVA, the model antigen, was shown in the conjugate system compared with a mixture of unconjugated OVA and TLR7/8 agonist (37.8% vs. 8.8%, respectively), validating the above hypothesis³²⁴. This work supported that of Kedl et al., who showed that TLR7/8-antigen bioconjugates increased the sensitivity of responding T cells to low amounts of antigen³²⁵.

An important issue in preparing antigen-IMD conjugates is ensuring that the IMD is not linked to the antigen at an important site for neutralizing antibody recognition. To this end, Hedestam and colleagues showed that attaching a TLR7/8 agonist onto surface-exposed lysine residues on the external subunit of the HIV-1 envelope glycoprotein gp120 led to reduced antibody recognition of the CD4 binding site, depending on the concentration of TLR7/8 agonist conjugated to gp120³²⁶. Work by O'Hagan and colleagues also highlighted the potential loss of conformation that can occur with bioconjugation reactions in this context and noted that a disperse mixture of conjugated species can form due to the high number of equivalent surface-exposed amino acids available for conjugation³²⁷. These authors used an *ortho*-activated benzaldehyde instead of a non-substituted derivative to overcome the need to increase the reactivity of lysine amino groups, thus reducing the complexity of the reaction and purification steps and increasing the product

homogeneity.

The above bioconjugate studies all focused on linkage of IMDs to single protein antigens. Work done by Alexander-Miller and colleagues allowed for multiple antigenic targets (i.e., incorporating all viral proteins) by conjugating an amine-modified R848 onto reduced inactivated influenza virus A particles (IPR8) using an amine to sulfhydryl crosslinker featuring N-hydroxysuccinimidyl ester and maleimide groups that connect the amine of the drug and the thiols on the virus particles respectively (SM(PEG)₄; **Fig. 15A**)³²⁸. This system was tested in the African Green Monkey (AGM) model of neonatal vaccination and resulted in a 10-fold increase in anti-influenza virus IgG levels, increased levels of influenza-specific IgM and IFN- γ ⁺ influenza-specific T cells, and decreased viral load in the trachea. This improved response was again tied to an increase in the total number of DCs in the dLNs and increased DC expression of maturation markers such as CD80 and CD86³²⁹. The R848-IPR8 conjugate was further tested for long-term responses in the AGM model and showed significantly increased levels of long-lived IgG antibody response 6 months after dosing³³⁰. Recent work from the same group explored the development of second-generation R848-IPR8 conjugates prepared via a two-step synthesis process³³¹. First, R848 was modified with different crosslinker moieties to introduce maleimide groups that were then conjugated to the reduced virus containing thiol groups. These systems were tested in RAW264.7 cells for TNF- α production with the *N*- γ -maleimidobutyl-oxysuccinimide ester (GMBS, ThermoFisher) linker showing higher CD40 expression (by an order of magnitude) compared with both the unconjugated control and the first-generation SM(PEG)₄ linker (**Fig. 15A**). These conjugate vaccine strategies highlight the necessity for improved formulation approaches in order to maximize the potential of TLR7/8 adjuvantation.

2.4.1.2 Polymer and particulate formulations of TLR7/8 agonists

While the above examples demonstrate bioconjugation of TLR7/8 agonists onto soluble proteins, another approach pioneered by Seder and colleagues involves the intentional design of conjugate formulations that self-aggregate into larger particulates^{332,333}. They attached a number of antigens or neoantigens using a charge modification conjugation approach that comprised peptide antigens linked to both a charge-modifying polypeptide and a hydrophobic polypeptide

block through enzyme-degradable linkers at the N and C termini, respectively. Then, the oligopeptide-based hydrophobic blocks were linked to a precise number of TLR7/8 agonists. This work further strengthens the hypothesis that antigen form (soluble vs. particulate) is a critical aspect of CD8⁺ T cell immunogenicity. Vaccination with particle antigens, either covalently attached or mixed with adjuvant, led to 20-fold-higher CD8 T cell responses compared to soluble antigen, with the particle conjugates being retained longer in dLNs and showing higher uptake by CD11c⁺ DCs (**Fig. 15B**). Another example of this approach was demonstrated by Hubbell and colleagues using a reversible linker strategy³³⁴. In this system, protein antigens were conjugated via a cleavable linkage to a statistical copolymer containing mannose-binding receptors and a TLR7 agonist called P(Man-TLR7). Antigens were modified with an amine-reactive heterobifunctional bicyclononyne-decorated linker, which is sensitive to disulfide reduction (stable in serum and cleaves on endocytosis). Vaccination with a P(Man-TLR7) conjugate linked to CSP (circumsporozoite protein from *Plasmodium falciparum* malaria) induced a significant increase in CSP-specific CD8⁺ T cell response (TNF- α ⁺ and IFN- γ ⁺ T cells) compared with controls, including the adjuvant currently used in the malaria vaccine being studied in clinical trials (**Fig. 15C**).

The rationale for particulate formulations has been bolstered by extensive work by Seder and colleagues, wherein TLR7/8 agonists were covalently conjugated onto synthetic polymer scaffolds to further explore the mechanistic effects of different linker structures and TLR7/8 agonist densities on the physicochemical properties of the prodrug particles³³⁵. Particulate TLR7/8 conjugates showed enhanced lymph node cytokine production and uptake by migratory APCs as well as an order of magnitude increase in the influx of CD11c⁺ DCs and monocytes in the dLN compared with soluble forms (**Fig. 16A**). These authors probed further into how the carrier size and morphology of these conjugates correlate with immune activation by comparing 3 types of carriers: a random coil polymer (~4 nm), a micelle nanoparticle (~10 nm), and a sub-micrometer particle (~300 nm)³³⁶. A significantly increased CD8⁺ response for the sub-micrometer particles as well as direct correlations between hydrodynamic radii and magnitude of lymph node IL-12 production as well as uptake by APCs were observed (**Fig. 16A**). Interestingly, the uptake of the sub-micrometer particles was 5-fold higher for monocytes and macrophages than for DCs, suggesting that monocytes and/or macrophages play a crucial role in adjuvant activity in this size

range. Particulate polymer or peptide formulations thus represent a promising approach to improve LN accumulation and retention of these agonists.

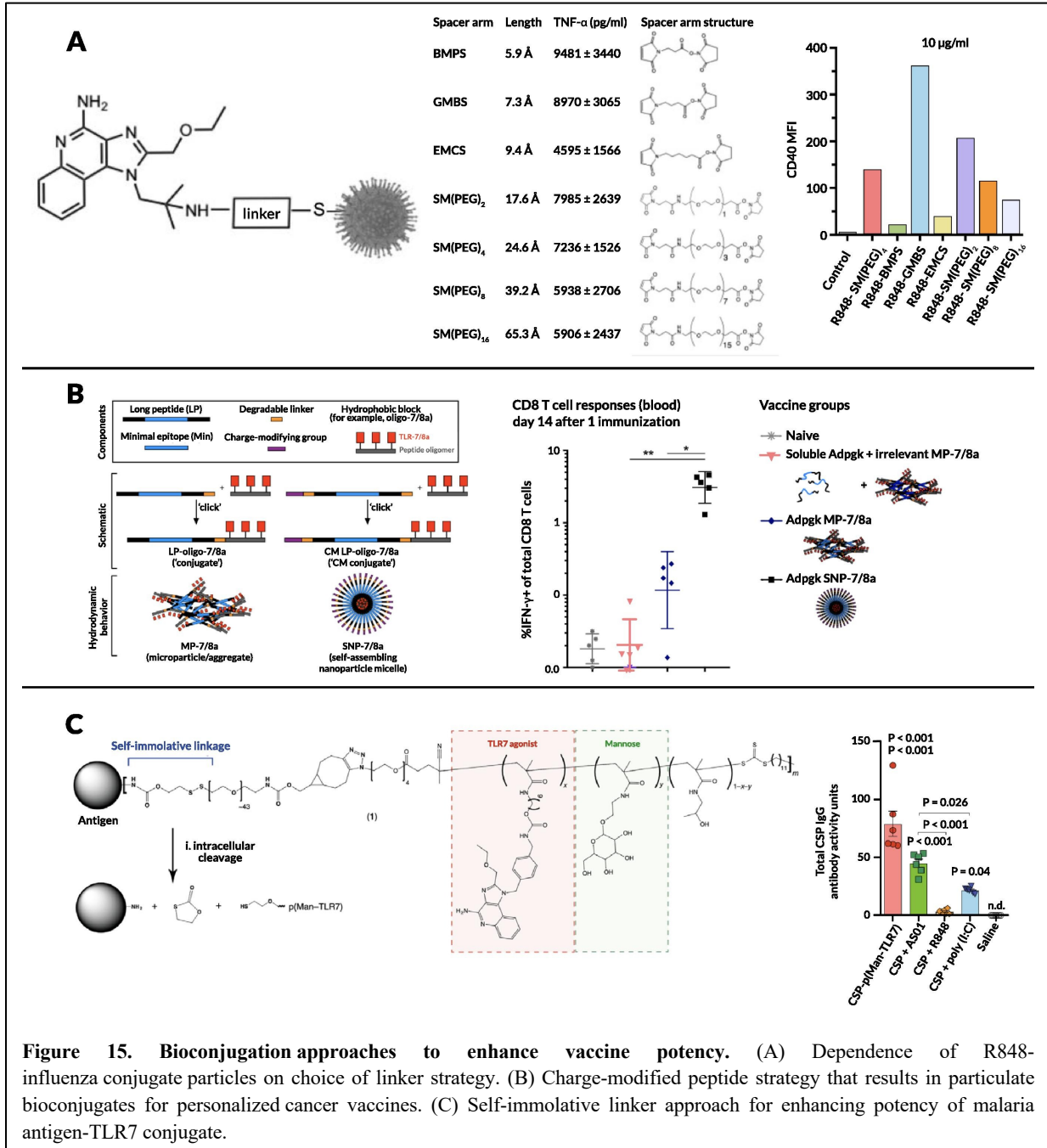


Figure 15. Bioconjugation approaches to enhance vaccine potency. (A) Dependence of R848-influenza conjugate particles on choice of linker strategy. (B) Charge-modified peptide strategy that results in particulate bioconjugates for personalized cancer vaccines. (C) Self-immolative linker approach for enhancing potency of malaria antigen-TLR7 conjugate.

In a similar vein, De Geest and colleagues used bis-amino-ketal 2,2-bis(aminoethoxy)propane cross-linkers to create amphiphilic copolymer nanogels that were attached to IMD TLR7/8 agonists^{337,338}. Compared to free TLR7/8a, immunization with TLR7/8a-

conjugated nanogels led to increased internalization by multiple subsets of immune cells in LNs including DCs, B cells, macrophages, and monocytes, with the vast majority of the nanogel localized to the subcapsular and medullary sinuses of the lymph node (**Fig. 16B**). The same group developed lipid-polymer amphiphiles consisting of cholesterol as a lipid motif and a hydrophilic polymer conjugated to a TLR7/8 agonist³³⁹. They demonstrated that this polymer binds to albumin with high affinity (as assessed using bio-layer interferometry), allowing for highly efficient passive translocation to lymphoid tissue via “albumin hitchhiking” and leading to a significant increase in DCs in the dLN along with high expression of CD80 and CD86. This lymph node targeting approach was verified using IFN- β reporter mice, with bioluminescent imaging showing minimal systemic activation with a strong signal in the dLN. David and colleagues conjugated a TLR7/8 agonist onto hyaluronic acid via a 2-chloro-4,6-dimethoxy-1,3,5-triazine-activated amidation strategy, which resulted in an immunologically “silent” conjugate that was activated via proteolysis or enzymatic cleavage of the amide bond³⁴⁰. Upon co-administration of the conjugate with diphtheria toxoid (CRM197) as a model antigen, they observed a significant increase in antigen-specific IgG titers after a single boost. Kishimoto and colleagues showed that conjugating R848 onto polymer particles via an acid-labile bond resulted in an order of magnitude increase in antibody titer (Th1 focused; i.e., higher IgG_{2c}/IgG₁ ratio), increased antigen-specific T cells, and a significant influx of myeloid DCs, granulocytes, and macrophages into the dLN³⁴¹. Another synthetic conjugate approach toward increasing DC activation and internalization in dLNs was shown by Hong and colleagues, wherein a TLR7/8 agonist with a terminal alkyne moiety was conjugated onto azide-coated iron oxide nanoparticles (NPs) through copper-catalyzed azide-alkyne cycloaddition and co-administered with OVA³⁴². The resultant increased antigen-specific T cell activity reinforced the use of the synthetic conjugation approach as a method to improve vaccine potency. Likewise, Appel et al. conjugated a TLR7/8 agonist onto a copolymer of dimethyl acrylamide and neopentyl glycol diacrylate formulated with beta-cyclodextrin³⁴³. Upon co-injection with either OVA or gp120, the adjuvant formulation exhibited significantly improved IgG_{2c} antibody titers.

An alternate approach to promote lymph node accumulation and reduce systemic dissemination of TLR7/8a adjuvants is to engineer their binding to existing clinical adjuvants such as alum. A team at Novartis pursued this approach by screening TLR7 agonists functionalized with

polyethylene glycol (PEG) linkers and terminal phosphonate groups¹⁰⁵. The PEG linkers allowed for increased solubility at neutral pH while the anionic phosphonate functional groups facilitated efficient adsorption to alum (**Fig. 16C**). Alum-bound TLR7 agonist adjuvants were tested in multiple vaccination mouse models; they demonstrated enhanced activation of APCs, priming of IFN- γ ⁺CD4⁺ T cells, and, most importantly, antigen-specific B cell responses (both antibody-secreting and memory phenotypes)³⁴⁴⁻³⁴⁸. Alum-TLR7 conjugates were subsequently evaluated in a phase I clinical trial with the antigen present in the Menjugate (meningococcal group C–CRM197 conjugate) vaccine. In this study, the highest dose (100 μ g) caused severe irAEs in one-fifth of patients, which correlated with high plasma levels of TLR7 agonist, while lower doses were deemed safe and effective in eliciting antibody responses similar to Menjugate (which contains alum as an adjuvant), though a larger-scale clinical trial was deemed necessary for verification³⁴⁹. TLR7 agonists have also been adsorbed to alum through mixing lipid tail-modified 3M-052 with phospholipids to generate very small lipid nanoparticles, which subsequently adsorb to alum via phosphate groups³⁵⁰. Upon co-injection of these alum/lipid nanoparticle-TLR7a complexes with a tuberculosis vaccine antigen, improved Th1 responses were observed relative to free 3M-052, with increased levels of antigen-specific CD4⁺ T cells and high levels of serum antibodies, which raises the question of whether there is potential synergy between TLR7/8 agonists and alum beyond simply a depot effect. This concept would be interesting to explore further, given that Seder and colleagues noted that adjuvant efficacy is lowered when TLR7 is co-formulated with an MF59-based nano-emulsion instead of alum, despite prior studies showing that MF59 induces higher binding titers than alum alone³⁵¹⁻³⁵³. More recently, an Alum/TLR7a-adjuvanted whole-virion inactivated SARS-Cov-2 vaccine received emergency approval by India's Central Drugs Standard Control Organization at the end of 2020³⁵⁴⁻³⁵⁹. At the time of writing this review, this vaccine has been administered to over ten million people, further underscoring the importance of formulated TLR7/8 agonists as vaccine adjuvants.

In addition to alum adsorption, a commonly studied approach for formulating IMDs has been through their encapsulation with or without vaccine antigens in biodegradable poly(lactic-co-glycolic acid) (PLGA) nanoparticles or other polymeric NPs. Pulendran and colleagues encapsulated soluble gp140 Env and lipophilic TLR7/8 agonist 3M-052 in PLGA NPs and showed an adjuvant effect comparable to that of alum-TLR7 and significantly higher than that of alum

alone in RMs^{360,361}. They demonstrated increased levels of Env-specific IgG antibodies in serum and vaginal secretions, high levels of neutralizing antibodies, and upregulated expression of CD86 on monocyte subsets 2 weeks after vaccination. Another interesting finding was the enhanced

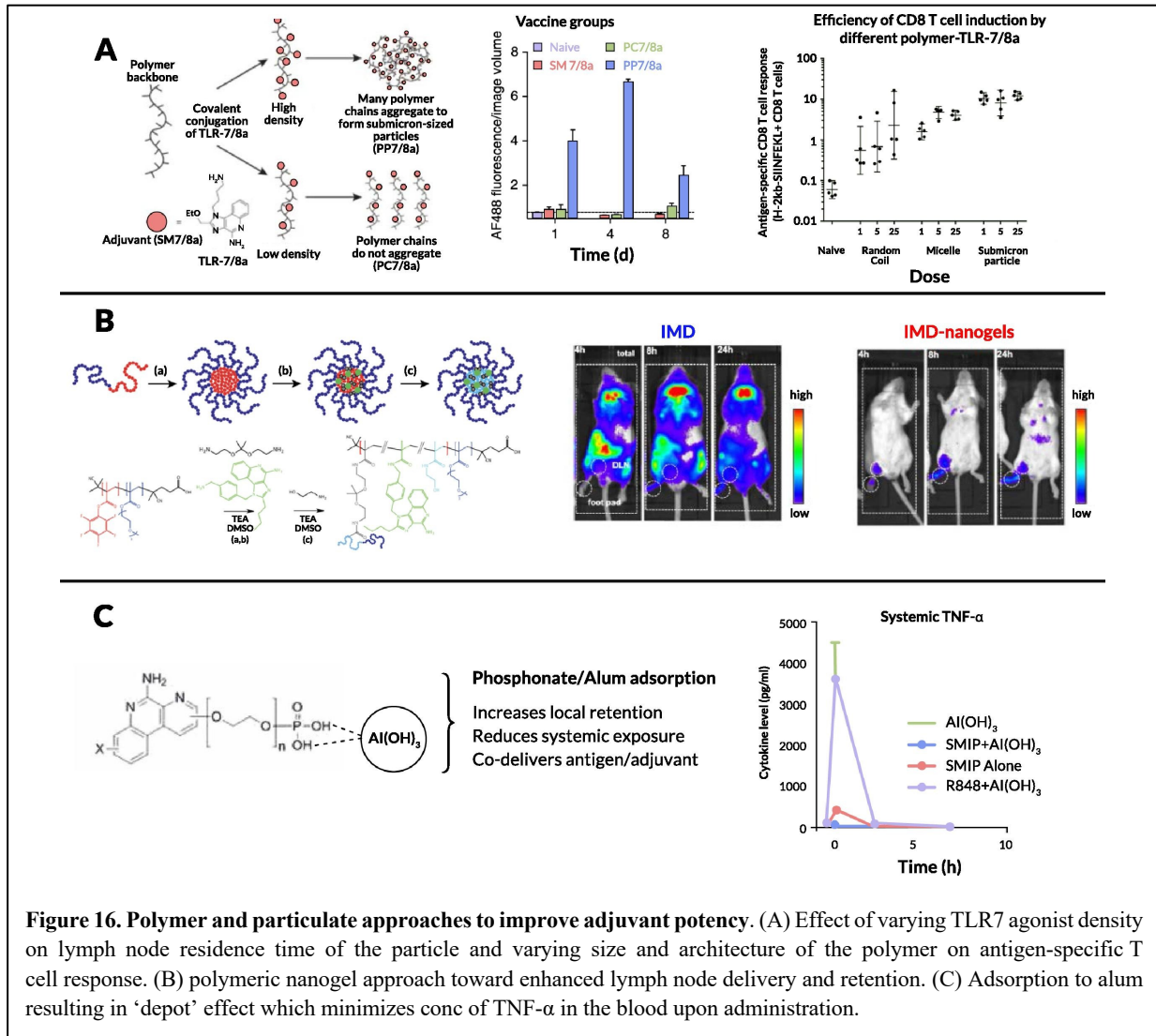


Figure 16. Polymer and particulate approaches to improve adjuvant potency. (A) Effect of varying TLR7 agonist density on lymph node residence time of the particle and varying size and architecture of the polymer on antigen-specific T cell response. (B) polymeric nanogel approach toward enhanced lymph node delivery and retention. (C) Adsorption to alum resulting in ‘depot’ effect which minimizes conc of TNF- α in the blood upon administration.

protection observed in young and adolescent RMs compared with older RMs, which could tie in to work done by Levy and colleagues that showed potent activity of TLR7/8 agonists on neonatal macaque blood cells³⁶². TLR7/8 PLGA-based vaccine formulations have also been studied in the context of mucosal and tumor immunizations^{363,364}. Other polymeric systems include block copolymers, developed by Wilson and colleagues, decorated with pyridyl disulfide ethyl methacrylate moieties for conjugation of thiol-containing antigen and a fatty acid-mimetic core for encapsulation of TLR7 agonist³⁶⁵. Vaccination with these block copolymer nanoparticles carrying

antigen (OVA) and TLR7 agonist elicited increased levels of antigen-specific CD8⁺ T cells in bronchoalveolar lavage fluid, lung vasculature, and lung interstitium in addition to enhanced antigen-specific IgG antibody titers upon intranasal administration compared to free protein/TLR7a immunization. In a similar approach, Levy and colleagues formulated a block copolymer system based on PEG-*block*-polypropylene-sulfide (PPS) polymersomes, encapsulating a TLR8 agonist that served as a potent adjuvant system when co-loaded with antigen³⁶⁶. Encapsulation in polymers has also been used to generate novel “needle-free” vaccination strategies, which represent potentially promising avenues for vaccine formulations based on TLR7 agonists^{367–369}.

2.4.2 Toward safe, systemic delivery via drug carrier approaches

As noted above, systemic toxicities associated with synthetic TLR7/8 agonists are a major roadblock to the clinical success of these compounds. Several drug carriers have been used in attempts to solve these issues, including PEGylation and other conjugation approaches, nano- and micro-particles, stimuli-responsive release, and molecular targeting moieties.

Carson and colleagues made a surprising observation when investigating PEGylation of TLR7 agonists. Specifically, while PEGylation improved solubility of these compounds, cytokine production *in vitro* was significantly lowered³⁷⁰. This loss of activity upon PEGylation was intriguing and the influences of PEG chain length (from 6 to 470 repeat units) on *in vitro* and *in vivo* effects of TLR7 ligands were examined. Short-chain PEGs displayed low potency to stimulate bone marrow-derived macrophages; however, when chain length exceeded 47, potency was restored, suggesting that spatially constrained conjugate ligands are limited in their ability to activate TLR7. Furthermore, conjugates with an amine end group were more potent than those ending with carboxyl. These data showing that conjugates using longer PEGs have improved solubility, circulation time, and plasma concentration, as well as increased IL-6 and TNF- α production *in vivo*, tie in nicely with previous observations that innate immune activity of PEG-TLR7 conjugates is affected by steric hindrance of the PEG linker³⁷¹. The same group has shown that upon conjugation of a TLR7/8 agonist onto a carrier protein (mouse serum albumin) via a succinimidyl 6-hydrazide nicotinamide acetone hydrazide linker, the immunostimulatory

potential of the agonist was significantly enhanced (**Fig. 17A**)³⁷². Further work on TLR7 conjugation onto primary amine-functionalized Ficoll (400 kDa) or dextran (70, 500, and 2,000 kDa) using benzoic acid functional groups showed higher potency (by an order of magnitude) of TNF- α and IL-6 induction *in vitro*³⁷³. It is interesting to note that 12 nm dextran conjugates with similar conjugation ratios showed 10-fold higher potency than 37 nm dextran conjugates, whereas 29 nm linear dextran showed 10-fold higher potency than 14 nm spherical Ficoll conjugates. These observations were validated *in vivo* along with admixed controls, wherein the synthetic conjugates were at least 500-fold more potent at inducing production of cytokines such as IL-6, TNF- α , and IFN- γ than the unconjugated TLR7 ligand. These studies reinforce the idea that size, composition, and molecular architecture of synthetic TLR7 conjugates significantly affect immune potencies due to efficiency of uptake by APCs which is required for the generation of an adaptive immune response. These studies culminated in the development of 1V270, a phospholipid-conjugated TLR7 agonist that spontaneously self-assembles into 110–120 nm liposomes³⁷⁴. This liposomal formulation was tested in multiple murine tumor models, where NK cells were responsible for early efficacy and CD8⁺ T cells were critical for sustained inhibition of lung metastasis.

Beyond molecular bioconjugates, numerous nano- and microparticle-based encapsulation approaches have been developed to enable intravenous delivery of TLR7 agonists. Ainslie and colleagues encapsulated R848 in acetylated dextran microparticles and showed efficacy in treating visceral leishmaniasis, a systemic parasitic disease³⁷⁵. Another significant stride toward systemic administration of TLR7/8 agonists was made by Weissleder and colleagues^{376–378}. They developed a single-cell high-content screening approach to identify compounds that could alter the polarization of macrophages from an M2 (wound-healing phenotype) to M1 (inflammatory) state *in vitro*³⁷⁶. Among the compounds tested, R848 was the most potent driver of macrophage re-education and they subsequently designed cyclodextrin NPs to encapsulate R848 based via host–guest interactions. Cyclodextrin NPs carrying R848 exhibited efficacy in both the MC38 colon cancer and B16.F10 melanoma models upon intravenous administration (**Fig. 17B**). Notably, toxicity was not addressed in this initial study; in a follow-up study, the same group attached adamantane to R848 via the tertiary alcohol group thus increasing the host-guest binding affinity and improving the stability of the drug-loaded supramolecular complex. They obtained antitumor

efficacy with lower weight loss than with R848-cyclodextrin NPs³⁷⁷. Another recent attempt at intravenous administration of TLR7/8 agonists was reported by Kabanov and coworkers; they encapsulated R848 in poly(2-oxazoline) particles and showed improved survival rates with low toxicity in a metastatic, orthotopic lung adenocarcinoma model³⁷⁹. They attributed the antitumor effects to higher levels of Ly6C⁺ monocytes and CD8⁺ T cells in the tumor microenvironment. Moving beyond polymeric systems, Bourquin and colleagues demonstrated that gold NPs coated with a mixture of 1-octanethiol and 11-mercaptoundecanesulfonic acid encapsulating R848 via hydrophobic interactions was a potent delivery vehicle, showing improved lymphatic accumulation and antitumor effects in the CT26 colon cancer mouse model³⁸⁰.

Stimuli-responsive nanomaterials are ubiquitous in the field of drug delivery and attempts to use this paradigm to minimize toxicity of TLR7/8 agonists have yielded fruitful results in preclinical studies. Hubbell and colleagues formulated TLR7 agonists in oxidation-sensitive polymersomes based on PEG-b-PPS, which would specifically release TLR7a on exposure to the oxidative environment within antigen presenting cell endosomes³⁸¹. They observed enhanced DC uptake and activation and proinflammatory cytokine secretion by these polymersomes compared to free TLR7a cultured with DCs *in vitro*. They hypothesized that this enhanced response was due to NOX-2-dependent reactive oxygen species in DC early endosomes and lysosomes triggering burst release of the encapsulated TLR7 agonist. Other oxidation-sensitive systems have been reported, including one developed by Broaders and colleagues that is based on a dextran polymer with stable boronic ester groups³⁸². Light is another stimulus that has been extensively studied in the context of responsive biomaterial systems. Esser-Kahn and colleagues reported the use of 2-(2-nitrophenyl)-propyloxycarbonyl, a photocleavable protecting group, to form a carbamate linkage with the C4-amines in R837 and R848, demonstrating release of the free drugs in response to 360 nm light³⁸³. Mancini et al. attached a β -galactopyranoside to R837 covalently at the C-4 amine and reported β -galactosidase-mediated immune cell activation (**Fig. 17C**)³⁸⁴. This enzyme-responsive activity represents another promising step toward synthetic TLR7/8 agonist-based formulations that can preferentially release active cargo based on specific cues in the tumor microenvironment. The same group furthered this work by developing glycosidase-directed R848 prodrugs, which release free R848 based on cancer cell metabolism³⁸⁵. Another recent attempt at enzyme-responsive release was demonstrated by Shi and colleagues, wherein a TLR7/8 agonist

was conjugated to PEG via benzyl carbamate residues capped by a β -glucuronidase (β -GUS)-sensitive glucuronide. The conjugates were then systematically studied by varying the number of benzyl repeat units (GL1, 2, or 3) and the molecular weight of PEG (0.75, 2, and 5 kDa)³⁸⁶. They found that PEG5k-GL2-IMD self-assembled into vesicular NPs and demonstrated native drug release in response to esterase and β -GUS.

Particulate formulations of TLR agonists favor uptake by APCs due to their natural propensity to phagocytose foreign material; however, enhancing delivery to these key cells and/or directing uptake by specific immune cell subsets is another strategy under investigation. One approach to enhance the concentration of IMDs in tumors is to target TLR7/8a-loaded nanoparticles to T cells circulating in the blood, which subsequently hone into tumors: Schmid et al. demonstrated this strategy by functionalizing TLR agonist-loaded PLGA NPs with anti-PD-1 antibody fragments (**Fig. 17D**)³⁸⁷. These fragments allow for preferential targeting of activated PD-1⁺ T cells in the circulation and tumors, leading to modestly enhanced antitumor efficacy of R848 in multiple mouse models. To more directly target DCs, Figdor and colleagues developed PLGA NPs coated with PEG-lipids displaying antibodies targeting the DC marker DC-SIGN³⁸⁸. They observed a significant increase in binding and uptake by human monocyte-derived DCs and increased expression of CD80 and TNF- α *in vitro*. DEC-205 is another marker of cDC1 dendritic cells; i.v. infusion of DEC-205-targeted NPs in mice elicited significantly lower levels of systemic type I IFNs compared with soluble TLR7 agonists, while still inducing potent cytotoxic T cell responses following OVA immunization. Edwards and colleagues conjugated a TLR7 agonist (UC-1V50) to an anti-hCD20 antibody, rituximab, through the use of a bifunctional *N*-hydroxysuccinimide (NHS) linker. They demonstrated a significant increase in IL-12p40 secretion from RAW264.7 macrophages and specific binding to CD20⁺CD19⁺ B cells *in vitro*³⁸⁹. Andresen and colleagues used maleimide functionalized liposomes attached to murine anti-human DCIR (dendritic cell immunoreceptor) monoclonal antibodies (IgG₁ specific for a nonhuman epitope) via Traut's reagent (i.e., 2-iminothiolane)³⁹⁰. They observed preferential uptake of the nanoparticles by monocytes and mDCs when evaluated *in vitro* in PBMCs and significantly enhanced secretion of inflammatory cytokines such as IL-6 and TNF- α . Beyond active targeting moieties, some promising attempts have been made to bias uptake toward specific immune cell subsets or tissues

by modifying the physicochemical properties of the carrier. Jensen and colleagues tested a TLR7 agonist encapsulated in liposomes composed of neutral, negatively charged, or positively charged phospholipids and found that positively charged formulations effectively biased the NPs to CD14⁺ monocytes in human whole blood, demonstrating a higher level of IL-12p40 secretion in these monocyte subsets and differentiation into CD14/DC-SIGN⁺ DCs, which are potent APCs that can stimulate both CD4 and CD8 T cell responses³⁹¹. Neither anionic nor neutral liposomes could produce these effects, demonstrating potential for charge-based cellular targeting, which has been highlighted recently in several other studies^{392,393}. These immune-cell biasing approaches in tandem with the other strategies described above could play a key role in making systemic administration of synthetic TLR7/8 agonists a clinical reality.

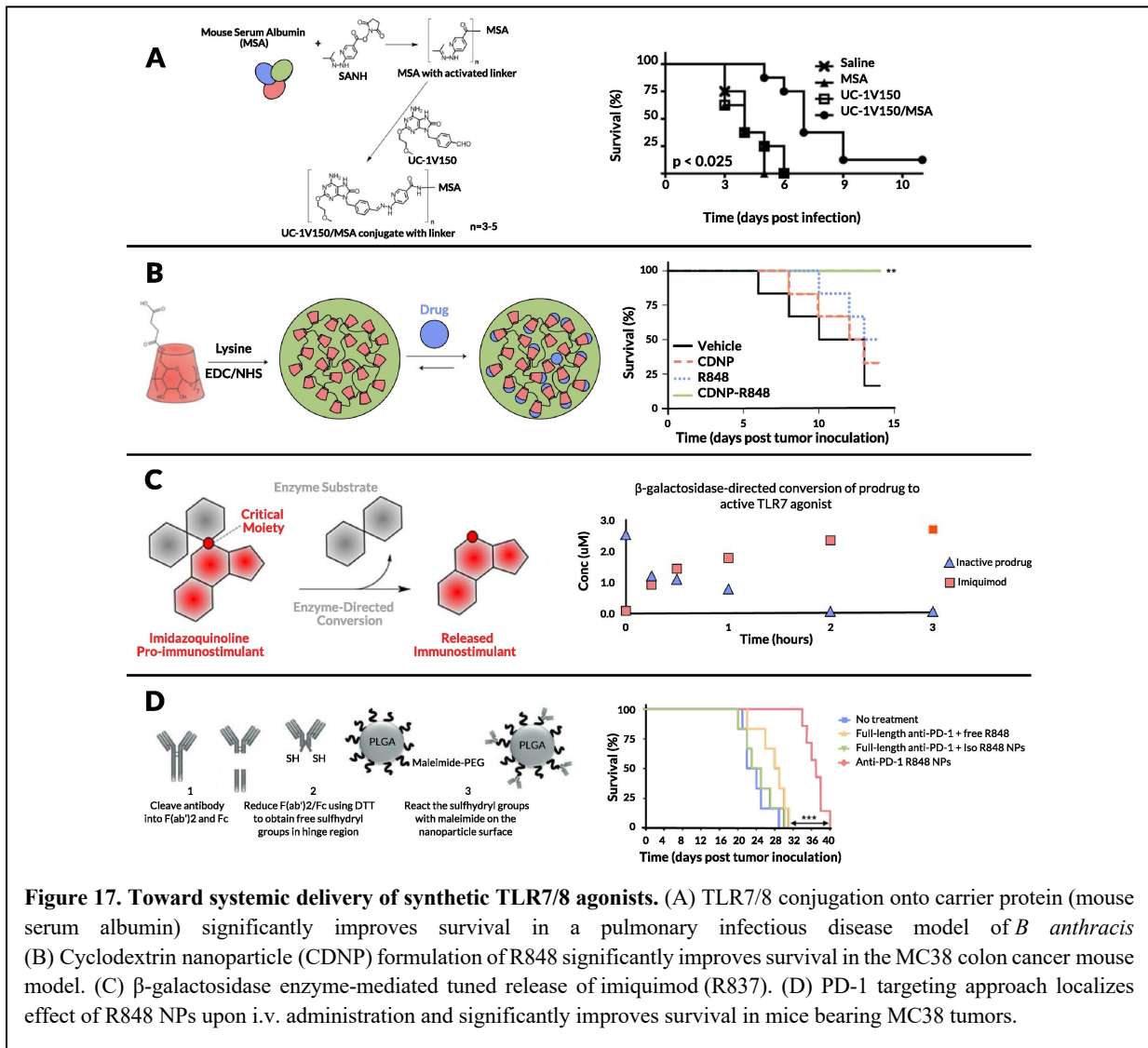


Figure 17. Toward systemic delivery of synthetic TLR7/8 agonists. (A) TLR7/8 conjugation onto carrier protein (mouse serum albumin) significantly improves survival in a pulmonary infectious disease model of *B anthracis* (B) Cyclodextrin nanoparticle (CDNP) formulation of R848 significantly improves survival in the MC38 colon cancer mouse model. (C) β-galactosidase enzyme-mediated tuned release of imiquimod (R837). (D) PD-1 targeting approach localizes effect of R848 NPs upon i.v. administration and significantly improves survival in mice bearing MC38 tumors.

2.4.3 Localized (in situ) delivery approaches to improve intratumoral efficacy

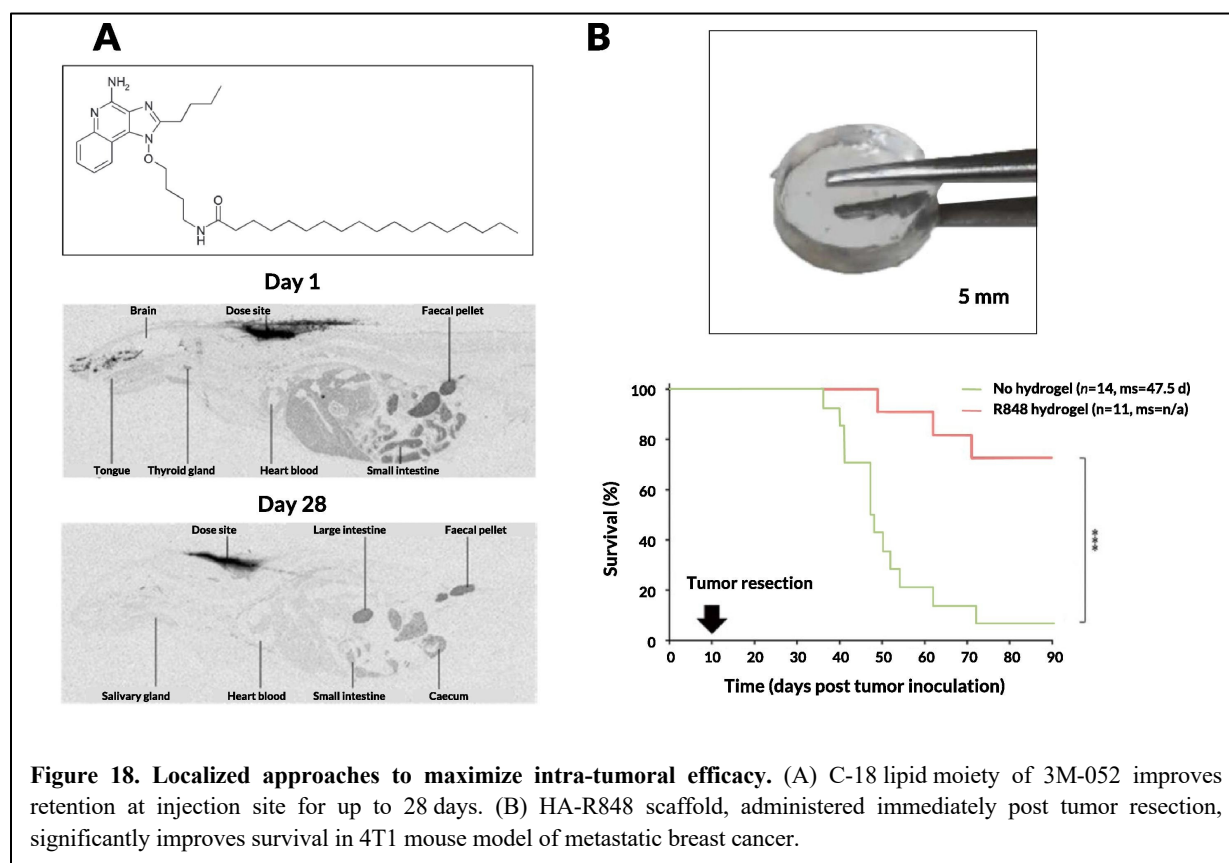
Although systemic administration remains the most common approach for delivery of anticancer therapies, significant advances in interventional radiology that allow for minimally invasive access to almost every organ in the body such that several malignant lesions can be treated simultaneously or sequentially have shifted clinical trends toward local administration^{394,395}. Following the FDA approval in 2015 of intratumoral delivery of talimogene laherparepvec (T-VEC), an oncolytic viral therapy³⁹⁶, key discoveries have been made in intratumoral delivery that have encouraged further preclinical and clinical development of this route of administration. Such local therapy is capable of eliciting systemic anti-tumor immunity, as tumor cell killing stimulated in the treated tumor leads to antigen presentation in tumor-draining lymph nodes, and priming of new T cell responses against the tumor, a concept now referred to as “*in situ* vaccination.” These tumor-specific T cells traffic to the treated tumor site as well as to distal, untreated tumors³⁹⁷, enabling systemic tumor regression following a localized treatment^{398,399}.

In Section 2.3.2, we briefly discussed localized delivery approaches for TLR7/8 agonists that have already made their way to the clinic. In particular, 3M-052/MEDI-9197, an imidazoquinoline bearing a C18 lipid moiety, has been extensively evaluated preclinically for antitumor efficacy as a monotherapy and in combination with checkpoint blockade, OX-40 agonist antibodies, and other anticancer therapies (**Fig. 18A**). Despite the minimal systemic immune activation observed in mouse models, however, the phase I clinical trial showed systemic toxicities following intratumoral administration, with most patients experiencing pyrexia, fatigue, chills, decreased lymphocyte count, nausea, injection site pain, and cytokine release syndrome⁴⁰⁰. Thus, although the C18 lipid moiety did lower systemic toxicity, it was not enough to justify phase II trials. Schwarz and colleagues demonstrated that a Poloxamer 407 thermogel formulation of 3M-052 showed a significant improvement in tumor pharmacokinetics, with 20% of the drug still present 2 weeks after intratumoral injection, as well as decreased tumor burden and improved survival in mice bearing melanoma tumors⁴⁰¹. An initial spike in serum drug concentration still occurred at 6 h post injection, however, indicating that further optimization was necessary to localize the drug in the tumor microenvironment. Wightman et al. showed an improved localized response when 3M-052 was formulated in liposomes, indicating potential for nano-formulations

to localize the effect of synthetic TLR7/8 agonists in the tumor microenvironment⁴⁰². Other localized TLR7/8 agonists discussed in Section 3.2 include NKTR-262, which is based on a 4-arm PEG star polymer to which 4 TLR7/8 agonists are attached via a hydrolysable glycine linker; this construct showed improved intratumoral retention and lowered plasma concentration compared to free drug. Alum-TLR7 was further optimized by Wu and colleagues via a medicinal chemistry approach to allow for phosphonate modification and maximum alum adsorption to minimize systemic dissemination⁴⁰³. One of these compounds, LHC165, is currently in phase I trials in combination with anti-PD-1 spartalizumab, administered intratumorally bound to alum⁴⁰⁴. In terms of preclinical formulations in industry, ALT-702 uses a depot-forming peptide with a fluorocarbon tail conjugated to a TLR7/8 agonist; it showed improved intratumoral retention and minimal systemic levels of inflammatory cytokines⁴⁰⁵. Finally, Ascendis Pharma is developing a long-acting prodrug of R848 formed by conjugation of R848 onto hydrogel microbeads via proprietary linkers⁵³.

Beyond these formulations advancing to the clinic via industry, some promising preclinical platforms have emerged from academic research that have also been able to localize the effect of TLR7/8 agonists using biomaterial-based strategies. De Geest and colleagues developed amphiphilic di-block copolymers that self-assembled into NPs⁴⁰⁶ that were bound to a TLR7/8 agonist and cross-linked with pH-sensitive bis-amino-ketals via amide bond formation between reactive PFP esters and primary amines of the TLR7/8 agonist and crosslinker. Upon peritumoral administration, they observed lower tumor burden in the B16 tumor model at levels similar to that of free TLR7/8 agonist but without the systemic side effects. Lim and colleagues developed squalene emulsions encapsulating R848 in oleic acid⁴⁰⁷. Upon intratumoral administration, they observed lowered systemic IL-6 and significantly improved local IL-6, MCP-1, and MIP-1 α kinetics. Forrest et al. formulated α -tocopherol-modified R848 with tocopherol-modified hyaluronic acid using an emulsification-solvent evaporation method⁴⁰⁸. Upon intratumoral administration in 6 canines with mast cell cancer, 4 demonstrated a reduction in tumor burden, and lesions disappeared in 1 animal. Recent work by Johnson et al utilized ring opening metathesis polymerization to synthesize injectable polynorbornene (pNb)-based triblock bottlebrush copolymer hydrogels that localize the effect of R848 therapy upon intra-tumoral administration to

minimize systemic side effects⁵⁴. Here, it was shown that co-delivery of R848 with paclitaxel in optimized multicompartiment hydrogels led to enhanced cure rates and reduced toxicity compared to free drugs and nanoparticle formulations in mice bearing CT26 tumors. Nuhn and colleagues also utilized ring opening metathesis polymerization to synthesize (pNb-PEG)-(pNb-pentafluorophenyl) micelles which were covalently conjugated to a TLR7 agonist and cross-linked with pH-responsive ketal bisamines to obtain nanogels⁴⁰⁹. Interestingly, the nanogels showed dose-dependent activation of RAW 264.7 cells, whereas the soluble chains obtained upon degradation of the nanogel were immunologically silent; that is, they did not show TLR7 activity. Finally, Zhang and coworkers demonstrated that platelet-membrane coated NPs carrying R848 improved therapeutic efficacy in the MC38 colon cancer model upon intra-tumoral administration as a result of enhanced bioavailability in the tumor⁴¹⁰.



In addition to these particulate formulations of TLR agonists, another paradigm is to implant drug-releasing biomaterial matrices into a tumor resection site to achieve sustained and localized TLR signaling at the site of surgical resection. For example, Goldberg et al. developed a

biodegradable hydrogel scaffold prepared from crosslinked hyaluronic acid (HA) that entrapped R848⁵⁵. In murine models of surgical implantation of TLR agonist-loaded gels into tumor resection sites, they observed no local tumor recurrence for at least one month and significantly improved survival, with the efficacy dependent on type I IFN signaling, NK cells, and CD4 and CD8 T cells (**Fig. 18B**). Interestingly, the authors showed that these antitumor effects were observed only upon local administration of the scaffold, with minimal survival following intravenous injections or a local bolus dose of the free drug.

2.4.4 In search of synergy: combination delivery approaches

The combination of synthetic TLR7/8 agonists with other therapies offers significant potential to further enhance their potency. Combination immunotherapies are particularly ubiquitous in the context of cancer, with countless preclinical investigations and more than 1800 ongoing clinical trials in the United States alone combining immune-checkpoint blockade with other immunotherapies. TLR7/8 agonists are showing promising preclinical results in overcoming tumor resistance to checkpoint blockade^{411–413}. In the vaccine realm, work by Pulendran and coworkers demonstrated that the live attenuated yellow fever vaccine, one of the most effective immunological interventions worldwide, administered to over 400 million people, in fact activates multiple TLRs on DCs to elicit an immune response⁴¹⁴. It has long been known that TLR agonists can exhibit synergistic activation of DCs; for example, R848 combined with either a TLR4 agonist or a TLR3 agonist allowed synergistic stimulation of inflammatory cytokines in multiple human DC subsets⁴¹⁵. It is likely that TLR7/8 activation may synergize with multiple innate immune sensors or other immunostimulatory pathways beyond just TLRs to potentiate vaccine or immunotherapy responses^{416,417}.

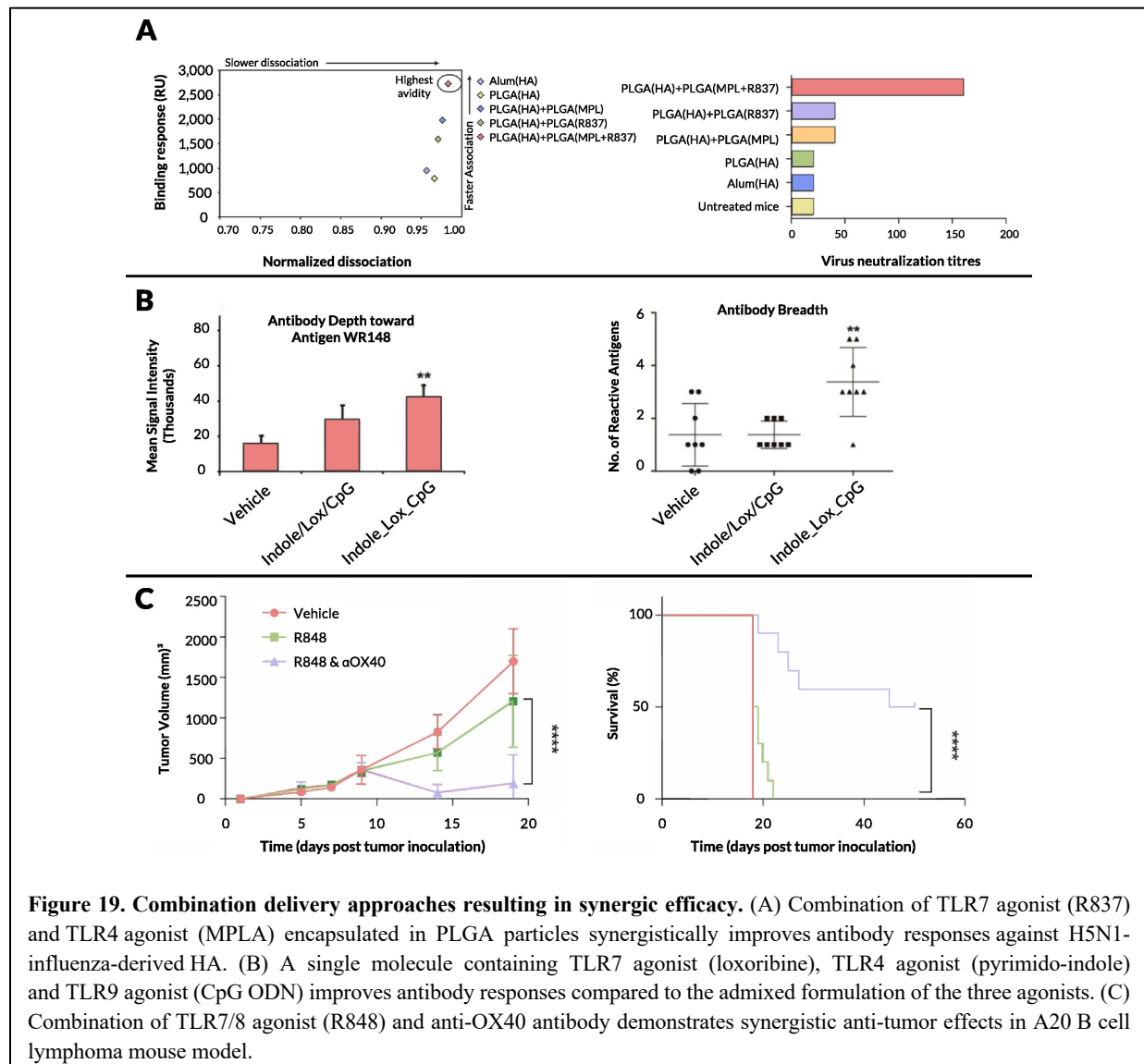
Drug carriers may have an important role to play in maximizing the impact of synergistic immune agonist drugs. Pulendran and coworkers utilized NPs similar to those described above in section 4.1.2. and demonstrated that R837 and monophosphoryl lipid A (a synthetic TLR4 agonist) encapsulated in PLGA NPs functioned synergistically when tested in multiple antigen models⁹³. They observed a significant increase in antigen-specific neutralizing antibodies and enhanced persistence of germinal centers and plasma cell responses (**Fig. 19A**). These antibody responses

were dependent on direct triggering of both TLRs on B cells and DCs, in addition to T cell help. The system was tested in other vaccination models of RMs and showed significantly improved levels of antigen-specific B cell responses as well as durable protection against rechallenge⁴¹⁸. Toxicity issues—a key concern when combining therapies—limited the dose of the TLR agonists in these NPs⁴¹⁹. This combination of TLR7/8 agonists with TLR4 agonists has been verified in numerous other studies^{420–422}. For example, Carter and colleagues tested this combination encapsulated in anionic liposomes with a recombinant malaria antigen⁴²⁰. They observed increased levels of antigen-specific IFN- γ production and IgG₂:IgG₁ levels indicative of an improved Th1 response. Hook and colleagues looked beyond liposomal structures toward cubosomes (i.e., cubic phase liquid crystalline nanostructures formed in this case from lipids), achieving similar responses⁴²¹. Additionally, Carson and colleagues observed rapid seroconversion, antigen sparing, and protective efficacy using their TLR4-TLR7 agonist combination⁴²². Shattock and colleagues demonstrated dose- and administration route-dependence of the synergy between TLR4 and TLR7/8 agonists in a Gottingen minipig model⁴²³.

Taking TLR combinations a step further, Haynes and colleagues added a TLR9 agonist into the mix and observed a durable antigen-specific antibody response⁴²⁴. Moreover, Roy and colleagues loaded this combination onto PLGA NPs and demonstrated synergistic activity in the context of antigen cross-presentation *in vitro* as well as lymph node germinal center and T helper cell responses *in vivo*⁴²⁵. Linking IMDs with other TLR agonists in a single molecule has also been shown to enhance activation of NF- κ B and inflammatory cytokines *in vitro* and improved antibody response *in vivo* (**Fig. 19B**)⁴²⁶. Analysis of APC activation by multifunctional conjugates linking ligands for multiple distinct TLRs into the same molecule indicates that synergy between TLR agonists depends upon the physical length of the linker bridging innate immune ligands, the choice of ligand combination, and the dose^{371,427}. These studies represent important early steps toward elucidating structure–activity dependence of TLR synergies, and complement work aiming to define rational TLR combinations based on the interplay between different intracellular signaling pathways^{428–434}.

In addition to studies of TLR agonist combinations as vaccine adjuvants, other groups have focused on the potential of TLR7/8 ligands to synergize with other immunotherapy modalities for cancer treatment. Illidge and colleagues combined radiation therapy with systemic R848 and

observed improved antitumor efficacy in multiple tumor models⁴³⁵. Levy et al. demonstrated that the synergistic effect of TLR7/8 agonists with anti-OX40 antibodies was explained by the fact that TLR7/8 agonists such as R848 induce expression of the OX40 target on CD4 T cells in the tumor microenvironment (Fig. 19C)⁴³⁶. Although TLR7/8 agonists could be substituted by TLR9 agonists, surprisingly, checkpoint inhibitors against PD-1, PD-L1, or CTLA-4 could not substitute for anti-OX40 antibodies. A number of other studies, however, have reported synergy between TLR7/8 agonists and checkpoint inhibitors in various other murine tumor models^{437–440}. Other attempts to augment the efficacy of synthetic TLR7/8 agonists have included combinations with antibodies such as anti-EGFR and anti-HER2/neu, cytokines such as IL-2, and photothermal therapies^{441–446}.



2.5 Conclusion and Future Outlook

Substantial evidence from preclinical studies and clinical trials suggests that synthetic TLR7/8 ligands have the potential to be powerful immunomodulators, vaccine adjuvants, and cancer therapeutics, but challenges in achieving suitable efficacy while avoiding toxicities remain a significant barrier. Recent elucidations of crystal structures, SAR analyses, and delivery approaches have led to steady progress, though systemic administration of TLR7/8 agonists still faces challenges⁴⁴⁷. Moreover, defining optimal dosing thresholds and timing intervals will be critical given that research on these compounds has followed closely on the heels of progress made on synthetic TLR4 and TLR9 agonists wherein significant efforts toward understanding tolerability and circadian effects have been pursued⁴⁴⁸⁻⁴⁵¹. TLR tolerance, which is defined as a transient state of refractoriness of TLRs to subsequent activation post initial dosing, has evolved to avoid the induction of auto-immunity through repeated TLR agonism; however, it has important implications for dosing schedules involving synthetic TLR7/8 agonists that aim to generate pro-inflammatory immune responses⁴⁵². Although TLR7 tolerance has been observed in multiple studies, the mechanism of induction is still an active area of research⁴⁵³⁻⁴⁵⁷. Initial studies provide confidence that dosing schemes can be devised that avoid TLR7 tolerance though this phenomenon must be studied in further detail to ensure maximum efficacy of these compounds^{458,459}. Moreover, the dependence of TLR expression and activity of agonists on circadian biology has yielded promising results in other agonist systems but is yet to be explored in detail for TLR7/8 agonism^{460,461}. Finally, as touched upon briefly in the previous sub-section, defining the synergistic role of synthetic TLR7/8 agonists in combination with established as well as emerging treatments is of utmost importance in our endeavor to achieve long-lasting cures to cancer, infectious diseases, and allergic and autoimmune conditions.

Chapter 3

Engineering kinetics of TLR7/8 agonist release from bottlebrush prodrugs enables tumor-focused immune stimulation

This chapter is adapted from Bhagchandani et al Science Advances (2023). This work was a collaborative effort wherein Dr. Farrukh Vohidov, Dr. Christopher Brown, Dr. Bin Liu assisted with synthesis of R848-BPDs. Dr. Lauren Milling assisted with biological assays and Evelyn Yuzuo Tong performed the single-cell RNA sequencing analysis.

3.1 Introduction

Therapies rooted in modulating the immune system have played a crucial role in the treatment of infectious diseases and, more recently, have paved the way for a paradigm shift toward re-defining cancer treatment. Cancer immunotherapies, such as antibodies blocking PD-1/PD-L1 interactions, have demonstrated clinical activity in diverse oncological indications⁴⁶². A majority of patients, however, still do not respond to currently available immunotherapies, possibly due to an inability to generate potent cytotoxic T lymphocyte (CTL) responses against tumor neoantigens as well as the immunosuppressive and tolerizing effects of the tumor microenvironment^{34,463,464}. In preclinical models of immunotherapy-resistant tumors, antigens derived from dying tumor cells are often not processed efficiently by myeloid cells such as dendritic cells (DCs), monocytes, and

macrophages due to a lack of activation and co-stimulatory signals that are necessary for presentation of tumor-derived peptides to T cells^{258,465–467}. Thus, shifting the myeloid activation state by promoting inflammation in the tumor microenvironment through innate immune stimulation has the potential to play an important role in reversing tumor microenvironment immunosuppression^{27,257,468,469}.

Therapeutic activation of Toll-like receptors (TLRs) is one of the most extensively studied approaches to activate myeloid cells, trigger acute inflammation, and stimulative adaptive immunity in tumors^{138,141}. In particular, targeting TLR7/8 has been shown to be very effective at eliciting acute inflammation: activation of TLR7 expressed by plasmacytoid DCs leads to production of type 1 interferons (IFNs), while TLR8 is expressed by conventional DCs, monocytes, and macrophages and its activation triggers the production of IL-12 and other pro-inflammatory cytokines⁴⁷⁰. A large body of work has focused on the development of synthetic ligands for TLR7/8 following the discovery that the anti-viral properties of imidazoquinolines (IMDs) was mediated by activation of these TLRs¹¹⁸. One of the first compounds in this class, imiquimod (R837), showed promising results in clinical trials for topical treatment of skin malignancies such as basal cell carcinoma and received FDA approval in 2004^{108,471}. This success led to the development of more potent IMDs such as resiquimod (R848) & 852-A for systemic treatment of metastatic cancers. Intravenous (*i.v.*) administration of these compounds in patients with solid tumors (colon, breast, ovarian and cervical cancers) showed promising results in terms of disease stabilization in a proportion of patients and increased levels of type I IFNs and pro-inflammatory cytokines such as tumor necrosis factor- α (TNF- α) and interferon- γ (IFN- γ), indicating potent immune activation^{250,251}. However, patients receiving these compounds experienced severe side effects due to systemic cytokine induction, ultimately leading to premature discontinuation of clinical trials. The prevalence of severe immune-related adverse events (irAEs) due to systemic exposure has presented a major bottleneck in expanding the use of IMDs and other innate immune stimulators⁴⁷². Thus, strategies to focus the action of IMDs in the tumor microenvironment are needed to unlock the potential of these TLR agonists for cancer immunotherapy.

One strategy to bias the delivery of IMDs to tumors involves their physical encapsulation in micro- & nano-particulate carriers;⁶⁰ however, to date, the tested formulations have had relatively short (<48 h) release half-lives that result in systemic toxicity^{365,376,377,473}. To overcome

this challenge, IMDs have been chemically conjugated to spherical “nanogel” scaffolds (~50 nm diam.)³³⁷ or aggregates of linear polymers (~700 nm diam.)³³⁵, which enabled enhanced innate immune cell uptake and retention in lymph nodes following parenteral injection. Vesicles (~200 nm diam.) formed from PEGylated IMD prodrugs have also been prepared, which are designed to release active TLR7 agonists (TLR7a) in endosomes in response to β -glucuronidase and esterase-mediated release³⁸⁶. While these strategies have suggested a benefit of using nanoscale particle structures to improve the activity of TLR7 agonists following subcutaneous dosing as vaccine adjuvants, they have not been tested in the context of *i.v.* administration, the preferred approach for treatment of metastatic disease where systemic toxicities are more challenging to overcome. In the setting of systemic administration, self-aggregating nanoparticles (~20 nm) based on peptides linked to a charge-modifying group and IMDs conjugated to a hydrophobic block showed no therapeutic efficacy in the absence of a tumor neoantigen when injected *i.v.* in the treatment of syngeneic mouse tumors³³². This study highlights the challenges associated with obtaining effective tumor-focused innate immune activation upon systemic treatment with IMDs. Key questions remain regarding the relation between kinetics of IMD release, systemic side effects, and anti-tumor efficacy, which could prove crucial to identifying a therapeutic window for these potent immunostimulators.

To address this challenge that continues to hamper progress in this field, we hypothesized that tuning drug release kinetics to align with the timing of tumor accumulation by a nanocarrier could open a therapeutic window for safe, systemic administration. We created a modular R848 bottlebrush prodrug (R848-BPD) library wherein activation kinetics are decoupled from carrier shape and size as an approach to enable fine tuning of IMD release to optimize potency and safety. R848-BPDs have antibody-like sizes (~10 nm), narrow size distributions, and an average of 10 R848 molecules are linked to a rigid polynorbornene backbone with PEG side chains. By carefully tuning the molecular structures of the cleavable linkers, a family of R848-BPDs that release active R848 at rates varying over 5 orders of magnitude, yet otherwise equivalent properties, were generated. Correlation of the prodrug activation kinetics with a range of safety and efficacy biomarkers enabled us to identify R848-BPDs that were both safe for systemic administration and resulted in potent tumor inhibition in multiple tumor models as a monotherapy or in combination with anti-PD-1 (α -PD-1) antibody treatment. Moreover, we show that anti-tumor efficacy of R848-BPDs was mediated by sustained myeloid activation and re-programming in the tumor

microenvironment and draining lymph nodes. Altogether, this work provides a new category of safe and effective TLR agonist prodrugs for potential clinical translation, and offers insights into how tissue exposure kinetics via molecular design can be leveraged to optimize immune stimulation, which may apply to other small-molecule innate immunomodulators such as STING agonists, RIG-I agonists, and other TLR agonists in the future.

3.2 Results

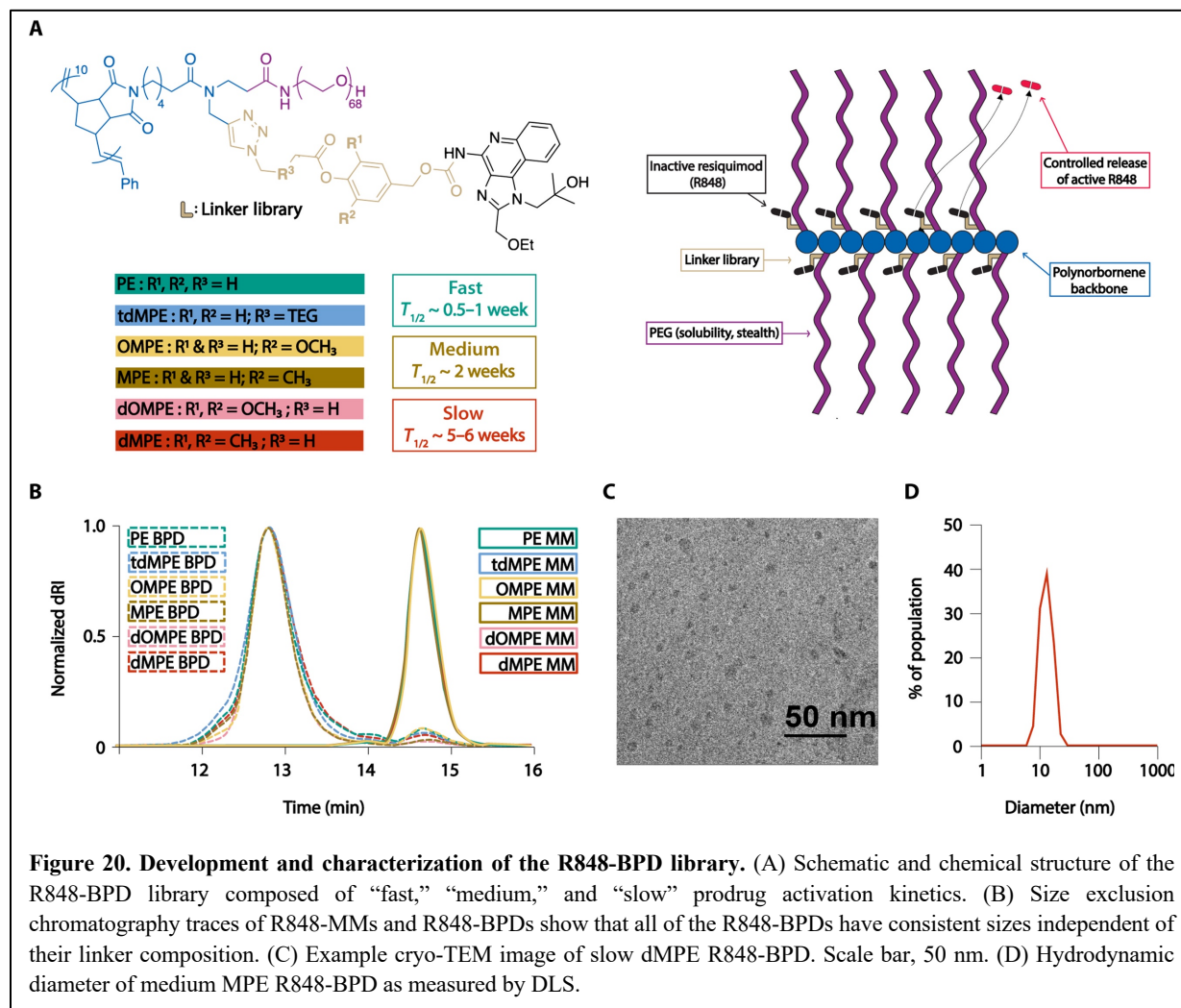
3.2.1 Synthesis and characterization of a library of R848-BPDs with varying linkers

The R848-BPD approach is summarized schematically in **Fig. 20A**. Macromonomers (MMs) bearing an *exo*-norbornene imide polymerizable group bound to 3 kDa poly (ethylene glycol) (PEG) and one of six azido-R848 ester-based prodrugs were prepared through copper-catalyzed azide-alkyne cycloaddition click chemistry. The aryl ester-based linkers were molecularly tuned to achieve release half-lives that span ~5 orders-of-magnitude in neutral buffer potentially allowing for controlled modulation of systemic versus tumor activation. Each of these six MMs (10 equivalents) was subjected to ring-opening metathesis polymerization (ROMP) using a Grubbs 3rd-generation initiator (1 equivalent) to provide six R848-BPDs with theoretical backbone degrees of polymerization (DP) of 10. The resulting polymers showed expected overlapping profiles by size exclusion chromatography (SEC), and had identical sizes and morphologies as assessed by dynamic light scattering (DLS) and cryogenic transmission electron microscopic (cryo-TEM) (**Fig. 20B-D**). The small-molecule prodrug precursors, MMs, and R848-BPDs were also characterized using ¹H and ¹³C nuclear magnetic resonance (NMR) spectroscopy and mass spectrometry where appropriate.

3.2.2 R848-BPDs display tunable release characteristics ranging from a few days to several weeks

Previously, we showed that MM prodrug cleavage rates determine the therapeutic index of BPDs based on bromodomain and extra-terminal protein inhibitors (BETi), with fast-activating

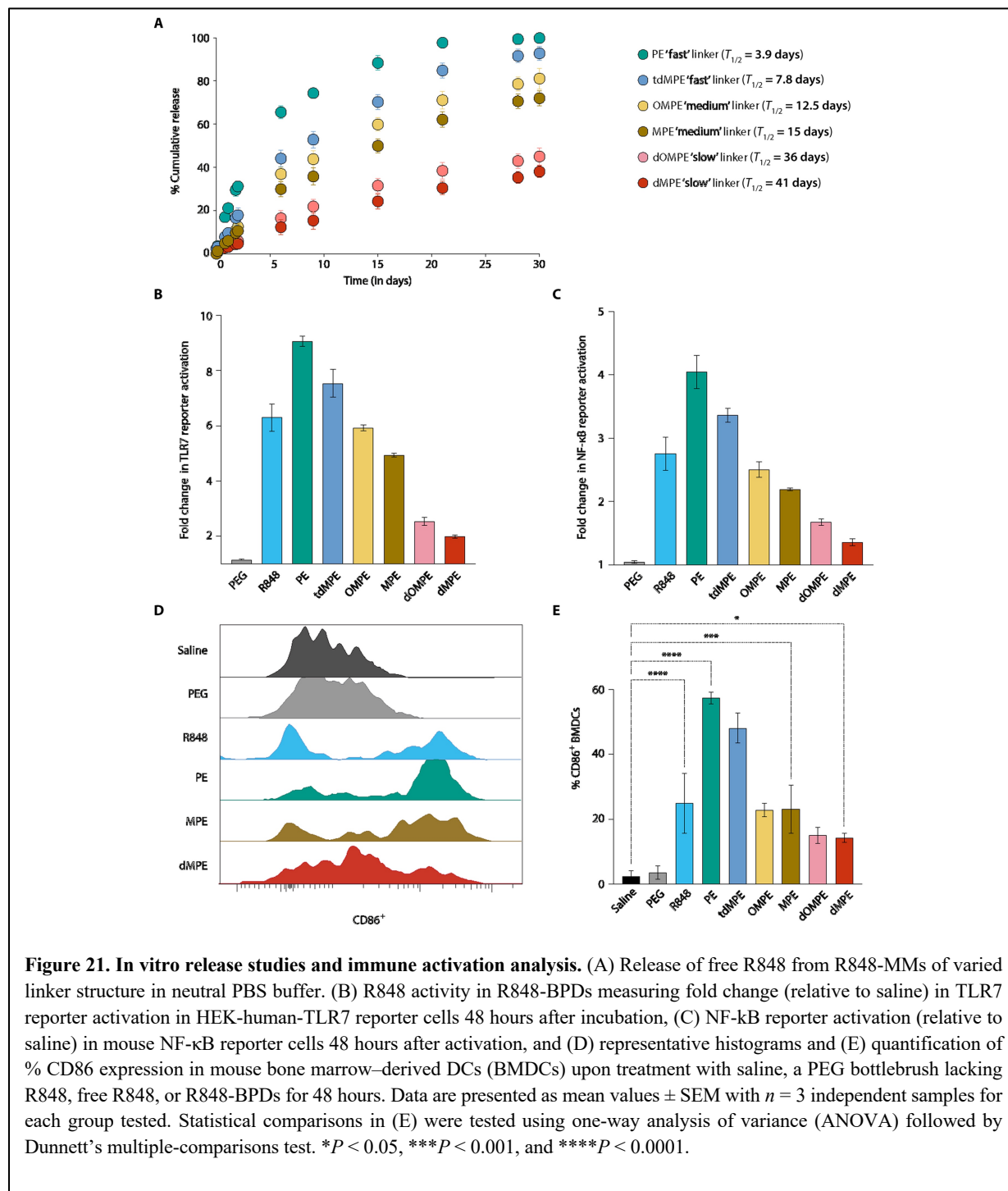
linkers ($t_{1/2}$ ~ hours) leading to toxicities similar to free drug, very slow linkers ($t_{1/2}$ ~ 30 d) lacking efficacy, and medium-rate linkers ($t_{1/2}$ ~4–6 d) eliciting optimal responses without toxicity in a murine breast cancer model⁴⁷⁴. Given that the R848-BPDs described here have very similar sizes, shapes, compositions, and active drug mass fractions (~10%), we hypothesized that their safety and efficacy should similarly be a function of the R848 aryl ester linker cleavage rate, which as noted above is a function of hydrolytic and esterase cleavage activity *in vivo*.



To assess the rate of hydrolytic cleavage under model conditions, each R848-MM was dissolved in pH 7.4 PBS buffer at 37 °C; samples were taken over time to quantify the amount of free R848 by LC-MS. Variations in R848 release $t_{1/2}$ values from ~4 days to ~40 days were observed (Fig. 21A), which correlated with the local steric and electronic environment of each aryl ester linker as defined by the substituents R₁ and R₂ as well as the composition of the linear

carbonyl component (R₃). For example, the fastest release was observed when R₁ and R₂ = H, the smallest substituents investigated (sample **PE**; $t_{1/2} \sim 3.9$ d, **Table S2**). Increasing the steric hindrance and electron density of R₁ and R₂ dramatically slows hydrolysis: when one (**MPE**) or two (**dMPE**) *ortho*-methyl groups are introduced, $t_{1/2}$ increases to 15 d and 41 d, respectively (**Table S2**). Similar effects were observed for less bulky yet more electron donating methoxy groups: when one (**OMPE**) or two (**dOMPE**) *ortho*-methoxy groups were introduced, $t_{1/2}$ values were 12.5 d and 36 d, respectively (**Fig. 2A, Table S2**). Finally, the steric and electronic effects of methyl substitution at R₁ and R₂ could be mitigated through the introduction of a more hydrophilic triethylene glycol at R₃ (**tdMPE**; $t_{1/2} \sim 7.8$ d, **Table S2**). Altogether, these 6 R848-BPDs are divided into “slow” (**MPE** and **OMPE**), “medium” (**dMPE** and **dOMPE**), and “fast” (**PE** and **tdMPE**) release in subsequent discussion based on these measured hydrolysis kinetics. Finally, we note that while ester cleavage is rate-limiting in this system, release of free R848 requires subsequent 1,6-elimination of a *para*-quinone methide derivative and expulsion of one molecule of CO₂ from the resulting carbonic acid. Under the conditions used for these release studies, we have never observed either the phenolic or carbonic acid intermediates, suggesting that these steps are very fast compared to ester cleavage. Moreover, we note that *para*-quinone methides are hydrolyzed rapidly under aqueous conditions to generate benign alcohols as products⁴⁷⁵.

Next, we sought to correlate these MM prodrug activation kinetics with the activity of each R848-BPD *in vitro* using TLR7 and NF- κ B reporter cell lines (both human and mouse). We note that while BPD hydrolysis is generally much slower than MM hydrolysis, the hydrolysis rates as a function of linker composition are expected to correlate⁴⁷⁴. In agreement with this concept, the R848-BPDs showed linker-dependent activation of both cell types compared to saline control that directly correlated with the measured half-lives of MM prodrug activation⁴⁷⁶. As shown in **Fig. 21B**, incubation of fast-releasing R848-BPDs with human TLR7 reporter cells for 48 hr triggered greater TLR activation than free R848, perhaps due to improved cell uptake, but medium and slow R848-BPDs displayed similar or lower activation compared to R848, as expected if the TLR agonist is inactive until released from the BPD carrier. Similar patterns of cellular activation were measured using NF- κ B reporter cells (**Fig. 21C**). When R848-BPDs were incubated with mouse bone marrow-derived dendritic cells or control conditions for 48 h, upregulation of activation marker CD86, as determined by flow cytometry²⁶², also correlated with linker composition.



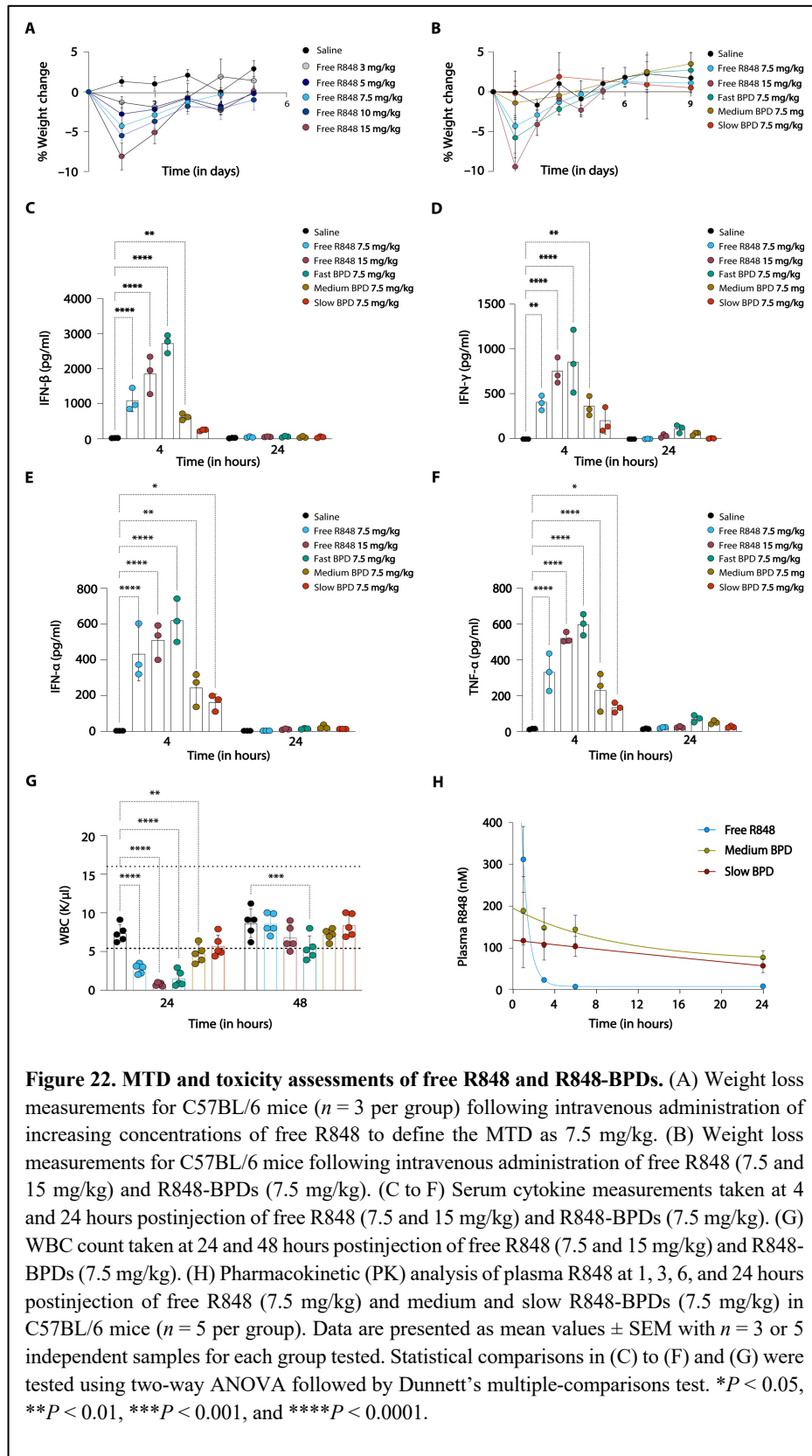
For example, fast, medium, and slow R848-BPDs upregulated CD86 expression in ~60%, ~25%, and ~10% of BMDCs, respectively (Fig. 21C). Altogether, these results demonstrate that the hydrolysis kinetics of R848-BPDs can be tuned through molecular design and that these kinetics correlate with TLR activation *in vitro*, yielding increased (for “fast”), similar (for “medium”), and

decreased (for “slow”) activation compared to R848 alone.

3.2.3 R848-BPDs with optimal linkers have greater maximum tolerated doses (MTDs) and broad therapeutic windows compared to free R848

The maximum tolerable dose (MTD) of free R848 was determined in healthy C57BL/6J mice by monitoring for weight loss and clinical signs (body condition score measurements) over a period of 1 week following a single dose⁴⁷⁷. Mice dosed at 10 mg/kg & 15 mg/kg demonstrated visible signs of restricted movement and lethargy in addition to weight loss greater than 5% of the original body weight (**Fig. 22A**); thus, 7.5 mg/kg was established as the MTD. We then evaluated 3 different R848-BPDs (‘fast BPD’, PE linker; ‘medium BPD’, MPE linker; ‘slow BPD’, dMPE linker) at doses of 75 mg/kg, 150 mg/kg, 300 mg/kg, 600 mg/kg, and 750 mg/kg, which, given the ~10% R848 loading of the BPDs, correspond to 1x, 2x, 4x, 8x and 10x the 7.5 mg/kg MTD of free R848, respectively (**Fig. 22B**). Notably, while the ‘fast PE’ BPD had a similar MTD compared to free R848 when normalized by the mass of R848, the ‘medium MPE’ and ‘slow dMPE’ BPDs exhibited MTDs at 4x and 8x higher R848 concentrations, respectively. Serum was collected 4 h, 24 h and 48 h post injection and assayed for cytokines commonly released downstream of TLR-7/8 activation; linker-dependent increases in type I IFNs (both IFN- α and IFN- β) as well as pro-inflammatory cytokines such as IFN- γ , IL-6, MCP-1, and TNF- α were observed (**Fig. 22C**). While the ‘fast PE’ BPDs induced even higher levels of systemic cytokine production (greater than or equal to 2x MTD of free R848), both the ‘medium MPE’ and ‘slow dMPE’ BPDs induced lower serum cytokine levels when given at equivalent R848 dosing levels (**Fig. 22C**). This reduced toxicity was not simply reflecting delayed activation of cytokine production by the slowed release kinetics, as cytokine levels remained low at 24 and 48 hr (**Fig. 22C**). Whole blood was collected in the different groups and subjected to a blood panel analysis wherein white blood cell (WBC) count served as a proxy for drug concentration in the blood, since R848 induces lymphocytes to leave blood transiently in a dose-dependent manner⁴⁷⁸. Free R848 and ‘fast PE’ showed a lowered WBC count, whereas ‘medium’ and ‘slow’ BPDs remained within limits of the normal range (**Fig. 22D**). Acute toxicities were also assessed via liver enzyme

biomarkers (alanine aminotransferase and aspartate aminotransferase) and blood urea nitrogen as



surrogates for liver and kidney function, respectively. In all cases, the ‘medium’ and ‘slow’ BPDs consistently showed normal levels of the relevant biomarkers (as opposed to free R848) even in the early time-points (acute phase), suggesting that they are safer than R848 alone. To understand these differences in toxicity, we analyzed the pharmacokinetics of R848 following dosing of free R848 or the R848-BPDs. The ‘medium’ and ‘slow’ BPDs showed lower initial free drug concentrations in serum compared to free R848, which display a peak at 30 min followed by clearance in a few hours (Fig. 22E, Table 4).

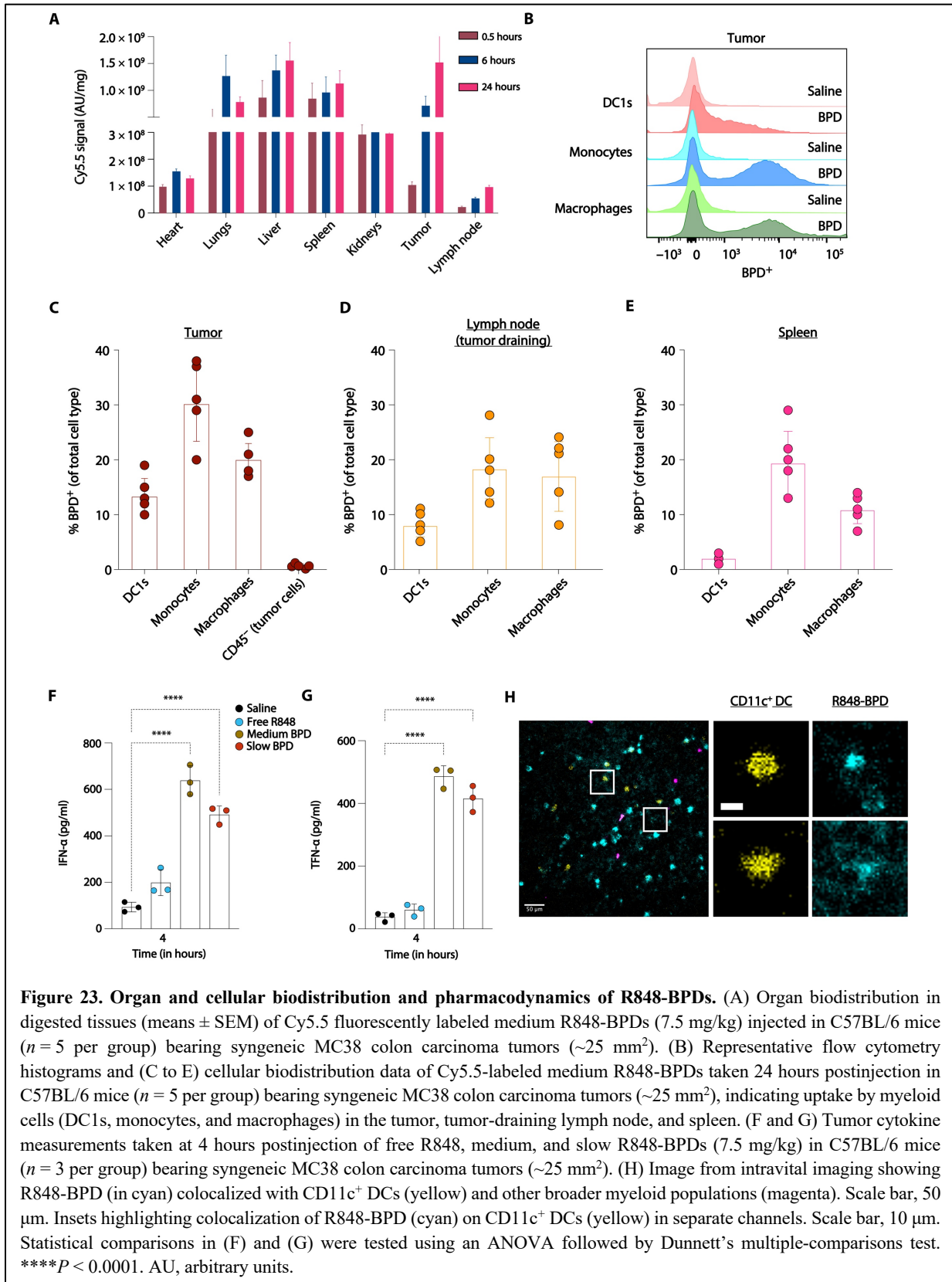
	Y0	Plateau	K	Half Life (hrs)	Tau	AUC
Free R848	1352	7.219	1.484	0.467	0.6738	525.1
Medium BPDs	195.1	66.18	0.101	6.843	9.873	110.4
Slow BPDs	118.5	-216.0	0.008	82.92	119.6	67.87

Table 4. One phase decay curve fitting of plasma concentrations for Free R848, Medium BPDs, & Slow BPDs in non-tumor bearing C57BL/6 mice

3.2.4 R848-BPDs display tumor accumulation and uptake by innate immune cells in the tumor and tumor-draining lymph nodes compared to R848

Based on its promising pharmacodynamic activity, we next evaluated the biodistribution of fluorescently-labeled R848-BPDs prepared with the medium-release rate MPE linker following *i.v.* injection in mice bearing syngeneic MC-38 colon carcinoma tumors. BPDs, by virtue of their small size and non-spherical shape, have been shown to display effective accumulation and penetration into subcutaneous and orthotopic murine tumors, with liver, spleen, and lungs as other major clearance tissues⁴⁷⁴. Here, the R848-BPD performed similarly, with the highest levels of tissue accumulation in tumors and the liver (**Fig. 23A**). The BPD continued to increase in accumulation in the tumor through 24 hr, and similar accumulation was observed in the tumor-draining lymph node albeit at much lower levels (**Fig. 23A**). Flow cytometry analysis of the tumor and tumor-draining lymph nodes revealed uptake of the R848-BPDs by innate immune cells, including conventional type 1 dendritic cells (cDC1s), monocytes, and macrophages (**Fig. 23B-C**). Approximately 20% of macrophages in the tumor were positive for R848-BPDs, along with 30% of monocytes and 15% of cDC1s (**Fig. 23B-C**). When we treated tumor-bearing mice with free R848, “slow-releasing” BPD-R848, or “medium” release rate BMD-R848, we found the substantial tumor accumulation of BPDs correlated with the generation of high levels of pro-inflammatory cytokines including type I IFN and TNF- α in the tumor microenvironment, which were not induced to statistically significant levels over saline-treated tumors by free R848 (**Fig. 23D**). Finally, we verified this cell uptake in the tumor microenvironment via intravital fluorescence imaging, showing the R848-BPDs (cyan) co-localized with CD11c⁺ DCs (yellow)

and other myeloid cells (magenta) (Fig. 23E).



3.2.5 Systemically administered R848-BPDs elicit therapeutic responses both as monotherapies and in combination with checkpoint blockade therapy in mouse models of colon carcinoma

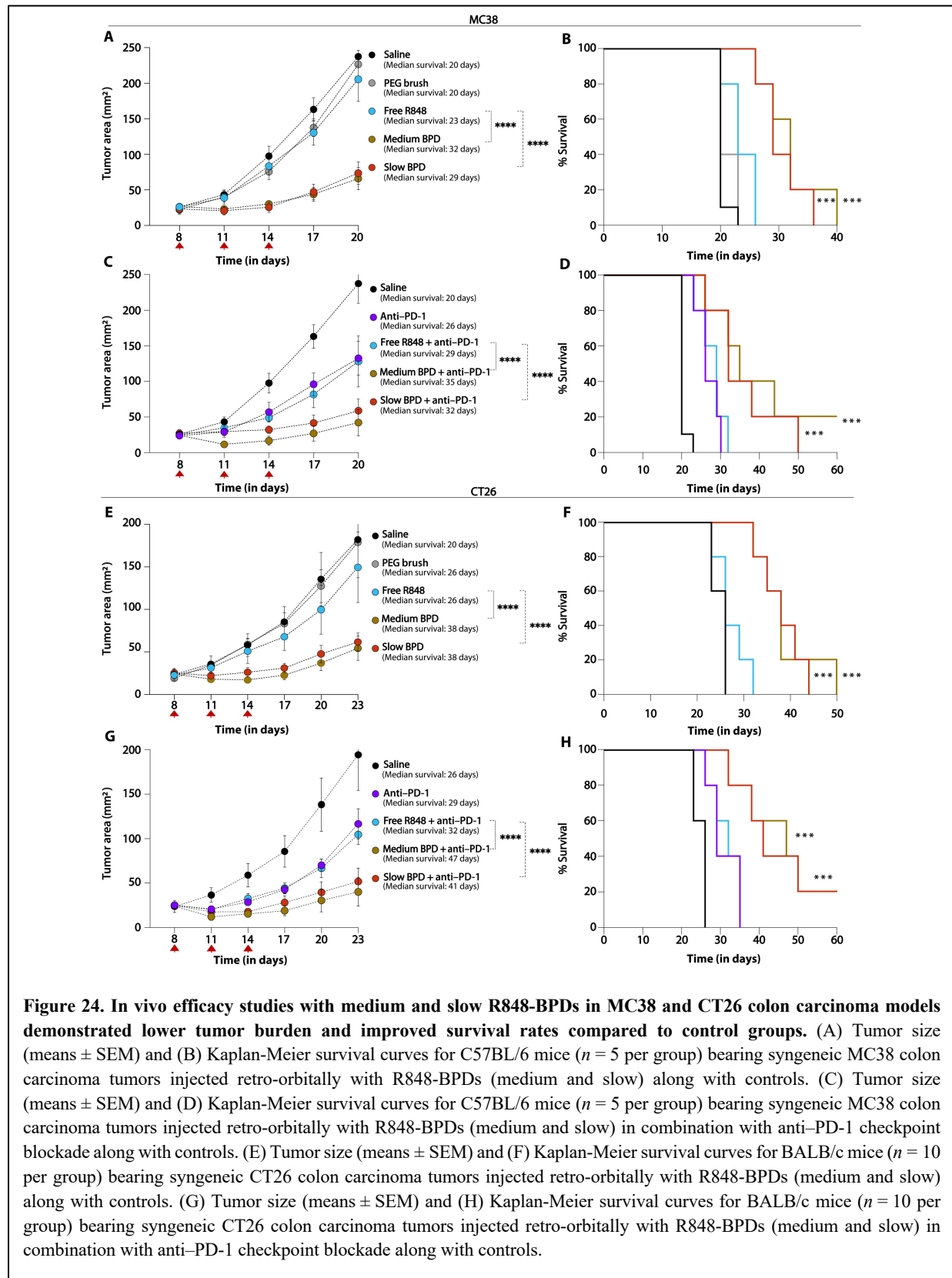
Given these promising biodistribution results, the therapeutic efficacy of R848-BPDs was evaluated in mice bearing subcutaneous MC38 tumors ($n = 5$). Two of the R848-BPDs (with medium-releasing MPE or slow-releasing dMPE linkers) along with free R848 were administered intravenously at their respective MTDs to the mice once every 3 days for 3 total doses. Notably, the R848-BPDs displayed a substantial slowing of tumor progression (p-value < 0.0001) and improved overall survival compared to mice given free R848 (**Fig. 24A**). As noted above, improved innate immune stimulation by TLR7/8 activation could boost responses to immunotherapies such as immune checkpoint blockade (ICB)⁴⁷⁹. Thus, following these monotherapy studies, we next performed combination multi-dose *in vivo* efficacy studies where mice bearing MC38 tumors were treated with R848-BPDs (MPE or dMPE) in combination with anti-PD-1 (200 ug). Animals treated with R848-BPDs combined with anti-PD-1 showed even better tumor control (p-value < 0.0001) and longer-term survival compared to mice given free R848 in combination with anti-PD-1 or anti-PD-1 alone (**Fig. 24B**).

In order to validate the generality of these treatment responses, we evaluated R848-BPDs (MPE & dMPE) in BALB/c mice bearing CT-26 colon carcinoma tumors ($n = 5$) with the same dosing pattern. Here, R848-BPDs (MPE & dMPE) treatment delayed tumor outgrowth (p-value < 0.0001) and significantly increased median survival compared to untreated tumors, while free R848 had no significant impact on tumor growth or overall survival (**Fig. 24C**). Finally, combining R848-BPDs with anti-PD-1 in the CT-26 model further boosted the response, extending survival and leading to complete responses in 20% of the animals (**Fig. 24D**).

3.2.6 R848-BPDs exert anti-tumor effects via sustained activation of innate immune cell subsets

Having shown that R848-BPDs display promising capability to control tumor growth and improve survival in murine tumor models, we next sought to examine whether their mechanism of action is due to immune stimulation via TLR activation since R848 canonically activates TLR7/8 expressed by myeloid cells. To determine which cell types contribute to the observed anti-tumor effects of the R848-BPDs, we performed single-cell RNA-sequencing (scRNA-seq) on tumors 24h

post dosing with either Saline (n=3), Free R848 (n=3), or R848-BPDs (n=2).



After removing MC38 tumor cells, we analyzed 8,017 non-malignant cells, resolving 8 broad cell types and 16 fine cell subsets across 3 conditions (**Fig. 25A**). First, we tested for changes in the relative frequencies of cell subsets across conditions. To account for compositional dependencies among cell subsets within each tumor, we conducted both Fisher exact tests and multivariate Dirichlet regression analysis⁴⁸⁰. This revealed distinct innate cell subsets enriched by the R848-BPDs: *Cd38⁺Saa3⁺* monocytes and *Cd38⁺Saa3⁺* macrophages, (Dirichlet p.adj = 7.55E-06 and Fisher p.adj = 2.33E-101, Dirichlet p.adj = 9.28E-06 and Fisher p.adj = 1.61E-124, respectively), in tandem with decreases in *Ly6c^{hi}* monocytes and *Spp1⁺* macrophages (Dirichlet p.adj = 1.33E-05 and Fisher p.adj = 9.29E-53, Dirichlet p.adj = 4.12E-06 and Fisher p.adj = 1.55E-119, respectively) when comparing R848-BPDs to free R848 (**Fig. 25B**). Further, when we performed differential expression analyses within each subset, we found that R848-BPD therapy induced distinct expression profiles in macrophages, monocytes, and conventional type I DCs (cDC1s), but not tumor-infiltrating lymphocytes. Gene set enrichment analyses over differentially expressed genes showed that *Cd38⁺Saa3⁺* macrophages were enriched in pathways related to inflammatory response, IFN and reactive oxygen species (**Fig. 25C**). Moreover, transcription factor inference analysis using DoRothEA confirmed that *Cd38⁺Saa3⁺* macrophages were enriched for expression of inflammation-related transcription factors (TFs), such as *Irf1*, *Irf9*, *Stat1* and *Foxo3*, compared to the *Spp1⁺* macrophages previously reported to be immunosuppressive with pro-tumorigenic roles (**Fig. 25D**)^{481,482}. Relatedly, as a nicotinamide adenine dinucleotide (NAD)-consuming enzyme, CD38 has been shown to be upregulated in M1 macrophages in both mice and humans upon acute or chronic inflammation, suggesting an anti-tumor pro-inflammatory effect of R848-BPDs in macrophages⁴⁸³.

Similarly, we identified an activated DC population, exhibiting high expression of *Ccr7*, *Ccl22*, *Ccl5*, *Cxcl16*, *Il12b* (**Fig. 25B**) and strong inflammation-related TF expression, including *Irf1* and *Nfkb1* (**Fig. 25C**), akin to previously reported tumor-infiltrating *CCR7⁺* DCs that secrete interleukin-12 and activate T cells to increase anti-tumor activity⁴⁸⁴. While resting and activated DC populations were present in all experimental conditions, activated DCs were modestly enriched upon R848-BPD treatment (Fisher p.adj = 6.96E-08 when comparing R848-BPDs to free R848; not significant by multivariate Dirichlet regression analysis). Collectively, our data suggest that R848-BPDs stimulate monocytes, macrophages, and DCs to yield a more pro-inflammatory state,

initiating anti-tumor activity.

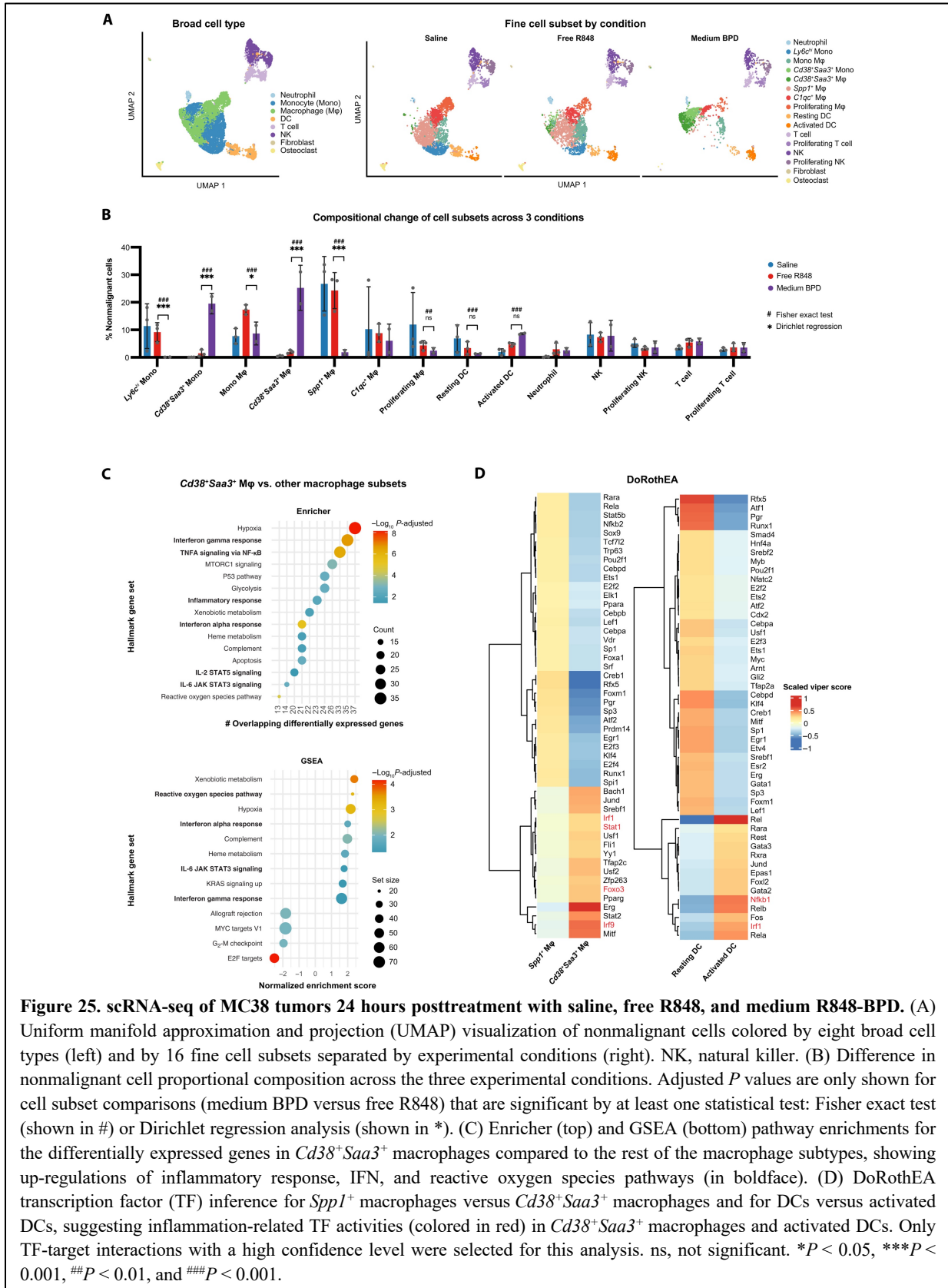


Figure 25. scRNA-seq of MC38 tumors 24 hours posttreatment with saline, free R848, and medium R848-BPD. (A) Uniform manifold approximation and projection (UMAP) visualization of nonmalignant cells colored by eight broad cell types (left) and by 16 fine cell subsets separated by experimental conditions (right). NK, natural killer. (B) Difference in nonmalignant cell proportional composition across the three experimental conditions. Adjusted P values are only shown for cell subset comparisons (medium BPD versus free R848) that are significant by at least one statistical test: Fisher exact test (shown in #) or Dirichlet regression analysis (shown in *). (C) Enricher (top) and GSEA (bottom) pathway enrichments for the differentially expressed genes in $Cd38^+Saa3^+$ macrophages compared to the rest of the macrophage subtypes, showing up-regulations of inflammatory response, IFN, and reactive oxygen species pathways (in boldface). (D) DoRoThEA transcription factor (TF) inference for $Spp1^+$ macrophages versus $Cd38^+Saa3^+$ macrophages and for DCs versus activated DCs, suggesting inflammation-related TF activities (colored in red) in $Cd38^+Saa3^+$ macrophages and activated DCs. Only TF-target interactions with a high confidence level were selected for this analysis. ns, not significant. * $P < 0.05$, *** $P < 0.001$, ## $P < 0.01$, and ### $P < 0.001$.

To assess if the changes induced in the TME extended to the tumor-draining lymph nodes (TDLNs), we carried out immunophenotyping studies at 24, 48 and 72h post R848-BPD dosing. CD86 expression levels measured for up to 72h pointed to sustained activation of cDC1s, monocytes, and macrophages when compared with free R848 and saline-treated controls (**Fig. 26A**). To gain further insight into the pathways and cell types most critical for the effectiveness of R848-BPD therapy, we analyzed therapeutic responses in mice lacking TLR7 or deficient in key DC/myeloid cell populations. As expected, there was a complete abrogation of anti-tumor efficacy in TLR7 knockout mice, indicating that TLR7 activation is necessary for the efficacy of the R848-BPDs even though IMDs have been shown to activate other innate immune pathways (**Fig. 26B**)¹²⁶. We tested the relative importance of macrophages to the therapeutic response by treating animals in the presence of depleting antibodies against F4/80. As shown in **Fig. 26B**, therapeutic efficacy was substantially reduced under this depletion condition.

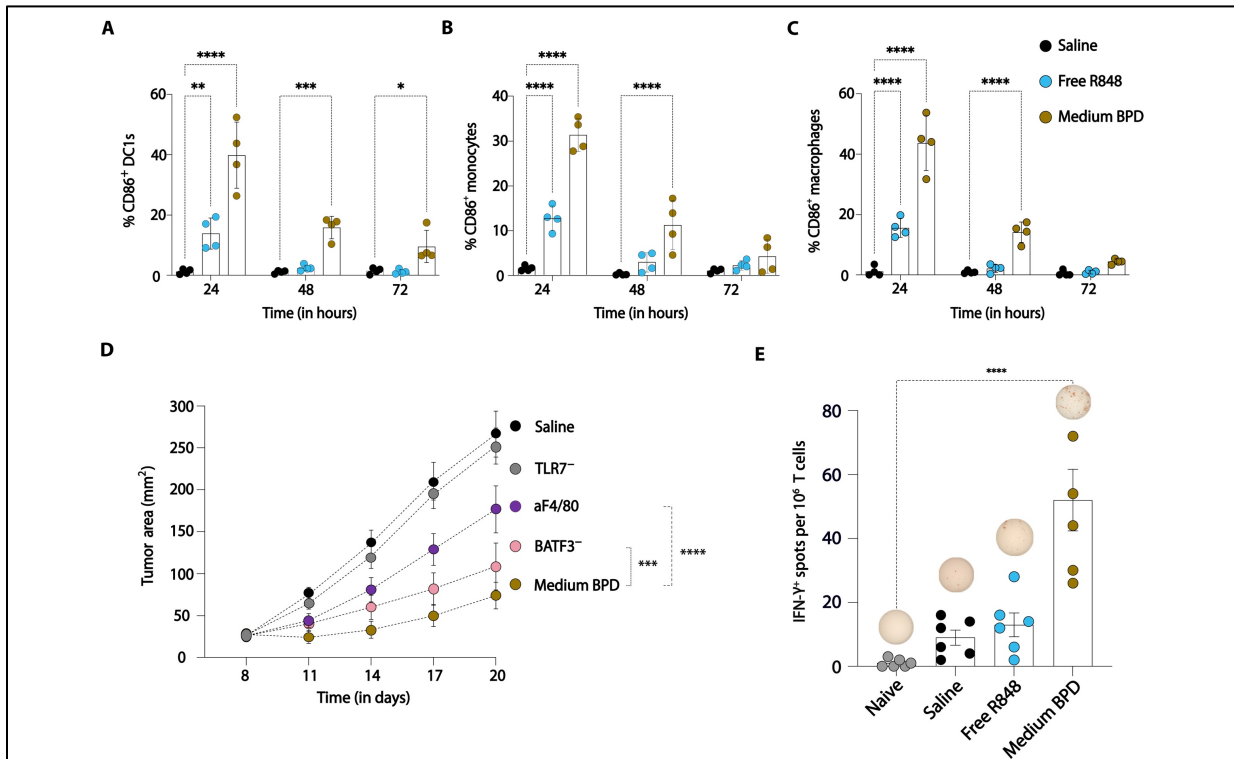


Figure 26. Myeloid cell activation is a key requirement for T cell priming and antitumor efficacy of R848-BPDs. (A to C) Immunophenotyping of tumor-draining lymph nodes 24, 48, and 72 hours after R848-BPD dosing of C57BL/6 mice ($n = 4$ per group) bearing syngeneic MC38 tumors ($\sim 30 \text{ mm}^2$). (D) Mice ($n = 5$ per group) bearing MC38 tumors ($\sim 25 \text{ mm}^2$) were treated with medium BPD (7.5 mg/kg on days 8, 11, and 14), and tumor growth was followed longitudinally. Treatment experiments in wild-type mice treated with depleting antibodies against F4/80, BATF3 knockout mice, and TLR7^{-/-} mice are shown. (E) C57BL/6 mice bearing MC38 tumors ($n = 6$ per group) were injected with R848-BPDs along with controls, and T cells were isolated on day 7 posttreatment and cocultured with irradiated MC38 cells for IFN- γ enzyme-linked immunosorbent spot (ELISpot) analysis.

Finally, an important potential mechanism of action for R848-BPD therapy would be activation of cross-presenting dendritic cell populations, which capture tumor antigens and migrate to tumor-draining lymph nodes to activate tumor-specific CD8⁺ T cells. Enzyme-linked immunosorbent spot (ELISPOT) analysis of IFN- γ production was performed on T cells isolated from the spleen of mice 7d after treatment with 1 dose of either saline, free R848 or R848-BPDs. Upon culturing with irradiated MC38 cells, we observed that even a single dose of R848-BPDs was able to amplify the endogenous T cell response against MC38 tumors (**Fig. 26C**). Consistent with this finding, treatment of mice deficient in Batf3-dependent cross-presenting DCs also led to a significant reduction in anti-tumor efficacy (**Fig. 26B**). Thus, we have demonstrated that our R848-BPD approach can efficiently activate myeloid cells to promote T cell responses against tumors to boost efficacy, while minimizing immune-related adverse events commonly associated with systemic administration of TLR7/8 agonists.

3.3 Discussion

Following imiquimod (R837) receiving FDA approval as a topical treatment for actinic keratosis and basal cell carcinoma, there was a significant push toward advancing more potent IMDs such as resiquimod (R848) into clinical studies using systemic administration in the context of melanoma and other solid malignancies^{273,485-487}. A striking observation in these clinical trials was the significant levels of inflammation that correlated with objective responses in primary and metastatic lesions in multiple tumor types; however, these anti-tumor responses occurred concomitant with severe grade 3 and 4 iRAEs, which halted the clinical progress of these compounds^{255,488,489}. This outcome was attributed to unacceptably high inflammatory cytokine levels (such as TNF- α) in the blood with multiple studies commenting on the narrow therapeutic index available for systemic delivery^{60,252}.

We hypothesized that a prodrug system that preferentially releases IMDs after they have accumulated in the tumor would be able to address this issue. Our approach involved designing a small library of novel linkers for tuning IMD release rates from BPDs, with the goal of maximizing tumor accumulation while minimizing free IMD exposure in off-target organs to enable safe, systemic delivery of IMDs. This library provides insight into the relationship between release rates of the active immunomodulator from drug carriers and systemic toxicities. Interestingly, we found

that BPDs with a sufficiently slow R848 release kinetics *in-vitro* ($t_{1/2} > \sim 12$ d) lower early acute peak levels of R848 in the peripheral blood following dosing, thereby blunting early systemic cytokine levels compared to free R848 dosing. However, at later times, BPDs show sustained low levels of the drug in circulation, which do not trigger systemic inflammation in the blood but may be important for the enhanced efficacy of these IMD prodrugs. This potentially indicates a threshold concentration of R848 in serum below which there is minimal systemic inflammation and allowed us to then focus on testing these BPDs for their anti-tumor potential. We have already established that BPDs preferentially accumulate in tumor tissues with the liver as the main route of clearance⁴⁹⁰. We leveraged this predictable biodistribution profile to our advantage: it is known that Kupffer cells in the liver have low pro-inflammatory cytokine production upon TLR7 engagement, a blunted response thought to be related to their role in maintaining tolerance^{491,492}. As a result, our IMD-BPDs accumulating in liver tissue did not induce immune toxicities as evidenced by minimal changes in ALT levels upon systemic administration; thus, we were able to focus on optimizing tumor versus blood drug release through linker design. By adding functional groups to our phenyl ester-based linker structures that connect R848 covalently to BPDs, we were able to find R848-BPDs that avoid systemic toxicities generated by premature exposure of drug in the blood. This system can be further enhanced by other tumor-specific linker strategies now that we have demonstrated a proof-of-concept approach to minimize systemic toxicities.

Non-linear dose-toxicity relationships confound MTD studies for IMDs such as R848 and are thus difficult to precisely define³⁷⁹. We determined the maximum tolerable dose (MTD) of free R848 in healthy C57BL/6J mice by monitoring for clinical signs and weight loss over a period of 1 week. Our preliminary decision was based on less than 5% of total body weight loss and no change in the body condition score of the mice. The R848-BPD library was also evaluated according to the above two parameters, and we observed linker-dependent increases in MTD values. Beyond weight loss and body condition score, cytokine levels in the blood were also assessed as a second layer of toxicity monitoring. Finally, whole blood analysis and toxicity panels were evaluated to obtain a final round of biomarkers to correlate systemic side-effects with serum concentrations of R848. We were able to successfully tune the levels of these markers through linker design allowing for controlled immune activation. Furthermore, fluorescently labeled R848-BPDs demonstrated increased tumor accumulation over time, significant uptake in myeloid populations in the tumor and draining lymph nodes as well as activation of inflammatory cytokines

in the tumor microenvironment. By directing uptake of BPDs into antigen presenting cells (APCs) rather than other cells within the tumor environment, we were able to enhance activation of APCs and downstream T cell priming while also improving their safety profiles. This effect resulted in significantly stronger tumor growth inhibition as well as improved survival rates compared to mice given R848 or a-PD-1 alone or the combination of these two therapies. Reprogramming subsets of macrophages and cDC1s played a crucial role in tumor control as depleting these cells abrogated anti-tumor efficacy demonstrated by R848-BPDs.

We note that this work comprises the first example of using bottlebrush polymer prodrugs as immune stimulants. The concept of using molecular design to tune release and understand in detail the impact of release kinetics on immune response has not been explored, and is uniquely enabled by our BPD platform. There are no other systems to our knowledge that allow for isolation of release as the key variable so readily while maintaining otherwise identical physical properties. Furthermore, the bottlebrush conformation has been shown to improve tissue penetration and cell uptake⁴⁹³. These are very small prodrug constructs that are in a size range not accessible to most other systems. Finally, we note that the bottlebrush configuration shields the payload from burst release in serum. We hypothesize that future work toward optimizing the dimensions of our R848-BPDs as well as attaching targeting moieties (such as antibodies against proteins expressed on tumors) can further increase their uptake in the tumor microenvironment^{16,494}. This is of particular relevance given that TLR7-antibody-drug conjugates (TLR7-ADCs) targeting human epidermal growth factor receptor 2 (HER-2) have shown promising anti-tumor inflammatory responses in mouse models and early clinical trials^{495,496}. However, the benefits of tumor antigen targeting and Fc γ -receptor-mediated phagocytosis come with significant issues such as highly limited drug loading, anti-drug antibodies and other immuno-toxicities which were associated with decreases in drug exposure in clinical studies⁴⁹⁷.

Finally, we showed that maximal therapeutic activity from R848-BPD therapy requires repeat dosing to drive the anti-tumor immune response. To achieve optimal efficacy, we hypothesize that defining optimal dosing and timing intervals will be critical. One key factor for defining an optimal dosing strategy is TLR tolerance: TLR tolerance is defined as a transient state of refractoriness of TLRs to subsequent activation post initial dosing. This hyporesponsiveness has evolved to avoid the induction of autoimmunity through repeated TLR agonism; however, it has important implications for dosing schedules involving IMDs such as R848 that aim to generate

anti-tumor immune responses. Although TLR7 tolerance has been observed in multiple studies, the mechanism of induction and avoidance remains undetermined^{453,458}. Using insights gained from tuning release rates via drug-linker chemistries, our future work involves understanding the appropriate dosing scheme to circumvent TLR7 tolerance and testing our optimized therapeutic strategy in more rigorous genetically engineered mouse models.

In summary, we have developed a BPD platform with distinct advantages for delivery of immune stimulants with narrow therapeutic indices such as IMDs, which allows for their systemic administration through improving their safety and enabling conversion of cold tumors into hot tumors via sustained myeloid cell activation. Our results establish our ability to: (i) generate R848 prodrugs and R848-BPDs of precise sizes; (ii) control release of free R848 *in vitro* and *in vivo*; and (iii) demonstrate anti-tumor effects of R848-BPDs in multiple syngeneic mouse models of colon carcinoma. We therefore conclude that finding an optimal tumor versus blood drug release window is a promising approach for safe, systemic delivery of small molecule immunomodulators to potentiate anti-tumor responses to existing cancer immunotherapies.

3.4 Methods

General procedure for synthesis of R848-MMs

One of six R848-N₃ compounds: R848-PE-N₃ (5a), R848-TEG-dMPE-N₃ (5f), R848-OMPE-N₃ (5b), R848-MPE-N₃ (5c), R848-dOMPE-N₃ (5d), or R848-dMPE-N₃ (5e) or Cy5.5-N₃ and PEG-Alkyne-MM were added to a 20 ml scintillation vial containing a stir bar. In a nitrogen-filled glovebox, the reagents were dissolved in THF (1ml THF per 100mg PEG-alkyne-MM) followed by addition of ~3 equiv. of copper (i) acetate. The reaction was stirred for 1h until consumption of PEG-alkyne-MM was observed by LC-MS analysis. The crude product was purified by preparative-gel permeation chromatography (prep-GPC). Fractions containing product were concentrated by rotary evaporation and the resulting residue was redissolved in THF and dried over sodium sulfate. Finally, the solid polymer was washed with cold diethyl ether 3 times to afford the desired R848-MM or Cy5.5-MM as white and green solids, respectively.

General procedure for synthesis of R848-BPDs.

R848-dMPE-MM (2.00 g, 9.9 equiv.) and Cy5.5-MM (20.1mg, 0.1 equiv.) were added to a 40ml vial containing a Teflon coated stir bar. In a nitrogen-filled glovebox, the G3 solution was prepared: G3 (49.8mg in 2.49ml THF = 0.02 gml⁻¹). An aliquot of G3 (1.75ml, 1 equiv.) was added to a stirred solution of MM (3.07ml, THF) as a single stream. The final volume in the reaction vial (3.07ml+1.75ml=4.82ml) afforded a MM concentration of 0.1M. The reaction was allowed to proceed for 25 min before removal from the glovebox and quenching with ethyl vinyl ether (0.300ml). The material was diluted with nanopure H₂O (~9.5ml, 1:1 dilution) and then transferred to dialysis tubing (RC, 8 kDa molecular weight cutoff) for dialysis against nanopure H₂O (10 l, 3×2–3h cycles). The contents of the dialysis tubing were then transferred to clean 20ml vials and lyophilized (48h) to afford a dry powder (2.1 g, 90%).

***In-vitro* R848 release assay in PBS**

Approximately 2mg of a given MM (PE, tdMPE, OMPE, MPE, dOMPE or dMPE) were weighed into a clean 4ml vial. 4ml of PBS (pH7.6) containing 4-bromobenzyl alcohol (100 uM, internal standard) was added into each vial. All vials were sealed and placed in an incubation oven set at 37 °C. At each time point, a vial for a given MM was removed from the incubation oven and 50ul aliquots were taken in LC-MS vials. To each vial was added 200 µl dimethylsulfoxide, and the resulting solution was briefly vortexed before filtering through a 0.45µm nylon syringe filter. Analysis by LC-MS provided insight into the amount of R848 released at a given time point. Quantifications were made by integration of the released R848 peak and disappearing MM peak (LC conditions: 5-95% MeCN/H₂O [0-7 min], 95 – 100% MeCN/H₂O [7-8 min], PES column).

Cells

Human TLR7, mouse TLR7 HEK293 and RAW BlueTM reporter cells were purchased from Invivogen and were cultured following the vendor's instructions. Murine bone marrow-derived dendritic cells (BMDCs) were harvested using a previous protocol⁴⁹⁸. Briefly, bone marrow harvested cells from 8–10-week-old female C57BL/6J mice were cultured in RPMI 1640 medium containing 10% fetal bovine serum (FBS), 100 units ml⁻¹ of penicillin and streptomycin (P/S), 50uM Beta-Mercaptoethanol, 600 ng/ml Flt3L and 5 ng/ml GM-CSF. Media was changed on Day 5 and on Day 9, non-adherent cells were harvested, counted and plated for the assay. MC38 cells

provided by J. Schlom (National Cancer Institute) and cultured in DMEM medium (GE Healthcare Life Sciences) supplemented with 10% FBS and 100 units ml⁻¹ of P/S. CT-26 cells were purchased from American Type Culture Collection (ATCC) and cultured in RPMI 1640 medium with 10% FBS, penicillin (100 U/ml) and streptomycin (100 ug/ml).

***In vitro* innate immune stimulation**

Human TLR7, mouse TLR7 HEK293 or RAW BlueTM reporter cells (InvivoGen) were seeded at 3×10^4 cells/96-well for 24 h then treated with R848, R848-BPDs, PBS or DMSO for 48 h. To assess innate immune stimulation, secreted alkaline phosphatase (SEAP) was measured from supernatants using QuantiBlue reagent (InvivoGen) to confirm dose-dependent activation of the target TLR receptor. We note that R848-BPDs were confirmed to have low endotoxin levels (<0.1 EU per dose) by the Endosafe Nexgen-PTS system (Charles River).

Alternatively, the immune stimulatory potential of R848 and R848-BPDs in BMDCs was assessed as well. BMDCs were seeded in a 96 well plate (Corning) at 200,000 cells/well. After 24 h of culture, medium was replaced with fresh medium or fresh medium with 75 μ l blank polymer or 75 μ l R848-BPD. After 48 h of incubation, induction of DC maturation by the R848-BPDs was assessed by flow cytometry analysis of the expression of the costimulatory receptor CD86.

Mice

All *in vivo* experiments were performed in the following mouse strains: 8–10-week-old female C57BL/6J mice (Jackson Laboratory), 8-10-week-old female BALB/c mice (Jackson Laboratory), 8-week-old BATF3⁻ mice (Jackson Laboratory, Strain # 013755), and 8-week-old TLR7⁻ mice (Jackson Laboratory, Strain # 008380). Experiments were performed in specific pathogen-free animal facilities at the MIT Koch Institute for Integrative Cancer Research. Mice were housed under standard 12-hour light - 12-hour dark conditions with ad libitum access to water and chow. All mouse studies were performed according to institutional and National Institutes of Health (NIH) guidelines for humane animal use and in accordance with the Association for Assessment and Accreditation of Laboratory Animal Care. Protocols were approved by the Institutional Animal Care and Use Committee (IACUC) at MIT.

Dose escalation and toxicity analysis to identify maximum tolerable dose *in vivo*

The maximum tolerable dose (MTD) of free R848 was determined in healthy C57BL/6J mice by *i.v.* injection at 5 different doses (3 mg/kg, 5 mg/kg, 7.5 mg/kg, 10mg/kg, and 15 mg/kg) followed by monitoring for clinical signs and weight loss over a period of 1 week. Body condition score parameters such as visible signs of restricted movement and lethargy were also noted for the mice. Next, we carried out dose escalation studies to identify the MTD for each BPD, starting from a dose of 7.5 mg/kg. MTD values for R848-BPDs were quantified in accordance with MIT Committee on Animal Care (CAC) policies. Healthy C57LB/6 mice were administered each R848-BPD sample at 5 different doses (7.5 mg/kg, 15 mg/kg, 30 mg/kg, 50mg/kg, and 75 mg/kg) by *i.v.* injection ($n = 5$ animals/group). The MTD was determined by monitoring for weight loss and clinical signs for up to two weeks.

In parallel, separate groups of mice were set-up where serum samples were collected by cheek bleeds 6, 24 and 48 hours after one injection (at MTD) of R848, R848-BPDs and frozen at 20°C until analysis. Samples were diluted 1:1 with Assay Buffer and assayed using the LEGENDplex mouse antiviral response panel (BioLegend) according to the manufacturer's instructions. The cytometric bead array readout was performed using a BD FACS LSR Fortessa cytometer and analyzed using LEGENDplex v8.0 software.

Finally, a third arm of the acute dosing analysis included blood chemistry analysis (complete blood count) and serum samples were also sent to IDEXX Reference Laboratories for analysis of liver enzyme levels (ALT) and blood urea nitrogen (BUN). For subsequent tumor imaging and therapy studies, the dose of R848 & R848-BPDs for safe administration was set as the MTD for R848 (*i.e.*, the maximum tolerated dose that results in < 5% weight loss in > 80% of animals). These studies outlined a tolerable dosing regimen for tumor therapy.

PK analysis *in vivo*

Free R848, R848-MPE-BPDs and R848-dMPE-BPDs were administered *i.v.* (at MTD dose) to C57LB/6 mice ($n=5$ animals/group). Blood PK was assessed by drawing blood for liquid chromatography with tandem mass spectrometry (LC-MS-MS) analysis to quantify free R848 levels at 1, 3, 6, and 24 hr.

Plasma samples were extracted by mixing 5 uL plasma with 45 uL extraction mix (acetonitrile/methanol 75:25 with 0.1% formic acid) containing 50 nM imiquimod as an internal

standard. Samples were vortexed at 4°C for 10 minutes and cleared by centrifugation at 4°C at 17,000 \times g for 10 minutes. Supernatants were transferred to LCMS vials for analysis. Working stocks of resiquimod were made by diluting resiquimod in extraction mix containing 50 nM Imiquimod as internal standard. A matrix-matched calibration curve was made by mixing 5 uL working stock resiquimod with 45 uL extracted control plasma. Analysis was conducted on a QExactive bench top Orbitrap mass spectrometer equipped with an Ion Max source and a HESI II probe, which as coupled to a Dionex Ulitmate 3000 HPLC system (both Thermo Fisher Scientific, San Jose, CA). 5 uL of sample was injected onto a Kinetex C18 50 \times 2.1 mm analytical column (2.6 μ m particle size, Phenomenex). The column oven and autosampler tray were held at 30°C and 4°C, respectively. The following conditions were used to achieve chromatographic separation: Buffer A was 0.1% formic acid; Buffer B was 0.1% formic acid in acetonitrile. The flow rate was 0.4 mL/min. The chromatographic gradient was run as follows: 0-3.5 min, linear gradient 5-80% B; 3.5-3.6 min, linear gradient 80-98% B; 3.6-4.5 min, the gradient was held at 98% B; 4.5-4.6 min, linear gradient 98-5% B; 4.6-6 min, the gradient was held at 5% B. The mass spectrometer was operated in positive mode and data acquisition was performed using targeted selected ion monitoring scans (tSIM) centering on 241.14477 m/z and 314.18155 m/z to detect Imiquimod and Resiquimod, respectively. The resolution was set at 70,000, the AGC target was 1e5 and the maximum injection time was 200 ms. Absolute quantification of Resiquimod was performed using XCalibur QuanBrowser 2.2 (Thermo Fisher Scientific), using a 5 ppm mass tolerance and referencing a matrix-matched calibration curve containing concentrations of resiquimod ranging from 1 nM – 100 uM and 50 nM imiquimod as internal standard. Curve fitting was achieved using a quadratic-log-log fit, with an R value of 0.9992.

MC38 syngeneic mouse model of colon adenocarcinoma

MC38 is derived from a colon tumor in a C57BL/6 mouse following long-term exposure to 1,2-dimethylhydrazine dihydrochloride (DMH). MC38 has a favorable response profile to immunomodulatory antibodies suggesting a tumor microenvironment amenable to immune activation⁴⁹⁹. Briefly, MC38 colon carcinoma cells were suspended at 0.5×10^6 cells in 100 μ L PBS and inoculated subcutaneously (s.c.) to induce tumors in C57Bl/6 mice.

Organ and cellular BD analysis *in vivo*

For tumor BD studies, 0.5×10^6 MC38 cancer cells were inoculated s.c. in the hind flank of C57BL/6 mice ($n = 5$ animals/group). When tumors reached $\sim 25 \text{ mm}^2$ in size, the animals received an i.v. injection of R848-Cy5.5-BPDs. Tumors and other organs were collected at 0.5, 6 and 24 hours, homogenized, and total fluorescence signal was measured on a fluorescence plate reader to quantify the R848-Cy5.5-BPD in each organ. Briefly, the extracted tissues were weighed and then mechanically dissociated until homogenous in lysis buffer (100 mM HEPES pH 7, 2 wt% Triton-X, 5mM EDTA) using disposable tissue grinder tubes (Kimble Biomasher). Subsequently, tubes were vortexed for 30 sec, centrifuged (300g, 2 min) and the supernatants were transferred to a black 96-well plate for quantification using fluorescence plate reader (excitation 675nm, emission 720nm). In parallel, flow cytometry was used to quantify cellular uptake of R848-Cy5.5-BPDs in homogenized tumor, tumor-draining lymph node, and spleen samples harvested 24 hours post i.v. injection of R848-Cy5.5-BPDs.

Intra-vital imaging

Dorsal imaging window was implanted into the dorsal skin of mice ($n = 1-2$ animals/group) with CD11c⁺ cells expressing the fluorescent protein, Venus. The imaging window permitted stable imaging via confocal fluorescence microscopy on a Leica SP8 microscope over several days consecutively. The mice were inoculated with MC38 cancer cells expressing the fluorescent protein Cerulean. This cell line contained a transgene in which yellow fluorescent protein (YFP) is expressed under the transcriptional control of the integrin alpha X (Cd11c) promoter, which is expressed primarily by DCs. After 5 d of tumor outgrowth, large areas of the tumor were imaged using a tilescan to ascertain the number of CD11c-Venus⁺ cells in the tumor microenvironment. Mice were injected i.v. with R848-Cy5.5-BPDs; after 24 h the same area was imaged again.

CT-26 syngeneic mouse model of colon carcinoma

CT26 is an N-nitroso-N-methylurethane-(NNMU) induced undifferentiated colon carcinoma cell line established from BALB/c mice with aggressive colon carcinoma. The CT-26 colon carcinoma cell line is moderately responsive to anti-PD-1 monoclonal antibody therapy providing a particularly relevant model for the development of new immunotherapies for metastatic disease⁴⁹⁹. Briefly, CT-26 cells were suspended at 1×10^6 cells in 100 μL PBS and inoculated subcutaneously

(s.c.) to induce tumors in BALB/c mice.

***In vivo* therapeutic efficacy**

Mice were injected with 0.5 or 1 x 10⁶ cells (MC38 or CT-26) subcutaneously (s.c.) on day 0. When tumors reached 25mm², animals were randomized into five groups and saline, blank polymer, free R848, R848-MPE-BPDs or R848-dMPE-BPDs were administered via intravenous injection either as a monotherapy or in combination with anti-PD-1 (200ug, intra-peritoneally) on days 8, 11 and 14. Tumor area measurements were taken using calipers and animal weights were assessed every 3 days starting on day 5 after tumor inoculation.

Sample processing for single-cell RNA-sequencing (scRNA-seq)

Mouse MC38 tumor samples (n=3 for saline group and free R484 group, n=2 for R848 with MPE brush group) were digested utilizing the Tumor Dissociation kit (Miltenyi Biotech) 24h post administration. Cells were then stained with CD45 microbeads and CD45+ and CD45- cells were separated using MACS Separator. CD45+ and CD45- single cells for each mouse were loaded in a ratio of 9:1 onto Seq-Well arrays. ScRNA-seq sample processing and library preparation followed the Seq-Well protocol (Gierahn et al., 2017; Hughes et al., 2020). cDNA was loaded onto Illumina Nextseq (75 Cycle NextSeq 500/550 v2.5 kit).

Single-cell RNA sequencing analysis

Quality control and clustering

ScRNA-seq reads from each sequencing run were demultiplexed and aligned to the mm10 reference genome, as previously described⁵⁰⁰. Raw feature-barcode matrices for each sample were used for further analysis. Initial quality control was conducted using Seurat V4.0.0 with following criteria: cells with 400<genes<10,000 and UMI<50,000 were retained and cells with >15% mitochondrial reads were excluded. Genes were filtered by retaining those expressed in at least in 10 cells. Initial clustering with the first 30 principal components (PCs) identified a cluster of poor-quality cells with high mitochondrial read fractions, which was subsequently excluded from downstream analyses. After identifying the top gene markers on each remaining cluster, we identified a cluster containing MC38 tumor cells based on expression of *Mtap*, *Rhox5*, *Col6a2*,

and *Fam159b*. We subsequently focused further analyses on the non-malignant clusters. After subsetting to only non-malignant cells, we re-scaled the dataset and identified 869 highly variable genes ($0.2 < \text{mean expression} < 6$ and $0.5 < \text{dispersion} < 20$). We then reran PCA and used the first 11 PCs to cluster with a resolution of 1.3. By running differential gene expression analyses for each cluster relative to the rest, we were able to identify marker genes to assign 16 fine cell subsets; based on expression of known markers, we combine clusters containing shared lineage information. For example, monocytes highly express *Ly6c2*, neutrophils highly express *SI100a8/9*, and T cells highly express *Cd3d/g*.

Proportion analysis

To account for the dependencies between cell subset proportions in scRNA-seq data, we used both Fisher exact tests and a Dirichlet-multinomial regression analysis as complementary approaches to look for shifts in cell frequencies across conditions. We performed Fisher exact tests using the number of cells from each cell subset between two conditions to test whether a cell type was enriched in one condition (with Benjamini-Hochberg multiple testing correction). To account for the proportions of all other cell types in comparison, we also used Dirichlet-multinomial regression model from *DirichletReg* R package and calculated the p values associated with abundance shifts (with Benjamini-Hochberg multiple testing correction)⁴⁸⁰. In the main figure, adjusted p values are shown for comparisons that are at least significant by one test. Of note, we also considered using Wilcoxon Rank Sum test on the cell subset proportions across conditions, but the statistical power for this method is limited by having only 2 replicates in the medium BPD condition, so we did not include this analysis in this study.

Gene Set Enrichment Analysis

To identify differentially expressed genes in each cell subset of interest, we used a Wilcoxon Rank Sum test to evaluate the significance of shifts in the frequently expressed genes (minimum expression in 25% of cells in either population), filtering for a minimum log fold change in expression of 0.25 and Benjamini-Hochberg corrected p value < 0.05 . Gene set enrichment analysis was performed for genes with adjusted p-value < 0.05 (Benjamini-Hochberg multiple testing correction) with *enricher* and *GSEA* function in *clusterProfiler* R package from Bioconductor⁵⁰¹.

Transcription Factor (TF) Enrichment Analysis

To identify the transcription factors enriched in each cell subset of interest, we used VIPER in combination with DoRothEA to estimate the TF activities from gene expression data⁵⁰². We used the “mm_pancancer” reference for TF-target interactions which contains 1,096 TFs targeting 17,695 genes⁴⁸². We only selected the TF-target interactions with high confidence (category A and B defined by DoRothEA) and defined adjusted p-value < 0.01 (Benjamini-Hochberg multiple testing correction) as significantly enriched TF between groups.

Immunophenotyping studies

For tumor BD studies, 0.5×10^6 MC38 cancer cells were inoculated s.c. in the hind flank of C57BL/6 mice ($n = 5$ animals/group). When tumors reached $\sim 30 \text{ mm}^2$ in size, the animals received an i.v. injection of R848-Cy5.5-BPDs. Tumor-draining lymph nodes were collected at 24, 48 and 72 h post dosing, mechanically dissociated and analyzed by flow cytometry. Antibodies to CD103 (2E7), Ly6C (HK1.4), F4/80 (BM8), CD11b (M1/70), CD86 (GL1), MHC2 or I-A/I-E (M5/114.15.2), CD24 (30-F1), CD11c (N418), CCR7 (4B12), CD169 (3D6.112), Ly6G (1A8) were obtained from BioLegend. Antibodies to CD45 (30-F11) and CD8 α (53-6.7) were purchased from BD Biosciences. All antibodies were diluted 1:100. Viability was assessed using Zombie Aqua (BioLegend, 1:1,000). Flow cytometry sample acquisition was performed on an LSRFortessa cytometer (BD Biosciences), and the collected data were analyzed using FlowJo v10.5.3 software (TreeStar).

Cellular depletion studies

To determine the relative importance of innate immune cell subsets in the efficacy of R848-BPDs, C57Bl/6 mice ($n = 5$ animals/group) were inoculated with MC38 tumor cells as above and treated with R848-BPDs in the presence of depleting antibodies against F4/80 (200ug, i.p.) every day (beginning 1 day prior to therapy) to ascertain the relative contribution of macrophages to therapeutic response. The role of cross-presenting DCs was assessed using *Batf3*^{-/-} mice, which lack this DC population while TLR7⁻ mice were used to validate the dependency on TLR7 activation.

Induction of activated T cell responses via Enzyme-linked ImmunoSpot assay (ELISpot)

To assess induction of tumor-specific T cell responses against treated tumors, we utilized IFN γ ELISpot assay of T cells co-cultured with irradiated MC38 tumor cells. Effector cells were CD3⁺ T cells isolated from MC38-tumor bearing mice 7d post treatment with saline, R848, or R848-BPDs. Spleens were isolated from mice, mechanically digested through 70 μ m nylon cell strainers to prepare single-cell suspensions for CD3⁺ T cell isolation by the CD3⁺ T cell isolation kit (Stem Cell Technology). Isolated CD3⁺ T cells were suspended in RPMI supplemented with 10% FBS, 1% P/S, 1 \times non-essential amino acids (Invitrogen), 1 \times sodium pyruvate (Invitrogen) and 1 \times 2-mercaptoethanol (Invitrogen). Target MC38 cells were treated with 50 U/ml mouse IFN- γ (Peprotech) for 12h and then irradiated (120 Gy) on the day of the experiment followed by trypsinization into a single cell suspension and washing 2 times in 1x PBS to remove residual IFN- γ and suspended in the same media as the effectors. Targets were seeded at 25,000 cells per well while effectors were seeded at 250,000 cells per well. Plates were wrapped in foil and incubated for 24h and then developed according to the manufacturer's protocol. Plates were scanned using a CTL-ImmunoSpot Plate Reader, and the data was analyzed using CTL ImmunoSpot software.

Statistics

Statistical analysis and graphing were done with GraphPad Prism. The two-tailed Student's *t* test was used to compare two experimental groups and two-way Anova with Dunnett's post hoc analysis was used for comparing more than two groups. Details of the statistical test and number of replicates are indicated in the figure legends. A value of $P < 0.05$ was considered statistically significant.

Chapter 4

Escalating-dose immunization of vaccines

4.1 Introduction

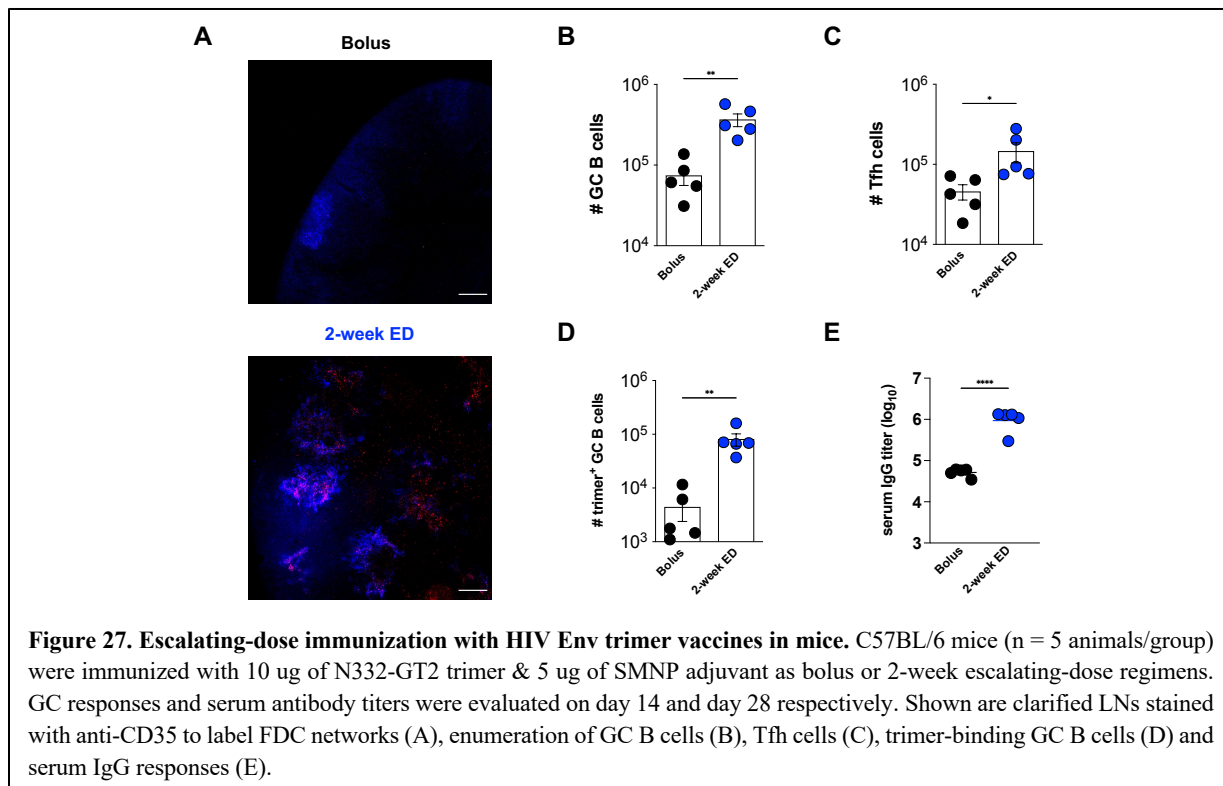
The efficacy of a vaccine formulation is influenced by a shared set of factors that govern the optimal generation of a desired immune response. Firstly, the identification of antigens capable of triggering protective antibody or T cell responses is crucial⁵⁰³. Secondly, it is also essential for antigen and inflammatory signals to reach the inductive sites, typically lymphoid tissues such as lymph nodes, and access specific compartments within these organs that orchestrate the activation of T cells and B cells⁵⁰⁴. The timing and concentration of antigen and inflammatory cues at these sites must be carefully regulated to proportionately initiate immune priming. Vaccine kinetics refers to the dynamic changes in the concentration of antigens and/or adjuvants to which the immune system is exposed over time, as these parameters significantly influence the response to immunization. Numerous studies, ranging from basic research to vaccine development-focused investigations, have revealed the multifaceted effects of antigen and inflammatory cue kinetics on the magnitude and quality of the immune response¹⁰¹. Extended exposure to these signals over a duration of at least a few weeks, resembling the persistence of antigens following acute infection, has been associated with enhancements in both cellular and humoral immune responses.

Escalating-dose immunization wherein a given dose of antigen/adjuvant is administered as 7 injections of increasing dose over 2 weeks (2-week ED) has proven to be a successful strategy to amplify humoral immunity elicited by vaccination⁵⁰⁵. The objective of the following studies was to assess the magnitude, durability, and functionality of the humoral responses elicited by the escalating dose regimen when compared to bolus immunization with two different vaccine formulations (HIV Env & Thyphim Vi) in mice.

4.2 Results

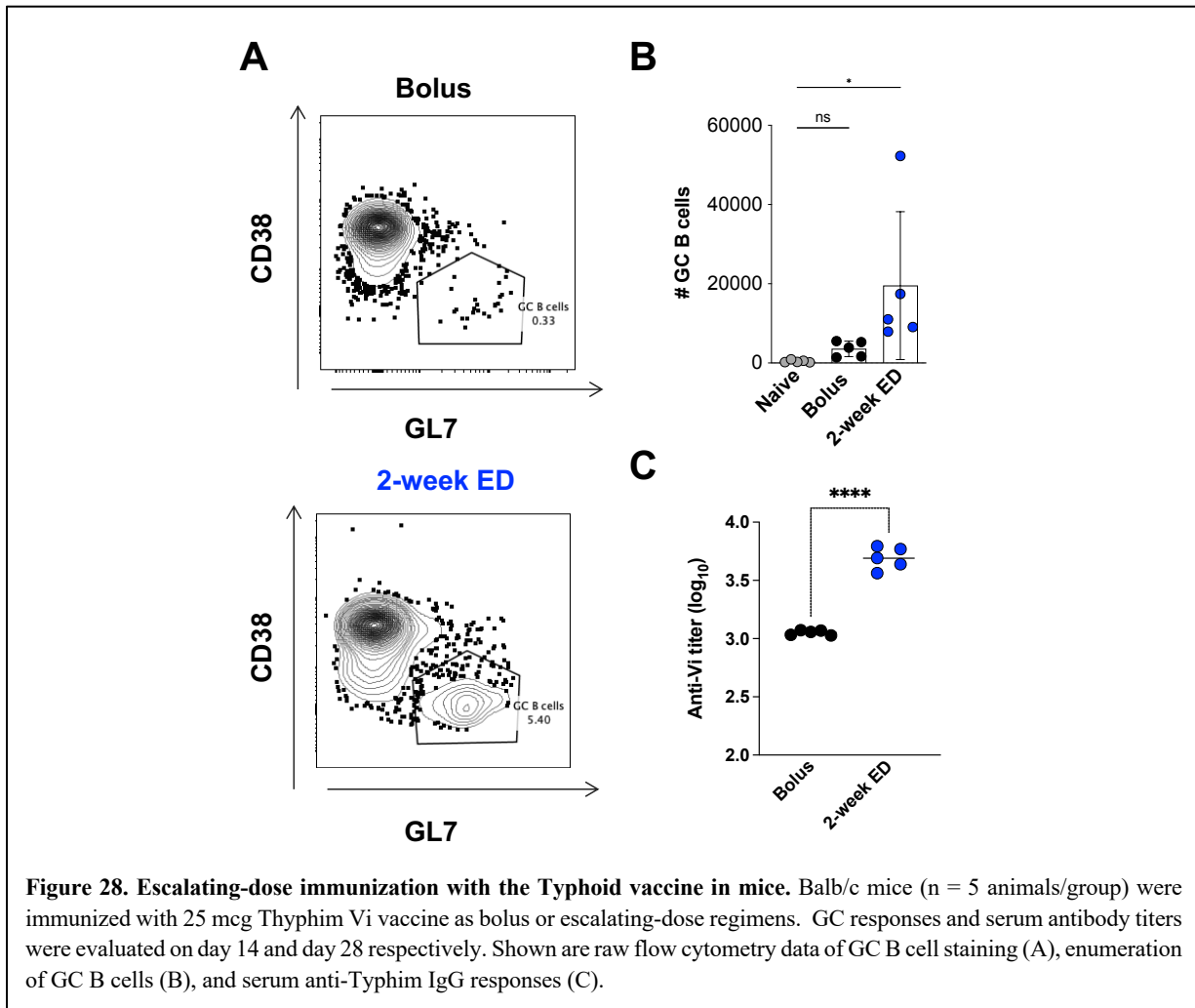
4.2.1 Escalating dose immunization improves antigen capture on follicles and enhances humoral immune responses to HIV Env trimers

We verified the effects of the 2-week ED regimen following immunization with the combination of N332-GT2 trimer (10 ug) and SMNP adjuvant (5 ug) in 8-week old C57BL/6 mice. We observed that the escalating dose immunization pattern prolonging antigen delivery to draining lymph nodes (dLNs) altered multiple facets of the immune response- causing enhanced antigen capture on FDCs (**Fig. 27A**), increasing the number of B cells entering GCs, improving the number of antigen-specific Tfh generated, significantly enhancing the number of trimer-binding B cells in the GC, and leading to increased total Ab titers (**Fig. 27B-E**). For the combination of N332-GT2 trimer and SMNP adjuvant, 2-week ED regimen demonstrated antigen capture on follicles which was absent on bolus immunization (**Fig. 27A**). 2-week ED regimen improved GC B cell and GC Tfh responses by 5-fold (**Fig. 27B-C**) and increased serum Ab titers by an order of magnitude relative to bolus immunization (**Fig. 27E**). Furthermore, we observed significantly improved trimer-binding GC B cell responses with the 2-week ED regimen that were 20-fold higher than bolus immunization (**Fig. 27D**).



4.2.2 Escalating dose immunization improves germinal center and serum antibody responses for the polysaccharide-based typhoid vaccine

To provide preliminary evidence for the utility of an escalating-dose immunization to amplify GC B cell responses for the polysaccharide-based Typhoid vaccine as we have seen with HIV protein immunogens, we carried out preliminary studies in mice, immunizing with 25 μg of the clinical Typhim Vi vaccine. As shown in **Fig. 28A-B**, ED immunization led to a ~ 10 -fold increase in the number of GC B cells elicited by the typhoid vaccine. Further, serum typhoid-specific IgG titers were increased ~ 5 -fold (**Fig. 28C**). Hence, the humoral immune response benefits of ED immunization seen with HIV protein immunogens appear to also hold for polysaccharide vaccines.



4.3 Discussion

High-affinity antibodies are typically generated through affinity maturation, a process driven by evolutionary competition among B cells within germinal centers (GCs)^{506,507}. GCs serve as microcosms of evolution, where B cell proliferation, accompanied by somatic mutations, and competition for limited resources, such as antigen and T cell help, occur. In order to undergo this evolutionary process, GC B cells undergo rapid proliferation, with a cell cycle of approximately 4-6 hours⁵⁰⁸. Following acute antigen exposure, GCs are often observed for a few weeks. In most model systems, antigen-specific GC B cells can be detected for a duration of 14 to 28 days, providing ample time for extensive exploration of antibody sequence space due to the fast division rate of GC B cells⁷⁵. Our findings demonstrate that escalating dose immunization, involving repeated small dose injections over a period of 2 weeks, enhances GC responses compared to traditional bolus immunizations, as evidenced by increased magnitude of germinal center B cells and antibody responses. However, the clinical feasibility of this approach is limited. Subsequent studies detailed in Chapter 5 aim to reduce the number of injections required and delve deeper into the underlying mechanisms of action associated with the escalating dose immunization strategy.

The Typhoid polysaccharide vaccine (Typhim Vi) is available for active immunization for the prevention of typhoid fever caused by *Salmonella typhi*. Typhim Vi is a sterile solution containing the cell surface Vi polysaccharide extracted from *Salmonella enterica* serovar Typhi, S typhi Ty2 strain and is administered by intramuscular injection as a single dose of 25mcg in 0.5mL. A single dose of Typhim Vi vaccine induced a four-fold or greater increase in antibody levels in 88% and 96% of an adult US population⁵⁰⁹. However, as antibody titers decline substantially, re-immunization is recommended every 24 months under conditions of repeated or continued exposure to the *S typhi* organism. We hypothesized that immunization of the Typhoid polysaccharide vaccine with the escalating dose regimen will result in increased GC development, as well as augmented and more durable antibody titers compared to bolus immunization. Our preclinical studies in mice revealed beneficial effects of escalating-dose immunization including the demonstration of a significant increase in the frequency of GC B cells and serum typhoid-specific IgG titers following 7-ED immunization with the Typhim ViTM vaccine. The future goals are to confirm these observations in humans and to generate new insights into B-cell induction and programming by vaccination.

4.4 Materials and Methods

HIV Immunogen

N332-GT2 trimers are expressed in FreeStyle 293F cells (Invitrogen, Cat no. R79007) and purified in two steps by affinity chromatography using a GE HisTrap column and size-exclusion chromatography using a GE S200 Increase column as described previously^{510,511}.

Adjuvant preparation

The saponin adjuvant is an ISCOM-like self-assembled nanoparticle consisting of Quillaja saponin, cholesterol, DPPC, and MPLA⁵¹². Briefly, solutions of cholesterol (20mg/ml final concentration, Avanti Polar Lipids Cat# 700000), DPPC (20mg/ml final concentration, Avanti Polar Lipids Cat# 850355), and MPLA (10mg/ml final concentration, PHAD) are prepared in Milli-Q water containing 20% w/vol MEGA-10 (Sigma D6277) detergent. Quil-A saponin (InvivoGen; vac-quil) was dissolved in Milli-Q water at a final concentration of 100 mg/ml. All components are mixed at a molar ratio of 10:10:2.5:1 (Quil-A:chol:DPPC:MPLA) and diluted in PBS to a final concentration of 1 mg/ml cholesterol. The solution is allowed to equilibrate overnight at room temperature and then dialyzed against PBS using a 10k MWCO membrane. The adjuvant solution is then sterile filtered, concentrated using 50k MWCO centricon spin filters, and purified by FPLC using a Sephacryl S-500 HR size exclusion column.

Typhim Vi™ and Diluent

Typhim Vi™, Typhoid Vi Polysaccharide Vaccine, produced by Sanofi Pasteur SA, for intramuscular use, is a sterile solution containing the cell surface Vi polysaccharide extracted from *Salmonella enterica* serovar *Typhi*, *S typhi* Ty2 strain. The organism is grown in a semi-synthetic medium. Phenol, 0.25%, is added as a preservative. The vaccine contains residual polydimethylsiloxane or fatty-acid ester-based antifoam. The vaccine is a clear, colorless solution. Each dose of 0.5 mL is formulated to contain 25 mcg of purified Vi polysaccharide in a colorless isotonic phosphate buffered saline (pH 7 ± 0.3), 4.150 mg of Sodium Chloride, 0.065 mg of Disodium Phosphate, 0.023 mg of Monosodium Phosphate, and 0.5 mL of Sterile Water for Injection. Diluent consisting of Sterile Water for Injection was used to make stock solutions for escalating dose immunization.

ELISA

To analyze on-target antibody response, high-binding ELISA plates (07-200-37, Fisher Scientific) were coated with 1 mg/ml trimer and blocked with 2% BSA in PBS overnight. To detect antigen-specific IgG responses, dilutions of serum or lymph node aspirate were added to the wells and incubated for 1.5 hours at 25°C. Plates were washed three times in PBS containing 0.2% Tween-20, and then anti-mouse IgG secondary antibody conjugated to HRP (172-1011, Bio-Rad Laboratories), diluted 1:5000 in blocking buffer as per manufacturer instructions, was added to the wells. After 1 hour of incubation, plates were again washed, developed with TMB, and the reaction was stopped with sulfuric acid. The optical density of the mixture was read out at 450 nm minus the absorbance at 540 nm according to the manufacturer's instructions.

Flow Cytometry Analysis of Lymph Nodes.

Inguinal lymph nodes were harvested and single-cell suspensions were obtained by passage of the lymph nodes through a 70- μ m filter (BD Biosciences). The isolated cells were stained with Live/Dead fixable aqua stain (L34957, Thermo Fisher Scientific) for 10 min at 25°C before washing twice in flow cytometry buffer. Cells were then incubated with Fc block for 10 min at 4°C before staining with antibodies listed (see the supplementary materials) for 20 additional min at 4°C. For trimer specific GC B cell analysis, cells stained with antibodies were distributed evenly and exposed to biotinylated trimer preincubated with streptavidin (30 min at molar ratio of 1:4 at 25°C) conjugated to phycoerythrin (405203, BioLegend) and/or BV421 (405226, BioLegend). Flow cytometry was carried out on a BD LSR Fortessa or LSR II.

Statistical analysis

Statistical analysis and graphing were done with GraphPad Prism. The two-tailed Student's *t* test was used to compare two experimental groups and one-way Anova with Tukey's post hoc analysis was used for comparing more than two groups. Details of the statistical test and number of replicates are indicated in the figure legends. A value of $P < 0.05$ was considered statistically significant.

Chapter 5

Two-dose “extended priming” immunization amplifies humoral immune responses by synchronizing vaccine delivery with the germinal center response

This chapter is adapted in part from a manuscript being prepared for submission. This work was a collaborative effort wherein Leerang Yang performed the computational studies, Laura Maiorino and Anna Romanov assisted with the imaging work.

5.1 Introduction

Vaccines are a critical public health tool for the control of infectious diseases and, most recently, their efficacy in mitigating severe outcomes during the COVID-19 pandemic has further highlighted their importance⁵¹³. However, despite significant advances, there remain a number of pathogens, including the human immunodeficiency virus (HIV), for which effective vaccines are unavailable, owing to challenges such as high mutation rates, immune evasion mechanisms, and unfavorable immunodominance patterns^{514,515}. HIV continues to pose a persistent global health threat, and the development of an effective vaccine against the virus remains an urgent priority⁵¹⁶. Based on non-human primate and human studies of antibody passive transfer, a vaccine capable of eliciting broadly neutralizing antibodies (bnAbs) against the HIV envelope trimer (Env) should be protective against HIV infection⁵¹⁷⁻⁵¹⁹. However, generation of antibodies capable of broad and potent native HIV neutralization via vaccination has proven challenging due to multiple factors

including immunodominance of non-neutralizing epitopes, high sequence variability of the trimer, and difficult structural accessibility of highly conserved epitopes^{515,520,521}.

Following vaccination, germinal centers (GCs) play a pivotal role in the evolution of the clonality and affinity of the antibody response, and influence the composition of the memory B cell and long-lived plasma cell compartments following immunization^{70,506}. The provision of antigen to GC B cells by follicular dendritic cells (FDCs), which efficiently capture complement- or antibody-decorated antigen, and support from follicular helper T cells (Tfh), which control GC B cell survival, are crucial factors in this process^{508,522}. Notably, the size of the early GC response correlates with the magnitude of neutralizing antibodies (Abs) generated by immunization with HIV Env trimers in rhesus macaques⁵²³. Furthermore, for difficult-to-neutralize pathogens such as HIV, increasing the number of clones entering the GC increases the likelihood that a rare neutralizing B cell undergoes affinity maturation^{520,524}.

One effective approach to enhance the GC response during vaccination is via the use of “extended prime” dosing regimens for administering HIV immunogens^{99–101,525}. In this approach, a given dose of antigen and adjuvant are provided over a prolonged window of time compared to traditional bolus vaccine injection, through methods such as repeated injections^{99,100,525}, implanted drug delivery devices^{99,100}, or through slow-release biomaterials^{526–528}. Among these approaches, a simple strategy that elicits profound changes to humoral immunity is escalating-dose immunization (EDI), where a given dose of vaccine is administered as a series of repeated injections over a period of 2 weeks. For stabilized HIV Env trimer immunogens, EDI using seven injections in an exponentially-increasing dosing pattern has been shown to increase the magnitude of the GC and Tfh response, increase the number of B cell clones entering the GC, increase the size of the memory B cell response, increase autologous tier 2 neutralizing antibody titers, and initiate a GC response that can persist for at least 6 months in non-human primates^{99,100,525}.

Although this extended-prime regimen is highly effective, it is not practical for mass vaccination. Slow-delivery technologies aiming to mimic the effects of extended dosing regimens following a single injection are in development^{104,526,529,530}, but it remains to be seen if these approaches can fully replicate the potency of EDI and they must meet a high bar of safety for implementation widely in vaccine development. Our early computational modeling work seeking to understand the mechanics of ED vaccine immune responses suggested that the key elements driving strong GC responses following ED immunization are the initiation of B cell priming and

GC formation by small amounts of antigen early in the dosing course, followed by later (~1-2 weeks) arrival of larger quantities of antigen that can be captured in immune complexes formed by newly-produced affinity-matured antibody in the lymph node⁹⁹. This late-arriving antigen becomes deposited on FDCs at high levels, providing a reservoir of antigen to drive the GC response.

Based on these mechanisms, we hypothesized that a “reduced escalating-dose” immunization could be possible, where we simplify the ED dosing regimen to just 2 injections, a first dose to initiate B cell priming followed by a second shot 1-2 weeks later that would provide antigen for capture on FDCs. Here, we explored the parameter space of EDI and carried out systematic studies varying the number of doses, dose ratio, and dose intervals using a model HIV Env stabilized trimer immunogen and potent saponin adjuvant in mice. We found that a reduced 2-shot extended-prime approach is able to retain much of the benefit of the 7-dose EDI regimen in amplifying the humoral response against Env trimers. Guided by computational modeling of T cell and B cell priming following bolus or multi-shot immunization, we show that even a two-shot priming approach is capable of greatly augmenting antigen deposition on FDCs to drive the GC response. Together these data suggest that a simple extended-prime immunization approach for subunit vaccines could provide substantial enhancements to the humoral response, and provide new insights into how the modulation of vaccine kinetics can be leveraged to augment the germinal center response of broad relevance to vaccines for infectious disease.

5.2 Results

5.2.1 A two-dose priming regimen greatly augments responses to HIV Env trimer protein immunization over traditional bolus immunization

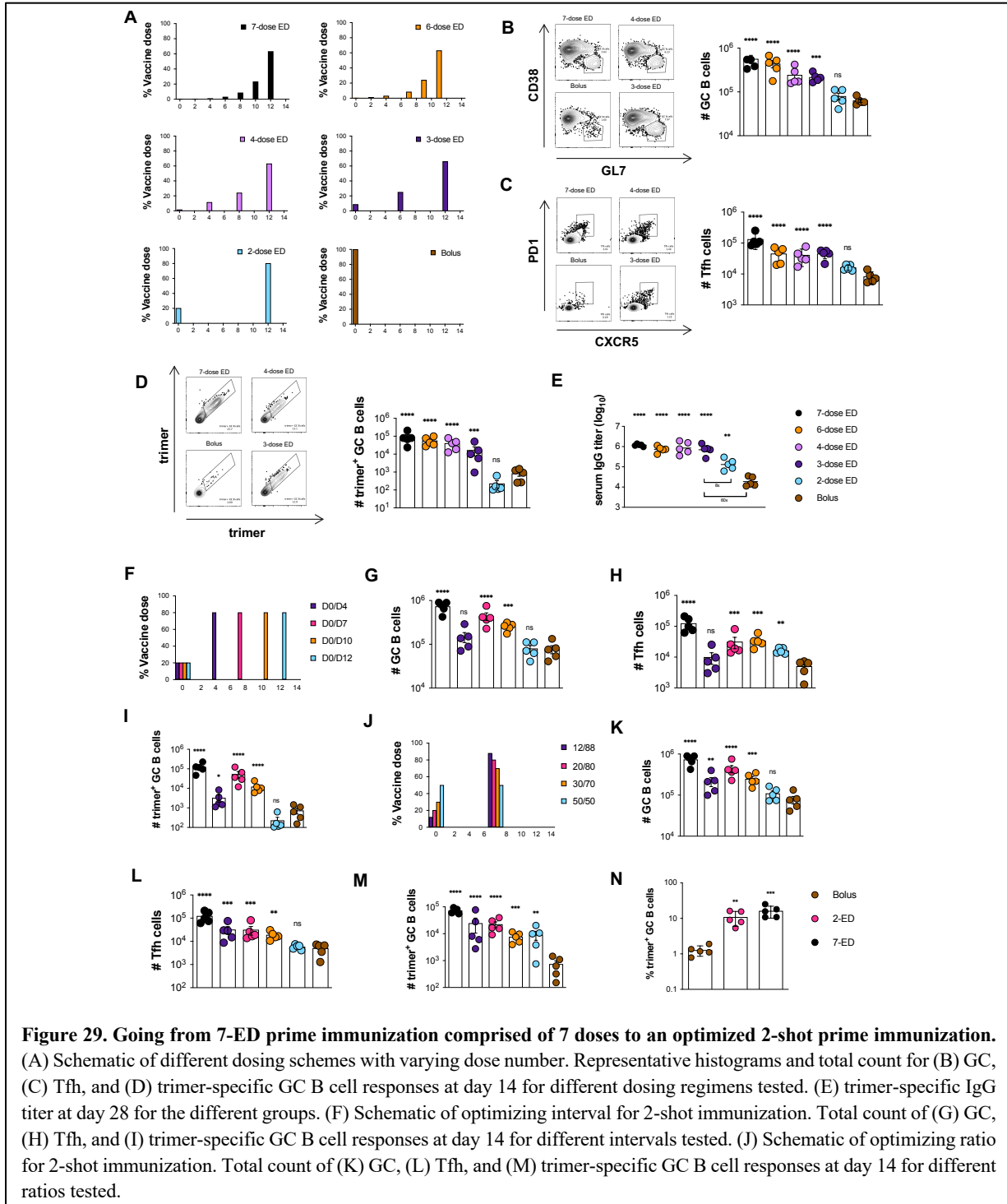
Previous reports found that administration of a given dose of protein antigen and adjuvant as 7 injections administered in an exponentially-increasing pattern over 12 days (hereafter, 7-ED regimen) could greatly augment GC and antibody responses in mice⁹⁹ and non-human primates^{100,525}. Though these immune response enhancements are compelling, such a regimen is impractical for general use in clinical immunization campaigns, and thus we sought to determine whether a “reduced” escalating-dose regimen involving fewer injections could still achieve some

or all of the effects of the full 7-dose immunization pattern. Using a stabilized HIV Env SOSIP trimer immunogen engineered to promote priming of N332-supersite-directed B cells (N332-GT2⁵¹¹) and a potent saponin nanoparticle adjuvant (saponin/MPLA nanoparticles, SMNP^{512,531}), we conducted an evaluation of simplified dosing regimens in mice. Given the large parameter space to explore, we opted to focus on analysis of GC responses at day 14 for all groups, as we previously found that GC responses in mice peaked at this timepoint for immunization patterns as disparate as bolus and the full 7-dose ED regimen⁹⁹. First, starting from the previously defined optimal 7-ED regimen, we found that as the total number of doses was reduced keeping the interval between the first and last dose fixed (**Fig. 29A**), the total size of the GC and Tfh responses steadily dropped (**Fig. 29B-C**). However, staining with fluorescent trimer probes to identify antigen-specific cells, the number of trimer-binding GC B cells dropped only ~5-fold moving from 7 doses down to 3 doses, while a 2-dose ED pattern elicited an antigen-specific GC B cell response not statistically different from bolus (**Fig. 29D**). Trimer-specific serum IgG antibody responses measured one month after dosing were similar for 7, 6, 4, and 3-dose ED, but 2-dose and bolus immunization were ~1 and ~2 logs lower, respectively (**Fig. 29E**). Thus, even a 3-dose escalating immunization pattern can substantially enhance many elements of the humoral immune response relative to traditional bolus immunization.

We hypothesized that the poor response to 2-dose escalating immunization could reflect that a 12-day interval between doses is too wide a gap to optimally feed antigen to the GC response, and thus we next tested two-dose escalating patterns administered at intervals ranging from 4 to 12 days, fixing the initial dose at 20% of the total, and the remaining 80% of the vaccine dose administered at the second injection (**Fig. 29F**). In this series, a two-dose escalating prime immunization with an interval of 7 days elicited an optimal response, eliciting 4-fold more total GC B cells and 5-fold more Tfh than bolus immunization (**Fig. 29G-H**). Remarkably, the 7-day 2-dose pattern elicited 10-fold more trimer-binding GC B cells than bolus immunization, only 3-fold fewer than the previously-optimized 7-dose two-week escalating dosing pattern (**Fig. 29I**).

Motivated by these findings, we next evaluated the impact of the dosing ratio (the proportion of total vaccine administered at dose 1 vs. dose 2, **Fig. 29J**). Administration of 12 or 20% of the vaccine in the first dose led to similar total GC, trimer-binding GC B cells, and Tfh responses, while increasing the initial immunization to 30 or 50% of the total dose led to decaying responses (**Fig. 29K-M**). The enhanced elicitation of antigen-binding GC B cells elicited by two-

dose ED priming reflects a combination of increased size of the GC and also an increased

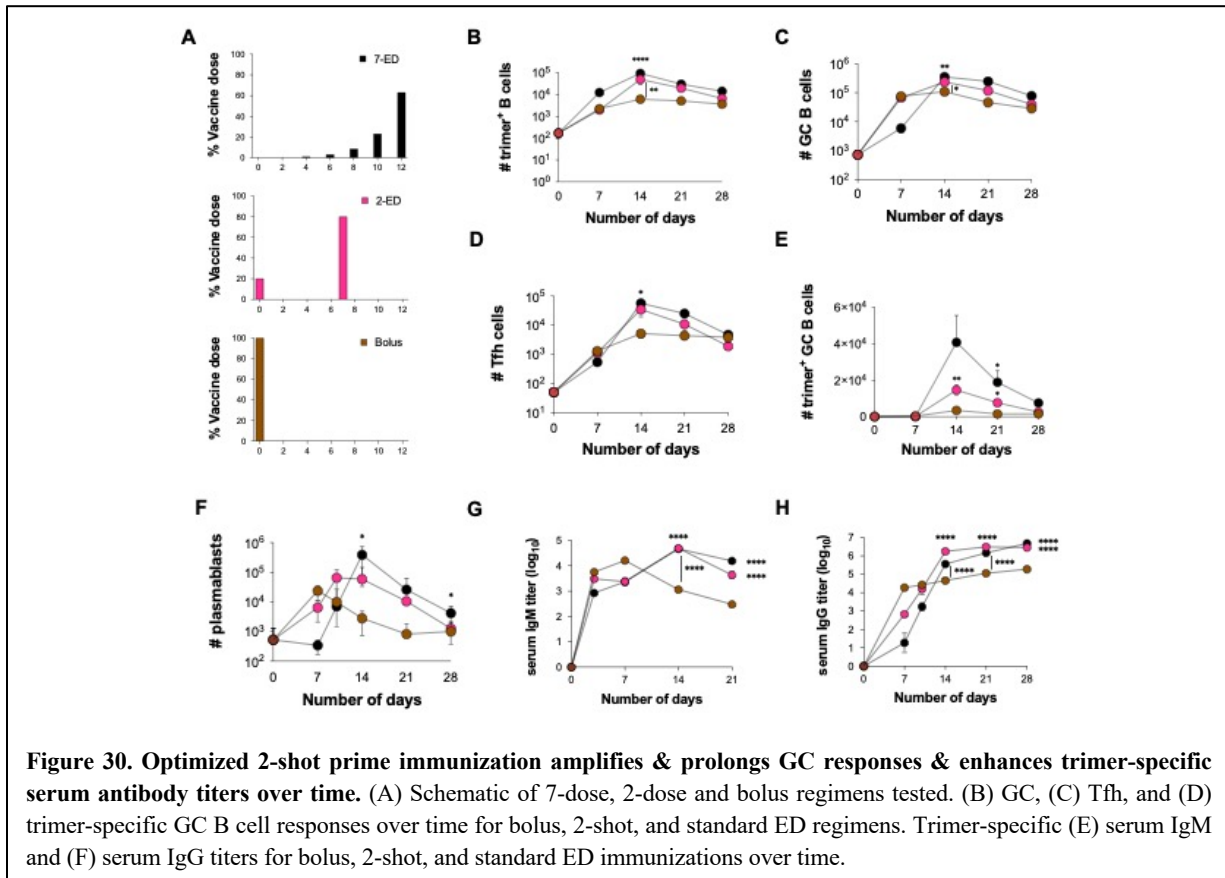


proportion of GC B cells recognizing intact antigen (Fig. 29N). Altogether, these data demonstrate the ability of even a minimal two-dose extended priming immunization to augment multiple facets of the humoral response to vaccination.

5.2.2 Optimized 2-dose ED priming amplifies both the magnitude and duration of GC responses compared to bolus immunization

We next assessed the evolution of the B cell response over time for the optimized 2-ED regimen compared to bolus or 7-ED immunization, to evaluate potential differences in the temporal dynamics or lifetime of the GC in each case (**Fig. 30A**). Trimer-binding B cells were detectable in all groups at day 7 and peaked at day 14, but total antigen-specific B cells were 15-fold and 5-fold greater in the 7-ED and 2-ED groups compared to bolus, respectively (**Fig. 30B**). Interestingly, despite the difference in initial vaccine dose administered, GC responses for bolus and 2-dose ED followed a similar kinetic trajectory until ~day 10, when they began to diverge (**Fig. 30C**). At this timepoint, the GC response for both ED groups continued to expand and followed a similar temporal trajectory distinct from the bolus immunization. The number of Tfh cells in the two ED groups also sharply expanded between day 10 and 14 (**Fig. 30D**). At the peak of the response at day 14, 7-ED and 2-dose ED vaccination elicited ~10- and ~6-fold greater numbers of Tfh cells compared to bolus immunization. Trimer-binding GC B cell numbers peaked for all 3 immunization conditions at day 14, and both ED regimens maintained higher levels of antigen-specific GC cells compared to bolus immunization through day 21 (**Fig. 30E**). Finally, lymph node plasmablasts were expanded by day 7 for both the bolus and 2-ED immunizations; these responses peaked at day 7 and day 10, respectively, then steadily decayed (**Fig. 30F**). In response to the 7-ED regimen, plasmablasts peaked later, at day 14, before contracting.

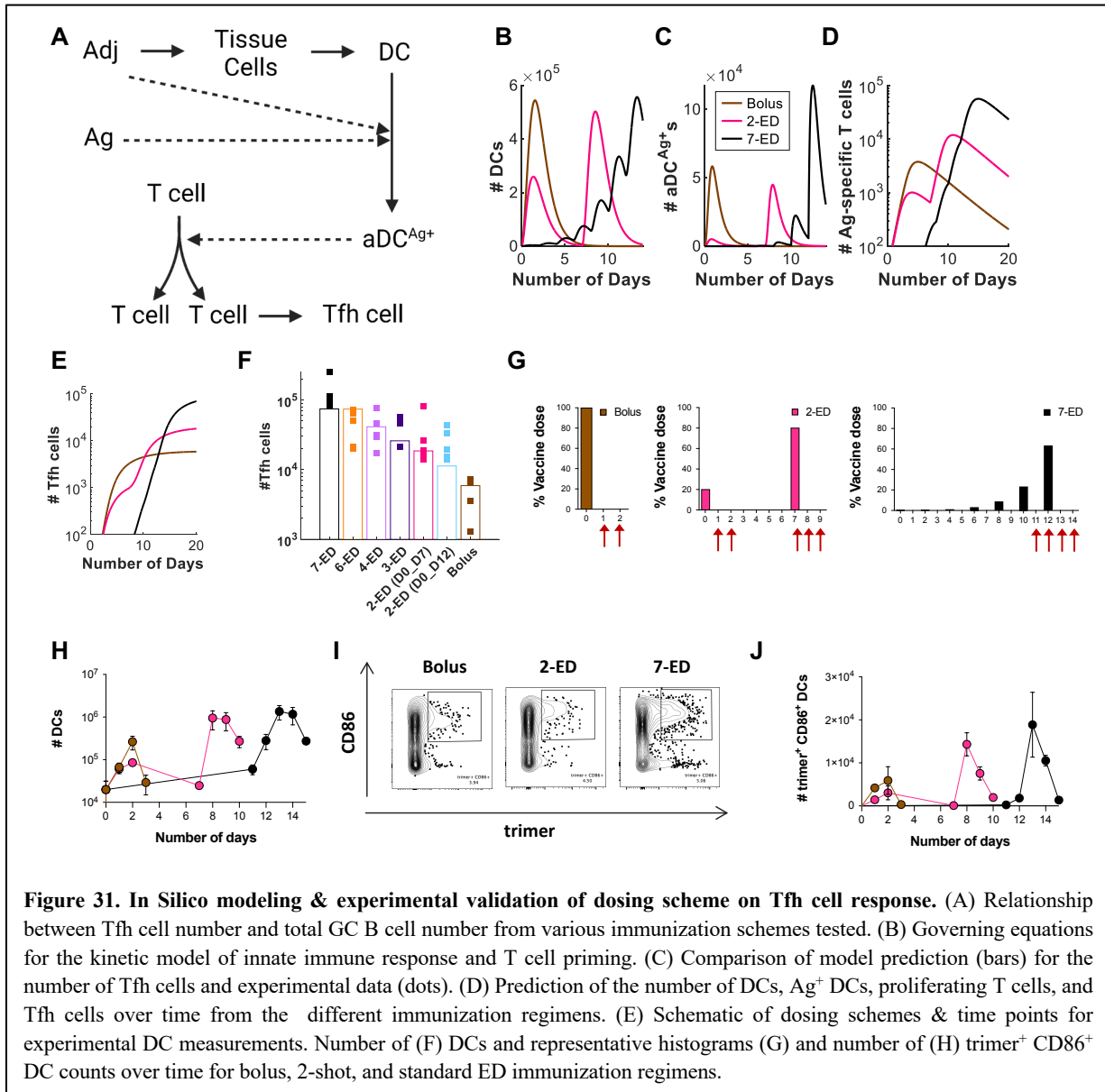
ED immunizations also impacted the evolution of serum antibody responses. IgM responses primed by bolus immunization peaked at day 7 then decayed steadily, while the two ED groups elicited IgM responses that peaked later, at day 14 (**Fig. 30G**). Bolus immunization elicited substantial serum IgG titers by day 7 which rose only slightly over the subsequent 3 weeks (**Fig. 30F**). By contrast, IgG responses for the two ED regimens increased sharply between day 7 and day 14, reaching levels ~10-fold greater than the bolus group by day 28 (**Fig. 30H**). Hence, both the 7-dose and simplified 2-dose ED regimens elicited changes in the humoral response that persisted over many weeks and primed strong, stable serum antibody responses greatly increased over traditional bolus immunization.



5.2.3 Extended and reduced dosing regimens boost innate inflammation in lymph nodes and allow for improved T cell responses

The data in Figures 29 and 30 demonstrate a substantial benefit of even a two-dose escalating immunization pattern over traditional bolus vaccination, thus we next turned to studies aiming to understand the mechanisms underlying this substantial amplification of the humoral immune response. Upon evaluating the relationship between Tfh cell number and total GC B cell number from the various immunization patterns that were tested, we observed a linear correlation between the two metrics (**Fig. 31A**). Such a relationship has been observed in prior studies^{532,533}, and is consistent with selection by Tfh cells acting as a key bottleneck controlling proliferation of GC B cells^{70,506,534}. To understand factors determining Tfh expansion during escalating dose immunization, we developed a coarse-grained kinetic model of the innate immune response and T cell priming (**Fig. 31B**). Briefly, in this model the adjuvant (Adj) activates tissue cells at the immunization site and/or draining lymph node, which release cytokines and chemokines that

recruit dendritic cells (DCs) to the tissue and trigger their activation coincident with antigen (Ag) uptake. Activated, antigen-loaded DCs (aDC^{Ag+}) then prime T cells in the draining lymph node. Adjuvant plays an important role in activating DCs and helps deliver antigen to DCs⁸⁴. As a proxy for these effects, we assume that adjuvant activity increases the rate of antigen uptake by DCs. The proliferation of T cells induced by the Ag^+ DCs is described according to a previously reported model⁵³⁵, and we assume proliferating T cells differentiate into Tfh cells at a constant rate⁵³⁶.



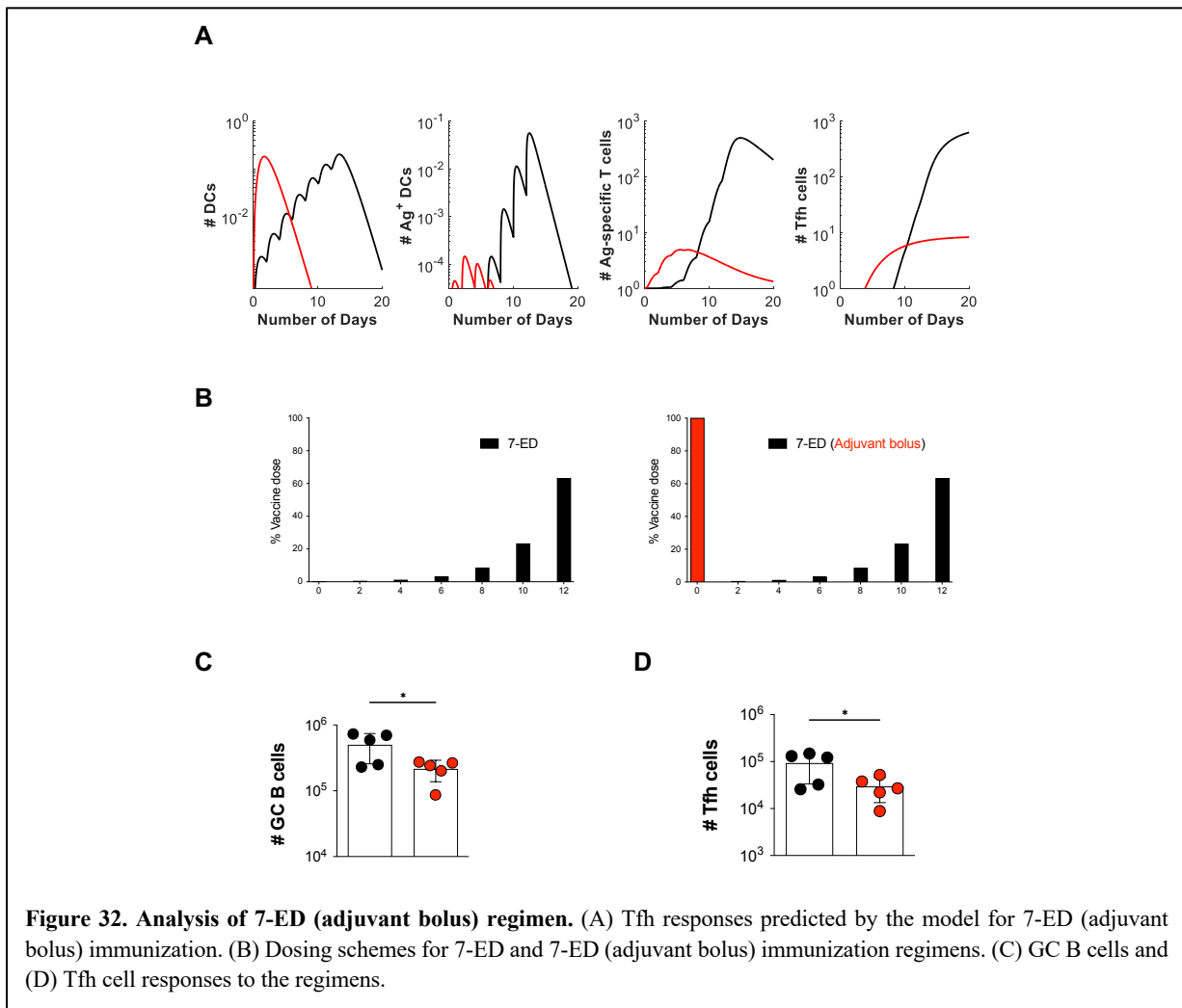
We first examined model predictions of the number of total DCs, Ag^+ activated DCs, antigen-specific proliferating T cells, and Tfh cells following bolus, optimal 2-ED, and 7-dose ED

immunization schemes (**Fig. 31C**). This analysis revealed that for bolus immunization, levels of total DCs and activated, antigen-loaded DCs peak within X days and rapidly decay due to rapid antigen clearance (**Fig. 31C-D**). By contrast, with 7-ED dosing, waves of DC recruitment induced by the sequential doses lead to DC accumulation in lymph nodes throughout the dosing time course (**Fig. 31C**). A significant number of DCs are already available when the final dose of standard ED is given at day 12, which leads to efficient uptake of antigen by activated DCs toward the end of the dosing course (**Fig. 31D**). Because T cells proliferate exponentially, extended stimulation by Ag⁺ DCs during the 7-ED regimen contributes to the substantially greater peak antigen-specific T cell expansion and Tfh production compared to the bolus (**Fig. 31E-F**), consistent with previous studies^{535,537}. For similar reasons, the model also predicts a greater T cell number with 2-dose immunization compared to bolus. However, the difference is smaller because, with realistic biological parameters, DC numbers are predicted to return to the baseline before the second dose (**Fig. 31C-F**).

We next modeled each of the escalating-dose regimens tested in **Fig. 29C**, and found that the model indeed captured the pattern of Tfh responses observed experimentally (**Fig. 30G**). Further, the model correctly predicts the enhanced Tfh response elicited by a day 0-day 7 two-dose vaccination (**Fig. 31G**). Because of the relationship between adjuvant and DC recruitment/activation, the model also predicts that optimal ED immunization requires co-administration of antigen and adjuvant across the timecourse- if antigen is administered in an escalating-dose pattern but adjuvant is administered as a bolus, poor synchronization of DC recruitment and antigen availability is predicted, and thus weak Tfh priming despite escalating dose antigen administration (**Fig. 32A**). In agreement with this prediction, vaccination of mice with a bolus adjuvant/7-ED antigen dosing schedule elicited much weaker GC and Tfh responses than escalating dosing of antigen and adjuvant together (**Fig. 32B-D**). Thus, this very simple model captures the relative magnitudes of increased Tfh expansion observed for the two ED regimens compared to traditional bolus immunization.

In order to further interrogate the predictions of the kinetic model, we immunized mice with fluorescently-labeled N332-GT2 trimer and SMNP adjuvant using ED or bolus dosing schemes, and analyzed DCs in the draining lymph node at key time points post immunization (**Fig. 31E**). After bolus immunization, both the total number of DCs and activated (CD86⁺) trimer⁺ DCs increased in LNs increased over 2 days (**Fig. 31E-H**). The initial dose of 2-ED also expanded

activated antigen-loaded DCs over the first two days, though at a lower level, and returned to baseline by day 7 when the second dose was administered, as predicted by the model (**Fig. 31H**). Interestingly for the 2-dose regimen, although the number of DCs in LNs return to the baseline as predicted by the model, the kinetics of DC influx after the 2nd dose are much faster than after the 2nd shot of the regimen, with antigen-bearing activated DCs numbers notably increased as early as 24h post injection (**Fig. 31E-H**). For the 7-ED regimen, lymph node DCs did not show substantial accumulation until day 12– when the final dose was administered– and continued to sharply accumulate to peak levels of trimer-specific CD86⁺ DCs at day 13 (~3x over bolus), prior to the start of contraction (**Fig. 31E-H**). Thus, the temporal evolution of activated, antigen-loaded DCs observed experimentally is consistent with the simple model of DC recruitment governed by adjuvant kinetics.

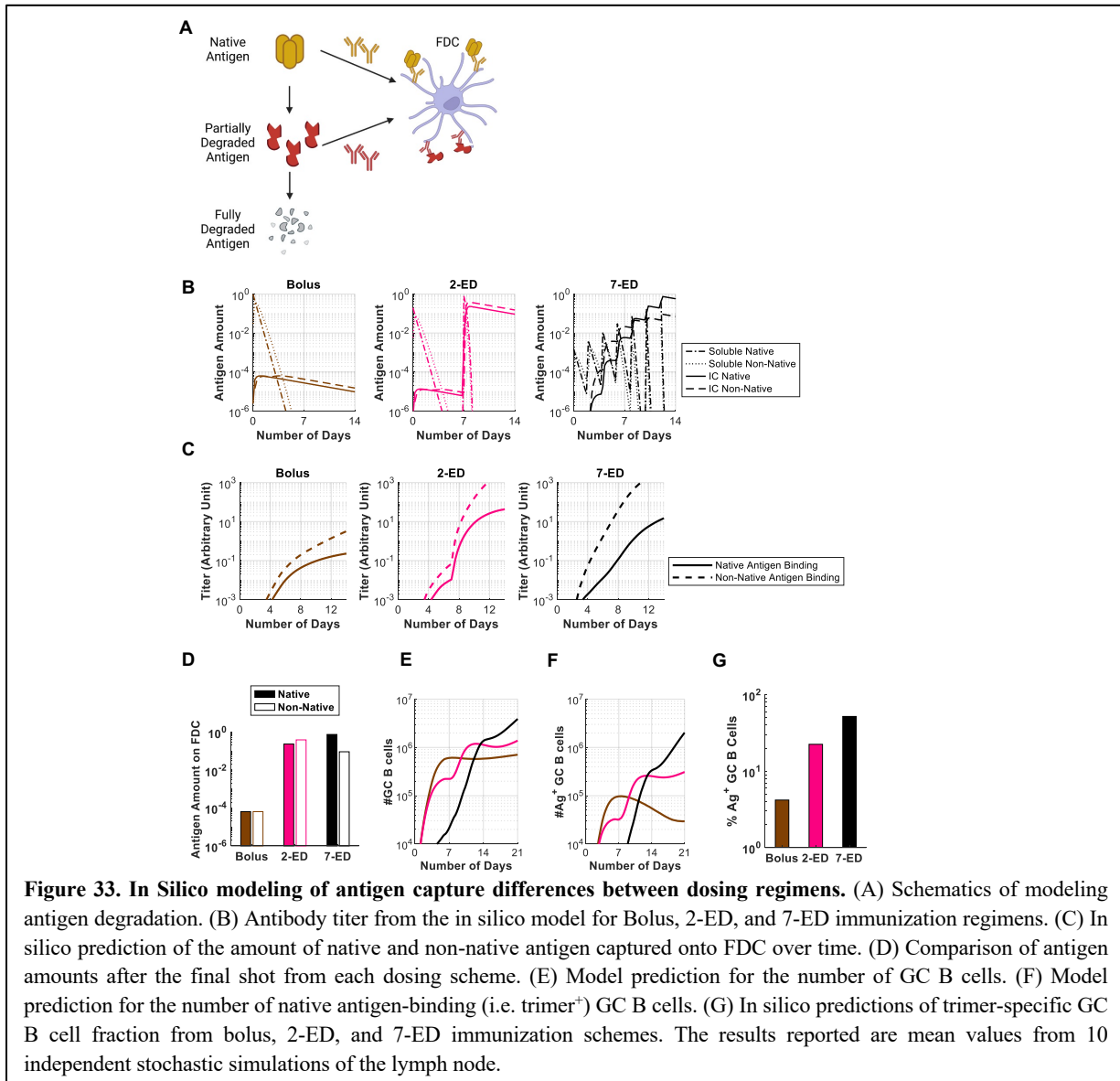


5.2.4 Computational modeling of the GC response predicts improved native antigen capture following extended-prime immunizations

Using a computational model of the germinal center reaction, we previously predicted that ED immunization can increase the size of the GC response via capture of antigen on follicular dendritic cells (FDCs)⁹⁹: initial vaccine doses in the ED regimen trigger initial B cell priming, and 7-10 days after the start of dosing, affinity-matured antigen-specific antibodies will begin to be produced. During ED immunization, antigen is still being delivered to the lymph node at this time point, and these newly produced antibodies form immune complexes with incoming antigen and facilitate its transport to FDCs, where it can promote expansion of the GC response. However, here we found that ED dosing also dramatically enhances the proportion of GC B cells that bind to the intact immunogen (10-fold and 5-fold vs. bolus for standard ED and 2-dose ED, respectively, **Fig. 29N**), an effect not captured in our previous simplified computational model. We recently reported that extracellular protease activity in lymph nodes plays an important role in modifying B cell responses, such that 24 hr post bolus-vaccine dosing onwards, ~50% of the available extracellular antigen pool in lymph nodes is degraded⁵³⁸. This antigen breakdown occurring in sinuses and extrafollicular regions of the node limits the quantity of intact antigen available to B cells and creates immunogen breakdown products that can prime competitive off-target B cell responses. However, protease activity was found to be low in B cell follicles, and we showed that capture of antigen by FDCs during ED immunization led to a much greater accumulation of intact antigen in follicles for escalating dose vs. traditional bolus immunization⁵³⁸.

To determine if greater levels of intact antigen captured in follicles could explain the greatly increased proportion of trimer-specific GC B cells detected for ED immunization, we modified our previously developed computational model of the B cell and antibody response⁵³⁹ (which combines the cellular dynamics of GC B affinity maturation and extrafollicular B cell expansion with the kinetics of antibody production and antigen capture), to incorporate effects of antigen degradation. Briefly, we assume that the B cells can target either native or partially degraded antigen, as schematically shown in **Fig. 33A**. Both types of antigens can be transported to FDCs by the corresponding antibodies that bind to them, where they are protected from further degradation. Additionally, to model the antibody response to HIV Env immunogens, we assume that the non-native antigen is more immunodominant— as HIV Env trimers are heavily glycosylated

and present few sites for high affinity antibody binding in the intact state, but are expected to expose more proteinaceous surfaces as they degrade⁵²⁰.



The model shows that very small overall amount of antigen is captured onto FDC after bolus immunization because most of the antigen decays before antigen-specific antibody responses are induced (**Fig. 33B-D**). As a result, highly stringent conditions are maintained for GC B cell survival, resulting in a GC response that is dominated by the immunodominant non-native epitope-targeting B cells (**Fig. 33E-G**). With the 2-dose regimen, antibody response against both the native and non-native epitopes are generated after the first dose (**Fig. 33B-C**). However, upon the second dose, much greater amounts of both types of antigens are captured onto FDCs over bolus

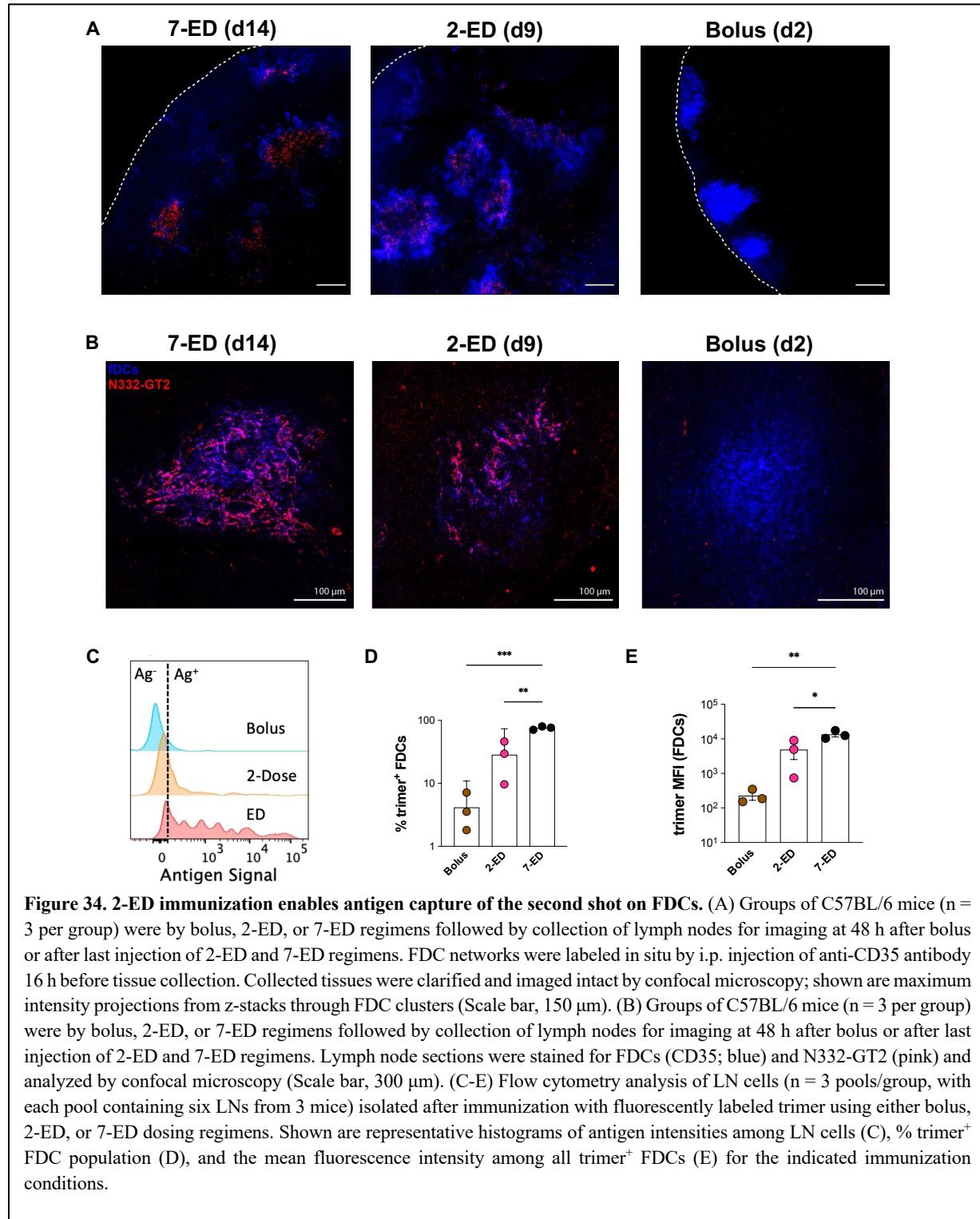
immunization (**Fig. 33C-D**). The increased antigen availability weakens the immunodominance hierarchy between the two antigens and leads to a much greater native trimer-binding GC B cell response (**Fig. 33C-D**)⁵³⁹. Finally, with 7-ED dosing, the antibody titer is already high when the final dose (63% of vaccine dose) is administered on day 12 (**Fig. 33B**). Although titer for both types of antigen is high, antigen can be rapidly captured by the high titer of antibodies and move to the follicles where it is protected (**Fig. 33C**). Therefore, the ratio of native and non-native antigen presented on FDC is shifted in favor of the former (**Fig. 33D**), allowing even better trimer-specific response compared to the 2-dose scheme (**Fig. 33E-G**). These predictions of the GC model align well with the experimentally-measured frequencies of intact trimer-binding GC B cells (**Fig. 29N**).

5.2.5 A two-dose escalating prime increases antigen capture in follicles compared to bolus immunization

A key prediction of the GC computational model is that a sufficient quantity of antibody specific for intact antigen can be produced by day 7 to enable antigen capture by FDCs to occur even following a 2-dose escalating prime immunization. As shown in Fig. 30G-H, antigen-specific IgM and IgG were both detectable in serum by day 7 in the 2-ED regimen. To test the model prediction, we immunized mice with fluorescently-labeled N332-GT2 trimer by each of the three dosing schedules, and analyzed the biodistribution of the antigen in lymph nodes via confocal imaging of lymph node histological sections and cleared whole lymph node tissues following bolus or ED immunizations. Both cleared whole LN (**Fig. 34A**) and traditional thin section imaging (**Fig. 34B**) revealed that presence of substantial amounts of antigen co-localized with FDCs 2 days following the last dose of the full ED regimen, while little if any antigen could be detected 2 days after bolus vaccination. Consistent with the model predictions and our prior studies, substantial amounts of FDC-localized antigen were also found in draining lymph nodes two days following the second dose of the 2-dose ED immunization (**Fig. 34A-B**)^{99,100}. High magnification imaging of the follicles of the ED groups suggested this follicle-localized antigen was associated with FDC dendrites (**Fig. 34B**).

Flow cytometry analysis of LNs pooled from multiple mice immunized with the dosing regimens revealed that 2-dose or standard ED immunizations increased the amount of FDC-trapped antigen by 20-fold and 60-fold over bolus immunization, respectively (**Fig. 34C-E**). Thus,

consistent with the computational model of GC dynamics, even a two-dose escalating prime vaccination is capable of achieving antigen targeting to FDCs and increasing the level of antigen retained within the LN.

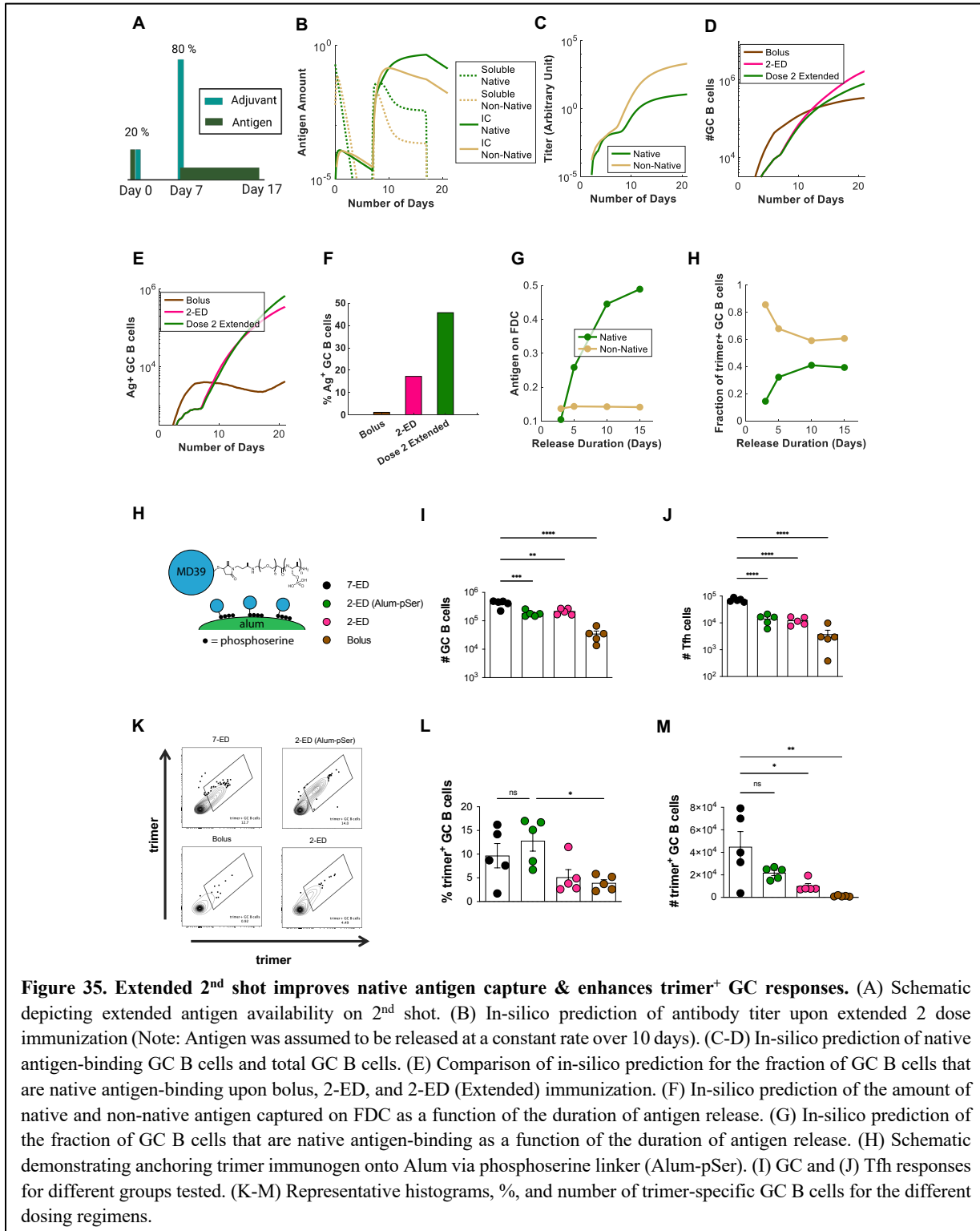


5.2.6 Extending antigen availability on the second immunization further boosts humoral responses as a consequence of innate immune activation and Tfh help

Given that the computational model of the GC reaction is able to provide qualitatively accurate predictions of the observed size GC and proportion of antigen-specific GC B cells, we next used the model to explore a much wider parameter space of dosing patterns than would be possible experimentally, to gain further insight into how humoral responses might be further bolstered using extended priming. The modeling and experimental data suggest that having a high trimer-binding antibody titer present before the majority of the antigen dose is cleared is an important factor governing the magnitude of the “on target” GC response. In the 2-ED prime immunization regimen, antibody titers increase steadily after the 2nd immunization because of extrafollicular expansion of the B cells, as predicted by the model (**Fig. 32B**) and shown by experimental measurements (**Fig. 30H**). However, because intact antigen in the lymph node decays rapidly (estimated half-life ~4.2 hours), most of the antigen arriving after the second immunization decays before high titers of antibody are reached, limiting immune complex formation and subsequent antigen capture by FDCs. Thus, we hypothesized that extending antigen availability over a longer time period at the second dose might substantially enhance GC responses. We thus simulated a 2-dose ED regimen where antigen was released from the injection site at a constant rate over 10 days after the second injection (**Fig 35A**). In this case, a significant fraction of the antigen dose arrives at the dLN after high titer levels of trimer-specific antibody are generated and is thus captured in immune complexes in an intact state (**Fig 35B-C**). Thus, the model predicted that such a scheme may lead to a superior trimer-specific GC B cell response compared to the 2-dose immunization (**Fig. 35D-F**). Varying the duration of antigen delivery after the second dose shows that a longer release duration leads to more native antigen on FDC (**Fig. 35G**) and better trimer-specific GC B cell response (**Fig. 35H**), highlighting the importance of dosing kinetics.

To experimentally test this idea, we employed using an approach we previously developed¹⁰⁴ to achieve slow-delivery effects in a manner readily translatable to clinical use: a C-terminally-modified SOSIP stabilized Env trimer termed MD39⁵⁴⁰ (very similar in sequence to the N332-GT2 trimer) was conjugated with short phosphoserine (pSer) peptide affinity tags (one tag per protomer at the base of the trimer). Phosphate groups in the affinity tags undergo a ligand exchange reaction with the surface of alum particles, enabling oriented high-avidity binding of the trimer to aluminum hydroxide adjuvant on simple mixing (**Fig. 35H**). By stably anchoring the

antigen to alum particles, on injection, the antigen is slowly released from the injection site as alum particles slowly disaggregate over time^{104,531}. Using this simple approach, alum-adsorbed MD39 trimers that normally clear from the injection site within a few days instead clear much more



slowly, over ~10 days¹⁰⁴. We thus tested a two-dose ED immunization giving 20% of the vaccine dose on day 0 as a bolus and 80% of the dose as an alum/pSer-trimer formulation on day 7. Consistent with the model's predictions, the extended 2-dose approach elicited a trend toward increased total GC B cells and Tfh cells (**Fig. 35I-J**), a 2-fold increase in both the total number and frequency of trimer-binding GC B cells compared to the 2-ED regimen (**Fig. 35K-M**), respectively. Thus, we have shown that an engineered 2-dose immunization, providing an initial “priming” dose followed by a larger extended-release vaccine dose retains much of the benefit to the GC response and fully amplifies the serum antibody response, substantially greater than bolus immunization.

5.3 Discussion

In previous studies, it was discovered that prolonging vaccine availability through extended dosing strategies such as via implantable osmotic pumps or repeated injections of a given dose of vaccine over time alters multiple facets of the immune response— increasing the number of B cells entering GCs, increasing the number of antigen-specific Tfh generated, increasing the number of unique clones in the GC, leading to increased total antibody titers, memory B cells, and neutralizing antibody production^{99,100,523}. In particular, an escalating-dose immunization of 7 shots administered in an exponentially-increasing dose pattern over two weeks was particularly effective in both mice and non-human primates for promoting humoral responses to HIV Env immunogens^{99,100,525}. However, administering seven doses is not practical for mass vaccination. Here we sought to better understand the critical elements of this potent dosing strategy, and based on our understanding of the mechanisms of ED-induced B cell responses, we hypothesized that a two-dose immunization, with an initial small dose of antigen to initiate B cell priming followed by a larger second dose that could be given to promote antigen deposition in follicles, might still offer substantial enhancements in humoral responses over traditional bolus vaccination. Such a scenario- two shots administered 1-2 weeks apart, would not be out of the realms of practicality (e.g., compare to current COVID-19 mRNA vaccines, administered twice at a 3- or 4-week interval). Through systematic studies varying the number of doses, dose ratio, and dose intervals in mice, we found that a two-shot reduced ED regimen, administering 20% of the vaccine dose on day 0 and 80% vaccine dose on day 7 elicited 10-fold increases in antigen-binding GC B cells,

prolonged the GC reaction, and increased serum antibody responses 100-fold relative to bolus immunization. and enabled antigen capture of the second shot on FDCs, though not reaching the immune response levels elicited by the standard ED regimen. Informed by computational modeling of the GC response, we further optimized an extended-release formulation on the 2nd shot by anchoring the antigen onto alum via a phosphoserine linker resulting in even better antigen-specific GC responses over the reduced 2-shot regimen. Thus, our work demonstrates the possibility of engineering an extended 2-shot prime to mimic the effects of standard ED-induced dosing without requiring as many injections.

To gain insight into factors governing these beneficial effects of even two-dose priming, we analyzed the parameter space of reduced dosing to gain insights into the requirements for extended dosing immunizations. Our preliminary studies showed that the two-shot immunization approach, with an initial priming dose followed by a larger vaccine dose, generated similar germinal center (GC) and serum antibody responses as the three-dose and four-dose approaches. We hypothesize that the early priming dose is sufficient to seed GCs and allow for antibody development, while the larger dose at later time-points enables native antigen capture and significantly improves the immune response over bolus immunization. Subsequent studies showed that administering a majority of the vaccine dose at later time-points for the three-dose and four-dose regimens improved GC responses compared to earlier administration of the doses, potentially indicating that native antigen capture is a key factor driving the enhanced GC responses observed. We also tested whether the reduced two-dose immunizations could match the potency of the standard ED regimen for driving robust GC and humoral responses. While it did not reach the level of standard ED, the two-dose regimen showed a substantially enhanced and prolonged GC response, over an order of magnitude higher than bolus immunization. This is particularly promising as previous studies have shown that the size of the early GC response predicts the magnitude of neutralizing antibodies generated by immunization with HIV Env trimers in rhesus macaques⁵²³. Long-lasting GCs can maximize polyclonal antibody titers against the trimer antigen and improve the diversity of antibodies generated, with special emphasis on immunologically subdominant responses that target relatively conserved epitopes on the spike of a highly mutable virus^{6,541}. Our studies highlight the impact of dosing regimen on the quantity, quality, and kinetics of GC development and the corresponding improvements that translate to orders of magnitude improved trimer-specific antibody responses over time. Furthermore, the dosing regimen also

augmented extra-follicular responses, with the peak of plasmablast numbers improved by an order of magnitude, also contributing to the enhanced immune response observed in these regimens. Early GC-derived plasmablasts are induced by IL-21 from Tfh cells and IL-6 from stromal cells. The standard and reduced ED dosing regimens demonstrate greater Tfh cell frequencies, thus suggesting an increased Tfh helper capacity as a consequence of the extended dosing regimens compared to bolus immunization. Therefore, optimizing the immunization schedule to engage humoral responses is a means of positively affecting Tfh help and should be carefully considered.

T follicular helper (Tfh) cells are essential for the germinal center (GC) reaction, providing support to B cells to generate long-lived plasma cells and memory B cells⁵⁴². Tfh cells secrete cytokines such as IL-21 and IL-4, which enhance B cell proliferation, differentiation, and immunoglobulin class switching⁵⁴³. Moreover, Tfh cells provide help through cell-to-cell interactions, including the T cell receptor (TCR) and B cell receptor (BCR), and CD40-CD40L signaling pathway⁵⁴⁴. Improved Tfh cell support in GC reactions can produce higher-affinity antibodies, which are more effective in neutralizing pathogens. Therefore, the improved humoral responses observed with extended dosing could be the result of newly activated Tfh cells entering existing GCs and augmenting & potentially prolonging the response. In particular, the 2-shot regimen benefits from the fact that T cells begin to concentrate in GCs 5-8 days post immunization^{545,546}. Thus giving the 2nd shot of greater antigen after the GC has matured has a potent effect on improving the T cell response as compared to giving it at an earlier time point. The 2-shot and standard ED regimens show an increasing number of Tfh cells, supporting this observation. Tfh cell development relies on antigen priming of naïve T cells by dendritic cells (DCs), which predominantly locate in T cell zones and have the greatest chance to prime CD4+ T cells⁵⁴³. Once primed by DCs, CD4+ T cells that receive Tfh cell-inductive signals upregulate Bcl6, promoting CXCR5 chemokine receptor expression and migration to the T-B border. The maintenance of Tfh cell phenotype requires sustained antigenic stimulation⁵³³. Repeated immunization enhances Tfh development, which informs the kinetic progression of the T cell response and provides insight into the appropriate interval of 6-8 days for our 2-shot approach. The 2-shot immunization leads to a rapid increase in MHC-II+ DCs after the 2nd dose, priming previously activated T cells and allowing pre-GC Tfh cells to develop into GC-Tfh cells, resulting in the improved Tfh response we observed. This approach overcomes the requirement for antigen/adjuvant during the effector phase to achieve optimum Tfh responses since Tfh cells are

heavily regulated in the early GC phase^{547,548}.

We observed that the amplification of GC/Tfh occurs towards the end of the dosing schedule, corresponding to the capture of native antigen on FDCs. Our study results show that an important mechanism underlying the efficacy of extended dosing regimens is the improved capture of native antigen on FDCs. In a reduced 2-shot immunization, administering a majority of the antigen on the 2nd shot allows for exploitation of pre-existing antibody responses from the lower 1st dose to form FDC-targeted immune complexes *in vivo* since the larger dose of immunogen is provided during a window of time when antigen-specific antibody is available for immune complex formation. Extending 2nd shot further takes advantage of the increasing concentration of antibody to improve native antigen capture & consequently boost trimer-specific GC responses since prolonging antigen availability when the first affinity-matured antibodies are being produced leads to even greater capture and retention of intact antigen on FDCs within follicles. Our synergistic deployment of computational and experimental studies offers new insight into the dynamics of antibody development & antigen capture that can have broad implications designing vaccine dosing regimens. With extended dosing, the kinetics of immune complex deposition are altered, allowing for synchronized native antigen availability with the GC. This is in contrast to bolus immunization where much of the antigen presented to GC B cells by FDCs is non-native protein and breakdown products, some of which can be immunodominant and distract the GC response from relevant targets^{549,550}. Extended dosing retains antigen in the draining LN significantly longer than mice given a bolus immunization which correlates with improved immune complex formation on FDCs. More antigen on FDCs during later stages of a GC likely increases GC B cell clonotypic diversity, allowing for significantly more BCR sequence space to be explored for high affinity BCR mutations. Extended dosing can also encourage SHM and favor B cells with nAb specificities over those with non-neutralizing specificities, such as those targeting breakdown products.

Several technologies are being developed to recapitulate the effects of the standard ED regimen. Our findings provide a strong rationale for utilizing reduced dosing immunization strategies that promote native antigen capture in the FDC network and enhance humoral responses. Developing a single-shot system that could mimic the effects of extended dosing would greatly improve compliance and increase vaccine coverage in developing countries. We have demonstrated the potential of a 2-shot regimen, but several single-shot approaches, such as

microfabrication-based PLGA particles or atomic layer deposition-based technologies, could also achieve this goal. The particles contain vaccine-infused core that can release its cargo at various timepoints based on chemical modifications to the PLGA polymer⁵⁵¹. Similarly utilizing a slow-dissolving alum coating to unmask and release the vaccine over tunable time periods can alter vaccine kinetics to mimic extended dosing effects⁵³⁰. These technologies could be particularly important for generating protective antibody responses against challenging pathogens such as HIV and for generating broadly neutralizing antibody responses against other variable pathogens. However, it is crucial to consider potential toxicities associated with these regimens, as multiple immunizations of potent adjuvants with the standard ED regimen could result in undesirable side effects. Similarly, extended delivery technologies must avoid injection site reactogenicity and chronic inflammation. Collectively, these efforts will establish effective strategies that can be broadly applied in vaccine design to achieve the benefits of extended dosing in real-world vaccines.

To summarize, we have optimized an extended two-dose priming approach that improves humoral immune responses to HIV trimers in an attempt to recapitulate responses achieved by the standard escalating dose regimen comprised of 7 doses. Our findings demonstrate our ability to: (i) augment GC and Tfh responses to HIV immunogens; (ii) increase trimer-specific serum antibody titers over bolus immunization; and (iii) highlight the critical role of antigen capture dynamics in driving the enhanced immune responses.

5.4 Materials and Methods

Immunogens

N332-GT2 trimers were expressed in FreeStyle 293F cells (Invitrogen, Cat no. R79007) and purified in two steps by affinity chromatography using a GE HisTrap column and size-exclusion chromatography using a GE S200 Increase column as described previously^{510,511}. MD39 HIV Env trimer was generated as previously described⁵¹⁰. Both trimers were administered at a dose of 10 ug per animal.

pSer-conjugation

Immunogens were expressed with a free terminal cysteine and reduced by incubation with 10

molar equivalents of tris(2-carboxyethyl)phosphine (TCEP, ThermoFisher) at a concentration of 1 mg/ml, followed by incubation at 25°C for 10 minutes. The reduced protein solutions were then processed using Amicon Ultra Centrifugal Filters (10 kDa MWCO, Millipore Sigma) to remove TCEP, and the resulting protein was mixed with 5 molar equivalents of pSer-maleimide linkers at a concentration of 1 mg/ml for 16 hours at 4°C in tris-buffered saline (TBS, Sigma Aldrich) at pH 7.2-7.4. After the reaction, unreacted pSer linker was removed using centrifugal filters in TBS, and pSer-antigen was buffer exchanged to PBS.

Adjuvant preparation

The saponin adjuvant used in this study was an ISCOM-like self-assembled nanoparticle consisting of Quillaja saponin, cholesterol, DPPC, and MPLA⁵¹². Briefly, solutions of cholesterol (20mg/ml final concentration, Avanti Polar Lipids Cat# 700000), DPPC (20mg/ml final concentration, Avanti Polar Lipids Cat# 850355), and MPLA (10mg/ml final concentration, PHAD) were prepared in Milli-Q water containing 20% w/vol MEGA-10 (Sigma D6277) detergent. Quil-A saponin (InvivoGen; vac-quil) was dissolved in Milli-Q water at a final concentration of 100 mg/ml. All components were mixed at a molar ratio of 10:10:2.5:1 (Quil-A:chol:DPPC:MPLA) followed by dilution with PBS to a final concentration of 1 mg/ml cholesterol. The solution was allowed to equilibrate overnight at room temperature, followed by dialysis against PBS using a 10k MWCO membrane. The adjuvant solution was then sterile filtered, concentrated using 50k MWCO centricon spin filters, and further purified by FPLC using a Sephacryl S-500 HR size exclusion column. Doses are reported in terms of the amount of saponin administered, calculated by measuring the concentration of cholesterol (Cholesterol Quantitation kit; Millipore Sigma; Cat# MAK043) in the preparation and assuming quantitative incorporation of the saponin during synthesis.

Antigen labeling and characterization

1 mg/mL solution of protein antigen (N332-GT2) in PBS was mixed with an equal volume of 0.2 M sodium bicarbonate buffer (pH 8.4) on ice. A fresh stock solution of Sulfo-Cyanine 5 NHS ester was prepared at a concentration of 1 mg/mL in 0.2 M sodium bicarbonate buffer (pH 8.4) and added to the antigen solution. The mixture was incubated at 4°C for 16 hours, and then desalted twice using a Zeba Spin Desalting column equilibrated in PBS. The labeled antigen was filtered

through 0.22 μm pore size Spin-X centrifuge tube filters and stored at 4°C until use. The degree of labeling of the antigen was determined by measuring the absorbance at 280 and 646 nm wavelengths for total protein and Cy5 dye, respectively. The extinction coefficient values of 113215 and 271000 $\text{M}^{-1}\text{cm}^{-1}$ were used to calculate the concentration of one subunit of N332-GT2 Trimer and sulfo-cy5 NHS ester, respectively. The degree of labeling for soluble antigen was determined by calculating the ratio of antigen concentration to Cy5 concentration.

Mice

All *in vivo* experiments were performed in 8-week-old female C57BL/6J mice (Jackson Laboratory). Experiments were performed in specific pathogen-free animal facilities at the MIT Koch Institute for Integrative Cancer Research. Mice were housed under standard 12-hour light - 12-hour dark conditions with ad libitum access to water and chow. All mouse studies were performed according to institutional and National Institutes of Health (NIH) guidelines for humane animal use and in accordance with the Association for Assessment and Accreditation of Laboratory Animal Care. Protocols were approved by the Institutional Animal Care and Use Committee (IACUC) at MIT.

Immunizations and sample collections

8-week-old female C57BL/6 mice were anesthetized and immunized with 10 μg of indicated antigens (N332-GT2 trimer or MD39 trimer) in the presence of 5 μg saponin adjuvant (SMNP) subcutaneously at the left and right sides of the tail base. In the case of the pSer-conjugated MD39 trimer antigen, immunizations were prepared by mixing 10 μg of antigen and 100 μg of alum in 100 μl of sterile TBS (Sigma-Aldrich, catalog no. T5912) per mouse unless otherwise specified. Antigen was loaded onto alum for 30 min on a tube rotator after which 5 μg of SMNP was added into the immunization and incubated with antigen-alum formulations for 30 min before immunization. This dose of SMNP corresponds to 5 μg of Quil-A and 0.5 μg of MPLA. Blood (from submandibular; 100 μL) was collected at indicated time-points into serum separator tubes (BD Corporation) and centrifuged at 4,000 \times g for 10 min at 4 °C. Sera extracted from blood samples were stored at -80 °C until ready for analysis. Inguinal LNs were harvested and added to Eppendorf tubes containing Protease inhibitor buffer (containing protease inhibitor cocktail and EDTA in PBS with 2% FBS). LNs were processed using a pestle and centrifuged at 16,000g for 5

min at 4 °C to pellet the cell/tissue debris. Supernatant was transferred to Spin-X tubes (Corning™ Costar™) and centrifuged again for 5 min with the flow through being transferred to final collection tubes, flash frozen and stored at –80 °C until ready for analysis.

ELISA

To analyze on-target antibody response, high-binding ELISA plates (07-200-37, Fisher Scientific) were coated with 1 mg/ml trimer and blocked with 2% BSA in PBS overnight. To detect antigen-specific IgG responses, dilutions of serum or lymph node aspirate were added to the wells and incubated for 1.5 hours at 25°C. Plates were washed three times in PBS containing 0.2% Tween-20, and then anti-mouse IgG secondary antibody conjugated to HRP (172-1011, Bio-Rad Laboratories), diluted 1:5000 in blocking buffer as per manufacturer instructions, was added to the wells. After 1 hour of incubation, plates were again washed, developed with TMB, and the reaction was stopped with sulfuric acid. The optical density of the mixture was read out at 450 nm minus the absorbance at 540 nm according to the manufacturer's instructions.

Immunofluorescence staining

Inguinal lymph nodes (LNs) extracted from euthanized mice were submerged into cryomolds containing O.C.T. (23-730-571, Fisher Scientific) compound and dipped into 2-methylbutane (M32631, Millipore Sigma) pre-chilled in liquid nitrogen. All frozen tissues were cryosectioned on a Leica CM1950 at 10 µm thickness, adhered to Superfrost Plus microscope slides (12-550-15, Fisher Scientific), and stored in -80°C until use. Frozen sections were retrieved from -80°C, quickly thawed, and incubated in 4% paraformaldehyde for 10 minutes at 25°C. The sections were washed 3 times in PBS with 10-minute incubation time between each wash. Excess PBS was removed after the final wash before incubating the slides in blocking buffer, comprised of 2% BSA and 2% Triton X-100 in PBS. After 30 minutes, the blocking buffer was aspirated and the slides were stained in 1:75 anti-CD35 (740029, BD Biosciences) primary antibody solution also made in blocking buffer for ~16 hours at 4°C. These slides were washed in PBS 3 times for 10 min, stained with 1:200 diluted secondary antibodies solution in blocking buffer (ab150063 Abcam, ab150061, Abcam) for 4 hours at room temperature, and washed again in PBS. To mount the slides, one drop of ProLong Diamond Antifade Mountant (Thermo) was added directly onto the stained tissues prior to gently placing a 20x20 mm coverslip on top of the droplet to sandwich the section. The

coverslip was sealed using CoverGrip coverslip sealant (23005, Biotium) and imaged immediately. For all experiments, imaging was performed on a Leica SP8 confocal microscope equipped with a white light laser and spectral emission filter to detect emission wavelengths between 470 and 670 nm with a minimum bandwidth of 10 nm. All images were recorded with a 25X water immersion lens and a 63X oil immersion lens for assessing antigen drainage in the LNs, laser settings were kept constant across different time points for each immunogen.

Whole tissue imaging

For whole tissue imaging, mice were injected with anti-CD35 BV421 antibody (clone 8C12) and lymph nodes were isolated after 16 hours and fixed overnight in 4% paraformaldehyde. Lymph nodes were then processed with a modified DISCO protocol as previously described⁵⁵². Briefly, the nodes were washed twice in PBS and excess fat and connective tissue was removed. Nodes were then gradually moved into solutions containing successively high concentrations (20, 50, 80%) of methanol for 30 mins, until they were incubated for half an hour in pure methanol. Nodes were then bleached for 2 minutes in hydrogen peroxide and returned to methanol for half an hour. They were then gradually moved into solutions containing increasing concentrations of tertiary-butanol (20, 50, 80%) before eventually being incubated in pure tertiary-butanol for one hour at 37° C. All solutions used after bleaching contained an additional 0.4% α -tocopherol (vitamin E). Nodes were then removed from solution and allowed to dry completely before being placed in dichloromethane for delipidation. After the 8 lymph nodes dropped to the bottom of tubes following swirling (indicating removal of remaining tertiary-butanol), they were stored in dibenzyl ether with 0.4% α -tocopherol, which was used as a refractive index matching solution. Cleared lymph nodes were imaged using an Olympus FV1200 Laser Scanning Confocal Microscope at 10x magnification. Lasers were set to minimize pixel saturation in the brightest samples. All laser and channel settings were then kept constant across groups for direct comparison between different samples. Each lymph node was imaged over a depth of 300 μ m with line average of 3. FDC occupancy calculations were performed with a MATLAB script, where images for each channel were smoothed with a 3-D Gaussian filter ($\sigma = 0.5$), then binarized into a mask to identify follicle or antigen area. The fraction of FDC area occupied by antigen was achieved by calculating overlapping pixels in the two binary masks. This calculation was performed for each individual image in the z-stack (9 per image), as well as for the z-projection (sum of slices).

Flow Cytometry Analysis of Lymph Nodes.

Inguinal lymph nodes were harvested and single-cell suspensions were obtained by passage of the lymph nodes through a 70- μ m filter (BD Biosciences). The isolated cells were stained with Live/Dead fixable aqua stain (L34957, Thermo Fisher Scientific) for 10 min at 25°C before washing twice in flow cytometry buffer. Cells were then incubated with Fc block for 10 min at 4°C before staining with antibodies listed (see the supplementary materials) for 20 additional min at 4°C. For trimer specific GC B cell analysis, cells stained with antibodies were distributed evenly and exposed to biotinylated trimer preincubated with streptavidin (30 min at molar ratio of 1:4 at 25°C) conjugated to phycoerythrin (405203, BioLegend) and/or BV421 (405226, BioLegend). Flow cytometry was carried out on a BD LSR Fortessa or LSR II.

Statistical analysis

Statistical analysis and graphing were done with GraphPad Prism. The two-tailed Student's *t* test was used to compare two experimental groups and one-way Anova with Tukey's post hoc analysis was used for comparing more than two groups. Details of the statistical test and number of replicates are indicated in the figure legends. A value of $P < 0.05$ was considered statistically significant.

Chapter 6

Concluding thoughts and future directions

6.1 Modulating kinetics of cancer-immune interactions

While our results reveal that modulating release kinetics offers a promising route to safe immunostimulant prodrugs for combination cancer immunotherapies, we also note that our work highlights the inability of TLR7/8-induced inflammation in the tumor microenvironment to mediate tumor regressions in syngeneic mouse models of colon carcinoma. This sheds light on a key challenge that the field of cancer immunotherapy is currently facing with over a decade of clinical data highlighting failed attempts to make the tumor microenvironment more amenable to anti-PD1/PDL-1 therapy or other immune checkpoint therapies. Apart from modest successes with chemotherapy and vascular endothelial growth factor (VEGF)-targeted therapies, most of the immune agents, like TLR agonists mentioned above, cytokines like IL-2 or other co-stimulatory agonists like OX40 and CD27, have all met with failures in clinical trials despite promising preclinical data^{411,553,554}. One of the prevailing hypotheses revolves around immune-combination therapies struggling with the similar set of immune escape mechanisms. These mechanisms include loss of recognition, inhibition of immune activity, and/or decreased T cell functional state such as exhaustion or anergy⁵⁵⁵. To overcome these immune challenges, we require synthetic immune approaches to generate a powerful and specific anti-cancer immune response and broaden anti-tumor immunity by stimulating endogenous responses via stimulatory cytokines⁵⁵⁶. Advances in engineering are needed to enable therapeutic design characteristics that can achieve these goals by modulating pathways that enable immune escape. We can enable more effective cancer immunotherapies if our synthetic immune technologies can target the correct drivers and avoid overstimulation – and tuning kinetics will be essential to achieve these goals.

6.2 The next frontier for tuning kinetics of humoral responses

While protein-based immunizations have been most commonly employed for vaccinations against infectious disease, the success of mRNA vaccines during the Covid-19 pandemic have highlighted RNA-based immunizations as the next frontier for augmenting humoral immunity. Vaccines based on the delivery of mRNA using lipid nanoparticles (LNPs) are an exciting modality that now has proof of concept in humans. “ModRNA” employing modified bases that lower innate immune stimulation and enhance the lifetime of mRNA are used in these vaccines. These mRNA vaccines can elicit prolonged GC responses (post boost), substantial memory B cells responses and protective antibody levels^{557,558}. Although current mRNA formulations are generally thought to express only a few days at most *in vivo*, with peak reporter gene expression occurring within ~6 hr and decaying by 3 logs over ~3 days⁵⁵⁹, there remains the potential to enhance their function by engineering their kinetics to intrinsically achieve effects similar to our extended dosing (ED) regimens using only bolus or two-shot immunizations.

Future work evaluating how RNA design and LNP formulations can impact antigen and inflammatory kinetics could unlock our ability to further amplify “ED-like” effects in RNA vaccines. Using modRNA to deliver targeted immunogens could potentially achieve extended kinetics through prolonging antigen delivery to draining lymph nodes. The low cost and speed of mRNA vaccine production for clinical use motivates efforts to further enhance this technology. Furthermore, new modalities such as self-replicating RNAs based on alphavirus replicons are also in preclinical and clinical development^{560,561}. These technologies will enhance our ability to modulate vaccine kinetics to improve humoral responses against difficult to neutralize pathogens such as HIV.

7 References

1. Yousefpour, P., Ni, K. & Irvine, D. J. Targeted modulation of immune cells and tissues using engineered biomaterials. *Nat Rev Bioeng* **1**, 107–124 (2023).
2. Eberl, G. Immunity by equilibrium. *Nat. Rev. Immunol.* **16**, 524–532 (2016).
3. Hegde, P. S., Karanikas, V. & Evers, S. The Where, the When, and the How of Immune Monitoring for Cancer Immunotherapies in the Era of Checkpoint Inhibition. *Clin. Cancer Res.* **22**, 1865–1874 (2016).
4. Melero, I., Castanon, E., Alvarez, M., Champiat, S. & Marabelle, A. Intratumoural administration and tumour tissue targeting of cancer immunotherapies. *Nat Rev Clin Oncol* **18**, 558–576 (2021).
5. Hiam-Galvez, K. J., Allen, B. M. & Spitzer, M. H. Systemic immunity in cancer. *Nat Rev Cancer* 1–15 (2021) doi:10.1038/s41568-021-00347-z.
6. Quast, I. & Tarlinton, D. Time is of the essence for vaccine success. *Nat Immunol* 1–3 (2022) doi:10.1038/s41590-022-01347-3.
7. Delves, P. J. & Roitt, I. M. The Immune System. *New England Journal of Medicine* (2000) doi:10.1056/nejm200007063430107.
8. Medzhitov, R. Toll-like receptors and innate immunity. *Nat Rev Immunol* **1**, 135–145 (2001).
9. Vivier, E. & Malissen, B. Innate and adaptive immunity: specificities and signaling hierarchies revisited. *Nat. Immunol.* **6**, 17–21 (2005).
10. Primer to the Immune Response (Second Edition). *Part: Basic Immunol.* 3–20 (2014) doi:10.1016/b978-0-12-385245-8.00001-7.
11. Brightbill, H. D. & Modlin, R. L. Toll-like receptors: molecular mechanisms of the mammalian immune response. *Immunology* **101**, 1–10 (2000).
12. Jain, A. & Pasare, C. Innate Control of Adaptive Immunity: Beyond the Three-Signal Paradigm. *J. Immunol.* **198**, 3791–3800 (2017).
13. Paludan, S. R., Pradeu, T., Masters, S. L. & Mogensen, T. H. Constitutive immune mechanisms: mediators of host defence and immune regulation. *Nat. Rev. Immunol.* **21**, 137–150 (2021).
14. Grant, S. M. *et al.* The lymph node at a glance – how spatial organization optimizes the immune response. *J. Cell Sci.* **133**, jcs241828 (2020).

15. Brutkiewicz, R. R. Cell Signaling Pathways That Regulate Antigen Presentation. *J. Immunol.* **197**, 2971–2979 (2016).
16. Zeng, B. *et al.* Self-adjuvanting nanoemulsion targeting dendritic cell receptor Clec9A enables antigen-specific immunotherapy. *J Clin Invest* **128**, 1971–1984 (2018).
17. Langenkamp, A., Messi, M., Lanzavecchia, A. & Sallusto, F. Kinetics of dendritic cell activation: impact on priming of TH1, TH2 and nonpolarized T cells. *Nat. Immunol.* **1**, 311–316 (2000).
18. Yan, N. & Chen, Z. J. Intrinsic antiviral immunity. *Nat. Immunol.* **13**, 214–222 (2012).
19. Biron, C. A. Interferons α and β as Immune Regulators—A New Look. *Immunity* **14**, 661–664 (2001).
20. Davidson, S., Crotta, S., McCabe, T. M. & Wack, A. Pathogenic potential of interferon $\alpha\beta$ in acute influenza infection. *Nat. Commun.* **5**, 3864 (2014).
21. Chen, D. S. & Mellman, I. Oncology Meets Immunology: The Cancer-Immunity Cycle. *Immunity* **39**, 1–10 (2013).
22. Wculek, S. K. *et al.* Dendritic cells in cancer immunology and immunotherapy. *Nat Rev Immunol* 1–18 (2019) doi:10.1038/s41577-019-0210-z.
23. Oliveira, G. & Wu, C. J. Dynamics and specificities of T cells in cancer immunotherapy. *Nat. Rev. Cancer* **23**, 295–316 (2023).
24. Schwartz, R. H. T CELL ANERGY*. *Immunology* **21**, 305–334 (2003).
25. Ruijter, L. K. de *et al.* Whole-body CD8⁺ T cell visualization before and during cancer immunotherapy: a phase 1/2 trial. *Nat. Med.* **28**, 2601–2610 (2022).
26. Blank, C. U. *et al.* Defining ‘T cell exhaustion.’ *Nat. Rev. Immunol.* **19**, 665–674 (2019).
27. Binnewies, M. *et al.* Understanding the tumor immune microenvironment (TIME) for effective therapy. *Nat Med* **24**, 541–550 (2018).
28. Chen, D. S. & Mellman, I. Elements of cancer immunity and the cancer–immune set point. *Nature* **541**, 321–330 (2017).
29. Tauriello, D. V. F., Sancho, E. & Batlle, E. Overcoming TGF β -mediated immune evasion in cancer. *Nat. Rev. Cancer* **22**, 25–44 (2022).
30. Veglia, F., Sanseviero, E. & Gabrilovich, D. I. Myeloid-derived suppressor cells in the era of increasing myeloid cell diversity. *Nat. Rev. Immunol.* **21**, 485–498 (2021).

31. Togashi, Y., Shitara, K. & Nishikawa, H. Regulatory T cells in cancer immunosuppression — implications for anticancer therapy. *Nat. Rev. Clin. Oncol.* **16**, 356–371 (2019).
32. Rothschilds, A. M. & Wittrup, K. D. What, Why, Where, and When: Bringing Timing to Immuno-Oncology. *Trends Immunol* **40**, 12–21 (2019).
33. Anderson, N. M. & Simon, M. C. The tumor microenvironment. *Curr. Biol.* **30**, R921–R925 (2020).
34. Sharma, P. & Allison, J. P. Dissecting the mechanisms of immune checkpoint therapy. *Nat Rev Immunol* **20**, 75–76 (2020).
35. Valkenburg, K. C., Groot, A. E. de & Pienta, K. J. Targeting the tumour stroma to improve cancer therapy. *Nat. Rev. Clin. Oncol.* **15**, 366–381 (2018).
36. Kaufman, H. L., Kohlhapp, F. J. & Zloza, A. Oncolytic viruses: a new class of immunotherapy drugs. *Nat. Rev. Drug Discov.* **14**, 642–662 (2015).
37. Shalhout, S. Z., Miller, D. M., Emerick, K. S. & Kaufman, H. L. Therapy with oncolytic viruses: progress and challenges. *Nat. Rev. Clin. Oncol.* **20**, 160–177 (2023).
38. Sullivan, R. J. & Weber, J. S. Immune-related toxicities of checkpoint inhibitors: mechanisms and mitigation strategies. *Nat. Rev. Drug Discov.* **21**, 495–508 (2022).
39. Crittenden, M. R., Thanarajasingam, U., Vile, R. G. & Gough, M. J. Intratumoral immunotherapy: using the tumour against itself. *Immunology* **114**, 11–22 (2005).
40. Mathios, D. *et al.* Anti-PD-1 antitumor immunity is enhanced by local and abrogated by systemic chemotherapy in GBM. *Sci. Transl. Med.* **8**, 370ra180 (2016).
41. Wang, H. & Mooney, D. J. Biomaterial-assisted targeted modulation of immune cells in cancer treatment. *Nat. Mater.* **17**, 761–772 (2018).
42. Tselikas, L. *et al.* Interventional Radiology for Local Immunotherapy in Oncology. *Clin. Cancer Res.* **27**, 2698–2705 (2021).
43. Momin, N. *et al.* Maximizing response to intratumoral immunotherapy in mice by tuning local retention. *Nat. Commun.* **13**, 109 (2022).
44. Momin, N. *et al.* Anchoring of intratumorally administered cytokines to collagen safely potentiates systemic cancer immunotherapy. *Sci Transl Med* **11**, eaaw2614 (2019).
45. Messenheimer, D. J. *et al.* Timing of PD-1 Blockade Is Critical to Effective Combination Immunotherapy with Anti-OX40. *Clin Cancer Res* **23**, 6165–6177 (2017).
46. Spitzer, M. H. *et al.* Systemic Immunity Is Required for Effective Cancer Immunotherapy. *Cell* **168**, (2017).

47. Yazdi, M. T. *et al.* Standard radiotherapy but not chemotherapy impairs systemic immunity in non-small cell lung cancer. *OncImmunity* **5**, e1255393 (2016).
48. Krall, J. A. *et al.* The systemic response to surgery triggers the outgrowth of distant immune-controlled tumors in mouse models of dormancy. *Sci. Transl. Med.* **10**, (2018).
49. Bosiljcic, M. *et al.* Targeting myeloid-derived suppressor cells in combination with primary mammary tumor resection reduces metastatic growth in the lungs. *Breast Cancer Res.* **21**, 103 (2019).
50. Kallis, M. P. *et al.* Pharmacological prevention of surgery-accelerated metastasis in an animal model of osteosarcoma. *J. Transl. Med.* **18**, 183 (2020).
51. Lake, R. A. & Robinson, B. W. S. Immunotherapy and chemotherapy — a practical partnership. *Nat. Rev. Cancer* **5**, 397–405 (2005).
52. Zanker, D. J. *et al.* Intratumoral administration of the Toll-like receptor 7/8 agonist 3M-052 enhances interferon-driven tumor immunogenicity and suppresses metastatic spread in preclinical triple-negative breast cancer. *Clin. Transl. Immunol.* **9**, e1177 (2020).
53. Zuniga, L. A. *et al.* Intratumoral Delivery of TransCon™ TLR7/8 Agonist Provides Potent Anti-tumor Activity as a Monotherapy and in Combination With IL-2 While Minimizing Systemic Cytokine Induction. *J Immunother Cancer* **7**, 283 (2019).
54. Vohidov, F. *et al.* ABC triblock bottlebrush copolymer-based injectable hydrogels: design, synthesis, and application to expanding the therapeutic index of cancer immunochemotherapy. *Chem Sci* (2020) doi:10.1039/d0sc02611e.
55. Park, C. G. *et al.* Extended release of perioperative immunotherapy prevents tumor recurrence and eliminates metastases. *Sci Transl Med* **10**, eaar1916 (2018).
56. Agarwal, Y. *et al.* Intratumorally injected alum-tethered cytokines elicit potent and safer local and systemic anticancer immunity. *Nat Biomed Eng* 1–15 (2022) doi:10.1038/s41551-021-00831-9.
57. O’Day, S. *et al.* 423 Safety and preliminary efficacy of intratumoral cavrotolimod (AST-008), a spherical nucleic acid TLR9 agonist, in combination with pembrolizumab in patients with advanced solid tumors. *Regul. young Investig. award Abstr.* A257.2-A258 (2020) doi:10.1136/jitc-2020-site2020.0423.
58. Wang, C., Fiering, S. N. & Steinmetz, N. F. Cowpea Mosaic Virus Promotes Anti-Tumor Activity and Immune Memory in a Mouse Ovarian Tumor Model. *Adv. Ther.* **2**, 1900003 (2019).
59. Zaharoff, D. A., Hance, K. W., Rogers, C. J., Schlom, J. & Greiner, J. W. Intratumoral Immunotherapy of Established Solid Tumors With Chitosan/IL-12. *J. Immunother.* **33**, 697–705 (2010).

60. Bhagchandani, S., Johnson, J. & Irvine, D. J. Evolution of Toll-like receptor 7/8 agonist therapeutics and their delivery approaches: From antiviral formulations to vaccine adjuvants. *Adv Drug Deliver Rev* (2021) doi:10.1016/j.addr.2021.05.013.
61. Berek, C. & Milstein, C. Mutation Drift and Repertoire Shift in the Maturation of the Immune Response. *Immunol. Rev.* **96**, 23–41 (1987).
62. Papavasiliou, F. N. & Schatz, D. G. Somatic Hypermutation of Immunoglobulin Genes Merging Mechanisms for Genetic Diversity. *Cell* **109**, S35–S44 (2002).
63. Shlomchik, M. J. & Weisel, F. Germinal center selection and the development of memory B and plasma cells. *Immunol. Rev.* **247**, 52–63 (2012).
64. Heesters, B. A., Myers, R. C. & Carroll, M. C. Follicular dendritic cells: dynamic antigen libraries. *Nat. Rev. Immunol.* **14**, 495–504 (2014).
65. Garin, A. *et al.* Toll-like Receptor 4 Signaling by Follicular Dendritic Cells Is Pivotal for Germinal Center Onset and Affinity Maturation. *Immunity* **33**, 84–95 (2010).
66. Deshane, J. & Chaplin, D. D. Follicular Dendritic Cell Makes Environmental Sense. *Immunity* **33**, 2–4 (2010).
67. Cyster, J. G. B cell follicles and antigen encounters of the third kind. *Nat Immunol* **11**, 989–996 (2010).
68. Okada, T. *et al.* Antigen-Engaged B Cells Undergo Chemotaxis toward the T Zone and Form Motile Conjugates with Helper T Cells. *PLoS Biol.* **3**, e150 (2005).
69. Victora, G. D. *et al.* Germinal Center Dynamics Revealed by Multiphoton Microscopy with a Photoactivatable Fluorescent Reporter. *Cell* **143**, 592–605 (2010).
70. Victora, G. D. & Nussenzweig, M. C. Germinal Centers. *Immunology* **30**, 429–457 (2012).
71. McHeyzer-Williams, L. J., Milpied, P. J., Okitsu, S. L. & McHeyzer-Williams, M. G. Class-switched memory B cells remodel BCRs within secondary germinal centers. *Nat. Immunol.* **16**, 296–305 (2015).
72. Schwickert, T. A. *et al.* In vivo imaging of germinal centres reveals a dynamic open structure. *Nature* **446**, 83–87 (2007).
73. Akkaya, M., Kwak, K. & Pierce, S. K. B cell memory: building two walls of protection against pathogens. *Nat. Rev. Immunol.* **20**, 229–238 (2020).
74. Bachmann, M. F. & Jennings, G. T. Vaccine delivery: a matter of size, geometry, kinetics and molecular patterns. *Nat Rev Immunol* **10**, 787–96 (2010).

75. Mesin, L., Ersching, J. & Victora, G. D. Germinal Center B Cell Dynamics. *Immunity* **45**, 471–482 (2016).
76. Tangye, S. G., Ma, C. S., Brink, R. & Deenick, E. K. The good, the bad and the ugly — TFH cells in human health and disease. *Nat. Rev. Immunol.* **13**, 412–426 (2013).
77. Liu, D. *et al.* T–B-cell entanglement and ICOSL-driven feed-forward regulation of germinal centre reaction. *Nature* **517**, 214–218 (2015).
78. Gonzalez, D. G. *et al.* Nonredundant Roles of IL-21 and IL-4 in the Phased Initiation of Germinal Center B Cells and Subsequent Self-Renewal Transitions. *J. Immunol.* **201**, 3569–3579 (2018).
79. Goenka, R. *et al.* Local BLyS production by T follicular cells mediates retention of high affinity B cells during affinity maturation. *J. Exp. Med.* **211**, 45–56 (2014).
80. Tas, J. M. J. *et al.* Visualizing antibody affinity maturation in germinal centers. *Science* **351**, 1048–1054 (2016).
81. Victora, G. D. & Mesin, L. Clonal and cellular dynamics in germinal centers. *Curr. Opin. Immunol.* **28**, 90–96 (2014).
82. Weisel, F. J., Zuccarino-Catania, G. V., Chikina, M. & Shlomchik, M. J. A Temporal Switch in the Germinal Center Determines Differential Output of Memory B and Plasma Cells. *Immunity* **44**, 116–130 (2016).
83. Silva, N. S. D. & Klein, U. Dynamics of B cells in germinal centres. *Nat. Rev. Immunol.* **15**, 137–148 (2015).
84. Pulendran, B., Arunachalam, P. S. & O’Hagan, D. T. Emerging concepts in the science of vaccine adjuvants. *Nat Rev Drug Discov* 1–22 (2021) doi:10.1038/s41573-021-00163-y.
85. Adachi, Y. *et al.* Distinct germinal center selection at local sites shapes memory B cell response to viral escape. *J. Exp. Med.* **212**, 1709–1723 (2015).
86. Bachmann, M. F., Odermatt, B., Hengartner, H. & Zinkernagel, R. M. Induction of long-lived germinal centers associated with persisting antigen after viral infection. *J. Exp. Med.* **183**, 2259–2269 (1996).
87. Yewdell, W. T. *et al.* Temporal dynamics of persistent germinal centers and memory B cell differentiation following respiratory virus infection. *Cell Rep.* **37**, 109961 (2021).
88. Rothausler, K. & Baumgarth, N. B-cell fate decisions following influenza virus infection. *Eur. J. Immunol.* **40**, 366–377 (2010).
89. Yewdell, J. W. Antigenic drift: Understanding COVID-19. *Immunity* **54**, 2681–2687 (2021).

90. Vinuesa, C. G. *et al.* A RING-type ubiquitin ligase family member required to repress follicular helper T cells and autoimmunity. *Nature* **435**, 452–458 (2005).
91. Tew, J. G. & Mandel, T. E. Prolonged antigen half-life in the lymphoid follicles of specifically immunized mice. *Immunology* **37**, 69–76 (1979).
92. Smith, B. A. *et al.* Persistence of Infectious HIV on Follicular Dendritic Cells. *J. Immunol.* **166**, 690–696 (2001).
93. Kasturi, S. P. *et al.* Programming the magnitude and persistence of antibody responses with innate immunity. *Nature* **470**, 543 (2011).
94. Vinuesa, C. G. *de et al.* Germinal Centers without T Cells. *J. Exp. Med.* **191**, 485–494 (2000).
95. Long, Z., Phillips, B., Radtke, D., Meyer-Hermann, M. & Bannard, O. Competition for refueling rather than cyclic reentry initiation evident in germinal centers. *Sci. Immunol.* **7**, eabm0775–eabm0775 (2022).
96. Gitlin, A. D., Shulman, Z. & Nussenzweig, M. C. Clonal selection in the germinal centre by regulated proliferation and hypermutation. *Nature* **509**, 637–640 (2014).
97. Pape, K. A., Taylor, J. J., Maul, R. W., Gearhart, P. J. & Jenkins, M. K. Different B Cell Populations Mediate Early and Late Memory During an Endogenous Immune Response. *Science* **331**, 1203–1207 (2011).
98. Dogan, I. *et al.* Multiple layers of B cell memory with different effector functions. *Nat. Immunol.* **10**, 1292–1299 (2009).
99. Tam, H. H. *et al.* Sustained antigen availability during germinal center initiation enhances antibody responses to vaccination. *Proc National Acad Sci* **113**, E6639–E6648 (2016).
100. Cirelli, K. M. *et al.* Slow Delivery Immunization Enhances HIV Neutralizing Antibody and Germinal Center Responses via Modulation of Immunodominance. *Cell* **177**, 1153–1171.e28 (2019).
101. Irvine, D. J., Aung, A. & Silva, M. Controlling timing and location in vaccines. *Adv Drug Deliver Rev* (2020) doi:10.1016/j.addr.2020.06.019.
102. Morefield, G. L. *et al.* Effect of phosphorylation of ovalbumin on adsorption by aluminum-containing adjuvants and elution upon exposure to interstitial fluid. *Vaccine* **23**, 1502–1506 (2005).
103. Iyer, S., HogenEsch, H. & Hem, S. L. Relationship between the degree of antigen adsorption to aluminum hydroxide adjuvant in interstitial fluid and antibody production. *Vaccine* **21**, 1219–1223 (2003).
104. Moyer, T. J. *et al.* Engineered immunogen binding to alum adjuvant enhances humoral immunity. *Nat Med* **26**, 430–440 (2020).

105. Wu, T. Y.-H. *et al.* Rational design of small molecules as vaccine adjuvants. *Sci Transl Med* **6**, 263ra160-263ra160 (2014).
106. O'Hagan, D. T., Singh, M. & Gupta, R. K. Poly(lactide-co-glycolide) microparticles for the development of single-dose controlled-release vaccines. *Adv. Drug Deliv. Rev.* **32**, 225–246 (1998).
107. Tzeng, S. Y. *et al.* Stabilized single-injection inactivated polio vaccine elicits a strong neutralizing immune response. *Proc. Natl. Acad. Sci.* **115**, E5269–E5278 (2018).
108. Miller, R. L., Gerster, J. F., Owens, M. L., Slade, H. B. & Tomai, M. a. Review Article Imiquimod applied topically: a novel immune response modifier and new class of drug. *Int J Immunopharmacol* **21**, 1–14 (1999).
109. O'Neill, L. A. J., Golenbock, D. & Bowie, A. G. The history of Toll-like receptors — redefining innate immunity. *Nat Rev Immunol* **13**, 453–460 (2013).
110. Gerster, J. F. 1H-IMIDAZO[4,5-C]QUINOLIN-4-AMINES AND ANTIVIRAL USE. (1987).
111. Ryu, J. & Yang, F. C. A Review of Topical Imiquimod in the Management of Basal Cell Carcinoma, Actinic Keratoses, and Other Skin Lesions. *Clin Medicine Ther* **1**, CMT.S1969 (2009).
112. Tomai, M. A. *et al.* Immunomodulating and antiviral activities of the imidazoquinoline S-28463. *Antivir Res* **28**, 253–264 (1995).
113. Hirota, K. *et al.* Discovery of 8-hydroxyadenines as a novel type of interferon inducer. *Journal of medicinal chemistry* **45**, 5419–22 (2002).
114. Dockrell, D. H. & Kinghorn, G. R. Imiquimod and resiquimod as novel immunomodulators. *J Antimicrob Chemoth* **48**, 751–755 (2001).
115. WU, J., HUANG, D. & TYRING, S. Resiquimod: a new immune response modifier with potential as a vaccine adjuvant for Th1 immune responses. *Antivir Res* **64**, 79–83 (2004).
116. Szeimies, R. -M. *et al.* A phase II dose-ranging study of topical resiquimod to treat actinic keratosis. *Brit J Dermatol* **159**, 205–210 (2008).
117. Tarabdkar, E. S. & Shinohara, M. M. Skin Directed Therapy in Cutaneous T-Cell Lymphoma. *Frontiers Oncol* **9**, 260 (2019).
118. Hemmi, H. *et al.* Small anti-viral compounds activate immune cells via the TLR7 MyD88–dependent signaling pathway. *Nature Immunology* **3**, (2002).
119. Kawai, T. & Akira, S. TLR signaling. *Semin Immunol* **19**, 24–32 (2007).

120. Inglefield, J. R. *et al.* TLR7 agonist 852A inhibition of tumor cell proliferation is dependent on plasmacytoid dendritic cells and type I IFN. *J Interf Cytokine Res Official J Int Soc Interf Cytokine Res* **28**, 253–63 (2008).
121. Cheever, M. A. Twelve immunotherapy drugs that could cure cancers. *Immunol Rev* **222**, 357–68 (2008).
122. Engel, A. L., Holt, G. E. & Lu, H. The pharmacokinetics of Toll-like receptor agonists and the impact on the immune system. *Expert Rev Clin Phar* **4**, 275–289 (2014).
123. Dong, Z. *et al.* Holding the Inflammatory System in Check: TLRs and Their Targeted Therapy in Asthma. *Mediat Inflamm* **2016**, 1–8 (2016).
124. Anwar, M. A., Shah, M., Kim, J. & Choi, S. Recent clinical trends in Toll-like receptor targeting therapeutics. *Med Res Rev* **39**, 1053–1090 (2018).
125. Shimizu, T. Structural insights into ligand recognition and regulation of nucleic acid-sensing Toll-like receptors. *Curr Opin Struc Biol* **47**, 52–59 (2017).
126. Groß, C. J. *et al.* K + Efflux-Independent NLRP3 Inflammasome Activation by Small Molecules Targeting Mitochondria. *Immunity* **45**, 761–773 (2016).
127. Milling, L., Zhang, Y. & Irvine, D. J. Delivering safer immunotherapies for cancer. *Adv Drug Deliver Rev* **114**, 79–101 (2017).
128. Takeda, K., Kaisho, T. & Akira, S. Toll-like receptors. *Annual review of immunology* **21**, 335–76 (2003).
129. Diebold, S. S., Kaisho, T., Hemmi, H., Akira, S. & Sousa, C. R. e. Innate Antiviral Responses by Means of TLR7-Mediated Recognition of Single-Stranded RNA. *Science* **303**, 1529–1531 (2004).
130. Heil, F. *et al.* Species-Specific Recognition of Single-Stranded RNA via Toll-like Receptor 7 and 8. *Science* **303**, 1526–1529 (2004).
131. Takeuchi, O. & Akira, S. Pattern Recognition Receptors and Inflammation. *Cell* **140**, 805–820 (2010).
132. Leulier, F. & Lemaitre, B. Toll-like receptors — taking an evolutionary approach. *Nat Rev Genet* **9**, 165–178 (2008).
133. Akira, S., Takeda, K. & Kaisho, T. Toll-like receptors: critical proteins linking innate and acquired immunity. *Nature Immunology* **2**, (2001).
134. Janssens, S. & Beyaert, R. A universal role for MyD88 in TLR/IL-1R-mediated signaling. *Trends Biochem Sci* **27**, 474–482 (2002).

135. Kawagoe, T. *et al.* Essential role of IRAK-4 protein and its kinase activity in Toll-like receptor-mediated immune responses but not in TCR signaling. *J Exp Medicine* **204**, 1013–1024 (2007).
136. Kawai, T. & Akira, S. TLR signaling. *Cell Death Differ* **13**, 816–825 (2006).
137. Gay, N. J., Symmons, M. F., Gangloff, M. & Bryant, C. E. Assembly and localization of Toll-like receptor signalling complexes. *Nat Rev Immunol* **14**, 546–558 (2014).
138. Kawai, T. & Akira, S. The role of pattern-recognition receptors in innate immunity: update on Toll-like receptors. *Nat Immunol* **11**, 373–84 (2010).
139. Bell, E. Intracellular trafficking, IRF7 and type-I-IFN responses. *Nat Rev Immunol* **5**, 361–361 (2005).
140. Hornung, V. *et al.* Quantitative Expression of Toll-Like Receptor 1–10 mRNA in Cellular Subsets of Human Peripheral Blood Mononuclear Cells and Sensitivity to CpG Oligodeoxynucleotides. *J Immunol* **168**, 4531–4537 (2002).
141. Iwasaki, A. & Medzhitov, R. Toll-like receptor control of the adaptive immune responses. *Nat Immunol* **5**, 987–995 (2004).
142. Sousa, C. R. e. Toll-like receptors and dendritic cells: for whom the bug tolls. *Seminars in immunology* **16**, 27–34 (2004).
143. Iwasaki, A. & Medzhitov, R. Control of adaptive immunity by the innate immune system. *Nat Immunol* **16**, 343–353 (2015).
144. Trinchieri, G. & Sher, A. Cooperation of Toll-like receptor signals in innate immune defence. *Nat Rev Immunol* **7**, 179–190 (2007).
145. Petes, C., Odoardi, N. & Gee, K. The Toll for Trafficking: Toll-Like Receptor 7 Delivery to the Endosome. *Front Immunol* **8**, 1075 (2017).
146. Merad, M., Sathe, P., Helft, J., Miller, J. & Mortha, A. The dendritic cell lineage: ontogeny and function of dendritic cells and their subsets in the steady state and the inflamed setting. *Annu Rev Immunol* **31**, 563–604 (2013).
147. Larangé, A., Antonios, D., Pallardy, M. & Kerdine-Römer, S. TLR7 and TLR8 agonists trigger different signaling pathways for human dendritic cell maturation. *J Leukocyte Biol* **85**, 673–83 (2009).
148. Edwards, A. D. *et al.* Toll-like receptor expression in murine DC subsets: lack of TLR7 expression by CD8 α ⁺ DC correlates with unresponsiveness to imidazoquinolines. *European Journal of Immunology* **33**, 827–833 (2003).

149. Ketloy, C. *et al.* Expression and function of Toll-like receptors on dendritic cells and other antigen presenting cells from non-human primates. *Vet Immunol Immunop* **125**, 18–30 (2008).
150. Doxsee, C. L. *et al.* The Immune Response Modifier and Toll-Like Receptor 7 Agonist S-27609 Selectively Induces IL-12 and TNF- α Production in CD11c+CD11b+CD8– Dendritic Cells. *The Journal of Immunology* **171**, 1156–1163 (2003).
151. Worbs, T., Hammerschmidt, S. I. & Förster, R. Dendritic cell migration in health and disease. *Nat Rev Immunol* **17**, 30–48 (2017).
152. Kapsenberg, M. L. Dendritic-cell control of pathogen-driven T-cell polarization. *Nat Rev Immunol* **3**, 984–993 (2003).
153. Wagner, T. L. *et al.* Modulation of TH1 and TH2 Cytokine Production with the Immune Response Modifiers, R-848 and Imiquimod. *Cell Immunol* **191**, 10–19 (1999).
154. Peng, G. *et al.* Toll-Like Receptor 8-Mediated Reversal of CD4+ Regulatory T Cell Function. *Science* **309**, 1380–1384 (2005).
155. Kabelitz, D. Expression and function of Toll-like receptors in T lymphocytes. *Curr Opin Immunol* **19**, 39–45 (2007).
156. Slifka, M. K. & Whitton, J. L. Antigen-Specific Regulation of T Cell–Mediated Cytokine Production. *Immunity* **12**, 451–457 (2000).
157. Guiducci, C., Coffman, R. L. & Barrat, F. J. Signalling pathways leading to IFN- α production in human plasmacytoid dendritic cell and the possible use of agonists or antagonists of TLR7 and TLR9 in clinical indications. *J Intern Med* **265**, 43–57 (2009).
158. Krieg, A. M. Toll-like receptor 9 (TLR9) agonists in the treatment of cancer. *Oncogene* **27**, 161–167 (2008).
159. Ergun, S. L. & Li, L. Structural Insights into STING Signaling. *Trends Cell Biol* **30**, 399–407 (2020).
160. Larson, S. R. *et al.* Ly6C+ monocyte efferocytosis and cross-presentation of cell-associated antigens. *Cell Death Differ* **23**, 997–1003 (2016).
161. Janke, M. *et al.* Selective and direct activation of human neutrophils but not eosinophils by Toll-like receptor 8. *J Allergy Clin Immun* **123**, 1026–1033 (2009).
162. Regli, I. B. *et al.* TLR7 Sensing by Neutrophils Is Critical for the Control of Cutaneous Leishmaniasis. *Cell Reports* **31**, 107746 (2020).
163. Matsushima, H., Yamada, N., Matsue, H. & Shimada, S. TLR3-, TLR7-, and TLR9-Mediated Production of Proinflammatory Cytokines and Chemokines from Murine Connective Tissue Type

Skin-Derived Mast Cells but Not from Bone Marrow-Derived Mast Cells. *J Immunol* **173**, 531–541 (2004).

164. Hayashi, T. *et al.* Mast cell-dependent anorexia and hypothermia induced by mucosal activation of Toll-like receptor 7. *American Journal of Physiology-Regulatory, Integrative and Comparative Physiology* **295**, (2008).

165. Nagase, H. *et al.* Expression and Function of Toll-Like Receptors in Eosinophils: Activation by Toll-Like Receptor 7 Ligand. *The Journal of Immunology* **171**, 3977–3982 (2003).

166. Butchar, J. P. *et al.* Reciprocal Regulation of Activating and Inhibitory Fc γ Receptors by TLR7/8 Activation: Implications for Tumor Immunotherapy. *Clin Cancer Res* **16**, 2065–2075 (2010).

167. Applequist, S. E., Wallin, R. P. A. & Ljunggren, H. Variable expression of Toll-like receptor in murine innate and adaptive immune cell lines. *Int Immunol* **14**, 1065–1074 (2002).

168. Hayashi, F., Means, T. K. & Luster, A. D. Toll-like receptors stimulate human neutrophil function. *Blood* **102**, 2660–2669 (2003).

169. Wang, J. P. *et al.* Toll-like receptor-mediated activation of neutrophils by influenza A virus. *Blood* **112**, 2028–2034 (2008).

170. Hou, B., Reizis, B. & DeFranco, A. L. Toll-like Receptors Activate Innate and Adaptive Immunity by using Dendritic Cell-Intrinsic and -Extrinsic Mechanisms. *Immunity* **29**, 272–282 (2008).

171. Desch, A. N. *et al.* Dendritic cell subsets require cis-activation for cytotoxic CD8 T-cell induction. *Nature Communications* **5**, (2014).

172. Spörri, R. & Sousa, C. R. e. Inflammatory mediators are insufficient for full dendritic cell activation and promote expansion of CD4⁺ T cell populations lacking helper function. *Nat Immunol* **6**, 163–170 (2005).

173. Mouriès, J. *et al.* Plasmacytoid dendritic cells efficiently cross-prime naive T cells in vivo after TLR activation. *Blood* **112**, 3713–3722 (2008).

174. Bishop, G. A. *et al.* Molecular Mechanisms of B Lymphocyte Activation by the Immune Response Modifier R-848. *J Immunol* **165**, 5552–5557 (2000).

175. Gujer, C., Sundling, C., Seder, R. A., Hedestam, G. B. K. & Loré, K. Human and rhesus plasmacytoid dendritic cell and B-cell responses to Toll-like receptor stimulation. *Immunology* **134**, 257–269 (2011).

176. Pettengill, M. A. *et al.* Distinct TLR-mediated cytokine production and immunoglobulin secretion in human newborn naïve B cells. *Innate Immun* **22**, 433–443 (2016).

177. Gururajan, M., Jacob, J. & Pulendran, B. Toll-Like Receptor Expression and Responsiveness of Distinct Murine Splenic and Mucosal B-Cell Subsets. *PLoS ONE* **2**, (2007).
178. Bishop, G. A. *et al.* The Immune Response Modifier Resiquimod Mimics CD40-Induced B Cell Activation. *Cell Immunol* **208**, 9–17 (2001).
179. Rubtsova, K. *et al.* T Cell Production of IFN γ in Response to TLR7/IL-12 Stimulates Optimal B Cell Responses to Viruses. *Plos One* **11**, e0166322 (2016).
180. Tanji, H., Ohto, U., Shibata, T., Miyake, K. & Shimizu, T. Structural Reorganization of the Toll-Like Receptor 8 Dimer Induced by Agonistic Ligands. *Science* **339**, 1426–1429 (2013).
181. Zhang, Z. *et al.* Structural Analysis Reveals that Toll-like Receptor 7 Is a Dual Receptor for Guanosine and Single-Stranded RNA. *Immunity* **45**, 737–748 (2016).
182. Gerster, J. F. *et al.* Synthesis and Structure–Activity-Relationships of 1H-Imidazo[4,5-c]quinolines That Induce Interferon Production. *J Med Chem* **48**, 3481–3491 (2005).
183. Shukla, N. M., Malladi, S. S., Mutz, C. A., Balakrishna, R. & David, S. A. Structure–Activity Relationships in Human Toll-Like Receptor 7-Active Imidazoquinoline Analogues. *J Med Chem* **53**, 4450–65 (2010).
184. Ganapathi, L. *et al.* The Imidazoquinoline Toll-Like Receptor-7/8 Agonist Hybrid-2 Potently Induces Cytokine Production by Human Newborn and Adult Leukocytes. *Plos One* **10**, e0134640 (2015).
185. Shi, C. *et al.* Discovery of Imidazoquinolines with Toll-Like Receptor 7/8 Independent Cytokine Induction. *Acs Med Chem Lett* **3**, 501–504 (2012).
186. Schiaffo, C. E. *et al.* Structure–Activity Relationship Analysis of Imidazoquinolines with Toll-like Receptors 7 and 8 Selectivity and Enhanced Cytokine Induction. *J Med Chem* **57**, 339–347 (2014).
187. Larson, P. *et al.* Design and Synthesis of N1-Modified Imidazoquinoline Agonists for Selective Activation of Toll-like Receptors 7 and 8. *Acs Med Chem Lett* **8**, 1148–1152 (2017).
188. Beesu, M. *et al.* Structure-Based Design of Human TLR8-Specific Agonists with Augmented Potency and Adjuvanticity. *J Med Chem* **58**, 7833–7849 (2015).
189. Shukla, N. M. *et al.* Toll-Like Receptor (TLR)-7 and -8 Modulatory Activities of Dimeric Imidazoquinolines. *J Med Chem* **55**, 1106–16 (2012).
190. Shukla, N. M. *et al.* Potent Adjuvanticity of a Pure TLR7-Agonistic Imidazoquinoline Dendrimer. *Plos One* **7**, e43612 (2012).
191. Yoo, E. *et al.* Structure–activity relationships in Toll-like receptor 7 agonistic 1H-imidazo[4,5-c]pyridines. *Org Biomol Chem* **11**, 6526–6545 (2013).

192. Yoo, E. *et al.* Determinants of Activity at Human Toll-like Receptors 7 and 8: Quantitative Structure–Activity Relationship (QSAR) of Diverse Heterocyclic Scaffolds. *J Med Chem* **57**, 7955–7970 (2014).
193. Kokatla, H. P. *et al.* Toll-like receptor-8 agonistic activities in C2, C4, and C8 modified thiazolo[4,5-c]quinolines. *Org Biomol Chem* **11**, 1179 (2013).
194. Beesu, M. *et al.* Identification of High-Potency Human TLR8 and Dual TLR7/TLR8 Agonists in Pyrimidine-2,4-diamines. *J Med Chem* **60**, 2084–2098 (2017).
195. Asami, J. & Shimizu, T. Structural and functional understanding of the Toll-like receptors. *Protein Sci* (2021) doi:10.1002/pro.4043.
196. Zhang, Z. *et al.* Structural Analyses of Toll-like Receptor 7 Reveal Detailed RNA Sequence Specificity and Recognition Mechanism of Agonistic Ligands. *Cell Reports* **25**, 3371–3381.e5 (2018).
197. Miyake, K., Shibata, T., Ohto, U. & Shimizu, T. Emerging roles of the processing of nucleic acids and Toll-like receptors in innate immune responses to nucleic acids. *J Leukocyte Biol* **101**, 135–142 (2017).
198. Maeda, K. & Akira, S. TLR7 Structure: Cut in Z-Loop. *Immunity* **45**, 705–707 (2016).
199. Sakaniwa, K. & Shimizu, T. Targeting the innate immune receptor TLR8 using small-molecule agents. *Acta Crystallogr Sect D Struct Biology* **76**, 621–629 (2020).
200. Isobe, Y. *et al.* Synthesis and Biological Evaluation of Novel 9-Substituted-8-Hydroxyadenine Derivatives as Potent Interferon Inducers. *J Med Chem* **49**, 2088–2095 (2006).
201. Roethle, P. A. *et al.* Identification and Optimization of Pteridinone Toll-like Receptor 7 (TLR7) Agonists for the Oral Treatment of Viral Hepatitis. *J Med Chem* **56**, 7324–7333 (2013).
202. McGowan, D. C. Latest Advances in Small Molecule TLR 7/8 Agonist Drug Research. *Curr Top Med Chem* **19**, 2228–2238 (2019).
203. Patinote, C. *et al.* Agonist and antagonist ligands of toll-like receptors 7 and 8: Ingenious tools for therapeutic purposes. *Eur J Med Chem* **193**, 112238 (2020).
204. Wang, Y. *et al.* Small-Molecule Modulators of Toll-like Receptors. *Accounts Chem Res* **53**, 1046–1055 (2020).
205. Kurimoto, A. *et al.* Prodrugs of 9-Benzyl-8-hydroxy-2-(2-hydroxyethylthio)adenine: Potent Interferon Inducing Agents in Monkeys. *Chem Pharm Bull* **52**, 466–469 (2004).
206. Nakamura, T. *et al.* Synthesis and evaluation of 8-oxoadenine derivatives as potent Toll-like receptor 7 agonists with high water solubility. *Bioorg Med Chem Lett* **23**, 669–672 (2013).

207. Heil, F. *et al.* The Toll-like receptor 7 (TLR7)-specific stimulus loxoribine uncovers a strong relationship within the TLR7, 8 and 9 subfamily. *Eur J Immunol* **33**, 2987–2997 (2003).
208. Evans, J. T. *et al.* Synthetic Toll-like Receptors 7 and 8 Agonists: Structure–Activity Relationship in the Oxoadenine Series. *Acs Omega* **4**, 15665–15677 (2019).
209. Bazin, H. G. *et al.* Structural requirements for TLR7-selective signaling by 9-(4-piperidinylalkyl)-8-oxoadenine derivatives. *Bioorg Med Chem Lett* **25**, 1318–23 (2015).
210. Weterings, J. J. *et al.* 2-Azidoalkoxy-7-hydro-8-oxoadenine derivatives as TLR7 agonists inducing dendritic cell maturation. *Bioorg Med Chem Lett* **19**, 2249–2251 (2009).
211. Yu, H. *et al.* Toll-Like Receptor 7 Agonists: Chemical Feature Based Pharmacophore Identification and Molecular Docking Studies. *Plos One* **8**, e56514 (2013).
212. Harrison, L. I., Stoesz, J. D., Battiste, J. L., Nelson, R. J. & Zarraga, I. E. A pharmaceutical comparison of different commercially available imiquimod 5% cream products. *J Dermatol Treat* **20**, 160–164 (2009).
213. Chollet, J. L. *et al.* Development of a Topically Active Imiquimod Formulation. *Pharm Dev Technol* **4**, 35–43 (1999).
214. Sauder, D. N. Imiquimod: modes of action. *Brit J Dermatol* **149**, 5–8 (2003).
215. Samuel, C. E. Antiviral Actions of Interferons. *Clin Microbiol Rev* **14**, 778–809 (2001).
216. Silverman, R. H. Viral Encounters with 2',5'-Oligoadenylate Synthetase and RNase L during the Interferon Antiviral Response. *J Virol* **81**, 12720–12729 (2007).
217. Palamara, F. *et al.* Identification and Characterization of pDC-Like Cells in Normal Mouse Skin and Melanomas Treated with Imiquimod. *J Immunol* **173**, 3051–3061 (2004).
218. Vidal, D. Topical Imiquimod: Mechanism of Action and Clinical Applications. *Mini-rev Med Chem* **6**, 499–503 (2006).
219. Beglin, M., Melar-New, M. & Laimins, L. Human papillomaviruses and the interferon response. *J Interf Cytokine Res Official J Int Soc Interf Cytokine Res* **29**, 629–35 (2009).
220. Dahl, M. V. Imiquimod: A cytokine inducer. *J Am Acad Dermatol* **47**, S205–S208 (2002).
221. Suzuki, H. *et al.* Imiquimod, a Topical Immune Response Modifier, Induces Migration of Langerhans Cells. *J Invest Dermatol* **114**, 135–141 (2000).
222. Perry, C. M. & Lamb, H. M. Topical Imiquimod: A Review of its Use in Genital Warts. *Drugs* **58**, 375–390 (1999).

223. Edwards, L. *et al.* Self-administered Topical 5% Imiquimod Cream for External Anogenital Warts. *Arch Dermatol* **134**, 25 (1998).
224. Deza, G., Martin-Ezquerria, G., Curto-Barredo, L., García, J. V. & Pujol, R. M. Successful treatment of hypertrophic herpes simplex genitalis in HIV-infected patient with topical imiquimod. *J Dermatology* **42**, 1176–1178 (2015).
225. Miller, R. L., Imbertson, L. M., Reiter, M. J. & Gerster, J. F. Treatment of primary herpes simplex virus infection in guinea pigs by imiquimod. *Antivir Res* **44**, 31–42 (1999).
226. Schacker, T. W. *et al.* Imiquimod 5-Percent Cream Does Not Alter the Natural History of Recurrent Herpes Genitalis: a Phase II, Randomized, Double-Blind, Placebo-Controlled Study. *Antimicrob Agents Ch* **46**, 3243–3248 (2002).
227. Winters, U. *et al.* Clinical and Immunologic Results of a Phase II Trial of Sequential Imiquimod and Photodynamic Therapy for Vulval Intraepithelial Neoplasia. *Clin Cancer Res* **14**, 5292–5299 (2008).
228. Daayana, S. *et al.* Phase II trial of imiquimod and HPV therapeutic vaccination in patients with vulval intraepithelial neoplasia. *Brit J Cancer* **102**, 1129–1136 (2010).
229. Wouters, T. *et al.* Systemic adverse events in imiquimod use for cervical intraepithelial neoplasia – A case series. *Case Reports Women's Heal* **21**, e00105 (2019).
230. Hadley, G., Derry, S. & Moore, R. A. Imiquimod for Actinic Keratosis: Systematic Review and Meta-Analysis. *J Invest Dermatol* **126**, 1251–1255 (2006).
231. Uhlenhake, E. E. Optimal treatment of actinic keratoses. *Clin Interv Aging* **8**, 29–35 (2013).
232. Lebwohl, M. *et al.* Imiquimod 5% cream for the treatment of actinic keratosis: results from two phase III, randomized, double-blind, parallel group, vehicle-controlled trials. *J Am Acad Dermatol* **50**, 714–721 (2004).
233. Geisse, J. *et al.* Imiquimod 5% cream for the treatment of superficial basal cell carcinoma: results from two phase III, randomized, vehicle-controlled studies. *J Am Acad Dermatol* **50**, 722–733 (2004).
234. Wysocka, M. *et al.* Synthetic Imidazoquinolines Potently and Broadly Activate the Cellular Immune Response of Patients with Cutaneous T-Cell Lymphoma: Synergy with Interferon- γ Enhances Production of Interleukin-12. *Clin Lymphoma Myeloma* **7**, 524–534 (2007).
235. Suchin, K. R., Junkins-Hopkins, J. M. & Rook, A. H. Treatment of Stage IA Cutaneous T-Cell Lymphoma With Topical Application of the Immune Response Modifier Imiquimod. *Arch Dermatol* **138**, 1137 (2002).
236. Rook, A. H. *et al.* Topical resiquimod can induce disease regression and enhance T-cell effector functions in cutaneous T-cell lymphoma. *Blood* **126**, 1452–61 (2015).

237. Wolf, I. H. *et al.* Topical Imiquimod in the Treatment of Metastatic Melanoma to Skin. *Arch Dermatol* **139**, 273 (2003).
238. Narayan, R. *et al.* Immunomodulation by imiquimod in patients with high-risk primary melanoma. *J Investigative Dermatology* **132**, 163–9 (2011).
239. Adams, S. *et al.* Topical TLR7 agonist imiquimod can induce immune-mediated rejection of skin metastases in patients with breast cancer. *Clin Cancer Res Official J Am Assoc Cancer Res* **18**, 6748–57 (2012).
240. Campanelli, A., Krischer, J. & Saurat, J.-H. Topical application of imiquimod and associated fever in children. *J Am Acad Dermatol* **52**, E1 (2005).
241. Bauza, A., Pozo, L. J. D., Saus, C. & Martin, A. Pemphigus-like lesions induced by imiquimod. *Clin Exp Dermatol* **34**, e60–e62 (2009).
242. Kumar, B. & Narang, T. Local and systemic adverse effects to topical imiquimod due to systemic immune stimulation. *Sex Transm Infect* **87**, 432–432 (2011).
243. Borden, E. C. Interferons α and β in cancer: therapeutic opportunities from new insights. *Nat Rev Drug Discov* **18**, 219–234 (2019).
244. Chi, H. *et al.* Anti-tumor Activity of Toll-Like Receptor 7 Agonists. *Front Pharmacol* **8**, 304 (2017).
245. Schon, M. *et al.* Tumor-Selective Induction of Apoptosis and the Small-Molecule Immune Response Modifier Imiquimod. *Jnci J National Cancer Inst* **95**, 1138–1149 (2003).
246. Huang, S.-W. *et al.* Imiquimod activates p53-dependent apoptosis in a human basal cell carcinoma cell line. *J Dermatol Sci* **81**, 182–91 (2015).
247. Dajon, M., Iribarren, K. & Cremer, I. Dual roles of TLR7 in the lung cancer microenvironment. *Oncoimmunology* **4**, e991615 (2015).
248. Schön, M. P. & Schön, M. TLR7 and TLR8 as targets in cancer therapy. *Oncogene* **27**, 190–199 (2008).
249. Smits, E. L. J. M., Ponsaerts, P., Berneman, Z. N. & Tendeloo, V. F. I. V. The Use of TLR7 and TLR8 Ligands for the Enhancement of Cancer Immunotherapy. *Oncol* **13**, 859–875 (2008).
250. Harrison, L. I., Astry, C., Kumar, S. & Yunis, C. Pharmacokinetics of 852A, an Imidazoquinoline Toll-Like Receptor 7-Specific Agonist, Following Intravenous, Subcutaneous, and Oral Administrations in Humans. *J Clin Pharmacol* **47**, 962–969 (2007).
251. Dudek, A. Z. *et al.* First in Human Phase I Trial of 852A, a Novel Systemic Toll-like Receptor 7 Agonist, to Activate Innate Immune Responses in Patients with Advanced Cancer. *Clin Cancer Res* **13**, 7119–7125 (2007).

252. Dummer, R. *et al.* An Exploratory Study of Systemic Administration of the Toll-like Receptor-7 Agonist 852A in Patients with Refractory Metastatic Melanoma. *Clin Cancer Res* **14**, 856–864 (2008).
253. Pope, B. L. *et al.* Loxoribine (7-allyl-8-oxoguanosine) activates natural killer cells and primes cytolytic precursor cells for activation by IL-2. *J Immunol Baltim Md 1950* **151**, 3007–17 (1993).
254. Pope, B. L., Sigindere, J., Chourmouzis, E., MacIntyre, P. & Goodman, M. G. 7-Allyl-8-oxoguanosine (loxoribine) inhibits the metastasis of B16 melanoma cells and has adjuvant activity in mice immunized with a B16 tumor vaccine. *Cancer Immunol Immunother* **38**, 83–91 (1994).
255. Agarwala, S. S., Kirkwood, J. M. & Bryant, J. Phase I, Randomized, Double-blind Trial of 7-allyl-8-oxoguanosine (Loxoribine) in Advanced Cancer. *Cytokines Cell Mol Ther* **6**, 171–176 (2009).
256. Adlard, A. L. *et al.* A novel systemically administered toll-like receptor 7 agonist potentiates the effect of ionizing radiation in murine solid tumor models. *Int J Cancer* **135**, 820–9 (2014).
257. Disis, M. L., Bernhard, H. & Jaffee, E. M. Use of tumour-responsive T cells as cancer treatment. *Lancet Lond Engl* **373**, 673–83 (2009).
258. Durgeau, A., Virk, Y., Corgnac, S. & Mami-Chouaib, F. Recent Advances in Targeting CD8 T-Cell Immunity for More Effective Cancer Immunotherapy. *Front Immunol* **9**, 14 (2018).
259. Lu, H. TLR Agonists for Cancer Immunotherapy: Tipping the Balance between the Immune Stimulatory and Inhibitory Effects. *Front Immunol* **5**, 83 (2014).
260. Ota, Y. *et al.* Abstract 4726: Novel intravenous injectable TLR7 agonist, DSP-0509, synergistically enhanced antitumor immune responses in combination with anti-PD-1 antibody. 4726–4726 (2018) doi:10.1158/1538-7445.am2018-4726.
261. Ackerman, S. E. *et al.* Abstract 1559: TLR7/8 immune-stimulating antibody conjugates elicit robust myeloid activation leading to enhanced effector function and anti-tumor immunity in pre-clinical models. 1559–1559 (2019) doi:10.1158/1538-7445.am2019-1559.
262. Ackerman, S. E. *et al.* Immune-stimulating antibody conjugates elicit robust myeloid activation and durable antitumor immunity. *Nat Cancer* 1–16 (2020) doi:10.1038/s43018-020-00136-x.
263. Metz, H. *et al.* SBT6050, a HER2-directed TLR8 therapeutic, as a systemically administered, tumor-targeted human myeloid cell agonist. *J Clin Oncol* **38**, 3110–3110 (2020).
264. Moyes, K. *et al.* Abstract 3271: A systemically administered, conditionally active TLR8 agonist for the treatment of HER2-expressing tumors. 3271–3271 (2019) doi:10.1158/1538-7445.am2019-3271.

265. Tan, J. *et al.* The active metabolite of the TLR7 agonist prodrug ANA773 activates anti-tumor activity by natural killer cells. *Cancer Res* **67** (9 Supplement), 3556 (1AD).
266. Daniels, G. A. *et al.* Phase I open-label, dose-escalation study of ANA773 tosylate, an oral prodrug of a toll-like receptor-7 agonist, in patients with advanced solid tumors. *J Clin Oncol* **29**, 2524–2524 (2011).
267. Witjes, W. P. J. *et al.* Results of a European Comparative Randomized Study Comparing Oral Bropirimine versus Intravesical BCG Treatment in BCG-Naive Patients with Carcinoma in situ of the Urinary Bladder. *Eur Urol* **36**, 576–581 (1999).
268. Webber, J. R. A. S. E. Pharmacodynamic response in vitro and in vivo of novel orally administered Toll-like Receptor 7 agonists for systemic immunotherapy of cancer. in *Pharmacodynamic response in vitro and in vivo of novel orally administered Toll-like Receptor 7 agonists for systemic immunotherapy of cancer* (2019).
269. Wu, T. Y. -H. Strategies for designing synthetic immune agonists. *Immunology* **148**, 315–325 (2016).
270. Hayashi, T. *et al.* Intravesical Toll-like receptor 7 agonist R-837: Optimization of its formulation in an orthotopic mouse model of bladder cancer. *Int J Urol* **17**, 483–490 (2010).
271. Arends, T. J. H. *et al.* Pharmacokinetic, Pharmacodynamic, and Activity Evaluation of TMX-101 in a Multicenter Phase 1 Study in Patients With Papillary Non-Muscle-Invasive Bladder Cancer. *Clin Genitourin Canc* **13**, 204-209.e2 (2015).
272. Donin, N. M. *et al.* A phase 2 study of TMX-101, intravesical imiquimod, for the treatment of carcinoma in situ bladder cancer. *Urologic Oncol Seminars Orig Investigations* **35**, 39.e1-39.e7 (2017).
273. Northfelt, D. W. *et al.* A Phase I Dose-Finding Study of the Novel Toll-like Receptor 8 Agonist VTX-2337 in Adult Subjects with Advanced Solid Tumors or Lymphoma. *Clin Cancer Res* **20**, 3683–3691 (2014).
274. Facciabene, A. *et al.* Abstract 4745: TLR8 agonist and Doxil chemotherapy potently activate human antitumor immune response in a human immune system mouse model. 4745–4745 (2011) doi:10.1158/1538-7445.am2011-4745.
275. Dietsch, G. N. *et al.* Late-Stage Cancer Patients Remain Highly Responsive to Immune Activation by the Selective TLR8 Agonist Motolimod (VTX-2337). *Clin Cancer Res* **21**, 5445–5452 (2015).
276. Singh, M. *et al.* Effective innate and adaptive antimelanoma immunity through localized TLR7/8 activation. *J Immunol Baltim Md 1950* **193**, 4722–31 (2014).
277. Brown, T. D., Whitehead, K. A. & Mitragotri, S. Materials for oral delivery of proteins and peptides. *Nat Rev Mater* **5**, 127–148 (2019).

278. Patel, M. C. *et al.* Novel drugs targeting Toll-like receptors for antiviral therapy. *Future Virol* **9**, 811–829 (2014).
279. Horscroft, N. J., Pryde, D. C. & Bright, H. Antiviral applications of Toll-like receptor agonists. *J Antimicrob Chemoth* **67**, 789–801 (2012).
280. Melchjorsen, J. Learning from the messengers: innate sensing of viruses and cytokine regulation of immunity - clues for treatments and vaccines. *Viruses* **5**, 470–527 (2013).
281. Pockros, P. J. *et al.* Oral resiquimod in chronic HCV infection: Safety and efficacy in 2 placebo-controlled, double-blind phase IIa studies. *Journal of Hepatology* **47**, 174–82 (2007).
282. Fidock, M. D. *et al.* The innate immune response, clinical outcomes, and ex vivo HCV antiviral efficacy of a TLR7 agonist (PF-4878691). *Clin Pharmacol Ther* **89**, 821–9 (2011).
283. Xiang, A. X. *et al.* Discovery of ANA975: An Oral Prodrug of the TLR-7 Agonist Isatoribine. *Nucleosides Nucleotides Nucleic Acids* **26**, 635–640 (2007).
284. Suslov, A., Wieland, S. & Menne, S. Modulators of innate immunity as novel therapeutics for treatment of chronic hepatitis B. *Curr Opin Virol* **30**, 9–17 (2018).
285. Miller, R. L., Meng, T.-C. & Tomai, M. A. The antiviral activity of toll-like receptor 7 and 7/8 agonists. *Drug News Perspect* **21**, 69 (2008).
286. Luk, A. *et al.* A Single and Multiple Ascending Dose Study of Toll-Like Receptor 7 Agonist (RO7020531) in Chinese Healthy Volunteers. *Clin Transl Sci* (2020) doi:10.1111/cts.12791.
287. Grippo, J. F. *et al.* Safety, tolerability, pharmacokinetics and pharmacodynamics of a TLR7 agonist prodrug RO6870868 in healthy volunteers. *Clin Transl Sci* (2021) doi:10.1111/cts.13016.
288. Zhang, H. *et al.* Safety, Pharmacokinetics, and Pharmacodynamics of TQ-A3334, an Oral Toll-Like Receptor 7 Agonist, in Healthy Individuals. *Expert Opin Inv Drug* (2021) doi:10.1080/13543784.2021.1873275.
289. Gao, L. *et al.* O-015: Combination treatment of a TLR7 agonist RO7020531 and a capsid assembly modulator RO7049389 achieved sustainable viral load suppression and HBsAg loss in an AAV-HBV mouse model. *J Viral Hepatitis* **25**, 12–12 (2018).
290. Fosdick, A. *et al.* Pharmacokinetic and Pharmacodynamic Properties of GS-9620, a Novel Toll-Like Receptor 7 Agonist, Demonstrate Interferon-Stimulated Gene Induction without Detectable Serum Interferon at Low Oral Doses. *J Pharmacol Exp Ther* **348**, 96–105 (2014).
291. Gane, E. J. *et al.* The oral toll-like receptor-7 agonist GS-9620 in patients with chronic hepatitis B virus infection. *J Hepatol* **63**, 320–328 (2015).
292. Menne, S. *et al.* Sustained efficacy and seroconversion with the Toll-like receptor 7 agonist GS-9620 in the Woodchuck model of chronic hepatitis B. *J Hepatol* **62**, 1237–45 (2015).

293. Lanford, R. E. *et al.* GS-9620, an Oral Agonist of Toll-Like Receptor-7, Induces Prolonged Suppression of Hepatitis B Virus in Chronically Infected Chimpanzees. *Gastroenterology* **144**, 1508-1517.e10 (2013).
294. Korolowicz, K. E. *et al.* Liver-Targeted Toll-Like Receptor 7 Agonist Combined With Entecavir Promotes a Functional Cure in the Woodchuck Model of Hepatitis B Virus. *Hepatology Commun* **3**, 1296–1310 (2019).
295. Jo, J. *et al.* Toll-Like Receptor 8 Agonist and Bacteria Trigger Potent Activation of Innate Immune Cells in Human Liver. *Plos Pathog* **10**, e1004210 (2014).
296. Guidotti, L. G. *et al.* Viral Clearance Without Destruction of Infected Cells During Acute HBV Infection. *Science* **284**, 825–829 (1999).
297. Mackman, R. L. *et al.* Discovery of GS-9688 (Selgantolimod) as a Potent and Selective Oral Toll-Like Receptor 8 Agonist for the Treatment of Chronic Hepatitis B. *J Med Chem* (2020) doi:10.1021/acs.jmedchem.0c00100.
298. Daffis, S. *et al.* Toll-Like Receptor 8 Agonist GS-9688 Induces Sustained Efficacy in the Woodchuck Model of Chronic Hepatitis B. *Hepatology* (2020) doi:10.1002/hep.31255.
299. Bam, R. A. *et al.* TLR7 Agonist GS-9620 Is a Potent Inhibitor of Acute HIV-1 Infection in Human Peripheral Blood Mononuclear Cells. *Antimicrob Agents Ch* **61**, e01369-16 (2017).
300. Borducchi, E. N. *et al.* Ad26/MVA therapeutic vaccination with TLR7 stimulation in SIV-infected rhesus monkeys. *Nature* **540**, 284–287 (2016).
301. Borducchi, E. N. *et al.* Antibody and TLR7 agonist delay viral rebound in SHIV-infected monkeys. *Nature* **563**, 360–364 (2018).
302. Lim, S.-Y. *et al.* TLR7 agonists induce transient viremia and reduce the viral reservoir in SIV-infected rhesus macaques on antiretroviral therapy. *Sci Transl Med* **10**, eaao4521 (2018).
303. Eigenbrod, T. & Dalpke, A. H. Bacterial RNA: An Underestimated Stimulus for Innate Immune Responses. *J Immunol* **195**, 411–418 (2015).
304. Moen, S. H. *et al.* Human Toll-like Receptor 8 (TLR8) Is an Important Sensor of Pyogenic Bacteria, and Is Attenuated by Cell Surface TLR Signaling. *Front Immunol* **10**, 1209 (2019).
305. Cervantes, J. L., Weinerman, B., Basole, C. & Salazar, J. C. TLR8: the forgotten relative revindicated. *Cell Mol Immunol* **9**, 434–438 (2012).
306. Dowling, D. J. *et al.* TLR7/8 adjuvant overcomes newborn hyporesponsiveness to pneumococcal conjugate vaccine at birth. *Jci Insight* **2**, e91020 (2017).
307. Dowling, D. J. Recent Advances in the Discovery and Delivery of TLR7/8 Agonists as Vaccine Adjuvants. *Immunohorizons* **2**, 185–197 (2018).

308. Abt, M. C. *et al.* TLR-7 activation enhances IL-22-mediated colonization resistance against vancomycin-resistant enterococcus. *Sci Transl Med* **8**, 327ra25-327ra25 (2016).
309. Drake, M. G., Kaufman, E. H., Fryer, A. D. & Jacoby, D. B. The Therapeutic Potential of Toll-Like Receptor 7 Stimulation in Asthma. *Inflamm Allergy-drug Targets* **11**, 484–491 (2012).
310. Lebold, K. M., Jacoby, D. B. & Drake, M. G. Toll-Like Receptor 7-Targeted Therapy in Respiratory Disease. *Transfus Med Hemoth* **43**, 114–119 (2016).
311. Adner, M., Starkhammar, M., Georén, S. K., Dahlén, S.-E. & Cardell, L.-O. Toll-like receptor (TLR) 7 decreases and TLR9 increases the airway responses in mice with established allergic inflammation. *Eur J Pharmacol* **718**, 544–551 (2013).
312. Kline, J. N. Immunotherapy of asthma using CpG oligodeoxynucleotides. *Immunol Res* **39**, 279–286 (2007).
313. Barnes, P. J. New drugs for asthma. *Nat Rev Drug Discov* **3**, 831–844 (2004).
314. Drake, M. G. *et al.* Toll-like Receptor 7 Rapidly Relaxes Human Airways. *Am J Resp Crit Care* **188**, 664–672 (2013).
315. Ellis, A. K., Tsitoura, D. C., Quint, D., Powley, W. & Lee, L. A. Safety and pharmacodynamics of intranasal GSK2245035, a TLR7 agonist for allergic rhinitis: A randomized trial. *Clin Exp Allergy* **47**, 1193–1203 (2017).
316. Biggadike, K. *et al.* Discovery of 6-Amino-2-[[[(1S)-1-methylbutyl]oxy]-9-[5-(1-piperidinyl)pentyl]-7,9-dihydro-8H-purin-8-one (GSK2245035), a Highly Potent and Selective Intranasal Toll-Like Receptor 7 Agonist for the Treatment of Asthma. *J Med Chem* **59**, 1711–26 (2016).
317. Biffen, M. *et al.* Biological characterization of a novel class of toll-like receptor 7 agonists designed to have reduced systemic activity. *Brit J Pharmacol* **166**, 573–586 (2012).
318. Leaker, B. R. *et al.* Effects of the Toll-like receptor 7 (TLR7) agonist, AZD8848, on allergen-induced responses in patients with mild asthma: a double-blind, randomised, parallel-group study. *Respir Res* **20**, 288 (2019).
319. Royer, C. M., Rudolph, K., Dietsch, G. N., Hershberg, R. M. & Barrett, E. G. VTX-1463, a novel TLR-8 agonist, attenuates nasal congestion after ragweed challenge in sensitized beagle dogs. *Immun Inflamm Dis* **4**, 45–51 (2015).
320. Horak, F. VTX-1463, a novel TLR8 agonist for the treatment of allergic rhinitis. *Expert Opin Inv Drug* **20**, 981–6 (2011).
321. Blander, J. & Medzhitov, R. On regulation of phagosome maturation and antigen presentation. *Nat Immunol* **7**, 1029–1035 (2006).

322. Wille-Reece, U., Wu, C., Flynn, B. J., Kedl, R. M. & Seder, R. A. Immunization with HIV-1 Gag Protein Conjugated to a TLR7/8 Agonist Results in the Generation of HIV-1 Gag-Specific Th1 and CD8+ T Cell Responses. *J Immunol* **174**, 7676–7683 (2005).
323. Wille-Reece, U. *et al.* HIV Gag protein conjugated to a Toll-like receptor 7/8 agonist improves the magnitude and quality of Th1 and CD8+ T cell responses in nonhuman primates. *Proc National Acad Sci* **102**, 15190–15194 (2005).
324. Kastenmüller, K. *et al.* Protective T cell immunity in mice following protein-TLR7/8 agonist-conjugate immunization requires aggregation, type I IFN, and multiple DC subsets. *J Clin Investigation* **121**, 1782–96 (2011).
325. Oh, J. Z. & Kedl, R. M. The Capacity To Induce Cross-Presentation Dictates the Success of a TLR7 Agonist-Conjugate Vaccine for Eliciting Cellular Immunity. *J Immunol Baltim Md 1950* **185**, 4602–8 (2010).
326. Feng, Y. *et al.* Chemical cross-linking of HIV-1 Env for direct TLR7/8 ligand conjugation compromises recognition of conserved antigenic determinants. *Virology* **446**, 56–65 (2013).
327. Vecchi, S. *et al.* Conjugation of a TLR7 agonist and antigen enhances protection in the *S. pneumoniae* murine infection model. *European J Pharm Biopharm Official J Arbeitsgemeinschaft Für Pharmazeutische Verfahrenstechnik E V* **87**, 310–7 (2014).
328. Holbrook, B. C. *et al.* A Novel R848-Conjugated Inactivated Influenza Virus Vaccine Is Efficacious and Safe in a Neonate Nonhuman Primate Model. *J Immunol Baltim Md 1950* **197**, 555–64 (2016).
329. Holbrook, B. C. *et al.* An R848 adjuvanted influenza vaccine promotes early activation of B cells in the draining lymph nodes of non-human primate neonates. *Immunology* **153**, 357–367 (2018).
330. Holbrook, B. C. *et al.* Adjuvanting an inactivated influenza vaccine with conjugated R848 improves the level of antibody present at 6months in a nonhuman primate neonate model. *Vaccine* **35**, 6137–6142 (2017).
331. Westcott, M. M., Clemens, E. A., Holbrook, B. C., King, S. B. & Alexander-Miller, M. A. The choice of linker for conjugating R848 to inactivated influenza virus determines the stimulatory capacity for innate immune cells. *Vaccine* **36**, 1174–1182 (2018).
332. Lynn, G. M. *et al.* Peptide–TLR-7/8a conjugate vaccines chemically programmed for nanoparticle self-assembly enhance CD8 T-cell immunity to tumor antigens. *Nat Biotechnol* 1–13 (2020) doi:10.1038/s41587-019-0390-x.
333. Baharom, F. *et al.* Intravenous nanoparticle vaccination generates stem-like TCF1+ neoantigen-specific CD8+ T cells. *Nat Immunol* 1–12 (2020) doi:10.1038/s41590-020-00810-3.

334. Wilson, D. S. *et al.* Antigens reversibly conjugated to a polymeric glyco-adjuvant induce protective humoral and cellular immunity. *Nat Mater* **18**, 175–185 (2019).
335. Lynn, G. M. *et al.* In vivo characterization of the physicochemical properties of polymer-linked TLR agonists that enhance vaccine immunogenicity. *Nature Biotechnology* **33**, 1201–1210 (2015).
336. Lynn, G. M. *et al.* Impact of Polymer-TLR-7/8 Agonist (Adjuvant) Morphology on the Potency and Mechanism of CD8 T Cell Induction. *Biomacromolecules* **20**, 854–870 (2019).
337. Nuhn, L. *et al.* pH-degradable imidazoquinoline-ligated nanogels for lymph node-focused immune activation. *Proceedings of the National Academy of Sciences* **113**, (2016).
338. Nuhn, L. *et al.* Potent anti-viral vaccine adjuvant based on pH-degradable nanogels with covalently linked small molecule imidazoquinoline TLR7/8 agonist. *Biomaterials* **178**, 643–651 (2018).
339. Vrieze, J. D. *et al.* Potent Lymphatic Translocation and Spatial Control Over Innate Immune Activation by Polymer–Lipid Amphiphile Conjugates of Small-Molecule TLR7/8 Agonists. *Angewandte Chemie Int Ed* **58**, 15390–15395 (2019).
340. Yoo, E. *et al.* Hyaluronic Acid Conjugates of TLR7/8 Agonists for Targeted Delivery to Secondary Lymphoid Tissue. *Bioconjugate Chem* **29**, 2741–2754 (2018).
341. Ilyinskii, P. O. *et al.* Adjuvant-carrying synthetic vaccine particles augment the immune response to encapsulated antigen and exhibit strong local immune activation without inducing systemic cytokine release. *Vaccine* **32**, 2882–95 (2014).
342. Kim, W. G. *et al.* Covalent Conjugation of Small-Molecule Adjuvants to Nanoparticles Induces Robust Cytotoxic T Cell Responses via DC Activation. *Bioconjugate Chemistry* **27**, 2007–13 (2016).
343. Liong, C. S. *et al.* Enhanced Humoral Immune Response by High Density TLR Agonist Presentation on Hyperbranched Polymers. *Adv Ther* 2000081 (2021) doi:10.1002/adtp.202000081.
344. Buonsanti, C. *et al.* Novel adjuvant Alum-TLR7 significantly potentiates immune response to glycoconjugate vaccines. *Sci Rep-uk* **6**, 29063 (2016).
345. Bagnoli, F. *et al.* Vaccine composition formulated with a novel TLR7-dependent adjuvant induces high and broad protection against Staphylococcus aureus. *P Natl Acad Sci Usa* **112**, 3680–5 (2015).
346. Mancini, F. *et al.* One Dose of Staphylococcus aureus 4C-Staph Vaccine Formulated with a Novel TLR7-Dependent Adjuvant Rapidly Protects Mice through Antibodies, Effector CD4+ T Cells, and IL-17A. *Plos One* **11**, e0147767 (2016).

347. Misiak, A. *et al.* Addition of a TLR7 agonist to an acellular pertussis vaccine enhances Th1 and Th17 responses and protective immunity in a mouse model. *Vaccine* **35**, 5256–5263 (2017).
348. Malyala, P. *et al.* The preparation and physico-chemical characterization of aluminum hydroxide/TLR7a, a novel vaccine adjuvant comprising a small molecule adsorbed to aluminum hydroxide. *J Pharm Sci* **107**, 1577–1585 (2018).
349. Gonzalez-Lopez, A. *et al.* Adjuvant effect of TLR7 agonist adsorbed on aluminum hydroxide (AS37): A phase I randomized, dose escalation study of an AS37-adjuvanted meningococcal C conjugated vaccine. *Clin Immunol* **209**, 108275 (2019).
350. Fox, C. B. *et al.* Adsorption of a synthetic TLR7/8 ligand to aluminum oxyhydroxide for enhanced vaccine adjuvant activity: A formulation approach. *J Control Release* **244**, 98–107 (2016).
351. Francica, J. R. *et al.* Innate transcriptional effects by adjuvants on the magnitude, quality, and durability of HIV envelope responses in NHPs. *Blood Adv* **1**, 2329–2342 (2017).
352. Vaccari, M. *et al.* Adjuvant-dependent innate and adaptive immune signatures of risk of SIVmac251 acquisition. *Nat Med* **22**, 762–770 (2016).
353. Singh, M. *et al.* A preliminary evaluation of alternative adjuvants to alum using a range of established and new generation vaccine antigens. *Vaccine* **24**, 1680–1686 (2006).
354. Yadav, P. D. *et al.* Immunogenicity and protective efficacy of inactivated SARS-CoV-2 vaccine candidate, BBV152 in rhesus macaques. *Nat Commun* **12**, 1386 (2021).
355. Ella, R. *et al.* Safety and immunogenicity of an inactivated SARS-CoV-2 vaccine, BBV152: a double-blind, randomised, phase 1 trial. *Lancet Infect Dis* (2021) doi:10.1016/s1473-3099(20)30942-7.
356. Ganneru, B. *et al.* Th1 skewed immune response of whole virion inactivated SARS CoV 2 vaccine and its safety evaluation. *Isience* **24**, 102298 (2021).
357. Ella, R. *et al.* Safety and immunogenicity of an inactivated SARS-CoV-2 vaccine, BBV152: interim results from a double-blind, randomised, multicentre, phase 2 trial, and 3-month follow-up of a double-blind, randomised phase 1 trial. *Lancet Infect Dis* (2021) doi:10.1016/s1473-3099(21)00070-0.
358. Li, J.-X. & Zhu, F.-C. Adjuvantation helps to optimise COVID-19 vaccine candidate. *Lancet Infect Dis* (2021) doi:10.1016/s1473-3099(21)00094-3.
359. Jangra, S. *et al.* Sterilizing Immunity against SARS-CoV-2 Infection in Mice by a Single-Shot and Lipid Amphiphile Imidazoquinoline TLR7/8 Agonist-Adjuvanted Recombinant Spike Protein Vaccine. *Angewandte Chemie Int Ed* (2021) doi:10.1002/anie.202015362.

360. Petitdemange, C. *et al.* Vaccine induction of antibodies and tissue-resident CD8⁺ T cells enhances protection against mucosal SHIV-infection in young macaques. *Jci Insight* **4**, e126047 (2019).
361. Arunachalam, P. S. *et al.* T cell-inducing vaccine durably prevents mucosal SHIV infection even with lower neutralizing antibody titers. *Nat Med* **1–9** (2020) doi:10.1038/s41591-020-0858-8.
362. Philbin, V. J. *et al.* Imidazoquinoline Toll-like receptor 8 agonists activate human newborn monocytes and dendritic cells through adenosine-refractory and caspase-1-dependent pathways. *J Allergy Clin Immunol* **130**, 195-204.e9 (2012).
363. Primard, C. *et al.* Multifunctional PLGA-Based Nanoparticles Encapsulating Simultaneously Hydrophilic Antigen and Hydrophobic Immunomodulator for Mucosal Immunization. *Mol Pharmaceut* **10**, 2996–3004 (2013).
364. Kim, H. *et al.* Polymeric nanoparticles encapsulating novel TLR7/8 agonists as immunostimulatory adjuvants for enhanced cancer immunotherapy. *Biomaterials* **164**, 38–53 (2018).
365. Sevimli, S., Knight, F. C., Gilchuk, P., Joyce, S. & Wilson, J. T. Fatty Acid-Mimetic Micelles for Dual Delivery of Antigens and Imidazoquinoline Adjuvants. *Acs Biomater Sci Eng* **3**, 179–194 (2017).
366. Dowling, D. J. *et al.* Toll-like receptor 8 agonist nanoparticles mimic immunomodulating effects of the live BCG vaccine and enhance neonatal innate and adaptive immune responses. *J Allergy Clin Immun* **140**, 1339–1350 (2017).
367. Vicente, S. *et al.* Co-delivery of viral proteins and a TLR7 agonist from polysaccharide nanocapsules: A needle-free vaccination strategy. *J Control Release* **172**, 773–781 (2013).
368. Kim, N. W. *et al.* Enhanced Cancer Vaccination by In Situ Nanomicelle-Generating Dissolving Microneedles. *Acs Nano* **12**, 9702–9713 (2018).
369. Park, W., Seong, K. Y., Han, H. H., Yang, S. Y. & Hahn, S. K. Dissolving microneedles delivering cancer cell membrane coated nanoparticles for cancer immunotherapy. *Rsc Adv* **11**, 10393–10399 (2021).
370. Chan, M. *et al.* Synthesis and Characterization of PEGylated Toll Like Receptor 7 Ligands. *Bioconjugate Chem* **22**, 445–454 (2011).
371. Ryu, K. A., Slowinska, K., Moore, T. & Esser-Kahn, A. Immune Response Modulation of Conjugated Agonists with Changing Linker Length. *Acs Chem Biol* **11**, 3347–3352 (2016).
372. Wu, C. C. N. *et al.* Immunotherapeutic activity of a conjugate of a Toll-like receptor 7 ligand. *Proc National Acad Sci* **104**, 3990–3995 (2007).

373. Shinchu, H. *et al.* Enhancement of the Immunostimulatory Activity of a TLR7 Ligand by Conjugation to Polysaccharides. *Bioconjugate Chemistry* **26**, 1713–23 (2015).
374. Hosoya, T. *et al.* Induction of oligoclonal CD8 T cell responses against pulmonary metastatic cancer by a phospholipid-conjugated TLR7 agonist. *Proc National Acad Sci* **115**, 201803281 (2018).
375. Duong, A. D. *et al.* Electrospray Encapsulation of Toll-Like Receptor Agonist Resiquimod in Polymer Microparticles for the Treatment of Visceral Leishmaniasis. *Mol Pharmaceut* **10**, 1045–1055 (2013).
376. Rodell, C. B. *et al.* TLR7/8-agonist-loaded nanoparticles promote the polarization of tumour-associated macrophages to enhance cancer immunotherapy. *Nature Biomedical Engineering* **2**, 578–588 (2018).
377. Rodell, C. B., Ahmed, M. S., Garris, C. S., Pittet, M. J. & Weissleder, R. Development of Adamantane-Conjugated TLR7/8 Agonists for Supramolecular Delivery and Cancer Immunotherapy. *Theranostics* **9**, 8426–8436 (2019).
378. Koch, P. D., Rodell, C. B., Kohler, R. H., Pittet, M. J. & Weissleder, R. Myeloid Cell-Targeted Nanocarriers Efficiently Inhibit Cellular Inhibitor of Apoptosis for Cancer Immunotherapy. *Cell Chem Biol* **27**, (2020).
379. Vinod, N. *et al.* High-capacity poly(2-oxazoline) formulation of TLR 7/8 agonist extends survival in a chemo-insensitive, metastatic model of lung adenocarcinoma. *Sci Adv* **6**, eaba5542 (2020).
380. Mottas, I. *et al.* Amphiphilic nanoparticle delivery enhances the anticancer efficacy of a TLR7 ligand via local immune activation. *Biomaterials* **190**, 111–120 (2019).
381. Scott, E. A. *et al.* Dendritic cell activation and T cell priming with adjuvant- and antigen-loaded oxidation-sensitive polymersomes. *Biomaterials* **33**, 6211–6219 (2012).
382. Manaster, A. J. *et al.* Oxidation-Sensitive Dextran-Based Polymer with Improved Processability through Stable Boronic Ester Groups. *Acs Appl Bio Mater* **2**, 3755–3762 (2019).
383. Ryu, K. A., Stutts, L., Tom, J. K., Mancini, R. J. & Esser-Kahn, A. P. Stimulation of Innate Immune Cells by Light-Activated TLR7/8 Agonists. *J Am Chem Soc* **136**, 10823–10825 (2014).
384. Hantho, J. D., Strayer, T. A., Nielsen, A. E. & Mancini, R. J. An Enzyme-Directed Imidazoquinoline for Cancer Immunotherapy. *ChemMedChem* **11**, 2496–2500 (2016).
385. Ryan, A. T. *et al.* Comparing the immunogenicity of glycosidase-directed resiquimod prodrugs mediated by cancer cell metabolism. *Acta Pharmacol Sin* **41**, 995–1004 (2020).

386. Wang, B. *et al.* Potent and Prolonged Innate Immune Activation by Enzyme-Responsive Imidazoquinoline TLR7/8 Agonist Prodrug Vesicles. *J Am Chem Soc* (2020) doi:10.1021/jacs.0c01928.
387. Schmid, D. *et al.* T cell-targeting nanoparticles focus delivery of immunotherapy to improve antitumor immunity. *Nature Communications* **8**, 1747 (2017).
388. Tacken, P. J. *et al.* Targeted delivery of TLR ligands to human and mouse dendritic cells strongly enhances adjuvanticity. *Blood* **118**, 6836–6844 (2011).
389. Gadd, A. J. R., Greco, F., Cobb, A. J. A. & Edwards, A. D. Targeted Activation of Toll-Like Receptors: Conjugation of a Toll-Like Receptor 7 Agonist to a Monoclonal Antibody Maintains Antigen Binding and Specificity. *Bioconjugate Chem* **26**, 1743–1752 (2015).
390. Klauber, T. C. B. *et al.* Delivery of TLR7 agonist to monocytes and dendritic cells by DCIR targeted liposomes induces robust production of anti-cancer cytokines. *Acta Biomater* **53**, 367–377 (2017).
391. Johansen, P. T. *et al.* Monocyte targeting and activation by cationic liposomes formulated with a TLR7 agonist. *Expert Opin Drug Del* **12**, 1045–58 (2015).
392. Miller, J. B. *et al.* Non-Viral CRISPR/Cas Gene Editing In Vitro and In Vivo Enabled by Synthetic Nanoparticle Co-Delivery of Cas9 mRNA and sgRNA. *Angewandte Chemie Int Ed Engl* **56**, 1059–1063 (2016).
393. Cheng, Q. *et al.* Selective organ targeting (SORT) nanoparticles for tissue-specific mRNA delivery and CRISPR–Cas gene editing. *Nat Nanotechnol* **15**, 313–320 (2020).
394. Aznar, M. A. *et al.* Intratumoral Delivery of Immunotherapy—Act Locally, Think Globally. *J Immunol* **198**, 31–39 (2017).
395. Sloot, S., Rashid, O. M. & Zager, J. S. Intralesional therapy for metastatic melanoma. *Expert Opin Pharmacol* **15**, 2629–2639 (2014).
396. Rehman, H., Silk, A. W., Kane, M. P. & Kaufman, H. L. Into the clinic: Talimogene laherparepvec (T-VEC), a first-in-class intratumoral oncolytic viral therapy. *J Immunother Cancer* **4**, 53 (2016).
397. Hammerich, L. *et al.* Systemic clinical tumor regressions and potentiation of PD1 blockade with in situ vaccination. *Nature Medicine* **25**, 814–824 (2019).
398. Daud, A. *et al.* Systemic antitumor effect and clinical response in a phase 2 trial of intratumoral electroporation of plasmid interleukin-12 in patients with advanced melanoma. *J Clin Oncol* **32**, 9025–9025 (2014).
399. Hong, W. X. *et al.* Intratumoral Immunotherapy for Early-stage Solid Tumors. *Clin Cancer Res* clincanres.3642.2019 (2020) doi:10.1158/1078-0432.ccr-19-3642.

400. Gupta, S. *et al.* Abstract CT091: Safety and pharmacodynamic activity of MEDI9197, a TLR 7/8 agonist, administered intratumorally in subjects with solid tumors. CT091–CT091 (2017) doi:10.1158/1538-7445.am2017-ct091.
401. Fakhari, A. *et al.* Thermosensitive Gel–Based Formulation for Intratumoral Delivery of Toll-Like Receptor 7/8 Dual Agonist, MEDI9197. *J Pharm Sci* **106**, 2037–2045 (2017).
402. Smirnov, D., Schmidt, J. J., Capecchi, J. T. & Wightman, P. D. Vaccine adjuvant activity of 3M-052: An imidazoquinoline designed for local activity without systemic cytokine induction. *Vaccine* **29**, 5434–5442 (2011).
403. Cortez, A. *et al.* Incorporation of Phosphonate into Benzonaphthyridine Toll-like Receptor 7 Agonists for Adsorption to Aluminum Hydroxide. *J Med Chem* **59**, 5868–5878 (2016).
404. Study of the Safety and Efficacy of LHC165 Single Agent and in Combination With PDR001 in Patients With Advanced Malignancies.
405. Georges, B. IMMUNOGENIC COMPOUND. (2019).
406. Nuhn, L. *et al.* Nanoparticle-Conjugate TLR7/8 Agonist Localized Immunotherapy Provokes Safe Antitumoral Responses. *Adv Mater* **30**, 1803397 (2018).
407. Kim, S.-Y. *et al.* Lyophilizable and Multifaceted Toll-like Receptor 7/8 Agonist-Loaded Nanoemulsion for the Reprogramming of Tumor Microenvironments and Enhanced Cancer Immunotherapy. *Acs Nano* **13**, 12671–12686 (2019).
408. Lu, R. *et al.* Formulation and preclinical evaluation of a toll-like receptor 7/8 agonist as an anti-tumoral immunomodulator. *Journal of Controlled Release* **306**, 165–176 (2019).
409. Kockelmann, J. *et al.* Control over Imidazoquinoline Immune Stimulation by pH-Degradable Poly(norbornene) Nanogels. *Biomacromolecules* **21**, (2020).
410. Bahmani, B. *et al.* Intratumoral immunotherapy using platelet-cloaked nanoparticles enhances antitumor immunity in solid tumors. *Nat Commun* **12**, 1999 (2021).
411. Melero, I. *et al.* Evolving synergistic combinations of targeted immunotherapies to combat cancer. *Nat Rev Cancer* **15**, 457–472 (2015).
412. Lo, J. A. *et al.* Epitope spreading toward wild-type melanocyte-lineage antigens rescues suboptimal immune checkpoint blockade responses. *Sci Transl Med* **13**, eabd8636 (2021).
413. Wang, L. *et al.* Enhancing KDM5A and TLR activity improves the response to immune checkpoint blockade. *Sci Transl Med* **12**, eaax2282 (2020).
414. Querec, T. *et al.* Yellow fever vaccine YF-17D activates multiple dendritic cell subsets via TLR2, 7, 8, and 9 to stimulate polyvalent immunity. *J Exp Medicine* **203**, 413–424 (2006).

415. Napolitani, G., Rinaldi, A., Bertoni, F., Sallusto, F. & Lanzavecchia, A. Selected Toll-like receptor agonist combinations synergistically trigger a T helper type 1–polarizing program in dendritic cells. *Nat Immunol* **6**, 769–776 (2005).
416. Maisonneuve, C., Bertholet, S., Philpott, D. J. & Gregorio, E. D. Unleashing the potential of NOD- and Toll-like agonists as vaccine adjuvants. *Proceedings of the National Academy of Sciences* **111**, (2014).
417. Shekarian, T. *et al.* Pattern recognition receptors: immune targets to enhance cancer immunotherapy. (2017) doi:10.1093/annonc/mdx179.
418. Kasturi, S. P. *et al.* Adjuvanting a Simian Immunodeficiency Virus Vaccine with Toll-Like Receptor Ligands Encapsulated in Nanoparticles Induces Persistent Antibody Responses and Enhanced Protection in TRIM5 α Restrictive Macaques. *J Virol* **91**, e01844-16 (2017).
419. Kasturi, S. P. *et al.* 3M-052, a synthetic TLR-7/8 agonist, induces durable HIV-1 envelope-specific plasma cells and humoral immunity in nonhuman primates. *Sci Immunol* **5**, eabb1025 (2020).
420. Fox, C. B. *et al.* A nanoliposome delivery system to synergistically trigger TLR4 AND TLR7. *J Nanobiotechnol* **12**, 17 (2014).
421. Rizwan, S. B. *et al.* Cubosomes containing the adjuvants imiquimod and monophosphoryl lipid A stimulate robust cellular and humoral immune responses. *J Control Release* **165**, 16–21 (2013).
422. Goff, P. H. *et al.* Synthetic Toll-Like Receptor 4 (TLR4) and TLR7 Ligands as Influenza Virus Vaccine Adjuvants Induce Rapid, Sustained, and Broadly Protective Responses. *Journal of Virology* **89**, (2015).
423. McKay, P. F. *et al.* TLR4 and TLR7/8 Adjuvant Combinations Generate Different Vaccine Antigen-Specific Immune Outcomes in Minipigs when Administered via the ID or IN Routes. *Plos One* **11**, e0148984 (2016).
424. Moody, M. A. *et al.* Toll-Like Receptor 7/8 (TLR7/8) and TLR9 Agonists Cooperate To Enhance HIV-1 Envelope Antibody Responses in Rhesus Macaques. *J Virol* **88**, 3329–3339 (2014).
425. Madan-Lala, R., Pradhan, P. & Roy, K. Combinatorial Delivery of Dual and Triple TLR Agonists via Polymeric Pathogen-like Particles Synergistically Enhances Innate and Adaptive Immune Responses. *Scientific Reports* **7**, 2530 (2017).
426. Tom, J. K. *et al.* Modulation of Innate Immune Responses via Covalently Linked TLR Agonists. *Acs Central Sci* **1**, 439–448 (2015).
427. Kimani, F. W. *et al.* Receptor–Ligand Kinetics Influence the Mechanism of Action of Covalently Linked TLR Ligands. *Acs Chem Biol* (2021) doi:10.1021/acscchembio.0c00924.

428. Bagchi, A. *et al.* MyD88-Dependent and MyD88-Independent Pathways in Synergy, Priming, and Tolerance between TLR Agonists. *J Immunol* **178**, 1164–1171 (2007).
429. Whitmore, M. M. *et al.* Synergistic Activation of Innate Immunity by Double-Stranded RNA and CpG DNA Promotes Enhanced Antitumor Activity. *Cancer Res* **64**, 5850–5860 (2004).
430. Albin, T. J. *et al.* Linked Toll-Like Receptor Triagonists Stimulate Distinct, Combination-Dependent Innate Immune Responses. *Acs Central Sci* **5**, 1137–1145 (2019).
431. Manna, S., Maiti, S., Shen, J., Du, W. & Esser-Kahn, A. P. Pathogen-like Nanoassemblies of Covalently Linked TLR Agonists Enhance CD8 and NK Cell-Mediated Antitumor Immunity. *Acs Central Sci* **6**, 2071–2078 (2020).
432. Pradhan, P. *et al.* TRAF6-IRF5 kinetics, TRIF, and biophysical factors drive synergistic innate responses to particle-mediated MPLA-CpG co-presentation. *Sci Adv* **7**, eabd4235 (2021).
433. Ni, Q. *et al.* A bi-adjuvant nanovaccine that potentiates immunogenicity of neoantigen for combination immunotherapy of colorectal cancer. *Sci Adv* **6**, eaaw6071 (2020).
434. Toy, R. *et al.* TLR7 and RIG-I dual-adjuvant loaded nanoparticles drive broadened and synergistic responses in dendritic cells in vitro and generate unique cellular immune responses in influenza vaccination. *J Control Release* **330**, 866–877 (2021).
435. Dovedi, S. J. *et al.* Systemic delivery of a TLR7 agonist in combination with radiation primes durable antitumor immune responses in mouse models of lymphoma. *Blood* **121**, 251–259 (2013).
436. Sagiv-Barfi, I. *et al.* Eradication of spontaneous malignancy by local immunotherapy. *Science Translational Medicine* **10**, eaan4488 (2018).
437. Huang, C. *et al.* Immunostimulatory TLR7 Agonist-Nanoparticles Together with Checkpoint Blockade for Effective Cancer Immunotherapy. *Adv Ther* **3**, 1900200 (2020).
438. Sato-Kaneko, F. *et al.* Combination immunotherapy with TLR agonists and checkpoint inhibitors suppresses head and neck cancer. *JCI Insight* **2**, (2017).
439. Nishii, N. *et al.* Systemic administration of a TLR7 agonist attenuates regulatory T cells by dendritic cell modification and overcomes resistance to PD-L1 blockade therapy. *Oncotarget* **9**, 13301–13312 (2018).
440. Smith, A. A. A. *et al.* Nanoparticles Presenting Potent TLR7/8 Agonists Enhance Anti-PD-L1 Immunotherapy in Cancer Treatment. *Biomacromolecules* **21**, 3704–3712 (2020).
441. Kim, H. *et al.* TLR7/8 Agonist-Loaded Nanoparticles Augment NK Cell-Mediated Antibody-Based Cancer Immunotherapy. *Mol Pharmaceut* **17**, (2020).
442. Hayashi, T. *et al.* Additive melanoma suppression with intralesional phospholipid-conjugated TLR7 agonists and systemic IL-2. *Melanoma Res* **21**, 66–75 (2011).

443. Heo, M. B. & Lim, Y. T. Programmed nanoparticles for combined immunomodulation, antigen presentation and tracking of immunotherapeutic cells. *Biomaterials* **35**, 590–600 (2014).
444. Silva, C. G. D. *et al.* Co-delivery of immunomodulators in biodegradable nanoparticles improves therapeutic efficacy of cancer vaccines. *Biomaterials* **220**, 119417 (2019).
445. Khanna, V. *et al.* Novel TLR 7/8 agonists for improving NK cell mediated antibody-dependent cellular cytotoxicity (ADCC). *Sci Rep-uk* **11**, 3346 (2021).
446. Díaz-Carballo, D. *et al.* Enhanced antitumoral activity of TLR7 agonists via activation of human endogenous retroviruses by HDAC inhibitors. *Commun Biology* **4**, 276 (2021).
447. Smith, M. *et al.* Trial Watch: Toll-like receptor agonists in cancer immunotherapy. *Oncoimmunology* **7**, 1–15 (2018).
448. Biswas, S. K. & Lopez-Collazo, E. Endotoxin tolerance: new mechanisms, molecules and clinical significance. *Trends Immunol* **30**, 475–487 (2009).
449. Chen, J. & Ivashkiv, L. B. IFN- γ abrogates endotoxin tolerance by facilitating Toll-like receptor-induced chromatin remodeling. *Proc National Acad Sci* **107**, 19438–19443 (2010).
450. Miles, K. *et al.* A tolerogenic role for Toll-like receptor 9 is revealed by B-cell interaction with DNA complexes expressed on apoptotic cells. *Proc National Acad Sci* **109**, 887–892 (2012).
451. Silver, A. C., Arjona, A., Walker, W. E. & Fikrig, E. The Circadian Clock Controls Toll-like Receptor 9-Mediated Innate and Adaptive Immunity. *Immunity* **36**, 251–261 (2012).
452. Kondo, T., Kawai, T. & Akira, S. Dissecting negative regulation of Toll-like receptor signaling. *Trends Immunol* **33**, 449–458 (2012).
453. Shi, Y., White, D., He, L., Miller, R. L. & Spaner, D. E. Toll-like Receptor-7 Tolerizes Malignant B Cells and Enhances Killing by Cytotoxic Agents. *Cancer Res* **67**, 1823–1831 (2007).
454. Koga-Yamakawa, E. *et al.* TLR7 tolerance is independent of the type I IFN pathway and leads to loss of anti-tumor efficacy in mice. *Cancer Immunol Immunother* **64**, 1229–1239 (2015).
455. Hayashi, T. *et al.* Prevention of autoimmune disease by induction of tolerance to Toll-like receptor 7. *P Natl Acad Sci Usa* **106**, 2764–9 (2009).
456. Poovassery, J. S. & Bishop, G. A. Type I IFN Receptor and the B Cell Antigen Receptor Regulate TLR7 Responses via Distinct Molecular Mechanisms. *The Journal of Immunology* **189**, 1757–1764 (2012).
457. Michaelis, K. A. *et al.* Persistent Toll-like receptor 7 stimulation induces behavioral and molecular innate immune tolerance. *Brain Behav Immun* **82**, 338–353 (2019).

458. Bourquin, C. *et al.* Systemic Cancer Therapy with a Small Molecule Agonist of Toll-like Receptor 7 Can Be Improved by Circumventing TLR Tolerance. *Cancer Research* **71**, 5123–5133 (2011).
459. Tsitoura, D. *et al.* Early clinical evaluation of the intranasal TLR7 agonist GSK2245035: Use of translational biomarkers to guide dosing and confirm target engagement. *Clin Pharmacol Ther* **98**, 369–380 (2015).
460. Silver, A. C. *et al.* Daily oscillations in expression and responsiveness of Toll-like receptors in splenic immune cells. *Heliyon* **4**, e00579 (2018).
461. Greenberg, E. N. *et al.* Circadian control of interferon-sensitive gene expression in murine skin. *Proc National Acad Sci* **117**, 5761–5771 (2020).
462. Wolchok, J. D. *et al.* Overall Survival with Combined Nivolumab and Ipilimumab in Advanced Melanoma. *New Engl J Med* **377**, 1345–1356 (2017).
463. Gajewski, T. F. The Next Hurdle in Cancer Immunotherapy: Overcoming the Non-T-Cell-Inflamed Tumor Microenvironment. *Semin Oncol* **42**, 663–671 (2015).
464. Lu, B. & Finn, O. J. T-cell death and cancer immune tolerance. *Cell Death Differ* **15**, 70–79 (2007).
465. Staveley-O’Carroll, K. *et al.* Induction of antigen-specific T cell anergy: An early event in the course of tumor progression. *Proc National Acad Sci* **95**, 1178–1183 (1998).
466. Rabinovich, G. A., Gabrilovich, D. & Sotomayor, E. M. Immunosuppressive Strategies that are Mediated by Tumor Cells. *Annu Rev Immunol* **25**, 267–296 (2007).
467. Bonaventura, P. *et al.* Cold Tumors: A Therapeutic Challenge for Immunotherapy. *Front Immunol* **10**, 168 (2019).
468. Mahoney, K. M., Rennert, P. D. & Freeman, G. J. Combination cancer immunotherapy and new immunomodulatory targets. *Nat Rev Drug Discov* **14**, 561–584 (2015).
469. Juneja, V. R., LaFleur, M. W., Manguso, R. T. & Sharpe, A. H. Novel Immunotherapeutic Approaches to the Treatment of Cancer. 1–39 (2016) doi:10.1007/978-3-319-29827-6_1.
470. Coffman, R. L., Sher, A. & Seder, R. A. Vaccine Adjuvants: Putting Innate Immunity to Work. *Immunity* **33**, 492–503 (2010).
471. FDA Approval for Aldara Cream for Superficial Basal Cell Carcinoma. *Oncol Times* **26**, 20 (2004).
472. Lynn, G. M., Laga, R. & Jewell, C. M. Induction of anti-cancer T cell immunity by in situ vaccination using systemically administered nanomedicines. *Cancer Lett* **459**, 192–203 (2019).

473. Thauvin, C. *et al.* Development of resiquimod-loaded modified PLA-based nanoparticles for cancer immunotherapy: A kinetic study. *Eur J Pharm Biopharm* **139**, 253–261 (2019).
474. Vohidov, F. *et al.* Design of BET Inhibitor Bottlebrush Prodrugs with Superior Efficacy and Devoid of Systemic Toxicities. *J Am Chem Soc* **143**, 4714–4724 (2021).
475. Greenwald, R. B. *et al.* Drug Delivery Systems Employing 1,4- or 1,6-Elimination: Poly(ethylene glycol) Prodrugs of Amine-Containing Compounds. *J Med Chem* **42**, 3657–3667 (1999).
476. Mullins, S. R. *et al.* Intratumoral immunotherapy with TLR7/8 agonist MEDI9197 modulates the tumor microenvironment leading to enhanced activity when combined with other immunotherapies. *J Immunother Cancer* **7**, 244 (2019).
477. Foltz, M. H. U.-C. J. & Foltz, C. J. Body Condition Scoring: A Rapid and Accurate Method for Assessing Health Status in Mice. *Lab Anim Sci* (1999).
478. Perkins, H. *et al.* Therapy with TLR7 Agonists Induces Lymphopenia: Correlating Pharmacology to Mechanism in a Mouse Model. *J Clin Immunol* **32**, 1082–1092 (2012).
479. Goswami, S., Anandhan, S., Raychaudhuri, D. & Sharma, P. Myeloid cell-targeted therapies for solid tumours. *Nat Rev Immunol* 1–15 (2022) doi:10.1038/s41577-022-00737-w.
480. Smillie, C. S. *et al.* Intra- and Inter-cellular Rewiring of the Human Colon during Ulcerative Colitis. *Cell* **178**, 714-730.e22 (2019).
481. Cheng, S. *et al.* A pan-cancer single-cell transcriptional atlas of tumor infiltrating myeloid cells. *Cell* **184**, 792-809.e23 (2021).
482. Garcia-Alonso, L., Holland, C. H., Ibrahim, M. M., Turei, D. & Saez-Rodriguez, J. Benchmark and integration of resources for the estimation of human transcription factor activities. *Genome Res* **29**, 1363–1375 (2019).
483. Covarrubias, A. J. *et al.* Senescent cells promote tissue NAD⁺ decline during ageing via the activation of CD38⁺ macrophages. *Nat Metabolism* **2**, 1265–1283 (2020).
484. Garris, C. S. *et al.* Successful Anti-PD-1 Cancer Immunotherapy Requires T Cell-Dendritic Cell Crosstalk Involving the Cytokines IFN- γ and IL-12. *Immunity* **49**, 1148-1161.e7 (2018).
485. Pockros, P. J., Tong, M. & Wright, T. A phase IIa placebo-controlled, double-blind trial to determine the safety, tolerability, PK/PD of an oral interferon inducer, resiquimod, in chronic HCV. *Gastroenterology* **124**, A766 (2003).
486. Vascotto, F. *et al.* Intravenous delivery of the toll-like receptor 7 agonist SC1 confers tumor control by inducing a CD8⁺ T cell response. *Oncoimmunology* **8**, e1601480 (2019).

487. Kidner, T. B. *et al.* Combined intralesional Bacille Calmette-Guérin (BCG) and topical imiquimod for in-transit melanoma. *J Immunother Hagerstown Md* 1997 **35**, 716–20 (2012).
488. Geller, M. A. *et al.* Toll-like receptor-7 agonist administered subcutaneously in a prolonged dosing schedule in heavily pretreated recurrent breast, ovarian, and cervix cancers. *Cancer immunology, immunotherapy : CII* **59**, 1877–84 (2010).
489. Weigel, B. J. *et al.* Prolonged subcutaneous administration of 852A, a novel systemic toll-like receptor 7 agonist, to activate innate immune responses in patients with advanced hematologic malignancies. *Am J Hematol* **87**, 953–956 (2012).
490. Golder, M. R. *et al.* Reduction of liver fibrosis by rationally designed macromolecular telmisartan prodrugs. *Nat Biomed Eng* **2**, 822–830 (2018).
491. Movita, D. *et al.* Kupffer cells express a unique combination of phenotypic and functional characteristics compared with splenic and peritoneal macrophages. *J Leukocyte Biol* **92**, 723–733 (2012).
492. Roberts, A. W. *et al.* Tissue-Resident Macrophages Are Locally Programmed for Silent Clearance of Apoptotic Cells. *Immunity* **47**, 913-927.e6 (2017).
493. Rabanel, J.-M. *et al.* Deep Tissue Penetration of Bottle-Brush Polymers via Cell Capture Evasion and Fast Diffusion. *Acs Nano* **16**, 21583–21599 (2022).
494. Irvine, D. J. & Dane, E. L. Enhancing cancer immunotherapy with nanomedicine. *Nat Rev Immunol* 1–14 (2020) doi:10.1038/s41577-019-0269-6.
495. Sharma, M. *et al.* Preliminary results from a phase 1/2 study of BDC-1001, a novel HER2 targeting TLR7/8 immune-stimulating antibody conjugate (ISAC), in patients (pts) with advanced HER2-expressing solid tumors. *J Clin Oncol* **39**, 2549–2549 (2021).
496. Fang, S. *et al.* Design and Characterization of Immune-Stimulating Imidazo[4,5-c]quinoline Antibody-Drug Conjugates. *Mol Pharmaceut* **19**, 3228–3241 (2022).
497. Janku, F. *et al.* Preclinical Characterization and Phase 1 Study of an Anti-HER2-TLR7 Immune-Stimulator Antibody Conjugate in Patients with HER2+ Malignancies. *Cancer Immunol Res* (2022) doi:10.1158/2326-6066.cir-21-0722.
498. Amend, S. R., Valkenburg, K. C. & Pienta, K. J. Murine Hind Limb Long Bone Dissection and Bone Marrow Isolation. *J Vis Exp Jove* 53936 (2016) doi:10.3791/53936.
499. Mosely, S. I. S. *et al.* Rational Selection of Syngeneic Preclinical Tumor Models for Immunotherapeutic Drug Discovery. *Cancer Immunol Res* **5**, 29–41 (2017).
500. Macosko, E. Z. *et al.* Highly Parallel Genome-wide Expression Profiling of Individual Cells Using Nanoliter Droplets. *Cell* **161**, 1202–1214 (2015).

501. Wu, T. *et al.* clusterProfiler 4.0: A universal enrichment tool for interpreting omics data. *Innovation* **2**, 100141 (2021).
502. Alvarez, M. J. *et al.* Functional characterization of somatic mutations in cancer using network-based inference of protein activity. *Nat Genet* **48**, 838–847 (2016).
503. Sette, A. & Rappuoli, R. Reverse Vaccinology: Developing Vaccines in the Era of Genomics. *Immunity* **33**, 530–541 (2010).
504. Moyer, T. J., Zmolek, A. C. & Irvine, D. J. Beyond antigens and adjuvants: formulating future vaccines. *J. Clin. Investig.* **126**, 799–808 (2016).
505. Tan, H., Davenport, M. P., Kent, S. J. & Wheatley, A. K. Nice and slow make the germinal centers go: measured and escalating antigen delivery enhance durability and quality of humoral immune responses against HIV-1. *Immunol. Cell Biol.* **100**, 750–752 (2022).
506. Victora, G. D. & Nussenzweig, M. C. Germinal Centers. *Annu Rev Immunol* **40**, 1–30 (2022).
507. Cyster, J. G. & Allen, C. D. C. B Cell Responses: Cell Interaction Dynamics and Decisions. *Cell* **177**, 524–540 (2019).
508. Gitlin, A. D. *et al.* T cell help controls the speed of the cell cycle in germinal center B cells. *Science* **349**, 643–646 (2015).
509. Keitel, W. A., Bond, N. L., Zahradnik, J. M., Cramton, T. A. & Robbins, J. B. Clinical and serological responses following primary and booster immunization with Salmonella typhi Vi capsular polysaccharide vaccines. *Vaccine* **12**, 195–199 (1994).
510. Steichen, J. M. *et al.* HIV Vaccine Design to Target Germline Precursors of Glycan-Dependent Broadly Neutralizing Antibodies. *Immunity* **45**, 483–496 (2016).
511. Steichen, J. M. *et al.* A generalized HIV vaccine design strategy for priming of broadly neutralizing antibody responses. *Science* **366**, eaax4380 (2019).
512. Silva, M. *et al.* A particulate saponin/TLR agonist vaccine adjuvant alters lymph flow and modulates adaptive immunity. *Sci Immunol* **6**, eabf1152 (2021).
513. Barouch, D. H. Covid-19 Vaccines — Immunity, Variants, Boosters. *New Engl J Med* **387**, 1011–1020 (2022).
514. Lee, J. H. & Crotty, S. HIV vaccinology: 2021 update. *Semin Immunol* **51**, 101470 (2021).
515. Haynes, B. F. *et al.* Strategies for HIV-1 vaccines that induce broadly neutralizing antibodies. *Nat Rev Immunol* **23**, 142–158 (2023).
516. Feinberg, M. B. Uhambo — Twists and Turns on the Journey to an Efficacious HIV-1 Vaccine. *New Engl J Med* **384**, 1157–1159 (2021).

517. Burton, D. R. Advancing an HIV vaccine; advancing vaccinology. *Nat Rev Immunol* **19**, 77–78 (2019).
518. Gilbert, P. B. *et al.* Neutralization titer biomarker for antibody-mediated prevention of HIV-1 acquisition. *Nat Med* **28**, 1924–1932 (2022).
519. Corey, L. *et al.* Two Randomized Trials of Neutralizing Antibodies to Prevent HIV-1 Acquisition. *New Engl J Med* **384**, 1003–1014 (2021).
520. Havenar-Daughton, C., Lee, J. H. & Crotty, S. Tfh cells and HIV bnAbs, an immunodominance model of the HIV neutralizing antibody generation problem. *Immunol Rev* **275**, 49–61 (2017).
521. Klasse, P. J., Ozorowski, G., Sanders, R. W. & Moore, J. P. Env Exceptionalism: Why Are HIV-1 Env Glycoproteins Atypical Immunogens? *Cell Host Microbe* **27**, 507–518 (2020).
522. Shulman, Z. *et al.* Dynamic signaling by T follicular helper cells during germinal center B cell selection. *Science* **345**, 1058–1062 (2014).
523. Pauthner, M. *et al.* Elicitation of Robust Tier 2 Neutralizing Antibody Responses in Nonhuman Primates by HIV Envelope Trimer Immunization Using Optimized Approaches. *Immunity* **46**, 1073-1088.e6 (2017).
524. Abbott, R. K. *et al.* Precursor Frequency and Affinity Determine B Cell Competitive Fitness in Germinal Centers, Tested with Germline-Targeting HIV Vaccine Immunogens. *Immunity* **48**, 133-146.e6 (2018).
525. Lee, J. H. & Crotty, S. Long-primed germinal centres with enduring affinity maturation and clonal migration. *Nature* (2022) doi:10.1038/s41586-022-05216-9.
526. Boopathy, A. V. *et al.* Enhancing humoral immunity via sustained-release implantable microneedle patch vaccination. *Proc National Acad Sci* **116**, 16473–16478 (2019).
527. Roth, G. A. *et al.* Injectable Hydrogels for Sustained Codelivery of Subunit Vaccines Enhance Humoral Immunity. *Acs Central Sci* **6**, 1800–1812 (2020).
528. Gale, E. C. *et al.* Hydrogel-Based Slow Release of a Receptor-Binding Domain Subunit Vaccine Elicits Neutralizing Antibody Responses Against SARS-CoV-2. *Adv. Mater.* **33**, 2104362 (2021).
529. Roth, G. A. *et al.* Designing spatial and temporal control of vaccine responses. *Nat Rev Mater* 1–22 (2021) doi:10.1038/s41578-021-00372-2.
530. Garcea, R. L. *et al.* Single-administration, thermostable human papillomavirus vaccines prepared with atomic layer deposition technology. *Npj Vaccines* **5**, 45 (2020).

531. Rodrigues, K. A. *et al.* Phosphate-mediated coanchoring of RBD immunogens and molecular adjuvants to alum potentiates humoral immunity against SARS-CoV-2. *Sci Adv* **7**, eabj6538 (2021).
532. Havenar-Daughton, C. *et al.* Direct Probing of Germinal Center Responses Reveals Immunological Features and Bottlenecks for Neutralizing Antibody Responses to HIV Env Trimer. *Cell Reports* **17**, 2195–2209 (2016).
533. Baumjohann, D. *et al.* Persistent Antigen and Germinal Center B Cells Sustain T Follicular Helper Cell Responses and Phenotype. *Immunity* **38**, 596–605 (2013).
534. Mintz, M. A. & Cyster, J. G. T follicular helper cells in germinal center B cell selection and lymphomagenesis. *Immunol Rev* **296**, 48–61 (2020).
535. Mayer, A., Zhang, Y., Perelson, A. S. & Wingreen, N. S. Regulation of T cell expansion by antigen presentation dynamics. *Proc National Acad Sci* **116**, 5914–5919 (2019).
536. Johansen, P. *et al.* Antigen kinetics determines immune reactivity. *Proc National Acad Sci* **105**, 5189–5194 (2008).
537. Quiel, J. *et al.* Antigen-stimulated CD4 T-cell expansion is inversely and log-linearly related to precursor number. *Proc National Acad Sci* **108**, 3312–3317 (2011).
538. Aung, A. *et al.* Low protease activity in B cell follicles promotes retention of intact antigens after immunization. *Science* **379**, eabn8934 (2023).
539. Yang, L. *et al.* Antigen presentation dynamics shape the antibody response to variants like SARS-CoV-2 Omicron after multiple vaccinations with the original strain. *Cell Reports* **42**, 112256 (2023).
540. Kulp, D. W. *et al.* Structure-based design of native-like HIV-1 envelope trimers to silence non-neutralizing epitopes and eliminate CD4 binding. *Nat Commun* **8**, 1655 (2017).
541. Wang, S. *et al.* Manipulating the Selection Forces during Affinity Maturation to Generate Cross-Reactive HIV Antibodies. *Cell* **160**, 785–797 (2015).
542. Qi, H. T follicular helper cells in space-time. *Nat Rev Immunol* **16**, 612–625 (2016).
543. Crotty, S. T Follicular Helper Cell Biology: A Decade of Discovery and Diseases. *Immunity* **50**, 1132–1148 (2019).
544. Crotty, S. T Follicular Helper Cell Differentiation, Function, and Roles in Disease. *Immunity* **41**, 529–542 (2014).
545. Dominguez-Sola, D. *et al.* The proto-oncogene MYC is required for selection in the germinal center and cyclic reentry. *Nat Immunol* **13**, 1083–1091 (2012).

546. Shulman, Z. *et al.* T Follicular Helper Cell Dynamics in Germinal Centers. *Science* **341**, 673–677 (2013).
547. Devarajan, P. *et al.* Strong influenza-induced TFH generation requires CD4 effectors to recognize antigen locally and receive signals from continuing infection. *Proc National Acad Sci* **119**, e2111064119 (2022).
548. Deenick, E. K. *et al.* Follicular Helper T Cell Differentiation Requires Continuous Antigen Presentation that Is Independent of Unique B Cell Signaling. *Immunity* **33**, 241–253 (2010).
549. Cirelli, K. M. & Crotty, S. Germinal center enhancement by extended antigen availability. *Curr Opin Immunol* **47**, 64–69 (2017).
550. Hu, J. K. *et al.* Murine Antibody Responses to Cleaved Soluble HIV-1 Envelope Trimers Are Highly Restricted in Specificity. *J Virol* **89**, 10383–10398 (2015).
551. McHugh, K. J. *et al.* Fabrication of fillable microparticles and other complex 3D microstructures. *Science* **357**, 1138–1142 (2017).
552. Tokatlian, T. *et al.* Innate immune recognition of glycans targets HIV nanoparticle immunogens to germinal centers. *Science* **363**, 649–654 (2019).
553. Gandhi, L. *et al.* Pembrolizumab plus Chemotherapy in Metastatic Non–Small-Cell Lung Cancer. *N. Engl. J. Med.* **378**, 2078–2092 (2018).
554. Lee, W. S., Yang, H., Chon, H. J. & Kim, C. Combination of anti-angiogenic therapy and immune checkpoint blockade normalizes vascular-immune crosstalk to potentiate cancer immunity. *Exp. Mol. Med.* **52**, 1475–1485 (2020).
555. Vinay, D. S. *et al.* Immune evasion in cancer: Mechanistic basis and therapeutic strategies. *Semin. Cancer Biol.* **35**, S185–S198 (2015).
556. Hegde, P. S. & Chen, D. S. Top 10 Challenges in Cancer Immunotherapy. *Immunity* **52**, 17–35 (2020).
557. Röltgen, K. *et al.* Immune imprinting, breadth of variant recognition, and germinal center response in human SARS-CoV-2 infection and vaccination. *Cell* **185**, 1025–1040.e14 (2022).
558. Cho, A. *et al.* Anti-SARS-CoV-2 receptor-binding domain antibody evolution after mRNA vaccination. *Nature* **600**, 517–522 (2021).
559. Pardi, N. *et al.* Expression kinetics of nucleoside-modified mRNA delivered in lipid nanoparticles to mice by various routes. *J. Control. Release* **217**, 345–351 (2015).
560. Melo, M. *et al.* Immunogenicity of RNA Replicons Encoding HIV Env Immunogens Designed for Self-Assembly into Nanoparticles. *Mol. Ther.* **27**, 2080–2090 (2019).

561. Pollock, K. M. *et al.* Safety and immunogenicity of a self-amplifying RNA vaccine against COVID-19: COVAC1, a phase I, dose-ranging trial. *eClinicalMedicine* **44**, 101262 (2022).